Sediment dynamics in the Pearl River Estuary: evolution of estuarine turbidity maximum

Dissertation

with the aim of achieving a doctoral degree at the Faculty of Mathematics, Informatics and Natural Sciences Department of Earth System Sciences at University of Hamburg

submittend by

Mengyao Ma

Hamburg, 2024

Department of Earth Sciences

Date of Oral Defense: 18.06.2025

Reviewers:

Prof. Dr. Corinna Schrum
Dr. Wenyan Zhang

Members of the examination commission:

Prof. Dr. Corinna Schrum
Dr. Wenyan Zhang
Prof. Dr. Jörn Peckmann
Prof. Dr. Florian Scholz
PD Dr. Thomas Pohlmann

Chair of the subject Doctoral Committee:

Earth System Science: Prof. Dr. Hermann Held

Dean of Faculty MIN: Prof. Dr.-Ing. Norbert Ritter

Abstract

Estuarine Turbidity Maximums (ETMs) represent zones where suspended particulate matter (SPM) concentrations are significantly elevated, occurring at the interface between riverine and marine environments. This has a profound influence on the biogeochemistry and biology of the estuary. The formation and maintenance mechanisms of ETMs depend on the river discharge, sediment load, tides, and estuarine morphology. In the Pearl River Estuary (PRE), hydrodynamics (river discharge, tides, and coastal current) interact with seasonal sediment load and estuarine topography to influence the sediment dynamics. The PRE is a highly variable, complex estuary. In temporal terms, it has undergone significant human-induced changes in its morphology over time, and its sea level has been rising at a rate greater than the global average. In spatial terms, various topographic units have collectively shaped the PRE. This study elucidates the physical mechanism of ETM formation and its response to the historical development and future scenarios. Investigation on the variation of stratification provides the mechanism of hydrodynamic response to morphological changes and climatic changes. Numerical modeling studies on the formation of three ETMs provide insights into different domain mechanisms. Reconstruction of past morphology and simulations under future scenarios shed light on the historical evolution and potential challenges (e.g. sea level rise, coastline change due to land reclamation or natural processes of erosion and deposition, bathymetry change due to dredging etc.) facing the PRE. The thesis aims to provide a basis for the knowledge needed by decision makers to establish science-based management strategies for estuaries under climate change and rapid coastal development.

The estuarine circulation in the PRE is driven by several factors, including the seasonal river discharge, tides, and coastal currents. The hydrological environment of the Pearl River Estuary is notable for its stratification, a characteristic that places it within the category of partially stratified estuaries. The intensity and location of stratification in this estuary respond not only to the aforementioned factors affecting the estuarine circulation, but also to the morphology of the PRE and the relative sea level. The impact of these changes on stratification can be summarized as follows: (1) Morphological changes in the Lingding Bay (the main estuary of the PRE) from 1970s to 2010s resulted in a bay-scale enhancement of stratification by up to a factor of four, with maximum local enhancement (up to a factor of seven) at the western shoal of the bay. (2) Stratification in the PRE has become more sensitive to tidal forcing and river runoff impact after the morphological change. The variation is greatly amplified by the spring-neap tidal cycle. The maximum enhancement in stratification occurs in the transition period

from neap to spring tides due to the increase of advection of vertical salinity variance in water volume. (3) The relationship between depth changes and salt fluxes is nonlinear and varies among different morphological units. In the PRE, the eastern channel and the western shoal experience the greatest enhancement in both strength and stability of stratification caused by the morphological change. (4) Compared to an overwhelming impact of human-induced morphological change in the past few decades, future change of stratification driven by sea level rise will be further strengthened but to a much lesser extent. The maximum enhancement associated with sea level rise occurs during spring tides due to the increased vertical straining value.

The formation and maintenance mechanisms of ETMs in the Pearl River Estuary are influenced by the complex hydrological environment and topography, exhibiting a high degree of diversity. Three ETMs have been observed in the PRE and are reproduced by the numerical model: the west shoal, middle shoal, and west channel ETMs. In the two ETMs located at the west shoal and middle shoal, advection dominates the sediment transport flux, whilst tidal pumping plays a crucial role in maintaining those ETM. A sharp bathymetric gradient leads to an entrapment of sediment within the bottom layer in the west channel ETM, a phenomenon referred to as topographical trapping. Model analysis shows that the ETMs are interconnected, with sediment transport between the ETMs varying seasonally, which is attributed to the variation of stratification driven by the monsoon-mediated river runoff.

To facilitate a more accurate reference point for sediment management, an investigation was conducted into the historical evolution and future development scenarios of the PRE. The morphological changes and relative sea level rise (rSLR) resulting from climate change and human activities were identified as the principal driving forces in the evolutionary development of PRE. Based on the morphology, river discharge, sediment load, and sea level of 1970s, a validated model result from the 1970s was employed to investigate the hydrodynamics and sediment dynamics of that period. Additionally, this study reconstructed the distribution of estuarine bed sediment during the 1970s and demonstrated that the composition of estuarine bed sediments is a critical factor influencing the distribution and extension of ETMs. The remaining findings are listed as follows: (1) The morphological changes that occurred between the 1970s and 2010s resulted in a transition of the ETMs in PRE from a river-dominated system to one that is multi-factor dominated. (2) The rSLR between the 2010s and 2100s has the effect of increasing the depth of the water column, which, in general, results in a decrease in the concentration of SPM at the bottom layer, as well as a reduction in the concentration and

intensity of ETMs. This is attributable to an increase in stratification and a decrease in bottom shear stress. (3) In light of the potential impact of wind shifts on future outcomes, our findings indicate that a projected 40° anticlockwise rotation in wind direction and a reduction in wind speed are associated with an increase in the concentration of bottom layer SPM in the southwestern portion of West Shoal. (4) Upon activating the wave model in the simulation, it was observed that the wave effect exerted the most significant influence on SPM concentration at the bottom layer during the 1970s. As morphological alterations and water depth increased, the wave effect was observed to reduce the intensification effect on bottom SPM concentration, with an increase observed only in the western shoal. As rSLR occurred, the wave effect on bottom SPM concentration was observed to further diminish, with only a slight increase in bottom SPM concentration noted in the western shoal.

The findings presented in this thesis represent the inaugural demonstration of the evolutionary trajectory of ETMs in the PRE. This serves as a point of reference for the sustainable management of estuarine sediments, with implications for the future development of the PRE and other estuaries.

Zusammenfassung

Ästuarine Trübungsmaxima (ETM) sind Zonen, in denen die Konzentration von Schwebstoffen (SPM) an der Schnittstelle zwischen Fluss- und Meeresumwelt deutlich erhöht ist. Dies hat einen tiefgreifenden Einfluss auf die Biogeochemie und Biologie des Ästuars. Die Entstehungs- und Erhaltungsmechanismen von ETMs hängen von der Abflussmenge des Flusses, der Sedimentfracht, den Gezeiten und der Morphologie des Ästuars ab. Im Ästuar des Perlflusses (PRE) beeinflussen die Hydrodynamik (Flussabfluss, Gezeiten und Küstenströmung) in Wechselwirkung mit der saisonalen Sedimentbelastung und der Ästuartopographie die Sedimentdynamik. Das PRE ist ein äußerst variables, komplexes Ästuar. In zeitlicher Hinsicht hat sich seine Morphologie im Laufe der Zeit durch den Menschen erheblich verändert, und der Meeresspiegel ist schneller gestiegen als im globalen Durchschnitt. In räumlicher Hinsicht haben verschiedene topografische Einheiten den PRE gemeinsam geformt. In dieser Studie wird der physikalische Mechanismus der ETM-Bildung und seine Reaktion auf die historische Entwicklung und künftige Szenarien erläutert. Die Untersuchung der Variation der Schichtung liefert den Mechanismus der hydrodynamischen Reaktion auf morphologische Veränderungen und klimatische Veränderungen. Numerische Modellierungsstudien zur Bildung von drei ETMs geben Einblicke in verschiedene Domänenmechanismen. Die Rekonstruktion der Morphologie der Vergangenheit und Simulationen von Zukunftsszenarien geben Aufschluss über die historische Entwicklung und potenzielle Herausforderungen (z. B. Anstieg des Meeresspiegels, Veränderung der Küstenlinie durch Landgewinnung oder natürliche Erosions- und Ablagerungsprozesse, Veränderung der Bathymetrie durch Ausbaggerung usw.), denen sich die PRE gegenübersieht. Ziel der Arbeit ist es, eine Grundlage für das Wissen zu schaffen, das die Entscheidungsträger benötigen, um wissenschaftlich fundierte Managementstrategien für Ästuare unter den Bedingungen des Klimawandels und der raschen Küstenentwicklung zu entwickeln.

Die Ästuarzirkulation in der PRE wird von mehreren Faktoren bestimmt, darunter der saisonale Flussabfluss, die Gezeiten und die Küstenströmungen. Das hydrologische Umfeld des Perlflussästuars zeichnet sich durch seine Schichtung aus, ein Merkmal, das es in die Kategorie der teilweise geschichteten Ästuare einordnet. Die Intensität und die Lage der Schichtung in diesem Ästuar hängen nicht nur von den oben genannten Faktoren ab, die die Mündungszirkulation beeinflussen, sondern auch von der Morphologie des PRE und dem relativen Meeresspiegel. Die Auswirkungen dieser Veränderungen auf die Schichtung lassen sich wie folgt zusammenfassen: (1) Morphologische Veränderungen in der Lingding-Bucht (dem Hauptmündungsgebiet der PRE) von den 1970er bis 2010er Jahren führten zu einer buchtweiten Verstärkung der Schichtung um einen Faktor von bis zu vier, mit einer maximalen lokalen Verstärkung (bis zu einem Faktor von sieben) an der westlichen Untiefe der Bucht. (2) Die Schichtung in der PRE ist nach der morphologischen Veränderung empfindlicher gegenüber den Gezeiten und den Auswirkungen des Flussabflusses geworden. Die Schwankungen werden durch den Gezeitenzyklus im Frühjahr und im Winter stark verstärkt. Die maximale Verstärkung der Schichtung tritt in der Übergangszeit zwischen Nipp- und Springflut auf, was auf die Zunahme der Advektion der vertikalen Salzgehaltsschwankungen im Wasservolumen zurückzuführen ist. (3) Die Beziehung zwischen Tiefenänderungen und Salzflüssen ist nichtlinear und variiert zwischen den verschiedenen morphologischen Einheiten. In der PRE erfahren die östliche Rinne und die westliche Untiefe die größte Verstärkung sowohl der Stärke als auch der Stabilität der Schichtung durch die morphologische Veränderung. (4) Im Vergleich zu den überwältigenden Auswirkungen der vom Menschen verursachten

morphologischen Veränderungen in den letzten Jahrzehnten werden die zukünftigen Veränderungen der Schichtung durch den Anstieg des Meeresspiegels zwar weiter verstärkt, aber in einem viel geringeren Ausmaß. Die maximale Verstärkung im Zusammenhang mit dem Meeresspiegelanstieg tritt während der Springfluten auf, da der Wert der vertikalen Belastung steigt.

Die Entstehungs- und Erhaltungsmechanismen von ETMs im Perlflussmündungsgebiet werden durch die komplexe hydrologische Umgebung und die Topographie beeinflusst und weisen eine große Vielfalt auf. In der PRE wurden drei ETMs beobachtet, die durch das numerische Modell reproduziert werden: das westliche Untief, das mittlere Untief und das westliche Kanal-ETM. In den beiden ETMs an der westlichen Untiefe und der mittleren Untiefe dominiert die Advektion den Sedimenttransport, während das Pumpen durch die Gezeiten eine entscheidende Rolle bei der Aufrechterhaltung dieser ETMs spielt. Ein starkes bathymetrisches Gefälle führt zu einem Einschluss von Sedimenten in der Bodenschicht im ETM der westlichen Rinne, ein Phänomen, das als topographischer Einschluss bezeichnet wird. Die Modellanalyse zeigt, dass die ETMs miteinander verbunden sind, wobei der Sedimenttransport zwischen den ETMs saisonal schwankt, was auf die durch den monsunbedingten Flussabfluss bedingte Variation der Schichtung zurückzuführen ist.

Um einen genaueren Bezugspunkt für das Sedimentmanagement zu erhalten, wurde eine Untersuchung der historischen Entwicklung und der zukünftigen Entwicklungsszenarien der PRE durchgeführt. Die morphologischen Veränderungen und der relative Meeresspiegelanstieg (rSLR) infolge des Klimawandels und menschlicher Aktivitäten wurden als die wichtigsten treibenden Kräfte für die evolutionäre Entwicklung des PRE identifiziert. Auf der Grundlage der Morphologie, des Flussabflusses, der Sedimentfracht und des Meeresspiegels in den 1970er Jahren wurde ein validiertes Modell aus den 1970er Jahren verwendet, um die Hydrodynamik und die Sedimentdynamik in diesem Zeitraum zu untersuchen. Darüber hinaus wurde in dieser Studie die Verteilung der Ästuarsedimente in den 1970er Jahren rekonstruiert und gezeigt, dass die Zusammensetzung der Ästuarsedimente ein entscheidender Faktor ist, der die Verteilung und Ausdehnung der ETMs beeinflusst. Die übrigen Ergebnisse sind im Folgenden aufgeführt: (1) Die morphologischen Veränderungen, die zwischen den 1970er und 2010er Jahren stattfanden, führten zu einem Übergang der ETM in PRE von einem flussdominierten System zu einem multifaktoriell dominierten System. (2) Die rSLR zwischen den 2010er und 2100er Jahren hat zur Folge, dass sich die Tiefe der Wassersäule vergrößert, was im Allgemeinen zu einer Abnahme der Konzentration von SPM in der unteren Schicht sowie zu einer Verringerung der Konzentration und Intensität von ETMs führt. Dies ist auf eine Zunahme der Schichtung und eine Abnahme der Bodenschubspannung zurückzuführen. (3) In Anbetracht der möglichen Auswirkungen von Windverschiebungen auf künftige Ergebnisse deuten unsere Ergebnisse darauf hin, dass eine projizierte Drehung der Windrichtung um 40° gegen den Uhrzeigersinn und eine Verringerung der Windgeschwindigkeit mit einer Zunahme der Konzentration von SPM in der Bodenschicht im südwestlichen Teil von West Shoal verbunden sind. (4) Nach Aktivierung des Wellenmodells in der Simulation wurde festgestellt, dass der Welleneffekt in den 1970er Jahren den größten Einfluss auf die SPM-Konzentration in der Bodenschicht ausübte. Als die morphologischen Veränderungen und die Wassertiefe zunahmen, wurde beobachtet, dass der Welleneffekt den Verstärkungseffekt auf die SPM-Konzentration am Boden verringerte, wobei nur in der westlichen Untiefe ein Anstieg beobachtet wurde. Als rSLR auftrat, wurde beobachtet, dass der Welleneffekt auf die SPM-Konzentration am Boden weiter

abnahm, wobei nur ein leichter Anstieg der SPM-Konzentration am Boden in der westlichen Untiefe festgestellt wurde.

Die in dieser Arbeit vorgestellten Ergebnisse stellen den ersten Nachweis des Entwicklungsverlaufs von ETM in der PRE dar. Sie dienen als Bezugspunkt für die nachhaltige Bewirtschaftung von Ästuarsedimenten und haben Auswirkungen auf die zukünftige Entwicklung der PRE und anderer Ästuare.

List of publications

Publication related to this dissertation:

Appendix A

Ma, M., Zhang, W., Chen, W., Deng, J. and Schrum, C., 2023. Impacts of morphological change and sea-level rise on stratification in the Pearl River Estuary. *Frontiers in Marine Science*, *10*, p.1072080. DOI: 10.3389/fmars.2023.1072080

Appendix B

Ma, M., Porz, L., Schrum, C. and Zhang, W., 2024. Physical mechanisms, dynamics and interconnections of multiple estuarine turbidity maximum in the Pearl River estuary. Frontiers in Marine Science, 11, p.1385382. DOI: 10.3389/fmars.2024.1385382

Appendix C

Ma, M., Zhang, W., Porz, L., and Schrum, C., 2024. Evolution of Estuarine Turbidity Maximum in the Pearl River Estuary: historical development and future scenarios. (to be submitted)

Contents

1. Introduction

This thesis aims to investigate the impact of various factors on the formation and maintenance of ETMs in the PRE and to explore some potential factors that impact the evolution of ETMs. The various factors that affect the ETMs in PRE include river discharge, sediment load, tides, coastal current, morphology, sediment components on estuarine bed, and sea level. Collectively, these factors contribute to making PRE a typical complex hydrodynamics and sediment dynamics estuary system.

The first documented occurrence of ETMs was in the Gironde estuary, France, by *Glangeaud* (1938). This observation led to the realization that ETMs are pervasive characteristics of estuarine environments. A number of studies have demonstrated the significance of ETMs in estuarine ecosystems. (1) Light attenuation. In many estuaries light attenuation by suspended sediment confines the photic zone to a small fraction of the water column, such that light limitation is a major control on phytoplankton production and turnover rate. Spatial and temporal variability of phytoplankton biomass or productivity in estuaries can be explained by variations in the ratio of photic depth (turbidity) to mixed depth (*Campbell and Spinrad*, 1987; *Cloern*, 1987; *Gameiro et al.*, 2011). In Chesapeake Bay, benthic diatoms cannot inhabit the deep shipping channel due to high concentration of SPM (*D Y Lee et al.*, 2012), the impediment is worsened in ETMs zone, which causes rapid light attenuation (*Baross*[1], 1994). (2) Aggregation and sedimentation. ETMs plays an important role in aggregation and sedimentation of fine cohesive sediment particles. In an ETM, the flocculation-associated increase in particle settling velocity is enhanced by tidal asymmetry, which in turn increases the trapping of sediment in the ETM, and the rapid bottom sediment accumulation at the ETM results in the much larger bed thickness (*Xu et al.*, 2010). It also significantly affects the chemical behaviors of heavy metal elements and organic materials as well as their fate and transport in the water body(*Wai et al.*, 2004). As the fine sediment is incorporated into ETM aggregate and /or the estuarine bed. Thus contaminant trapping is a frequent occurrence in ETM (*Jay et al.*, 2015). (3) Oxygen depletion. Oxygen depletion due to the degradation of organic matter that is associated with the suspended sediment aggregates. A minimum of dissolved oxygen (DO) occurs near the ETM in Ems estuary, which results from the interaction of nutrients and algae and their residence time, and constant sediment oxygen demand drives oxygen depletion (*Talke et al.*, 2009). *Cui et al.* (2022) suggest that particle resuspension plays a vital role in maintaining the DO level of bottom hypoxia, as their observations indicate a profound correlation between bottom hypoxia and ETM in PRE. The role of ETM in the

aforementioned process is of significant consequence, and the study of ETM is therefore key to the advancement of sustainable estuarine ecosystems. For instance, an understanding of ETM may assist in the elucidation of harmful algal blooms or the development of hypoxia zones in the estuary, thereby enabling the development of an effective management method for the estuary.

1.1 Variation of stratification

The sediment distribution is consequence of estuarine hydrodynamic. The estuarine hydrodynamics affect the transportation of sediments, contaminants, nutrients, and larvae, as well as the condition of the estuarine species. Sediment plays a pivotal role in determining several key environmental variables, including the availability of nutrients, light penetration, turbidity, deposition/erosion processes, and the residual current (*Iglesias et al.*, 2024). From this perspective, an exact comprehension of the hydrodynamic patterns that characterise estuaries is of vital importance for the effective management and preservation of sediment management in the context of the current emergence of anthropogenic pressures and climate changes.

Stratification represents a fundamental hydrodynamic attribute of estuaries, which emerges as a consequence of the convergence of freshwater and saltwater. *Geyer and MacCready* (2014) defined estuarine parameter space based on freshwater Froude number[1] and mixing number[2] as: salt wedge, time-dependent salt wedge, strongly stratified, partially mixed, strain-induced periodic stratification (SIPS), well mixed. The stratification or mixing level of estuary depends on the tide, the river flow, the current induced by density gradients, the morphology and the climatic conditions (*MacCready*, 1999). In the PRE, the interaction of the longitudinal straining, lateral current shear, Coriolis force, and morphology contribute to the tidal, seasonal, and geographically varying stratification(*Lu and Gan*, 2015; *Qian et al.*, 2022; *F Yang et al.*, 2022a).

The morphological changes resulting from land reclamation and dredging, in addition to sea-level rise (SLR) caused by climate change, have the effect of influencing the variation of estuarine stratification. The channel deepening results in enhanced saltwater intrusion was reported across a range of rivers (Hudson River, *Ralston and Geyer* (2019); Missippi River, *F*

[1] Froude number $F_{rf} = U_0/(\beta g S_0 H)^{1/2}$ represents the ratio of the mean river velocity (U_0) to the gravitationally driven exchange flow that is scaled with the water depth H. Here, S_0 is the background ocean salinity and $\beta \cong 7.7 \times 10^{-4}$ is the coefficient of saline contraction.

[2] Mixing number $M = [C_d U_t^2/\omega N_0 H^2]^{1/2}$ represents the ratio between the tidal timescale and the timescale of vertical turbulent mixing. In, $N_0 = (\beta g S_0/H)^{1/2}$ is the buoyancy frequency for maximum top to bottom salinity variation in an estuary, where ω is the tidal frequency, U_t is the amplitude of the depth-averaged tidal velocity, C_d is the drag coefficient.

C Wang (1988); Ems and Elbe, *van Rijn and Grasmeijer* (2018); Changjiang River estuary, (*S Wu et al.*, 2016a)), including the PRE (*S Lin et al.*, 2021; *Y-H Wang et al.*, 2021b; *W Zhang et al.*, 2015a). The impact of SLR on estuarine dynamics was reviewed by *Khojasteh et al.* (2021), it was concluded that SLR affects a range of estuarine processes or/and parameters, including tidal parameters, mixing and circulation, salt water intrusion, stratification, and sediment dynamics.

The evolution of the PRE is characterized by active morphodynamical changes and continued rSLR. In light of the inherent complexity of the PRE, it becomes necessary to pose the following research question:

Q1: *How do human activities and climate changes impact the stratification of Pearl River Estuary?*

1.2 Mechanisms of ETM formation

The mechanisms of formation of ETM are complex. In general, convergence at the salt front of landward sediment flux by the gravitational circulation and seaward sediment flux by the river flow is considered a fundamental mechanism contributing to ETM formation (*Postma*, 1967). In most of estuaries, a spatially limited pool of resuspendable particles is present in the vicinity of the salt front (*Megina et al.*, 2023; *Sanford et al.*, 2001; *Xu et al.*, 2010). Tidal resuspension has been identified as a critical process in maintaining elevated SPM concentrations(*Sanford et al.*, 1991; *Shenliang et al.*, 2003). While tidal asymmetry also contributes to the ETM formation(*Burchard and Baumert*, 1998; *Q Yu et al.*, 2014). ETM formation is usually driven by one or a combination of the following drivers: 1 tidal asymmetry (tidal pumping), 2. Topographical trapping, 3. Convergence of current. The details of those driver and associated processes are outlined subsequently.

Tidal asymmetry in turbulent mixing due to tidal straining has been documented, with higher values of eddy viscosity occurring during the less stratified flood tide. As a result of this asymmetry, more sediment is resuspended during the flood phase of the tide resulting in up-estuary pumping of sediment in York River Estuary (*Scully and Friedrichs*, 2007). The upstream net transport of suspended sediment resulting from strong tidal asymmetry in stratification and flow field was also found in the Columbia River Estuary by *Jay and Musiak* (1994). *Geyer* (1993) show that the suppression of turbulence by density stratification tends to keep the particle near bed at the convergence zone. *Tidal asymmetry* refers to the distortion of tidal wave, which is defined as difference in the magnitude between maximum ebb and flood

velocities and/or difference in the duration of slack water. This distortion is a result of the interaction between tidal components and the geometry and bathymetry. In instances when the flood period unequal to the ebb period, it may generate residual sediment transport, if the period of water level rise is shorter than the period of water level fall, the tide is called flood-dominant and in the opposite case it is called ebb-dominant (*Z B Wang et al.*, 1999). The various factors that cause tidal asymmetry are not independent of one another. For example, *Jay and Musiak* (1994) describe the process of tidal velocity asymmetry in which the convective instability during the flood tide produces a bottom intensified velocity profile and convectively stable transport during the ebb yields increased shear and reduced near-bottom currents. This results with net upstream bottom currents, and because sediment concentrations increase near the bed, a net upstream transport of suspended material is generated.

Topographical trapping also plays a significant role in the formation of ETMs. A review paper by *Burchard et al.* (2018b) indicated that observations in numerous estuaries have found that ETMs are not necessarily associated with the limit of salinity or tidal propagation, but rather are spatially fixed and associated with bathymetric transition. Three simultaneous ETMs have been observed in the Columbia River estuary. The two landward ETMs are situated in proximity to the upstream limits of salinity intrusion in the two main channels and are predominantly sustained by internal tidal asymmetry. The more seaward of these ETMs, which are associated with topographic convergence, were documented by *Jay and Musiak* (1994). In San Francisco Bay, bottom topography controlling the location of ETMs in channels, especially sills in the channels. The location of ETMs is related to bottom topography because salinity stratification and gravitational circulation are enhanced seaward of sills (*Schoellhamer*, 2000). In a multi-ETM estuary, the PRE, the more seaward ETM is also fixed to the topography of the west channel (*Ma et al.*, 2024).

The lateral transport and trapping of SPM are inherently connected to longitudinal processes (*Burchard et al.*, 2018b). Examples of lateral trapping include: (1) Lateral depth variation resulting in lateral variations in bottom stress and lateral gradients in stratification, which in turn leads to the formation of a coarser bed in the deeper part of the channel and an accumulation of fines on the shoal. This phenomenon also serves to suppress the transport of materials between the channel and the shoal (*Geyer et al.*, 2001; *Ralston et al.*, 2012). (2) Differential advection of along-estuary salinity gradient, creating lateral salinity gradients that transport near-bed sediment out the channel towards to the shoal (*Kappenberg et al.*, 1995; *A Sottolichio et al.*, 2000; *Zhu et al.*, 2021). The trapping of sediment by lateral circulation affects the lateral

distribution of bed sediment and thus is fundamentally connected to the along-estuary SPM transport (*Burchard et al.*, 2018b).

River discharge is associated with gravitational circulation, in addition to the geographical configuration of estuaries. River discharge may be identified as a contributing factor in the seasonal variation of the ETM (*Y Yu et al.*, 2013; *M Zhang et al.*, 2014). The convergence of riverine flow and saltwater intrusion results in the formation of ETM, which is typically regarded as a consequence of tidal pumping (*Scully and Friedrichs*, 2007; *Q Yu et al.*, 2014). When the river discharge exhibits seasonal variation, the ETM assumes seasonal characteristics. In PRE, the suspended sediment concentration is enhanced and ETM is intensified during dry season with low riverine flow, whereas the center of the ETM moves upstream by a distance of 10 km during wet season with high riverine flow(*R Liu et al.*, 2016). In Changjiang River Estuary, the ETM was further upstream in dry seasons than wet seasons due to the decrease of river discharge (*Hua et al.*, 2020). In the upper Humber and Ouse Estuary, the monthly average runoff and tide were found to account for 88% of the variation in ETM locations. Following a period of high winter runoff, the ETM was observed to be situated downstream of the ETM in summer drought conditions, at a distance of approximately 50 km (*Uncles et al.*, 2006). The extent of the ETM is also influenced by river discharge, as evidenced by observations in the Elbe. During the winter time, the ETM zone is approximately twice as long (30 km) as it is during the summer (*Papenmeier et al.*, 2014).

The seasonal sediment load is dependent on the river discharge, and the effect of seasonal sediment load on ETM varies between rivers. The ETM occurs in the low salinity upper reaches of estuary. This phenomenon is primarily caused by local resuspension bed sediment, in which the effect of sediment load is largely limited (*Hesse et al.*, 2019; *Uncles et al.*, 1994; *Uncles and Stephens*, 2010; *Woodruff et al.*, 2001). In the study conducted by *Ma et al.* (2024), the riverine sediment components in the upstream ETMs were quantified. The results indicated that the sediment load in the ETMs of PRE consisted of approximately 10%–30% SPM, inclusive the effect of the seasonal fluctuations in sediment load.

It is noteworthy that the seasonal variation of ETM is also reflected in the seasonal variation of SPM settling velocity. Seasonal variation in settling velocity can drive variations in the location of the ETM and its trapping efficiency. *Sanford et al.* (2001) found that particles bypassed the ETM zone of Chesapeake during winter but were effectively trapped during the autumn; this was attributed to an order of magnitude decrease in the median settling velocity from 0.3 (winter) to 3 mm/s (autumn). This change may be attributed to biogenic alterations in the stickiness of

the packaging materials surrounding the aggregates (*Fettweis and Baeye*, 2015). The hindered settling due to high SPM concentration, larger than a few kg/m^3 (*Dankers and Winterwerp*, 2007), is ignored in this study.

The development of ETM is also influenced by *other factors*, including wave and wind conditions, which impact the estuarine circulation and increase the resuspension of sediment from the bed (*N Chen et al.*, 2018; *Kessarkar et al.*, 2009; *North et al.*, 2004). In the Seine Estuary, it is found that the suspended mass in the ETM caused by energetic wave conditions is three times higher that is caused by mean tides (*Grasso et al.*, 2018). *Christie et al.* (1999) reported that wave activity maintains elevated SSC over high water level. This suspended sediment was transported offshore during ebb tides in stormy conditions in the Humber Estuary. Wave effects in sediment transport can be significantly influenced by typhoon(*Y Chen et al.*, 2019), and morphological change (*Tönis et al.*, 2002). In the PRE, modeled SSC is elevated by 1.3~1.5 times with inclusion of wave-enhanced bottom shear stress compared to that without wave effect during a typhoon landfall (*Yun Yang et al.*, 2022b). As reported by *S Lin et al.* (2022), the narrowing of the PRE estuary due to land reclamation has resulted in a general increase in wave-induced bottom stress in the estuary leading an increase in the area of SSC greater than 100 mgL^{-1} by 183.4%.

The aforementioned drivers of ETM formation can lead to multiple ETMs within one estuary. Multiple ETMs were identified in many estuaries over the world, including York River (*J Lin and Kuo*, 2001), Delaware estuary (*Biggs et al.*, 1983), Cam-Nam Trieu estuary (*Duy Vinh et al.*, 2018), the Ems river (*de Jonge et al.*, 2014),the PRE (*Ma et al.*, 2024). The existence of multiple ETMs within an estuary can be attributed to a number of different factors. For instance, in York River, the upstream ETM was found to be in close vicinity to the head of salt intrusion, whereas the downstream ETM was typically situated in the transition zone between upstream well-mixed and downstream more stratified water columns. This suggests that the occurrence and location of downstream ETM are closely associated with the stratification patterns observed in the York River (*J Lin and Kuo*, 2001). Additionally, topographical trapping can facilitate independent ETM from the limits of salinity or tidal propagation (*Burchard et al.*, 2018a).

1.3 Fast-paced changes across estuaries

The ETM is the result of complex estuarine dynamics, and thus, is susceptible to alteration as a consequence of the modification of the estuary. Estuaries are of significant social and economic importance, yet they are vulnerable to human activities and climate change. The factors that shape the estuarine hydrodynamic and sediment dynamics are constantly

undergoing modification due to shifting natural forces and anthropogenic impact. Common pressures from human activities include alterations to land use and hydrology, land reclamation, sand mining, harbor dredging, pollution and eutrophication, and overexploitation such as overfishing, all in the context of climate change (*Cloern et al.*, 2016). The multitude of anthropogenic and climate change impacts can be summarized into several categories in the future. These are as follows: 1. Morphological changes due to land reclamation and dredging. 2. Variation of riverine sediment load due to dam construction. 3. Relative sea level rise due to climate change and human activities. 4 shifting of wind conditions due to climate change. Details of these factors are presented below.

Morphological changes resulting from land reclamation, sand mining, dredging, and other activities were documented in numerous estuaries. **Land reclamation** in an estuary can change an estuary from a sink to a source, such as in the Yalu River Estuary, where the expansion of an inner island in the Yalu River Estuary by approximately 80 km² was observed to result in a reduction in landward sediment flux, which could potentially lead to the estuary becoming a sediment source rather than a sink if further land reclamation occurs in the future (*Cheng et al.*, 2020), or vice versa, as in Jiaozhou Bay, a potential trend of transition from erosion to siltation as a result of loss of tidal flats due to land reclamation has been reported by *Gao et al.* (2018). **Dredging** in the estuary to serve navigation has a profound effect on the distribution of SPM in the estuary. Channel deepening combined with land reclamation can often lead to a combination of tidal amplification, increased estuarine circulation, and increased flood dominance of tidal asymmetry (*Winterwerp*, 2011), which increases up-estuary sediment transport. As a result of increased up-estuary sediment transport, SPM concentrations have increased significantly in most estuarine systems. Some examples are the Ems (*Pein et al.*, 2014), the Elbe(*M Li et al.*, 2014), and the Seine estuary (*Grasso and Le Hir*, 2019).

The sediment load is dependent upon the river discharge, and is also modified by the presence of artificial constructions (*Walling*, 2008). Globally, an estimated 50% of the gross sediment flux has been trapped in reservoirs (*Nilsson et al.*, 2005). A marked reduction in the volume and concentration of sediment transported in runoff following the construction of dams was observed to result in a corresponding decline in ETM levels. Such observations were made in the Changjiang Estuary(*Yunping Yang et al.*, 2014), the PRE (*S Zhang et al.*, 2008), and the Danube Estuary (*Panin and Jipa*, 2002).

Most of the examples of changes in estuary introduced above are related to specific anthropogenic impacts. However, climate change is also a pervasive pressure affecting the

estuarine systems. Changes in estuary by anthropogenic impacts could, for example, be superimposed on changes associated with variation of sea level rise and/or the Southern Oscillation Index, which would like to reduce the clarity of the signal generated by human impact (*Walling*, 2008).

Relative sea level rise (rSLR) can be attributed to a combination of factors, including sea level rise due to climate change and vertical land motion. According to the IPCC report (*Kikstra et al.*, 2022), on the global scale, mean sea level change over the 20th century, which is dominated by glacier (52%) and Greenland Ice Sheet mass loss (29%) and the effect of ocean thermal expansion (32%), with a negative contribution from the land water storage (LWS) changes (-14%). The projections by SROCC (Special Report on Ocean and Cryosphere in a Changing Climate, *Holland et al.* (2022)), the global mean sea level will rise between 0.4 (0.26-0.56, likely range) m (RCP2.6) and 0.81 (0.58-1.07m, likely range) m (RCP 8.5) by 2100 relative to 1995-2014. In coastal regions, *Bindoff and McDougall* (2000) reached the statistically significant conclusion that the majority of these regions will experience changes in tidal amplitudes through the 21st century as a result of rSLR (*Haigh et al.*, 2020). Tidal dynamics, as a primary driver of estuarine sediment dynamics has been identified as a crucial factor influenced by rSLR, as evidenced by studies. The rSLR can shift the tidal wave asymmetry, which is significant for sediment dynamics and net transport (*Passeri et al.*, 2015), in the Tagus estuary (*Valentim et al.*, 2013), in the Tamar estuary (*Palmer et al.*, 2019), in the Gironde estuary (*van Maanen and Sottolichio*, 2018).

Regional wind situation responses to climate change may also influence the dynamics of estuarine sedimentation. Different trends in wind speed and direction may emerge in the future (*Kulkarni et al.*, 2013). For example, weakened summer south Asian monsoon circulation results in overall suppression of summer precipitation (*Swapna et al.*, 2017). A pronounced increase in the mean wind speed by 0.5 m/s in the northern part of the Baltic Sea and a notable decline in the Mediterranean by 2.0 m/s by 2070 to 2099 have been projected (*Walter et al.*, 2006). A study by *De Winter et al.* (2013) suggested a shift in wind direction, with more extreme wind from the west, in the North Sea during 2050-2100. Even a small change in winds may exert a remarkable influence on sediment transport in coastal environments by altering the residual circulation and waves (*Barnard et al.*, 2013; *Green and Coco*, 2014; *King et al.*, 2019). As a consequence of climate change, the regional frequency of extreme events variation has been documented by *Wigley* (2009), in which storm events exert a significant influence on coastal sediment transport. In German Wadden Sea, the typical ebb-dominance occurring

during fair-weather conditions was temporarily neutralized and even reversed to a flood-dominated situation (*Bartholomä et al.*, 2009). In the Changjiang Estuary, the winter storm resulted in a notable increase in wind and wave activity, leading to a substantial rise in the SPM concentration to 3 g/L. This is a significant deviation from the typical range, exceeding the concentration by more than threefold (*Tang et al.*, 2019).

1.4 Motivation

The formation of ETM is the result of complex estuarine dynamics, which are highly variable in time and space and differ substantially among estuaries. Furthermore, human activities and climate change have introduced increasing environmental pressures to the estuarine system. These pressures cause coastal/estuarine erosion and subsidence, flooding, freshwater shortage, pollution, and loss of biodiversity (*Xiong et al.*, 2024). For example, the extent and intensity of estuarine hypoxia are reported to be increasing in the PRE (*X Li et al.*, 2020). Studies on the summertime hypoxia of PRE demonstrated that particle-attached bacteria are more prevalent than free-living bacteria (*J-L Li et al.*, 2018a; *Y Liu et al.*, 2020; *Y Wang et al.*, 2020). It is therefore important to investigate the role of particle resuspension in the dissolved oxygen budget in order to gain a more accurate understanding of the estuarine hypoxia. Thus, particle resuspension has gain growing interest, given it is highly associated with oxygen dynamic (*Cui et al.*, 2022). In another example, the estuary turbidity controls the phytoplankton biomass and productivity significantly. The drastic decline (~70%) in sediment load from the Changjiang River reduced turbidity in the Changjiang Estuary and contribute to the increase frequency of harmful algal blooms in the buoyant discharge plume, the Chl *a* concentration in 2002-2003 was at least twice as high as that in the 1980s (*B Wang et al.*, 2016). Therefore, understanding the estuarine sediment dynamic, especially the formation and maintenance of the ETM in estuaries is essential for dealing with the estuary environment problems and preparing for the potential impacts of future changes.

The spatial and temporal variations of ETMs in the PRE are the result of a complex interplay of processes, including those involved in the formation and evolution of ETM in the PRE. Previous studies have concentrated on the formation mechanism of a single ETM (described in Chapter 2). However, in a complex, large, stratified estuary, multiple ETMs exist for various reasons, and the interconnection between these ETMs is rarely investigated, and the role of stratification in those processes remains uncertain. It is crucial to investigate the ETMs as a holistic system, based on a well understanding of hydrodynamic. Furthermore, human activities and climate change have been shown to have a significant impact on hydrodynamic and

sediment dynamics. Consequently, it is important to investigate the influence of human activities and climate change on ETM formation and evolution. Given the complex hydrodynamic environment, coupled with the effects of active human activities and climate change in the PRE, research focusing on the prototypical Pearl River Estuary (PRE) is conducted in this thesis. In order to gain an understanding of the sediment dynamic response to morphological change and sea level rise, it is first necessary to investigate the formation mechanism of ETM in the PRE. Further, It would be an oversight to disregard the interconnectivity between ETMs within the estuary, which often exhibits multiple ETMs, leading to the second and third research question:

Q2: what is the formation of mechanism of ETM in the PRE?

Q3: Is there interconnection between ETMs? If so, what determines the pathway of SPM between ETMs in estuaries with multiple ETMs?

As outlined in section 1.3, estuaries exhibit clear evidence of morphological change and rSLR resulting from human activities and climate change. Yet, a holistic approach to examining the role of estuarine evolution in sediment dynamics has not been undertaken. In view of this, the present research was designed with the specific aim of answering the following question:

Q4: How is the ETM evolving, from its formative history to its projected future, in the PRE?

This thesis investigates the formation and evolution of ETM as a holistic system. Model simulations are employed to illustrate the variation of stratification and formation mechanism of ETMs and examine the impact of human activity and climate change-related factors on the stratification and evolution of ETMs. This thesis can serve as a reference for the sustainable management of sediments in estuaries.

Balancing the need for development with the need to protect the estuary's natural resources is a major challenge and will require careful planning and management, and accurate forecasting to ensure that the estuary remains a healthy and sustainable ecosystem. Future solutions should be based on the new pattern of changes in the PRE, focusing on estuary evolution and management of water quality. However, very little research has been conducted on how the estuary has responded and will respond to changes. Key scientific issues related to spatiotemporal changes in estuaries driven by intense human activities are therefore investigated in this thesis.

This thesis is structured as follows: Chapter 2 gives an account of current knowledge and background information on the PRE. Chapter 3 summarizes the results of the studies conducted

in the context of this dissertation, and Chapter 4 discusses the results in the context of estuarine management and gives an outlook toward directions of future research.

2. Characterizing the Pearl River Estuary

2.1 Historical evolution of PRE

The Pearl River Delta (PRD), situated in the south of China, hosts several megacities (Guangzhou, Shenzhen and Hong Kong) with a total population of 83.01 million by 2020 (*Q Zhang et al.*, 2021b) (Figure 1). The Pearl River is one of the world's 25th largest rivers with an average annual discharge of 336×10^9 m^3 and an annual mean sediment load of approximately 30 million tons, with over 90% discharged during the wet season in summer. Approximately 80% of the deposited sediment is found within the estuary (*Wai et al.*, 2004). The Pearl River Estuary is fed by eight tributaries (Humen, Jiaomen, Hongqili, Hengmen, Modaomen, Jitimen, Hutiaomen, and Yamen). The estuary's topography is divided into three sections by two channels (east channel and west channel): the east shoal, the middle shoal, and the west shoal. The west shoal is directly connected to the four tributaries (Humen, Jiaomen, Hongqili, Hengmen), which together receive 65% of the pearl river discharge and 56.8% of the Pearl River sediment load annually(*G Zhang et al.*, 2019). The estuary is host to several islands, though most of these are located in the outer reaches of the estuary. Tides are mainly semi-diurnal (M2) and diurnal (K1) inside the PRE, the average tidal range in the PRE increases gradually from the offshore region to the estuary, reaching a maximum at the head of the PRE (Humen) due to the bell-shape of estuary(*Mao et al.*, 2004). The interaction between river discharge and tides produces a seasonal and tidal variation in the stratification of the estuary(*Zu and Gan*, 2015). Beside the tidal forcing and buoyancy from river discharge, the estuarine circulation is also forced by the winds, and it interacts with the coastal current. Under the impact of East Asian Monsoonal circulation, about 80% of the rainfall comes in the period of April-September(*Weng*, 2007). During the East Asia summer monsoon, coastal upwelling with the northeastward along-shore currents is formed along the coast off PRE (*Ou et al.*, 2009). The seasonal circulation and associated forcing in the PRE and coastal current can be summarized based on the research conducted by (*Weng*, 2007; *Wong et al.*, 2003; *Zu and Gan*, 2015), as illustrated in Figure 1.

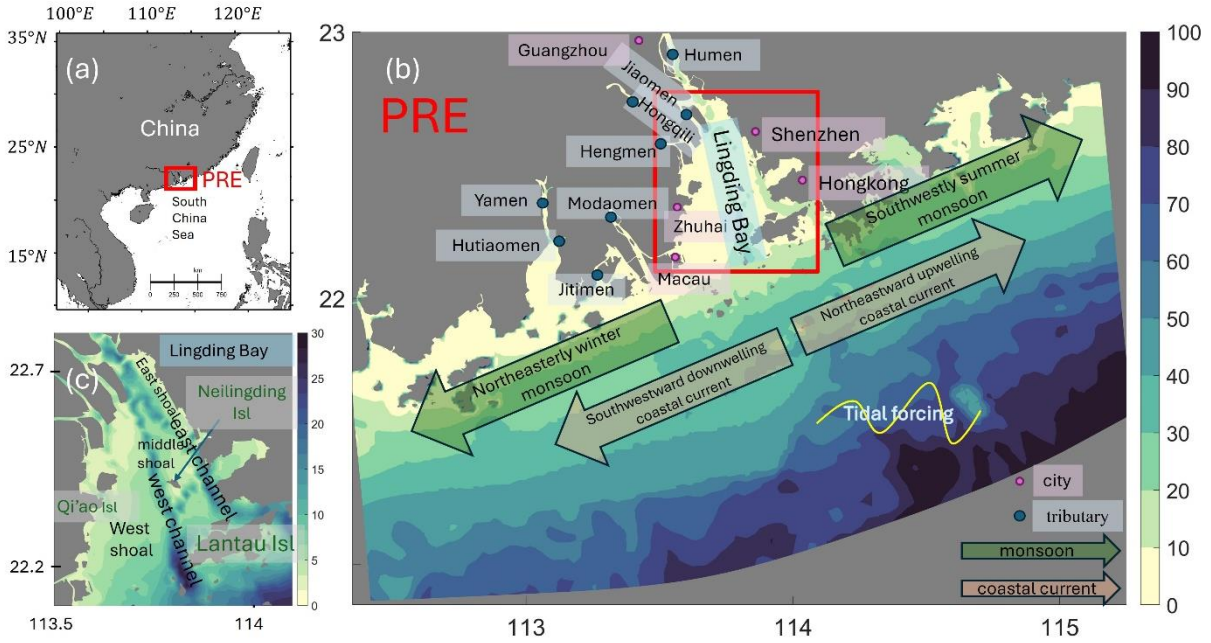

Figure 1 The location, the topographical characteristics, the monsoon and coastal current of PRE. The red box in (a)indicates the location of PRE. The red box in (b) indicates the location of Lingding Bay. (depth unit: m).

Before the 1980s, the evolution of the PRE was mainly dominated by natural processes because human activities based on the agricultural industry had a little impact on the drainage basin and estuary. However, with the implementation of the national reform and opening policy in the 1980s, the population (increased from approximately 10 million in 1978 to 83 million by 2020) and economy of the Pearl River Basin began to develop rapidly(*Weng*, 2007). The rapid urbanization is very distinct when comparing satellite images (USGS) from 1973 and today (Figure 2d), in many areas vegetation has been replaced by urbanized area.

Human activities, including dam construction in the river basin, land reclamation, channel dredging, and sand extraction in the estuary, have greatly accelerated in the Pearl River Basin and the PRE. Consequently, the sediment load from the river and morphological evolution of the estuary have been severely disturbed. The sediment load rate was 71.9 million tons/yr in the 1950s, dropping to 23.7 million tons/yr in the 2010s. It is noteworthy that the water discharge during the past seven decades fluctuated narrowly between 260 and 300 billion m^3/yr, a trend that is clearly different from the one of the sediment load (*Wei et al.*, 2020). The average advancing rate of coastline of PRE to the sea from 1972 to 2017 reached approximately 64.8m/year (*Wei et al.*, 2021). The subaqueous decreased by $\sim 170 km^2$ from 1955 to 2010, and the water volume of PRE decreased by $615 \times 10^6 m^3$ (*ZY Wu et al.*, 2016b). The bathymetric data show that the main change occurred in the west coast move seaward, and the deepening of channels in Lingding Bay (Figure 2 a, c). The combined influences of channel dredging, sand mining, and sediment load reduction caused by dam construction have contributed to those

changes. A negative liner regression relationship between annual sediment load and cumulative storage capacity was described by *C Wu et al.* (2019). The number of dam construction and river discharge and sediment load show in the Figure 2.

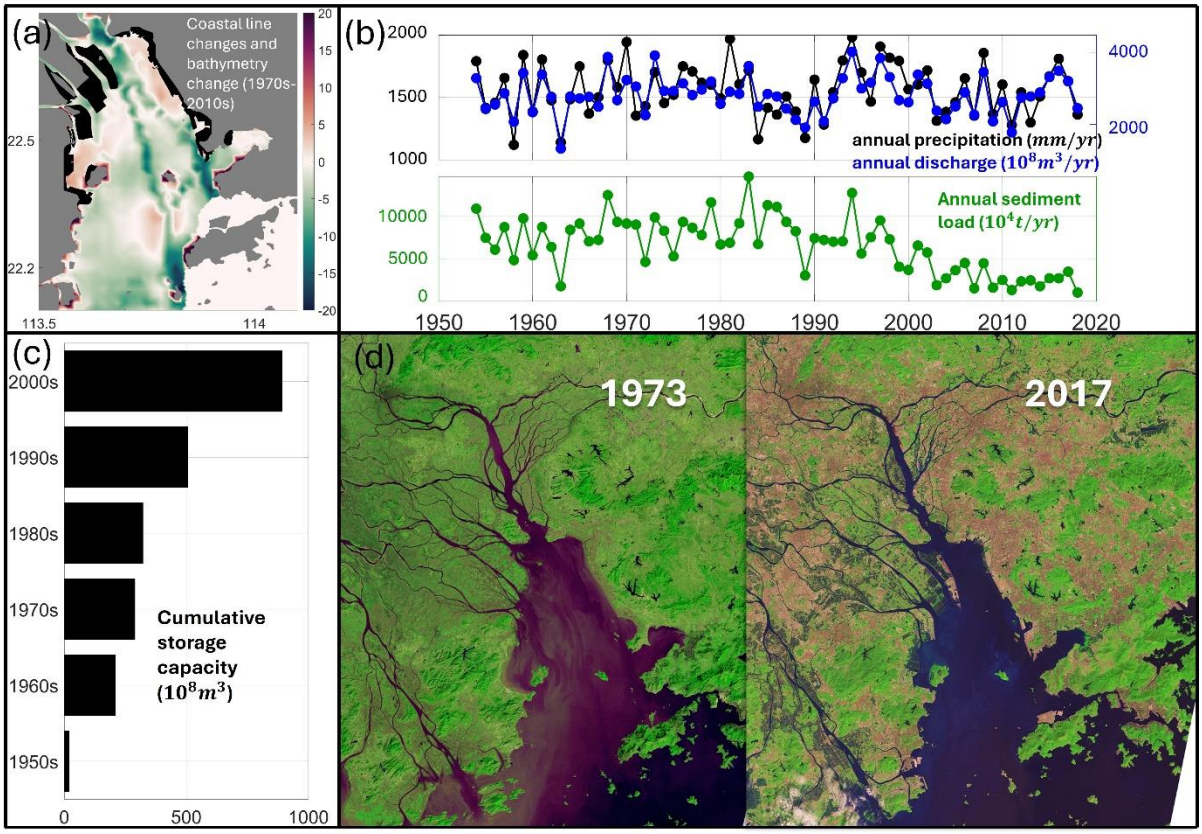

Figure 2 Historical development of PRE. (a) Morphological change in the Lingding Bay from 1970s to 2010s. Black polygons refer to the land reclaimed during this period. Negative values (in green color) indicate a deepening of the bathymetry in 2010s compared to 1970s, vice versa. (b)Time series of annual basin-wide precipitation (black solid line) in the Pearl River basin, and water discharge (blue solid line) and sediment load (green solid line) into the sea from 19854 to2018. The data modified from Wei et al. (2020). (c) Temporal changes in the cumulative storage capacity of major dams in the Pearl River basin. The data modified from F Liu et al. (2018). (d) Landsat images of PRE in 1973 and 2017, image source: USGS (U.S. Geological Survey).

Since the PRE is a hotspot for human activities, it is important to explore the combined effects of climatic and human stressors in the PRE as a typical coastal system. For example, the relative rise in sea level caused by climate change and land subsidence caused by over-extraction of groundwater pose serious threats (flooding, saltwater intrusion) to coastal cities such as Guangzhou in China (*Du et al.*, 2020), Shanghai in China (*Yun Zhang et al.*, 2015b), and Semarang in Indonesia(*Abidin et al.*, 2013). Therefore, whether studying the development of ETM or exploring appropriate sediment management methods, the effects of climate change should be taken into account. In the PRE, the most notable consequences of climate change are sea level rise (*Hong et al.*, 2020), ocean warming and precipitation (*Zeng et al.*, 2019), and shifts in wind condition (*Hong et al.*, 2022). Details are given below.

Tidal gauge data analysis has shown that the rate of sea level rise in the Hongkong coastal area was 31 mm/decade from 1954 to 2023 (Figure 3 a), and this rate is increasing, under the intermediate (SSP2-4.5) and very high (SSP5-8.5) greenhouse gas emissions scenarios, the annual mean sea level in Hong Kong in 2100 is likely to rise by 0.37-0.82m and 0.57-1.08 respectively (Figure 3 b). Figure 3 a illustrates a notable surge in sea level during the 1990s. This phenomenon may be attributed to land subsidence, a documented occurrence in numerous PRD studies by satellite and on-site observations (*Ren et al.*, 2024; *H Wang et al.*, 2012; *Jun Wang et al.*, 2021a; *Ziyin Wu et al.*, 2018). In study of *Ziyin Wu et al.* (2018), a land subsidence of approximately 250mm was assumed for the 1850-2015 period in order to account for geomorphological changes in PRD. InSAR data from 2007 to 2010 show that the average subsidence within 500m of the coast is about $2.5\ mm/yr$, and maximum is up to $6\ mm/yr$ (*H Wang et al.*, 2012). The recently published study, which is based on InSAR data spanning the period from 2016 to 2021, by *Ren et al.* (2024) has reached the conclusion that the coastal area of PRE is experiencing prolonged and intense subsidence. The relative sea level rise, including land subsidence, throughout the PRD region is therefore of critical importance for the conduct of risk assessments, given the current global rate of sea level rise of approximately $2-3mm/yr$.

The annual mean sea surface temperature recorded at Hong Kong Observatory showed an increasing trend (rate: $0.18℃/decade$) during 1975-2023. Under the intermediate (SSP2-4.5) and very high (SSP5-8.5) greenhouse gas emissions scenarios, the annual mean temperature in Hong Kong by 2100 is projected to increase by approximately $2.0℃$ and $3.6℃$ respectively, in comparison to the average temperature over the period 1995-2014; the annual rainfall in Hong Kong by 2100 is projected to increase by about 7.0% and 9.0% respectively, compared to the average by 1995-2014 (*J-Y Lee et al.*, 2021). As a consequence of the weakening of the East Asian monsoon, there have been notable alterations in the wind conditions prevailing in PRE. Based on the monthly mean wind data recorded at Macau airport and ERA5 data, (*Hong et al.*, 2022) concluded that summer wind direction in the PRE shift anticlockwise at a rate of $-0.36°/yr$, reduction rate on wind speed is $-0.025m/s$ over the period 1979-2020, the mean wind direction in July shift and is predicted as $142.1°$ by 2100. The shift of wind conditions will exert a significant impact on the estuarine circulation of the PRE.

2.2 Current issues and solution approaches

In response to the current pressures exerted by human activities and climate change, local administrations have put forth a series of measures. For example, engineering measures (such

as sluice construction) and non-engineering measures (such as reservoir operation and administrative regulation) are used for prevention of saltwater intrusion (*B Liu et al.*, 2019), floods, and storm surges (*Chan et al.*, 2021). In the meanwhile, under the combined influence of human activities and global climate change, riverine ecosystems and environments have undergone significant transformations over the past half century (*Giosan et al.*, 2014). In the ecological monitoring area of the PRE, there has been an increase in nitrogen-to-phosphorus-ratio (N/P), hypoxia, acidification, and alterations in biodiversity (*Dai et al.*, 2023; *Niu et al.*, 2021). These are characterized by unstable planktonic community structures and frequent occurrences of harmful algal blooms (*Bi et al.*, 2022). In order to achieve an environment-friendly sustainable development situation, a wide range of industries have relocated from the PRD metropolitan area to the neighboring prefectures or other inland provinces. The regulation of sand mining and dredging in estuarine bays and rivers is strictly implemented in order to prevent the resuspension of contaminants from sediments (*Miu*, 2005; *Xiong et al.*, 2024).

The current suite of management measures exhibits inconsistencies. For instance, the use of interconnected enclosures and sluices, in combination with reservoirs, has proven effective in the prevention of upstream flood disasters (*Xiong et al.*, 2020). However, the deployment of these structures has the effect of impeding the natural exchange of water and material (sediments) between the inner river and the outer distributaries or estuary. This, in turn, has the consequence of undermining the hydrodynamic conditions of the estuary and its capacity for self-purification with regards to water pollution, affecting water quality and leading to the occurrence of environmental issues in the estuary (*Chakraborty*, 2021).

2.3 ETM studies in PRE

The sequence of PRE management was proposed in *Xiong et al.* (2024) as follows: "estuary change mechanism and trends—management targets—technology research and development—application demonstration." In order to establish a more effective management target and reduce inconsistencies, it is essential to gain a comprehensive understanding of the estuary change mechanism and trends.

The estuarine hydrodynamic and sedimentary dynamics represent the physical setting of the estuarine system and serve as a primary factor in understanding ongoing changes within the PRE. Sediment serves as a carrier of a variety of pollutants, marine protists, and bacterial communities(*R Li et al.*, 2018b; *Mai et al.*, 2018; *Sun et al.*, 2011). Furthermore, water turbidity has direct impacts on phytoplankton growth. A strong correlation between SPM and Chl a was identified in the PRE (*G Wang et al.*, 2010; *Jinkun Yang and Chen*, 2007). Therefore, taking

PRE as example, this thesis analyzes and studies the sediment dynamic and evolution of ETM based on a solid understanding of the hydrodynamic processes within the estuary. The PRE exhibits the typical topographic and dynamic settling, and its complexity renders it a prototypical case study in sedimentary dynamics research.

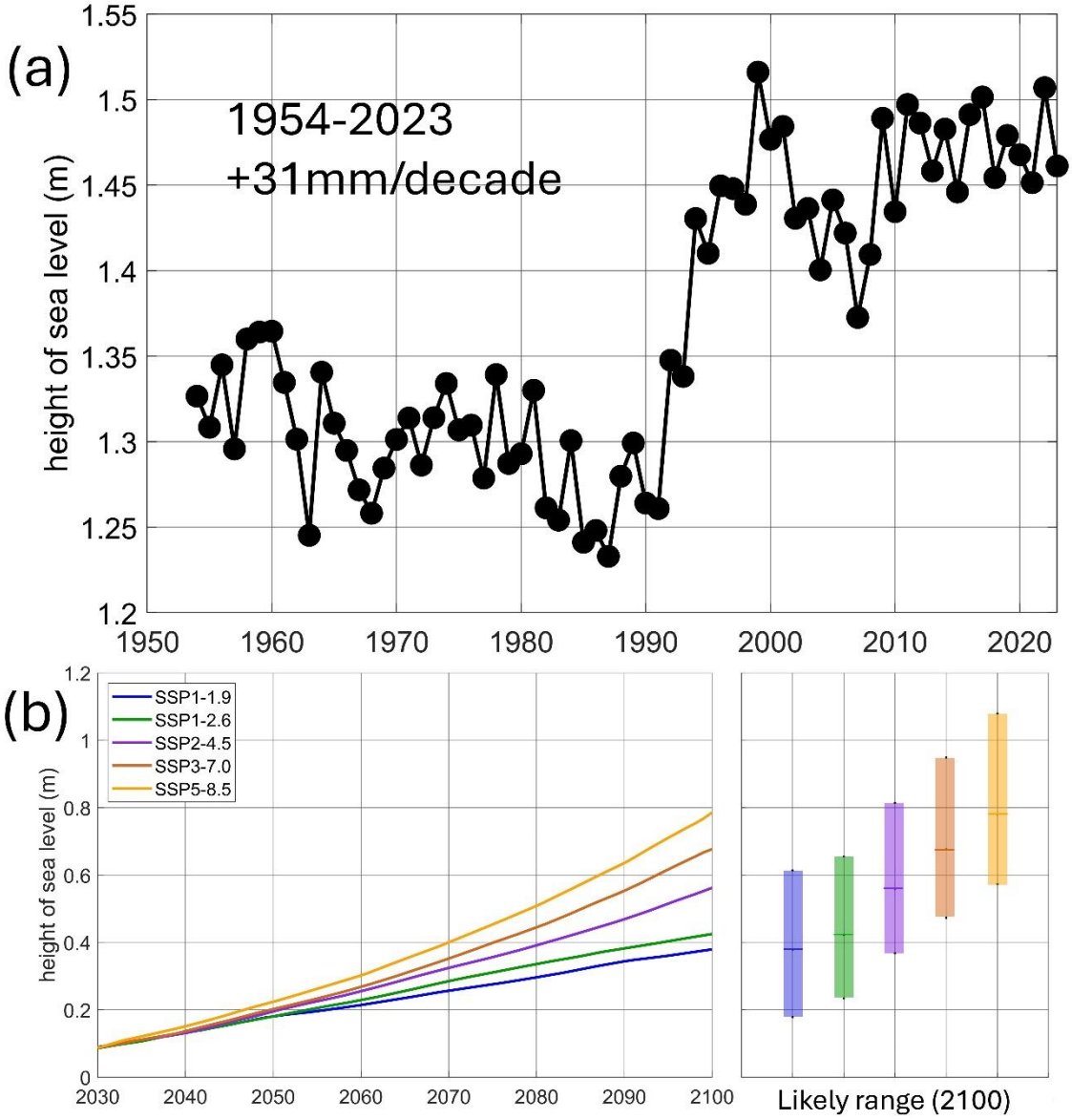

Figure 3 Sea level situations. (a) Annual mean sea level at Hong Kong from 1954 to 2023, data source: Hong Kong Observatory. (b) Projected change in annual mean sea level in Hong Kong relative to the average of 1995-2014. Colored solid curves show median projections under 5 emissions scenarios. Colored bars indicate likely ranges in 2100 under 5 emissions scenarios. Image modified from Hong Kong Observatory. Data source: IPCC AR6.

In the PRE, it has been reported that the formation of ETM is influenced by a combined effect of tides, river discharge, and topography, wherein sediment resuspension is the dominant factor influencing the variation of ETM (*H Li et al.*, 2022; *R Liu et al.*, 2016; *Ma et al.*, 2024; *Wai et al.*, 2004). As evidenced by existing observations, multiple ETMs are present in both the upper and lower regions of the PRE. The presence of ETMs in the upper estuary was observed

between Qi'ao Island and Neilingding Island. The intensity and extent of the ETMs were found to be weaker during the wet season than during the dry season, which can be attributed to variations in stratification. Additionally, the center of the ETMs was observed to move upstream in conjunction with the movement of the salt wedge by a distance of approximately 10 km during the wet season (*R Liu et al.*, 2016). Based on analysis of observation data, *Wai et al.* (2004) proposed that gravitational circulation and tidal pumping are the principal formation mechanisms of the ETMs in PRE. In the lower estuary, an ETM was observed close to the west channel, situated to the west of Lantau Island, during the wet season (*Cui et al.*, 2022). The occurrence of elevated SPM concentrations of ETM is primarily observed in the bottom water, which is a consequence of the strong stratification of salinity distribution during the wet season. During the dry season, when there is a weak stratification, the high SPM concentration is observed in the entire water column and at the same location. The occurrence of ETM is a result of tidal pumping, as evidenced by [Liu, et al. 2016], However, the role of stratification in this process remains unclear, particularly when the examination is extended to the entire estuary.

A time series investigation of total suspended soil (TSS) concentration during 1987-2015 based on remote sensing data in PRE revealed a significant decreasing trend in TSS concentrations in shoals and channels of PRE, primarily due to the construction of the dam. The average annual TSS concentration decreased by 5.7-10.1 mg/l in the wet season from 1988 to 2015 (*Chongyang Wang et al.*, 2018). By employing long-term hydrographic survey data, *Jiangping; Yang and Liu* (2015) demonstrate that a northeast-southwest large turbidity zone has undergone a process of evolution into multiple independent ETMs, as a consequence of morphological changes that have occurred since the 1970s to the 2010s. *Jiaxi Wang and Hong* (2021) examined the correlation between water turbidity and various factors including sediment load, wind speed, tidal range, and sea level. Their analysis highlighted that SLR could lead to both longitudinal and lateral landward retreat of ETMs, directly contributing to the decline of water turbidity.

3. Synthesis: Hydrodynamics and sediment dynamics of the Pearl River Estuary

This chapter summarizes the research findings on the aforementioned questions (*Q1, Q2, Q3,* and *Q4*). This chapter illustrates the hydrodynamic processes through an examination of the variation in stratification in 3.1. The formation of ETMs as a consequence of hydrodynamic and sediment dynamics is described in sections 3.2 and 3.3. Section 3.2 is dedicated to an

analysis of the formation mechanisms of ETMs, while Section 3.3 presents an investigation of the impact of human activities and climate change on these ETMs.

3.1 Hydrodynamics: variation of stratification

The essence of this study is to quantify each of the influencing factors in order to ascertain the dominant factors under different conditions and the interactions between the factors, and in order to make sure that sediment dynamic model is reliable. For this purpose, the study I[3] in this thesis presents a series of hydrodynamic simulations based on varying morphologies and sea levels of the PRE. A high-resolution 3-D hydrodynamic model was used to investigate the impact of mainly human-induced morphological change (from 1970s till 2010s) and climate-induced sea level rise (from 1970s till 2050s) on the stratification in the PRE. The answers of *Q1* are detailed study I:

1) Morphological change in the Lingding Bay (the main estuary of the PRE) from 1970s to 2010s results in a bay-scale enhancement of stratification by up to four times, with maximum enhancement (up to seven times) at the western shoal of the bay.
2) Stratification in the PRE becomes more sensitive to tidal and river runoff impact after the morphological change. The variation is greatly amplified by the spring-neap tidal cycle. The maximum enhancement in stratification occurs in the transition period from neap to spring tides due to the increase of advection of salinity variance.
3) The relationship between depth changes and salt fluxes is nonlinear and varies among different morphological units. In the PRE, the eastern channel and the western shoal experience the greatest enhancement in both strength and stability of stratification caused by the morphological change.
4) Compared to an overwhelming impact of human-induced morphological change in the past few decades, future change of stratification driven by sea level rise would be further strengthened but to a much less extent. The maximum enhancement associated with sea level rise occurs in spring tides due to the increased negative straining.

The results suggest a highly amplified and irreversible impact of human-induced morphological change on estuarine environments in terms of stratification, which should be taken into account in future planning of estuaries. The results of our research might have potential implications for the estuarine management, in particular, human intervention such as the planning of land

[3] See appendix A: Ma, M., Zhang, W., Chen, W., Deng, J. and Schrum, C., 2023. Impacts of morphological change and sea-level rise on stratification in the Pearl River Estuary. *Frontiers in Marine Science*, *10*, p.1072080. DOI: 10.3389/fmars.2023.1072080

reclamation or sand mining in Lingding Bay, etc. As the human intervention is the main driving factor of variations of the hydrodynamic environment in PRE.

3.2 Sediment dynamics: formation and dynamics of ETMs

The influence of human activities and climate change on hydrodynamics of the PRE are well investigated by *Ma et al.* (2023).

To answer the *Q2* and *Q3*, in study II[4], a sediment dynamics model was constructed based on the hydrodynamics model developed in study I inorder to explain ETM formation in the PRE. In summary, the ETM is the result of a combination of gravitational circulation and tidal pumping, with additional contributions from topographic trapping and wave effects. Resuspended sediment represents the primary component of the ETM. The concentration of SPM in the ETM zone can be several or more than tenfold higher than in other areas within an estuary, with a considerable quantity of SPM being retained within the ETM zone.

Three sediment classes are applied in the model to represent clay, silt and sand. The classification of sediment is further distinguished by the addition of the labels "riverine sediment" and "resuspended sediment," which serve to differentiate between the sources of SPM. The wave module is active in discussing the impact of waves on sediment dynamics. This study explores the flocculation effect on sediment dynamics based on the flocculation module developed by *P Arlinghaus et al.* (2022). Based on the simulation results that are confirmed by observation, the relative contribution of specific physical mechanisms for the formation of the ETMs, the temporal and spatial dynamics of the ETMs as well as their interconnections were investigated. The following main conclusions are drawn from the study:

1) Three ETMs exist in the Lingding Bay of the PRE, and they are formed by different physical mechanisms. The two upstream ETMs (TM_shoalw and TM_shoalm) situated on the shoals are a result of convergence of residual flow and sediment transport associated with tidal pumping. The downstream ETM located in the west channel (TM_channel) is formed mainly by topographical trapping.
2) All three ETMs exhibit distinct seasonal and spatial variations. Advection and tidal pumping are the main processes mediating the sediment flux of the ETMs. These factors are largely influenced by river runoff and stratification dynamics. The TM_shoalw

[4] See appendix B. Ma, M., Porz, L., Schrum, C. and Zhang, W., 2024. Physical mechanisms, dynamics and interconnections of multiple estuarine turbidity maximum in the Pearl River estuary. Frontiers in Marine Science, 11, p.1385382. DOI: 10.3389/fmars.2024.1385382.

exhibits spatial extension in wet seasons and shrinks in dry seasons, whereas TM_channel and TM_shoalm show an opposite pattern.

3) The ETMs are interconnected through sediment exchange. In the wet season, a 'TM_channel-TM_shoalm-TM_shoalw' sediment transport pathway across the three ETMs and a 'TM_channel-TM_shoalw' pathway between two ETMs are prominent. In the dry season, these transport pathways become less stringent, and sediment exchange between TM_channel and TM_shoalm becomes more active.
4) Discussion of the flocculation effect and the wave effect. The comparable distribution pattern of ETMs between simulations with and without flocculation in the PRE indicates that flocculation influences SSC in the ETMs, yet it is not the primary mechanism responsible for the formation of ETMs. A notable rise in SSC can be attributed to the wave effect within the estuary. In the simulations with and without the wave effect, the core of the three ETMs remained unaltered.

3.3 Historical development and future scenarios: evolution of ETMs

The evolution of the coast is the result of morphodynamic processes that occur in response to changes in external conditions. Coastal morphodynamics can be defined as the 'mutual adjustment of topography and fluid dynamics involving sediment transport' (*Wright and Thom*, 1977). However, human impacts upon coastal zones have increased dramatically through the last half of twentieth century. This is partly driven by increasing population pressure and utilization of coastal regions, and by the ongoing sea level rise. The impacts of these changes are acutely felt in estuarine areas, underscoring the urgent need for a comprehensive examination of the intricate issues inherent to estuary management.

The answer to *Q4* is addressed in study III[5]. This study examines the impact of morphological changes and rSLR on ETMs in PRE. The morphological changes and rSLR resulting from climate change and human activities were identified as the principal driving forces in the evolutionary development of PRE. From the 1970s to the 2010s, the Pearl River estuary experienced significant alterations in its morphological characteristics in conjunction with the economic growth and development of the region. These changes included a narrowing of the estuary due to land reclamation from the sea and an increase in the depth of the channel resulting

[5] See appendix C. Ma, M., Zhang, W., Porz, L., and Schrum, C., 2024. Evolution of Estuarine Turbidity Maximum in the Pearl River Estuary: historical development and future scenarios. (to be submitted)

from sand dredging and other human activities. In order to ensure the sustainable development of the PRE, large-scale reclamation and sand dredging are prohibited. Consequently, it can be assumed that the primary factor influencing the future development of the Pearl River Estuary is the rSLR. The rSLR between the 2010s and 2100s was determined by employing a methodology that integrated the findings of the IPCC report with the insights gleaned from recent observational data, taking into account the impacts of climatic sea level rise and land subsidence. The rSLR will result in a notable change in the water depth of the Pearl River Estuary.

In this study, I set up 13 simulations (8 simulations for the evolution of PRE, 2 simulations for the wind shifting effect, and 3 simualtions for the wave effect) to investigate the response of ETMs to the aforementioned factors in the PRE.

1. An ETM with a relatively large spatial extent between the river mouth of Humen and the Qi'ao island (>30 km in length) existed in 1970s according to both observation and our model results. This ETM evolved into several locally confined but interconnected ETMs in 2010s. Human-induced morphological change mainly associated with land reclamation and deepening of bathymetry by channel dredging and sand mining is the main driver behind such change.
2. Sediment composition in the estuarine bed has also been altered significantly during the past decades. Clay content has largely been depleted since 1970s and the present-day estuarine bed is dominated by silts. The SSC in the PRE is enhanced by a change from clay-dominance to silt-dominance in the estuarine bed, sustaining the multiple ETMs. The most significant change occurs in the channel, where the ETM becomes not only larger but also persistent throughout the year.
3. A remarkable reduction in riverine sediment load from 1970s to 2010s leads to a notable decrease in the spatial extent of ETMs in the wet season. However, it has minor effect on the dynamics of ETMs in the dry season. Our results also show that the PRE has become increasingly starved in SPM along with the morphological change and this trend will likely remain with an accelerated rSLR.
4. The rSLR during the past decades leads to a mild reduction of the spatial extent of the ETMs from 1970s to 2010s. In the forthcoming decades, an accelerated rSLR will likely result in a substantial reduction of SSC in the PRE, particularly on the shoals, with a maximum reduction by up to ~ 3 times larger than the impact of a rSLR following the

same rate in the past decades and thereby greatly reduce the spatial extent of ETMs in the PRE.

5. A gradual shift in the mean wind direction and reduction in wind speed in summer during the past decades have a minor influence on ETMs when compared to the effect of morphological change. However, in future scenarios, a continuous change of wind direction and speed would jointly lead to a lower bottom SSC in the northern part of the western shoal and higher bottom SSC in the southern part of the shoal and the channels, which consequently affect the spatial extent of the ETMs.
6. Wind waves exert a considerable impact on SSC in the 1970s and sustain the ETM on the shoal. An increase of the mean water depth of the PRE from 1970s to 2010s by human activities leads to a weakening of the wave effect in a vast part of the estuary except for the western shoal. The same pattern is projected in future scenarios.

The study provides a diagnosis of the historical and current status of ETM, as well as an analysis of the potential factors that may influence it in the future. This will facilitate the sustainable management of the estuary.

4. Discussion and outlook

This thesis endeavor thereby seeks to contribute to estuary management by advancing our understanding of hydrodynamics and sediment dynamics. Study I aims to identify the physical drivers of stratification. This includes river discharge, tides, and topography, which interact with each other to influence the location and intensity of stratification. This study also highlights the response of stratification to morphological changes and SLR. Study II elucidates the formation mechanisms of ETMs and provided the inaugural analysis of the interconnection between ETMs in the PRE, emphasizing the role of stratification in the formation, variation, and interconnection of ETMs. Study III illustrates the evolution of ETMs from historical development to future scenarios. Additionally, the study evaluates the impact of morphological change-related and climate change-related factors on the evolution of ETMs. This thesis provides evidence that climate change and human activities exert a profound impact on estuarine sediment dynamics, particularly with regard to the formation and distribution of ETMs.

To reproduce the observational data presented in (*Cui et al.*, 2022; *Jiangping; Yang and Liu*, 2015; *Ying Zhang et al.*, 2021c), three classes of sediments (clay, silt, and sand) were defined in PRE. The fraction of sediments in bed and the riverine sediment load varies with decades. Given the lack of certainty regarding the available sediment data, the bed sediment fraction from the 1970s was calculated based on the conditions observed in other estuaries that have been less affected by human activities. Morphological changes represent the primary factor in the patchy evolution of ETM, while changes in the sediment fraction can be considered the secondary factor in the formation of current (2010s) verifiable ETMs. This finding aligns with the observation by *Cui et al.* (2022) that the resuspended sediment primarily composes the ETM in the PRE. Accordingly, when using models to study the ETM, it is important to set up appropriate sediment fractions in the estuaries, as sediment resuspension is the important source of SPM in the ETM, for example, in the Weser Estuary (*Kösters et al.*, 2014), the Seina Estuary (*Schulz et al.*, 2018). The occurrence of resuspension is more pronounced when the proportion of silt in the sediment fraction is elevated (*Te Slaa et al.*, 2013) Human activities such as dredging, dumping, as well as changes in sediment load, may result in changes to the sediment fraction (*Chakrapani*, 2005; *Torres et al.*, 2009). Consequently, the management of these activities should take into account their potential impact on ETM.

The absence of flocculation effects in the model simulations may result in an overestimation of the SPM concentration in the channel area. This is because, with the flocculation effect,

deposition caused by turbulence is significant in the channel area. However, the flocculation is not a factor that can affect the existence of ETMs in PRE (*Ma et al.*, 2024). In addition to the effects of turbulent mixing on flocculation, the concentration of SPM, salinity, and biological process also impact the flocculation process (*Eisma*, 1986). These factors should therefore be considered in future model explorations. However, their selection should be guided by the main characteristics of the estuary, given the inherent limitations of computing resources.

The incorporation of wind wave effects into the simulations results in a change in the distribution of SPM, although this change is insufficient to alter the characteristics of ETM. The most significant impact is on the western shoal. The wind wave effects increase the SPM concentration in the western shoal, due to two main factors. Firstly, the enhanced westward residual transport increases the SPM concentration. Secondly, the wind waves effect enhances the resuspension on shallow west shoal. This same pattern has been identified by (*G Zhang et al.*, 2021a). However, the wind wave effect will weaken with the increase of relative depth (Ma et al., 2024).

By demonstrating the validity and importance of various drivers of ETM, this study not only provides a qualitative analysis of the effects, but also a quantitative calculation of the effects, which may contribute to sediment management in estuaries to achieve more standardized construction and ecological objectives, or sustainable development. For example, the rSLR and reduction in riverine sediment load may result in a decrease in estuarine turbidity, which could potentially give rise to environmental concerns, as turbidity as a control on phytoplankton biomass and productivity in estuaries (*Cloern*, 1987). In the PRE, The alterations in hydrodynamics and sediment load resulting from human activities exert a more pronounced influence on phytoplankton chlorophyll than the effects of nutrients and temperature in long-term (*Niu et al.*, 2020). The findings of our study indicate that the shrinking of ETMs could potentially result in a more pronounced phytoplankton bloom. In accordance with the projections by (*Scown et al.*, 2023), 49 estuaries across the globe are estimated to experience a 26~37% decline in riverine sediment load by 2100, due to the prevailing socio-economic pressures (fisheries, navigation, etc.). Consequently, it is imperative to direct global attention towards the adverse effects of shrinking of ETM.

The findings in this thesis suggest that the sediment transport between the west shoal and west channel will be diminished in response to the rSLR. This is due to the rSLR's ability to weaken the wave effect, which in turn reduces the enhanced sediment transport between the shoal and channel(*Ma et al.*, 2024). This phenomenon has also been identified in the study of ideal

channel-shoal system embayment (*Elmilady et al.*, 2022) and in the Hudson River Estuary (*Geyer et al.*, 2001). The resuspension of sediment may be suppressed by the increased stratification [Appendix C], and the increased stratification may promote or inhibit the sediment transport between ETMs (*Ma et al.*, 2024). These changes have a significant impact on the sediment redistribution in the estuary, particularly in consequence of a reduction in SPM and extension of ETMs. The decline in ETMs indicates a reduction in resuspension, which may necessitate an increase in dredging activities within the PRE. The quantitative examination of the factors involved in the formation and maintenance of ETMs provides the possibility of manipulating currents and tides with deflecting walls. A reduction in suspended sediment may be caused by a decrease in convergence flow (*Heininger et al.*, 2015). Furthermore, the enhancement of ebb tide can result in the flushing out of more sediment from the estuary. The same method was proposed by (*Colby et al.*, 2010) to moving a lagoon towards a self-flushing mode through a program of strategic dredging by manipulating the natural tidal asymmetry. It is essential to conduct a detailed examination of the specific relationships between currents, tides, topography and sediment dynamics before any alterations can be made to the system in a beneficial manner. Furthermore, the impact of human activities and climate change should be considered on these processes.

The investigation conducted in this thesis has revealed the significance of rSLR, which involves the relatively deepening of the channel in an estuary, as an independent effect apart from the deepening impact of regular dredging. The rSLR will exert considerable pressure on coastal areas, as river channels are required to deal with higher water levels and the associated flood safety concerns. However, it could be argued that rSLR may also result in a reduction in the intensity of dredging efforts (*Cox et al.*, 2022). Further research is required to gain a holistic understanding of the impact of sea level rise on sedimentation. The findings of this thesis indicate that sea level rise will also increase sediment deposition due to the enhancement of stratification, and future research should therefore consider whether there is a balance between channel deepening and siltation caused by rSLR.

From a global perspective, changes in land-ocean sediment transfer will result in changes in the global biogeochemical cycle, since sediment is important in the flux of many key elements and nutrients. Equally this transfer will also reflect the intensity of soil erosion and land degradation and thus the longer-term sustainability of the global soil resource (*Walling*, 2008). In light of this necessity, model studies must incorporate the interconnection between sediment dynamics and ecological dynamics. It is imperative that considerations be given not only to coastal

engineering projects such as dam construction and dredging, but also to ecosystem function-based research and exploration. Coastal ecosystems like salt marshes, mangroves, seagrass meadows, beaches, dunes, coral, and shellfish or oyster reefs provide benefits and support beneficial processes for Water, Nature and People alike (*Chowdhury et al.*, 2021; *Forrester et al.*, 2024; *Jordan and Fröhle*, 2022). The functions of certain species can be employed to stabilize or destabilize the bed, thereby facilitating the trapping, settling, or resuspension of sediment (*Gutiérrez et al.*, 2011). For example, the mussel beds which can grow on stable artificial structures can result in the mitigation of wave and storm surges, a reduction in current velocities, the trapping of sediment particles, and the processes of bioaccumulation (*P P Arlinghaus et al.*, 2023; *Borsje et al.*, 2011). In this context, with the notable increase in the implementation of ecological engineering for coastal protection and the corresponding lack of knowledge regarding its long-term effects, it is imperative to adopt a long-term model study. To avoid the limitations of short-term consequences, model studies should assess the long-term effects of these solutions.

A diachronic analysis of an estuary is a crucial undertaking to predict its future fates. In the industrial age, when human activities flourish, the effects of climate change and human impact on estuaries are becoming increasingly pronounced. This is leading to significant alterations in the factors that maintain estuary hydrodynamic and sediment dynamic(*Grasso and Le Hir*, 2019; *Hutton et al.*, 2017; *Aldo Sottolichio et al.*, 2013). Each estuary exhibits unique natural geographical conditions. However, the modifications implemented by humans are broadly similar, including activities such as dredging, damming and land reclamation. On the other hand, climate change occurs globally. The joint effect of climate change and human activities has led to similar response of estuaries during the past decades (*Cloern et al.*, 2016; *Talke and de Swart*, 2006; *Chenglong Wang et al.*, 2017) and likely similar fates in future. Successful examples in mitigation of climate change and anthropogenic impact in some estuaries thus have global implications. Our work presents an effort towards a comprehensive understanding of the evolution of ETMs and may contribute to development of guidelines for mitigation in one of the largest estuaries worldwide.

Appendices

Appendix A

Impacts of morphological change and sea-level rise on stratification in the Pearl River Estuary

frontiers | Frontiers in Marine Science

TYPE Methods
PUBLISHED 01 February 2023
DOI 10.3389/fmars.2023.1072080

OPEN ACCESS

EDITED BY
Selvaraj Kandasamy,
Xiamen University, China

REVIEWED BY
Peng Yao,
Hohai University, China
Huawei Wang,
Southern University of Science and Technology, China
Sandeep Kizhur,
Central University of Kerala, India

*CORRESPONDENCE
Mengyao Ma
mengyao.ma@hereon.de
Wenyan Zhang
wenyan.zhang@hereon.de

SPECIALTY SECTION
This article was submitted to Marine Biogeochemistry, a section of the journal Frontiers in Marine Science

RECEIVED 17 October 2022
ACCEPTED 20 January 2023
PUBLISHED 01 February 2023

CITATION
Ma M, Zhang W, Chen W, Deng J and Schrum C (2023) Impacts of morphological change and sea-level rise on stratification in the Pearl River Estuary.
Front. Mar. Sci. 10:1072080.
doi: 10.3389/fmars.2023.1072080

Impacts of morphological change and sea-level rise on stratification in the Pearl River Estuary

Mengyao Ma[1,2*], Wenyan Zhang[1*], Wei Chen[1], Junjie Deng[3] and Corinna Schrum[1,2]

[1]Institute of Coastal Systems – Analysis and Modeling, Helmholtz-Zentrum Hereon, Geesthacht, Germany, [2]Institute of Oceanography, Center for Earth System Research and Sustainability, University of Hamburg, Hamburg, Germany, [3]Research Centre for Coastal Ocean Science and Technology, School of Marine Sciences, Sun Yat-Sen University, Guangzhou, China and Southern Marine Science and Engineering Guangdong Laboratory (Zhuhai), Zhuhai, China

The Pearl River Delta (PRD), where several megacities are located, has undergone drastic morphological changes caused by anthropogenic impact during the past few decades. In its main estuary, the water area has been reduced by 21% whilst the average water depth has increased by 2.24 m from 1970s to 2010s. The mainly human-induced morphological change together with sea level rise has jointly led to a remarkable change in the water stratification. However, the spatial and temporal variability of stratification in the estuary and associated driving mechanisms remain less understood. In this study, stratification in the Pearl River Estuary (PRE) in response to morphological change and external forcing is investigated by 3-dimensional numerical modeling. Simulation results indicate that stratification in the PRE exhibits distinct spatial and temporal variabilities. At a tidal-to-monthly time scale, variation of stratification is mainly driven by advection and straining through tidal forcing. At a monthly-to-seasonal scale, monsoon-driven river runoff and associated plume and fronts dominate the variation of stratification. Human-induced morphological change leads to an enhancement of stratification by up to four times in the PRE. Compared to an overwhelming human impact in the past few decades, future sea level rise would further enhance stratification, but to a much lesser extent than past human impacts. In addition, stratification in different areas of the estuary also responds differently to the driving factors. The western shoal of the estuary is most sensitive to changes in morphology and sea level due to its shallowness, followed by the channels and other parts of the estuary, which are less sensitive.

KEYWORDS

stratification, salinity variation, morphological change, sea level rise, scenario

1 Introduction

Water column stratification is an essential characteristic of estuaries. Conventionally, according to stratification or vertical salinity structure, estuaries can be classified as salt wedge, strongly stratified, weakly stratified and well mixed types (Pritchard, 1955; Cameron

and Pritchard, 1963). In tidal estuaries, stratification is normally determined by salinity gradients which result from a balance between the stratifying tendency of estuarine circulation and mixing by tides, with additional but short-term impacts generated by energetic weather events (Zhang et al., 2018). Stratification has important consequences for estuarine ecology and matter transport (Li et al., 2018a; Zhang et al., 2020; Zhang et al., 2021b) and environmental hazards such as hypoxia or anoxia may be triggered by a persistently stable stratification (Cui et al., 2019).

Estuaries and coastal seas are transition areas between land and ocean with profound changes exerted by human activities and climate change (Wu et al., 2016; Ralston and Geyer, 2019; Deng et al., 2020). Numerous observational and modeling studies have confirmed a significant modification in estuarine stratification by morphological changes and sea level rise. For example, the dredging of shipping channels results in enhanced estuary circulation and salinity intrusion in many estuaries (Kennish, 2003). Chant et al. (2018) demonstrated that a relatively small (15%) increase in depth by dredging in a short reach of an estuary may double the exchange of salt flux and remarkably increase stratification in the estuary. In contrast, Ralston and Geyer (2019) showed that channel deepening due to dredging may result in an increase in salinity intrusion but almost no change in the estuarine circulation, suggesting that the impact of channel dredging on stratification is nonlinear and site dependent. Sea level rise also influences the stratification of estuaries. Gong and Shen (2011) simulated the hydrodynamics of Chesapeake Bay in response to the projected sea level rise scenarios in the 21st century. Their results show that the bay-scale averaged stratification would strengthen along with a sea level rise and characterized by obvious seasonal and inter-annual variations. Through scenario simulation Chua and Xu (2014) found that sea level rise would increase the strength of gravitational circulation, resulting in higher vertical stratification by increasing the strength of salinity gradient and reducing the bottom-generated turbulence.

The Pearl River, located in the south of China, with an annual mean discharge of $336\times10^9 m^3$ (Zhang et al., 2009), is one of the world largest rivers in terms of river discharge (Figure 1A). The Pearl River Estuary (PRE) is featured by a complex channel network through its delta that hosts several megacities (Guangzhou, Shenzhen and Hong Kong) with a total population of 63.01 million (Zhang et al., 2021a). A major portion (~61%) of river discharge from the Pearl River to the continental shelf of the South China Sea is delivered through Lingding Bay (Figure 1C) (Han et al., 2021), where is subject to intense morphological changes by human activities (Wu et al., 2016). Since 1970s, frequent dredging in the two main shipping channels (i.e., east and west channels) have deepened the mean channel depth by more than 15% till 2010s. Meanwhile, the water area of Lingding Bay has decreased by ~170 km^2 (8.1% of the total Lingding Bay water area in 1970s) due to land reclamation, and sediment input to the bay has been reduced by 70% by human activities at the catchment like river damming (Dai et al., 2007). A joint accumulative effect of land reclamation, channel dredging, river damming and sand excavation resulted in a decrease of water areas and a deepening of the mean water depth by 2.24 m from 1970s to 2010s over the entire Lingding Bay, with annual variation at local sites up to ± 5m/yr (Wu et al., 2016).

The mean sea level at the mouth of PRE rose at a rate of 3.1 mm/yr during 1954-2021 (https://www.hko.gov.hk/en/climate_change/obs_hk_sea_level.htm), and exhibits an accelerating trend in recent decades (Wong et al., 2003; Masson-Delmotte et al., 2021). Existing studies show that the impact of sea level rise on the estuarine circulation and stratification in the PRE is through a modification of tides and estuarine circulation. Based on three-dimensional hydrodynamic modeling, Hong et al. (2020) found that the salinity, stratification and tidal range all increase as sea-level rises and are characterized by clear spatial and seasonal variations. By calculating the water flux, Yuan et al. (2015) found that the upstream salinity

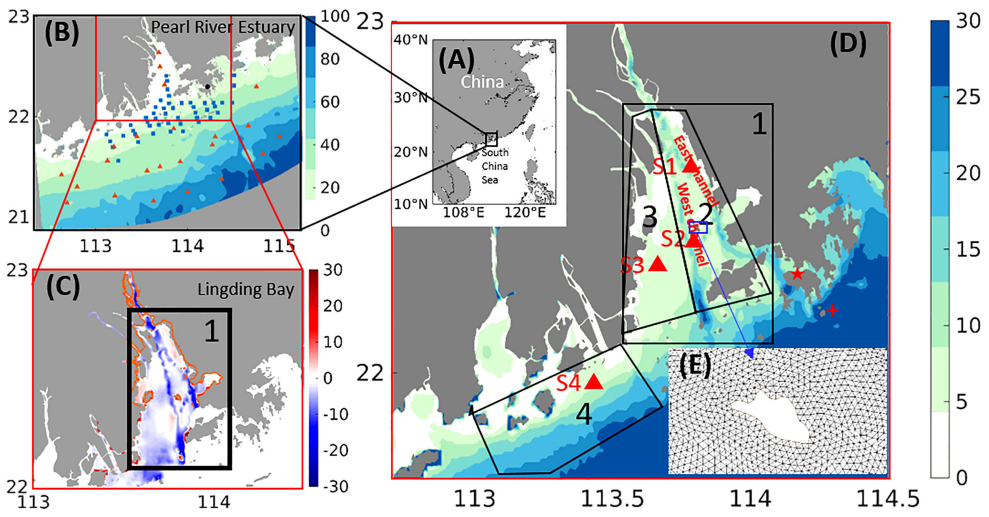

FIGURE 1
Location maps. **(A)** The location of the Pearl River Estuary in south China. **(B)** The model domain. Squares represent sites for salinity validation; triangles represent sites for temperature validation; the black dot is the location of the tidal gauge. **(C)** Bathymetric change from the 1970s to 2010s. The black frame indicates the Lingding Bay. The orange line refers to the shoreline in the 1970s. **(D)** Bathymetry (unit: m) of the PRE in 2010s, the marksed areas are: Zone 1 (Lingding Bay), Zone 2(channels), Zone 3 (west shoal), and Zone 4 (river plume dominated area). The four red triangles indicate the selected sites which are used to assess the stability of stratification. The five-pointed star indicates the location of Victoria harbor. The four-pointed star indicates the location of Waglan Island. **(E)** An example of computational grid around small island.

intrusion increased linearly in the main channel (Modaomen) of the estuary with sea level rise, meanwhile the isohaline of 0.45 (which is the salinity standard for drinking water) moved offshore in other two smaller channels Jiaomen and Hongqimen.

Previous studies of stratification in the PRE mainly focused on the extent of saltwater intrusion. The spatial and temporal variation of stratification in the PRE in response to decadal-scale morphological change and sea-level rise remains largely unknown. As the PRE is a bell-shaped estuary, the tidal range and current in response to the morphological change and sea-level rise are highly nonlinear (Hong et al., 2020; Valentim et al., 2013). In the short term, the stratification strength varies from days to seasons, with a prominent variation in the tidal cycle (Luo et al., 2009). In the longer term, how the interaction between tides and river runoff responds to morphological change and sea-level rise and consequent impact on stratification are yet to be explored (Hong et al., 2020). The aim of this study is to contribute to addressing this question and quantify the role of morphological change and sea level rise in driving the variation of stratification in the PRD at multi-temporal and spatial scales by high-resolution 3-dimensional numerical modeling.

2 Data and methods

We used a 3-D model to simulate three scenarios, namely one historical scenario based on the morphology (bathymetry and coastline configuration) in 1970s, one present day scenario based on the morphology in 2010s and one future scenario for 2050s based on the present day morphology superposed by a moderate sea level rise of 20cm, which are represented by Run_1970s, Run_2010s and Run_2050s, respectively. Data for model setup and performance assessment as well as methods for result analysis are described in following sections.

2.1 Data

Several observational datasets obtained *via* field surveys and gauge stations in the study area as well as global hydrographic datasets and projections were used to initialize and validate the model. The topographic data used in this study primarily consist of historical bathymetrical maps of Lingding Bay (Deng et al., 2020). Two topographic datasets of Lingding Bay derived from the 1970s and 2010s were used for modeling in this study. Another two topographic datasets from 1980s and 1990s were additionally used for the analysis of morphological change during the period of 1970s - 2010s.

Compared to dominance by the human-induced morphological change between 1970s and 2010s, future change of stratification in the PRE would be mainly driven by climate change especially the sea-level rise because of a legal prohibition of land reclamation and sand excavation initiated in recent years (Zhao et al., 2015).

The historical mean sea level recorded at the estuary mouth (Vitoria Harbor at Hong Kong, https://www.hko.gov.hk/en/climate_change/proj_hk_msl.htm) was used in the simulation of the scenarios 1970s and 2010s. A sea level rise by 20 cm from present day level was used to study the sensitivity of stratification to a moderate sea level rise for a futures scenario corresponding to 2050. Recorded data from the Hong Kong Observatory indicate that the mean sea level in the station Victoria Harbour rose at a rate of ~3 mm/year during 1954-2021 (https://www.hko.gov.hk/en/climate_change/obs_hk_sea_level.htm). However, it is expected that future sea-level rise rate would be accelerated. The scenario simulation for 2050s in this paper is based on SSP2-4.5 from IPCC AP6, showing that the mean sea level of the world sea would rise at a mean rate of 5 mm/year in the future, which means that the sea level would rise by 20 cm until 2050s compared to that in 2010s. The SSP2-4.5 scenario considers intermediate greenhouse gas emissions, in which CO2 emissions around current level until 2050, then falling but not reaching zero by 2100. The probability for likely range of SSP2-4.5 to cover the outcome is at least 66% (IPCC, 2021). Thermal expansion of a warming ocean makes up 21-43% of the total global mean sea level rise in the scenario SSP2. The melting of land ice (glaciers and ice sheets) adds mass to the ocean (as freshwater), and makes up most of the remainder of global mean sea level rise (Couldrey et al., 2022).

Monthly river discharge data are available from the China Sediment Report (http://www.mwr.gov.cn/sj/tjgb/zghlnsgb/). Daily river discharge from July to September 2017 was collected from existing publications (Liu and Gan, 2020) to assess model performance against observations. In addition, historical data from the eight main outlets of the PRE (Liu and Gan, 2020; Yu et al., 2021) were collected to calculate the proportion of river tributary discharge.

The Copernicus Marine Environment Monitoring Service (CMEMS) data were used to specify the initial fields of temperature and salinity as well as to provide open boundary conditions in the study area (Shen et al., 2018). The CMEMS data is a reanalysis product of the global ocean eddy-resolving model (with 1/12 degree horizontal resolution and 50 vertical levels). Cruise data for surface water temperature and salinity during the period of July to September 2017 were collected from existing publications (Liu and Gan, 2020) to assess model performance.

Atmospheric forcing driven by monsoons was included in open boundary (CMEMS data) and interpolated into our model grid using wind, air pressure, precipitation, and net solar radiation obtained from European Centre for Medium Range Weather (ECMWF) ERA-interim (https://cds.climate.copernicus.eu/cdsapp#!/dataset/reanalysis-era5-single-levels?tab=overview). The spatial resolution of ERA-interim data is 0.25° × 0.25° and the temporal resolution is 1 day.

Eight primary tidal constituents (M2, S2, N2, K2, K1, O1, P1, Q1) were specified at the open boundary. The tidal data were extracted from the global TPXO9-atlas (https://www.tpxo.net/global/tpxo9-atlas). In addition, daily data of water level, salinity, temperature, and currents (u, v) from 1th June 2017 to 1th June 2018 obtained from CMEMS were specified at the open boundary. At the upstream river boundaries, a constant salinity of 3 psu was specified with a daily varying temperature extracted from the Himawari-8 satellite product (http://www.data.jma.go.jp/mscweb/en/index.html) from 1th June 2017 to 1th June 2018.

2.2 Methods

2.2.1 Hydrodynamic model and setup for the study area

The hydrodynamic model used in this study is the Semi-implicit Cross-scale hydroscience Integrated system Model (Zhang et al., 2016).

SCHISM is developed from the SELFE model and includes new features that ensure its robustness in application to estuarine and coastal areas with complex coastline and morphology. In particular, SCHISM includes (1) a new advection scheme for the momentum equation which includes an iterative smoother to reduce excess mass produced by higher-order kriging method, (2) a new viscosity formulation to work robustly for generic unstructured grids and effectively filter out spurious modes without introducing excessive dissipation, and (3) a new higher-order implicit advection scheme for transport (TVD^2) to effectively handle a wide range of Courant number as commonly found in typical cross-scale applications. In addition, the model shows a good performance in the eddying regime, which represents the last missing link for cross-scale modeling (Zhang et al., 2016).

The model domain covers the PRE and its eight river outlets spanning from 21 to 23°N in latitude and 112.4 to 115.25°E in longitude (Figure 1B), with a high grid resolution (~50 m) in the Lingding Bay and coarsening resolution (till ~1000 m) toward the open boundary at the shelf of the South China Sea. In particular, sparsely distributed islands in the PRE are resolved by a high-resolution grid so that their impact on hydrodynamics is included (Figure 1E). Three scenarios, namely Run_1970s, Run_2010s and Run_2050, were designed. The morphological data of 1970s and 2010s were used in the Run_1970s and Run_2010s, respectively. Land reclamation and sand excavation in the PRE were officially banned during the past decade (Tang et al., 2016). Therefore, it is expected that future morphological change until 2050 would not be as dramatic as the historical change between 1970s and 2010s. Dredging in the two main shipping channels is expected to continue to maintain the depth. Based on this, the Run_2050s adopted the morphology in 2010s but superposed by a 20 cm higher sea level compared to that of 2010s. The 3D hydrodynamic model time step was 60 seconds and the simulation period was one year (starting from 1st June 2017) in each scenario and adopted the same atmospheric forcing from 1st June 2017 to 6th July 2018. The simulation results of Run_2010s are assessed by observation data from 2017. Further details of model setup are provided in the Supplementary Material (Supplementary Table 1).

2.2.2 Potential energy anomaly

In this study, potential energy anomaly (PEA) φ (Simpson and Bowers, 1981) is used as a measure for stratification:

$$\varphi = \frac{1}{H}\int_{-h}^{\eta}(\bar{\rho}-\rho)gzdz, \tag{1}$$

Where ρ is the vertical density profile over the water column of depth H, given by $H = \eta + h$, η is the free surface, h is the bed level, $\bar{\rho}$ is the depth average density, z is the vertical coordinate, and g is the gravitational acceleration. The value of φ indicates the work required per unit of volume to cause a complete vertical mixing of the water column.

The water column is considered as stratified when φ exceeds the threshold 10 J/m^3 (Chegini et al., 2020). Based on the scenario Run_2010s, the average value of φ>10J/m^3 covers 89% of the time over the entire simulation in a major part of the study area. In order to distinguish strong stratification, another threshold φ>50J/m^3 is used, above which the water column is highly stratified.

2.2.3 Gradient Richardson number

To evaluate the stability of vertical stratification, the gradient Richardson number R_i is computed by:

$$R_i = \frac{N^2}{V_s^2}, \tag{2}$$

with the definition of buoyancy frequency

$$N = \left(-\frac{g}{\rho}\frac{\partial\rho}{\partial z}\right)^{\frac{1}{2}}, \tag{3}$$

and the vertical shear

$$V_s = \left[\left(\frac{\partial u}{\partial z}\right)^2 + \left(\frac{\partial v}{\partial z}\right)^2\right]^{\frac{1}{2}}. \tag{4}$$

The water column is considered stably stratified when $log10(Ri)\geq 1$ (Chen, 2018).

2.2.4 Salinity variance balance

MacCready et al. (2018) introduced the concept of salinity variance to understand the budget change of salinity. Salinity variance is given by $s'^2 = (s-\bar{s})^2$, where s is the *in-situ* salinity, $\bar{s}$ is the salinity averaged over the entire water body of the estuary. According to Wang et al. (2017), the total salinity variance of an estuary can be calculated by:

$$SVAR = \iiint_V s'^2 dV, \tag{5}$$

where V indicates the whole estuarine water volume. Li et al. (2018b) separated the total salinity variance into two parts corresponding to the horizontal and the vertical components:

$$\iiint (s')^2 dV = \iiint (s_h')^2 dV + \iiint (s_v')^2 dV, \tag{6}$$

where $(s_h')^2$ represents the horizontal salinity variance and $(s_v')^2$ represent the vertical salinity variance.

In this study, we focus on vertical density stratification. For this reason, only the vertical salinity variance is considered. Based on the conservation of vertical salinity variance $(s_v')^2$, Li et al. (2018) proposed a dynamic equation to describe the temporal change of the vertical salinity variance integrated over the entire water column:

$$\frac{\partial\int(S_v')^2dz}{\partial t} + \nabla_h\int U_h(S_v')^2dz = \int -2u_v'S_v'\cdot\nabla\overline{S_v}dz - \int 2K_{zz}\left(\frac{\partial S}{\partial z}\right)^2dz, \tag{7}$$

where $\overline{S_v}$ is the vertically averaged salinity, ∇_h is the horizontal gradient operator, U_h is the horizontal velocity vector, and K_{zz} is the vertical eddy diffusivity. In a physical process-based understanding, Equation (7) can be expressed as *Tendency + advection = straining + dissipation*.

By using the above equations, Li et al. (2018b) quantified the influence of straining and mixing on stratification in the Yangtze estuary. Their research indicated that the salinity variance method could be used as a useful approach for examining the spatial and temporal variability of stratification in estuaries and coastal environments.

2.2.5 Sub-division of the study area for process understanding

To better understand the spatial variation in stratification, the study area is divided into four zones, as shown in Figure 1D, taking

into account their distinct features in hydrodynamic conditions and morphology. Zone 1 covers the entire Lingding Bay. Zone 2 covers the channel area in the Lingding Bay, including two channels and the area in between. Zone 3 covers the west shoal of the Lingding Bay and Zone 4 covers the coastal area dominated by the river plume.

3 Results

3.1 Model validation

To assess the model performance, simulation results of the scenario Run_2010s were compared to observation data (salinity and temperature) collected in a cruise from 11th to 21th of July 2017 (Yu et al., 2021) as well as water level recorded at a fixed gauge station (Waglan Island, Figure 1B).

The comparison demonstrates a general satisfactory model performance in capturing both spatial and temporal variations of water level, salinity and temperature (Figure 2). The recorded tidal amplitude is ~2 m at the gauge station (Waglan Island) and the Root Mean Square Error (RMSE) of the simulated water level is 0.15 m, corresponding to 7.5% deviation from observation. The data show a dominance of semi-diurnal tides with a distinct spring-neap cycle in the study area. Salinity constantly changes under the effect of tides (Figure 2B). The correlation coefficient between the simulated surface water salinity and field data is 0.93, and the RMSE is 2.7 psu. The Taylor diagram of the simulated sea surface temperature compared to field data indicates a high correlation coefficient between 0.95 and 0.99, and a RMSE within 1°C. Based on the satisfactory agreement between observation and simulation for the surface water, and the understanding that surface water dynamics in the estuary, especially temporal and spatial variation of temperature and salinity, is jointly controlled by interaction between freshwater discharge and bottom saline water, we therefore believe that the model also reliably captures the bottom water dynamics which is not covered by existing observation data. The overall good model performance allows for using the extended simulation results (for 400 days in each scenario) to derive insights into the impact of morphological change and sea-level rise on variation of stratification in the PRD at multi-temporal and spatial scales.

3.2 Variability of stratification and driving factors

The morphology of the PRE changed considerably from 1970s to 2010s, especially in the Lingding Bay (Figure 1C). The average depth of Lingding Bay (Zone 1) increased by 2.24 m. The most significant deepening occurred in the channels (Zone 2) due to dredging, with a mean depth increase of 4.85 m and local maximum of 12 m in the southern Lingding Bay, close to the Lantau island. Depth of the western shoal area (Zone 3) was increased by approximately 1 m on average (the calculation is based on the water area of 2010s), whilst the area close to the west bank became shallower and the coastline extend to the sea due to land reclamation. The total water area of the Lingding Bay decreased by approximately 170 km^2 because of land reclamation, accounting for 8.1% of the total water area in the 1970s. Most reduction of water area occurred in west shoal (Zone 3), with

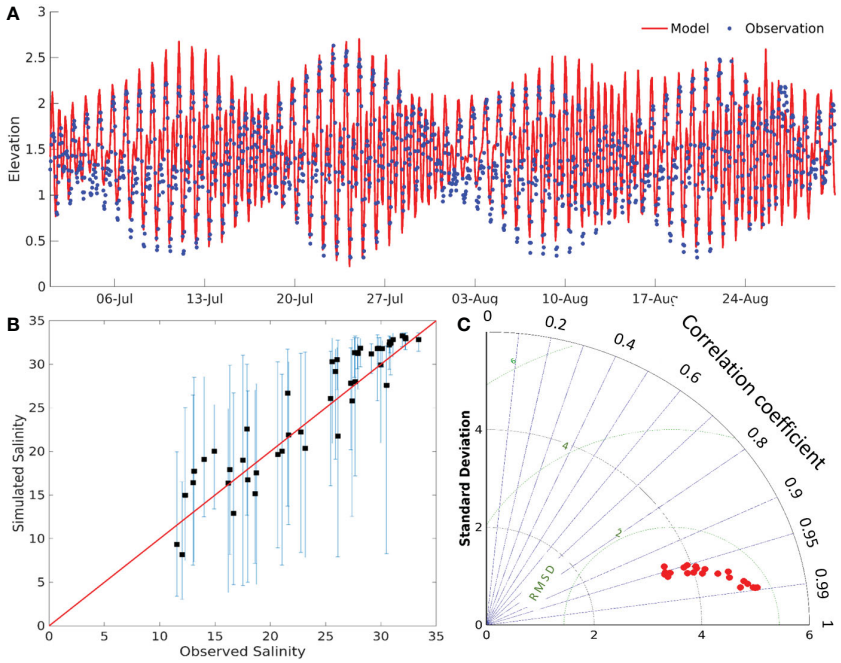

FIGURE 2
Comparison between model result and field data of **(A)** water level at the gauge station Waglan Island and **(B)** surface salinity collected during a research survey in July 2017 by Yu et al. (2021). In addition, simulated temporal variation of surface salinity within a tidal cycle at each measuring station is indicated by the bar crossing the measured value. Location of the stations is shown in Figure 1B. **(C)** Taylor diagram showing the standard deviation, the correlation coefficient, and the RMSE of simulated surface temperature against field data at 23 stations. Location of the stations is shown in Figure 1B by red dots.

14.32% of its total water area in the 1970s transformed to land till 2010s by artificial reclamation. The overall trend of changes in the Lingding Bay was narrowing and deepening from 1970s to 2010s.

River runoff in the PRE has a remarkable seasonality driven by monsoon. A direct comparison of the spatial distribution of stratification among the three scenarios can be seen in the salinity difference between the bottom and surface water averaged in two representative seasons (Figure 3). The wet season from 1st July to 1st September is characterized by a mean river runoff of $2.5\times10^4 m^3/s$, while the dry season from 1st October to 1st December has a much reduced mean river runoff of $0.75\times10^4 m^3/s$. Model results indicate a salinity increase in the bottom water of Lingding Bay by about 70% during the wet season and about 50% during the dry season from 1970s to 2010s. In contrast, the increase of salinity in the bottom water of the Lingding Bay from the 2010s to 2050s is 3.5% and 2.1% in the wet and dry seasons, respectively.

The salinity difference of 12 psu between the bottom and surface water can be used as a simple indicator for stratification (depicted by the brown line in Figure 3) as proposed by Li et al. (2017). As shown in Figure 3, the morphological change from 1970s to 2010s has notably changed the spatial distribution of stratification in the Lingding Bay. In the simulation result of 1970s, we found that the 7-m isobaths (described by the black lines in Figure 3) roughly describe the northern edge of stratification in the wet season. Stratification is mainly located in the outer the Lingding Bay and the river plume dominated area (Zone 4). Whilst in the 2010s, although the northern edge of stratification is still mostly limited by the 7-m isobaths in the wet season, stratification extends to the interior the Lingding Bay along the two channels (Zone 2) and appears in the western shoal (Zone 3) and further expands in Zone 4 due to the morphological change. Compared to the wet season, stratification in the dry season is weaker but with a different spatial pattern (Figure 3). Due to decrease in river runoff, stratification appears in the upper part of the Lingding Bay and extends into the rivers. Stratification in the Run_2050s shows very minor difference with the Run_2010s in both wet and dry seasons, suggesting a minor role of sea level rise (by 20 cm) in controlling the spatial pattern of salinity difference between bottom and surface water in the study area.

3.2.1 Variation caused by morphological change

To further understand the spatial and temporal variation of stratification and driving processes behind, the potential energy anomaly (φ) the four terms in Equation 4 are quantified for each sub-region for each scenario and compared accordingly. A variation index σ_{mc}, calculated by $\sigma_{mc}=\varphi_{2010s}/\varphi_{1970s}$ where φ_{2010s} and φ_{1970s} represent the potential energy anomaly in the Run_2010s and Run_1970s, respectively, is used to indicate the change of stratification induced by the morphological change between the 1970s and 2010s, while $\sigma_{sc}=\varphi_{2050s}/\varphi_{2010s}$ is used to indicate the change of stratification induced by sea-level rise.

The daily value of φ for each sub-region in the three scenarios is shown in Figure 4. The results cover the period of simulation, which includes variation in wet and dry season. Results of both wet season and dry season were shown. There exists a persistently strong stratification ($\varphi\geq50 J/m^3$) in the PRE during the wet season in all scenarios (Run_1970s, Run_2010s and Run_2050s), due to the large river runoff. Morphological changes mainly occurred in the Lingding Bay (Zone 1). Consequently, enhancement of stratification also mainly occurs in the Lingding Bay. In the channel area (Zone 2), stratification is always strong in the wet season, whilst in the dry season the strength of stratification becomes much weaker with φ normally ranging between 10 and 30 J/m^3 in all three scenarios (Run_1970s, Run_2010s and Run_2050s). In the west shoal area (Zone 3), strong stratification does not occur before the morphological change (Run_1970s), but occasionally occurs after the morphological change (Run_2010s and Run_2050s) in the wet season. Stratification in the river plume dominated area (Zone 4) exhibits similar change to that in Zone 3 in the wet season, but in the dry season the value of φ is almost the same in all scenarios in Zone 4 whilst periodic enhancement in φ is seen in Zone 3.

The enhancement of stratification due to morphological change in the entire PRE is most significant in the wet season. In the wet

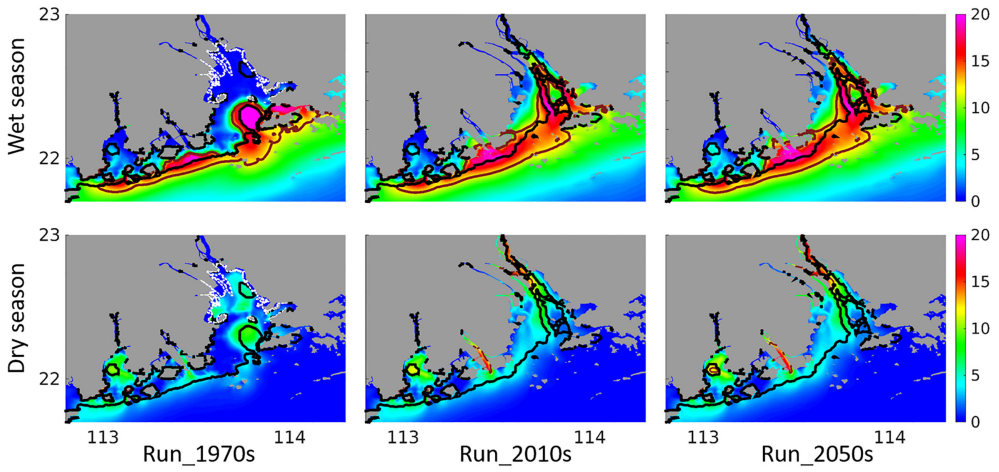

FIGURE 3
The salinity difference from bottom to surface in wet and dry season of Run_1970s, run_2010s and Run_2050s, areas with salinity difference values greater than 12 psu is surrounded by brown lines. The black line indicates the 7-m isobath. The white dashed line in the Run_1970s refers to the location of coastline in 2010s. (Unit: psu).

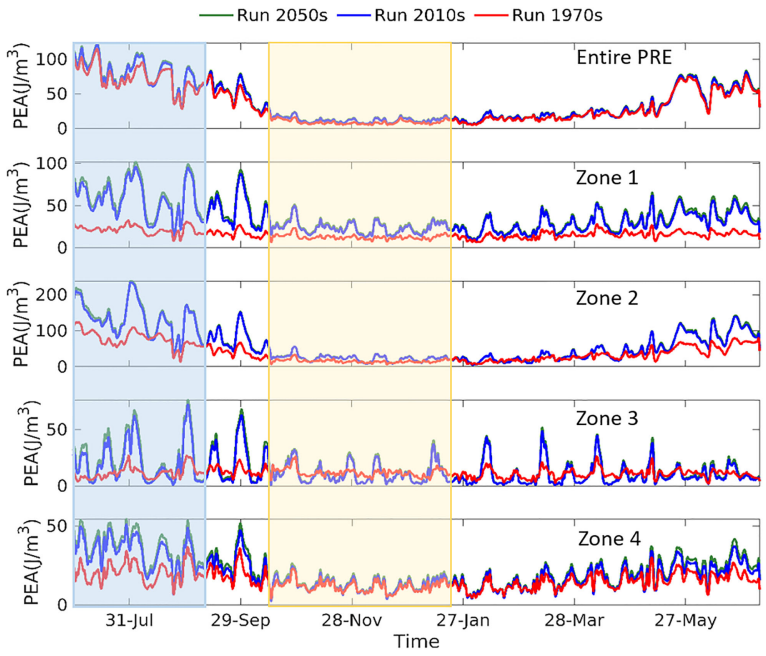

FIGURE 4
Time series of daily-averaged potential energy anomaly (φ) in the entire PRE and different sub-regions in the three scenarios (Run_1970s, Run_2010s and Run_2050s). The light blue and yellow rectangles indicate the wet season (July and August) and dry season (October, November and December), respectively.

season, the strength of stratification averaged over the Zone 1 and 2 is up to 4 times and in Zone 3 even up to 7 times stronger in the Run_2010s than that in the Run_1970s, while in the dry season the enhancement of stratification by morphological change becomes less prominent (Table 1). Besides a general strengthening of stratification in the wet season, the enhancement also exhibits some obvious periodic cycles (Figure 4). Figure 5 indicates that this periodic enhancement is caused by the spring-neap tidal cycle. These results indicate that the stratification of the Lingding Bay becomes much more sensitive to tidal and river runoff impact after the morphological change.

Tides affect stratification in the PRE mainly at short time scales from hours extending to spring-neap cycle. Tidal signals are clearly seen in the time series of φ at each sub-region (Figure 5). Spectral analysis of φ in the Run_2010s shows that the tide-driven fluctuation of φ is mainly at M4, M2, and K1 cycles, which is consistent with field observation (Mao et al., 2004). According to the simulation results, morphological change in the Lingding Bay (Zone 1) from 1970s to 2010s results in an increase intidal in this region, the increase range gradually decreases from north to south, and the maximum increase can reach 0.5 m in the northern of the Lingding Bay near the coastline. The increase of tidal amplitude caused by the changes of coastline (Shen et al., 2018); and the deepening of the channels area (Zone 2) makes stronger tidal flow than before(Run_1970s) in the Lingding Bay, which leads to stronger salt water intrusion. Both the increase of tidal amplitude and the intensification of tidal flow lead to a nonlinear response of stratification.

Before the morphological change (i.e. in the Run_1970s), φ_{1970s} in the Lingding Bay (Zone 1) fluctuates mildly around 25 J m^{-3} in the wet season and slightly higher than 15 J m^{-3} in the dry season. The impact of spring-neap tidal cycle is hardly visible. By contrast, φ_{2010s} exhibits a positive correlation with the tidal cycle, and fluctuates between 25 to 100 J m^{-3} during the spring-neap tidal cycle (Figures 4, 5). The enhancement of stratification caused by the morphologic change σ_{mc} ranges between 1 and 4 depending on the tidal phase. The peaks of σ_{mc} appear normally before the peak of spring tides, and the troughs appear after the spring peaks but before the neap tides. Advection is primarily responsible for this phenomenon (Figure 6), as

TABLE 1 The factor by which the stratification is enhanced due to morphological changes and sea-level rise in different areas.

	Wet season		Dry season	
	Morphologic change (σ_{mc})	SLR (σ_{sc})	Morphologic change (σ_{mc})	SLR (σ_{sc})
1. Entire PRE	1-1.4	1.02-1.04	1-2	1.04-1.1
2.Lingding Bay(Zone 1)	1-4	1.05-1.2	1-3.5	1.05-1.13
3.Channels(Zone 2)	1-4	1-1.1	0.8-3	0.95-1.15
4.West shoal(Zone 3)	0-7	1.1-2.5	0-3	1-1.5
5.River plume dominated area (Zone4)	1-2.5	1.05-1.25	0.8-1.2	1-1.15

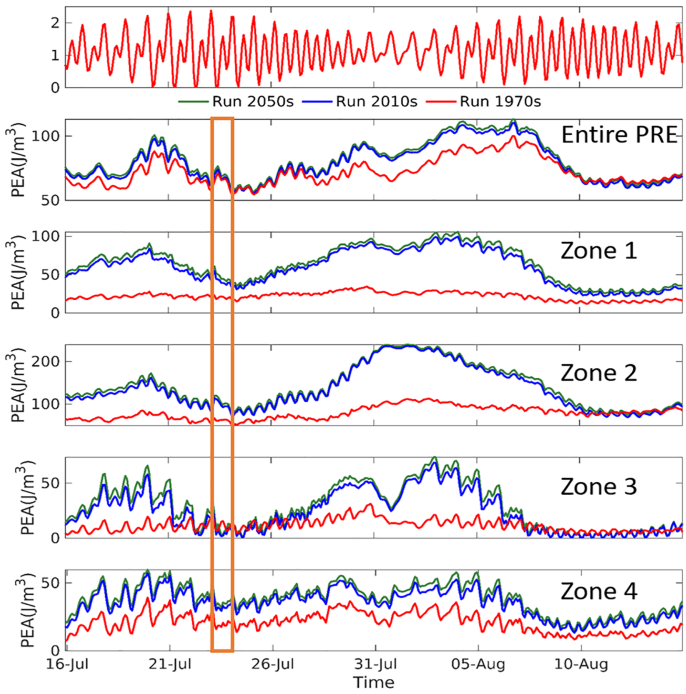

FIGURE 5
Potential energy anomaly (φ) in different sub-regions in the three scenarios from 16 July to 15 August. Duration of the typhoon Roke is marked by the orange rectangle.

the advection term (Equation 4) increases by about three times during the transition from neap tides to spring tides. It can be seen in Figure 6 that the advection of the horizontal gradient of salinity variance is the main contributor to stratification. During the advection process, the vertical salinity variance $(S_v')^2$ increases significantly (by about 200% on average) with a strong saltwater intrusion from the bottom, resulting in an import of salinity variance to the Lingding Bay.

In the channels of the Lingding Bay (Zone 2), stratification is more significant than in other sub-regions, which is attributed to a strong saltwater intrusion, similar to many other estuarine channels (Xu et al., 2008; Ralston and Geyer, 2019). The response of stratification to morphological deepening in the channels is similar to that in the entire Lingding Bay (Zone 1) as seen in Figures 4, 5 as well as Table 1. Advection is the main controlling process for variation of stratification in the channels. In the west shoal area (Zone 3), φ_{1970s} fluctuates mildly around 10 J m^{-3} without obvious seasonal variation. This means that water is between well mixed and weakly stratified in this area before the morphological change (Run_1970s). By contrast, a clear fluctuation related to the spring-neap tidal cycle is seen in $\varphi_{2010s,}$ which can reach up to 70 J m^{-3} in the wet season during the transition from the neap tides to spring tides, approximately 7 times larger than that in the Run_1970s. This result indicates that the morphological change alters the west shoal (Zone 3) from a well mixed/weakly stratified environment in 1970s to periodically strongly stratified environment in 2010s.

Compared to the sub-regions Zone 1-3, the river plume dominated area (Zone 4) appears to be less affected by the morphological change (Figures 4, 5; Table 1). In the dry season, stratification is only slightly enhanced by morphological change (up to 1.2 times) and sea level rise (up to 1.15 times), while in the wet season, stratification is persistently enhanced by morphological change (up to 2.5 times) and sea level rise (up to 1.25 times) and can exceed the threshold of strong stratification (φ=50 J m^{-3}) episodically during neap tides and transition to spring tides.

Short-term extreme events such as typhoons also impact the stratification in the PRE. Three typhoons (Roke on 23rd July, Hato on 22-23rd August, Pakhar on 26-27th August, www.hko.gov.hk) occurred in 2017 and were included in the simulations. Impact of the typhoon Roke (23rd July) was shown in Figure 5. In the Run_1970s, there is no obvious response to the typhoon in the channels (Zone 1 and 2) and the shoal area (Zone 3). The reduction in stratification occurs only in the river plume-dominated area (Zone 4). After the morphological change, stratification is significantly reduced by the typhoon in every sub-region in the Run_2010s and 2050s. This is caused by a higher landward advection of salt water induced by the typhoon, as well as higher straining and dissipation (Figure 6). However, typhoons impact stratification in the PRE only for a short-term and the system rapidly (in 2 days after the typhoon Roke) restores to a tide-driven status after the typhoon passage.

At a monthly-to-seasonal scale, monsoon-driven river runoff dominates the variation of stratification (Figure 4). The location of stratification is bounded by the estuarine fronts. The fronts in the PRE are formed by salinity gradient between the riverine water and saline shelf waters (Wong et al., 2004).

To identify the location of the fronts, the horizontal salinity gradient in surface and bottom water is calculated respectively in the three scenarios with peak values (>0.0015 psu/m) indicating the fronts (Figure 7). Results show that in the surface water (Figure 7A),

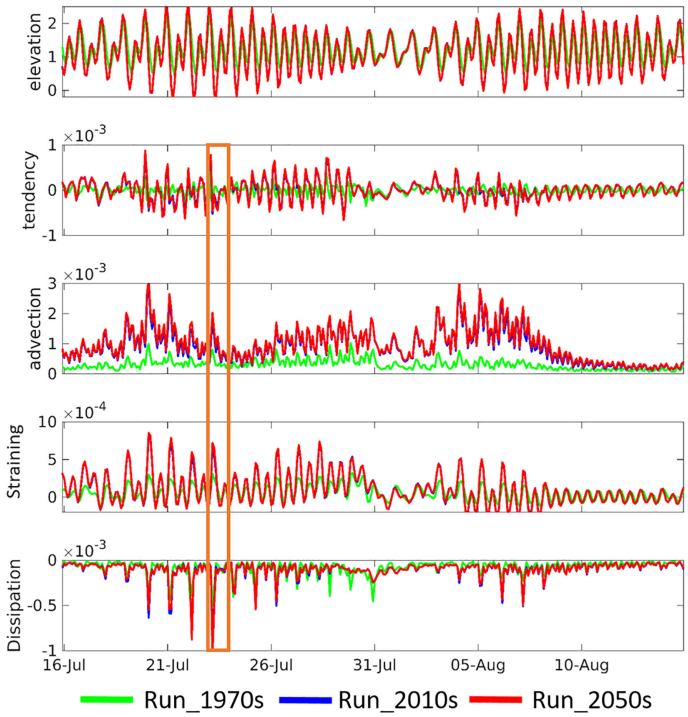

FIGURE 6
Spring-neap tidal cycle reflected in the change of water level and corresponding change in the vertical salinity variance (tendency, advection, straining, dissipation) in the Lingding bay (Zone 1). Duration of the typhoon Roke is marked by the orange rectangle.

the front is dominated by the river runoff, and is mostly located in the outer estuary and the estuarine plume area (Zone 4) in the wet season of all three scenarios. As river runoff decreases, the surface front moves landward in the dry season. In the Run_1970s, the surface front is located in the middle of the Lingding Bay, exhibiting a belt-like shape. After the morphological change (Run_2010s), the surface front is located in the inner part of the Lingding Bay and close to the river outlets. This is also the case in the Run_2050s. In the bottom water (Figure 7B), result of the Run_1970s shows that the front is roughly limited by the 7m isobath of the Lingding Bay in the wet season, whilst in the Run_2010s and Run_2050s, the front is located along both sides of the two shipping channels, on the shoal between the channels and the western shoal (Zone 3). These results indicate that the shoals have become the place for the frontogenesis (in the wet season) after the morphological change. In the dry season, the bottom front in the Run_1970s is located quite close to the surface front, indicating a vertically homogeneous but horizontally stratified state. After the morphological change, the fronts retreat onshore and are located close to the river outlets (Run_2010s and Run_2050s).

3.2.2 Variation caused by sea-level rise

Sea level rise is one of the main drivers of the variation in future scenarios. As seen in Figures 4, 5; Table 1, the enhancement of stratification due to sea-level rise (Run_2050s) is minor compared with that caused by morphological change, but it varies among the sub-regions. The strongest enhancement of stratification due to sea-level rise occurs in the west shoal (Zone 3) in both wet and dry seasons. In Zone 3, stratification is enhanced up to 2.5 times in the wet season while 1.5 times in the dry season by a sea-level rise of 20 cm (Run_2050s). In other sub-regions, stratification is enhanced by maximum of 1.25 times in the wet season and 1.15 times in the dry season by the sea level rise.

The study of Chua and Xu (2014) mentioned that sea-level rise results in a stronger baroclinic pressure gradient proportional to the water depth, indicating an increase in the strength of gravitational circulation, thereby resulting in higher vertical stratification. The enhancement of stratification is through a tidal straining of the density field (Cheng et al., 2011). In Equation (7), the straining term $-2u_v'S_v' \cdot \nabla\bar{S}$ describes a transformation of horizontal salinity gradient to vertical salinity gradient. A positive value of the straining term means destruction of stratification (destratification), while a negative value refers to enhancement of stratification. The temporal variation of the straining term (Figure 8) shows amplified negative straining during spring tides, which means that stratification is enhanced during the spring tides, as the negative straining leads to increased salinity variance. The peaks of enhancement of stratification caused by sea level rise also appear during spring tides (Figure 8). This result means that the sea level rise would cause a transformation of horizontal salinity gradient to vertical salinity gradient, with most significant effect in spring tides caused by negative straining, thereby increasing the vertical stratification. Thus, the impact of sea level rise on stratification is different from the morphological change, as the morphological change mainly alters the advection process as described previously.

3.2.3 Variation of stability in stratification

To further assess the impact of morphological change and sea level rise on stratification in the PRE, stability of stratification in the

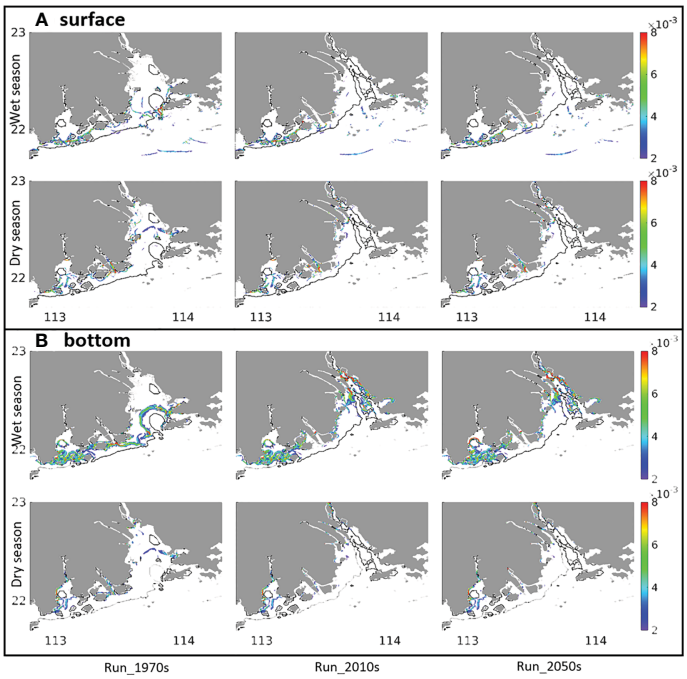

FIGURE 7
Location of estuarine fronts in the **(A)** surface and **(B)** bottom water (identified by salinity gradient greater than 0.0015 psu/m) in the PRE in the three scenarios. The black line indicates the 7-m isobaths. (Unit: psu/m). Supplementary Material provides a zoom in view of Lingding Bay (Supplementary Figure 1).

four selected sites (Figure 1D) is calculated based on the gradient Richardson number R_i. As already indicated by results from previous sections (3.2.1), stratification is most significant in the wet season. Therefore, the analysis of the stability of stratification is focused on the wet season.

Figure 9 shows one-month variation of the vertical distribution of the gradient Richardson number R_i at the four sites in the wet season. In the Run_1970s, stratification does not exist in the eastern channel (S1), where water depth is around 3 m. Stable stratification ($log10(Ri)$ >1) frequently occurs in the western channel (depth > 7 m, S2) and the river plume-dominated area (depth is around 3.5 m, S4). By contrast, stable stratification in the shallow western shoal (Zone 3) mainly appears during neap tides and is absent for the rest of the time. In the Run_2010s, stability of stratification is enhanced at all four sites, with most significant change in the eastern channel (S1, Table 2), where the channel depth is increased by ~ 3 m. Similar to the strength of stratification represented by φ, stability of the stratification also presents fluctuations following the spring-neap tidal cycle. The strongest enhancement of R_i occurs during neap tides and their transition to spring tides, whilst is weakened or completely destroyed by strong mixing during spring tides.

The stability of stratification at the two channels and the west shoal exhibits similar temporal variation in response to the spring-neap tidal cycle, meanwhile is characterized by a vertical variation in its maximum value (Figure 9). Maximum R_i migrates downward to the deeper part of the water column during a transition from spring to neap tides, and then starts to rebound towards surface during the transition from neap to spring tides. However, such pattern is not observed at S4 located in the river plume-dominated area (Zone 4). The reason is attributed to the spatial variation of the river plume and its front. During neap tides, the river plume and its front reach their maximum extent in Zone 4. The site S4 is mainly dominated by well mixed fresh water which greatly dampens stratification. During the transition from neap to spring tides, the river plume and its fronts retreat to the inner shore, and stratification at S4 becomes more stable.

It is worth to note that typhoons exert only short-term perturbations to the stability of stratification. As can be seen in Figure 5, it takes around two days for the stratification to restore to a tide-driven state after the typhoon passage. The stability of stratification exhibits similarly (Figures 9, 10). Further, our simulation results show that the instability of stratification is controlled by a joint impact of spring-neap tidal cycle and typhoons (Figure 10). Stratification is quite unstable and relatively weak during the typhoon period overlapping with the transition from spring tide to neap tides. However, stratification rapidly restores with a significantly enhanced stability after the typhoon passage and during the transition from neap tides to spring tides. In addition, morphological change results in a delay of the restoration by half a day as seen by a comparison between the Run_1970s and Run_2010s, whilst the impact of sea level rise is hardly seen.

Sea-level rise also increases the stability of stratification in the PRE, although the extent is much weaker than that caused by the morphological change (Figure 9; Table 2). The extent also varies among the sites, with maximum increase (by ~15%) at S1 (Zone 2) and S3 (Zone 3), and minimum increase at S4 (Zone 4).

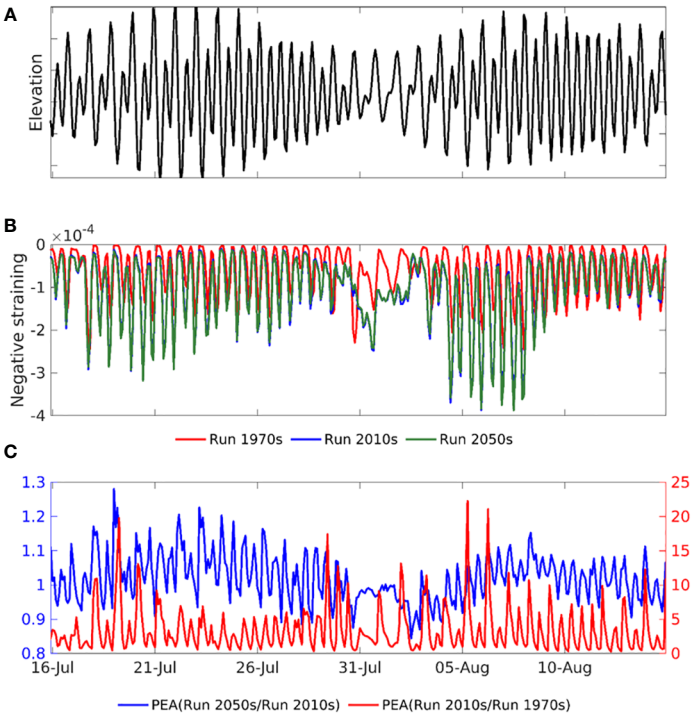

FIGURE 8
Time series of **(A)** water level, **(B)** straining and **(C)** magnification of negative straining due to morphologic change and sea-level rise.

4 Discussion

Geyer and MacCready (2014) provided a quantitative means of classification of estuaries in terms of stratification, which are based on two dimensionless parameters. The first parameter, i.e., the Freshwater Froude number $F_{rf}=U_0/(\beta g S_0 H)^{1/2}$, represents the ratio of the mean river velocity (U_0) to the gravitationally driven exchange flow that is scaled with the water depth H. Here, S_0 is the background ocean salinity and $\beta \cong 7.7\times10^{-4}$ is the coefficient of saline contraction. The second is the mixing parameter $M = [C_d U_t^2/\omega N_0 H^2]^{1/2}$, which measures the ratio between the tidal timescale and the timescale of vertical turbulent mixing. In, $N_0=(\beta g S_0/H)^{1/2}$ is the buoyancy frequency for maximum top to bottom salinity variation in an estuary, where ω is the tidal frequency, U_t is the amplitude of the depth-averaged tidal velocity, $C_d \cong (1–2.5)\times10^{-3}$ is the drag coefficient.

Estuaries can be classified into different stratification conditions based on the freshwater Froude number F_{rf} and the mixing number M (Figure 11). The range of M is calculated from the variation of tidal current velocities and water depth in a spring-neap cycle, whereas the range of F_{rf} is estimated by the variation of the monthly mean river runoff within a year. Many estuaries, including the Puget sound, the Chesapeake Bay, the Pearl River Estuary and the Yangtze River, are characterized by a broad range of M not only due to the variation of spring-neap tides but also owing to the signification variation of water depth (Geyer and MacCready, 2014; Chen, 2018). Data from these estuaries show that M decreases along with an increase in the average water depth, which is evidenced by a decrease of M for the Lingding Bay from the 1970s to the 2010s (Figure 11). Compared to the Yangtze Estuary which mainly falls into the type of salt wedge because of its large F_{rf}, stratification in the PRE in 2010s is more variable and encompasses three types (salt wedge, strongly stratified and partially mixed) in the wet season, and two types (strongly stratified and partially mixed) in the dry season (Chen, 2018). However, F_{rf} of the PRE seems to be underestimated in our simulation, since salt wedge intrusion in the area has been reported by several studies (Mao et al., 2004; Cui et al., 2019) both during the wet and dry seasons. The main reason for underestimation is likely caused by an exclusion of tributaries on the western coast of the bay in our model, therefore U_0 is underestimated in our results.

The morphological change in the Lingding Bay between 1970s and 2010s not only causes a remarkable decrease of M but also a mild decrease of F_{rf}. According to the simulation results in the Run_1970s, stratification in the PRE mainly encompasses three types (salt wedge, strongly stratified and partially mixed) in the wet season, whilst in the dry season salt wedge is replaced by strain-induced periodic stratification (SIPS) (Figure 11). In the Run_2010s, SIPS does not exist in the dry season anymore, and the whole system is shifted toward strongly stratified conditions. By contrast, a sea level rise of 20 cm (Run_2050s) only shows a minor impact on M and F_{rf} when comparing with the Run_2010s scenario. The range of M shifts slightly to the left due to a sea level rise-induced decrease in mixing. The range of F_{rf} remains unchanged, suggesting that a 20 cm-sea level rise alone would not affect river flows in the study area.

The PRE shows both similarity (e.g. decrease of M along with an increase of depth) and difference with other estuaries which have also experienced human-induced deepening. In the Hudson estuary, modification for navigation since the late 1800s has increased the channel depth by 10-30%, which results in a strong salinity intrusion

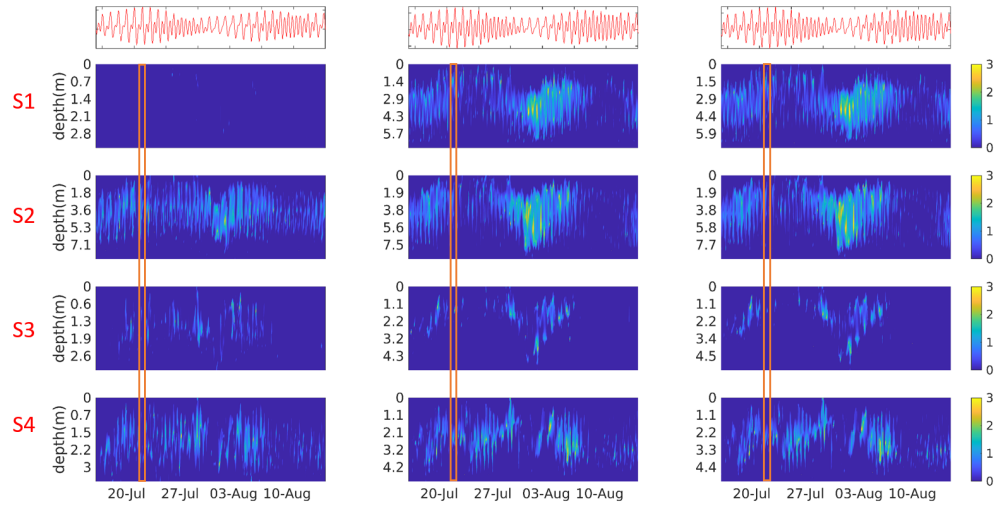

FIGURE 9
Time series of vertical profile of the gradient Richardson number R_i (*plotted in log10*(*Ri*)) in the wet season at the four selected sites in the Run_1970s (left column), Run_2010s (middle column) and Run_2050s (right column). Duration of the typhoon Roke is marked by the orange rectangle.

but almost no change in the estuarine circulation according to the study by Ralston and Geyer (2019), which argued that the import of salt by estuarine circulation is balanced by the export of salt by the mean advection due to river discharge. Our results demonstrated that both the import of salt and the estuarine circulation are enhanced by the morphological change. The difference is likely to be attributed to that (a) the Lingding Bay experienced not only deepening but also reduction in water area by 8.1%, which have consequent impact on tidal velocity and amplitude (Shen et al., 2018), and (b) an exclusion of the effect of tidal mixing in the estimate by Ralston and Geyer (2019).

The relationship between depth change and salt fluxes is nonlinear in estuaries. Chant et al. (2018) found that a relatively small (15%) increase in depth by dredging in a short reach of an estuary may double the exchange salt flux and remarkably increase stratification in the estuary. Ralston and Geyer (2019) found that channel deepening by 10%-30% in the Hudson estuary increases salinity intrusion by 30% and enhanced stratification during neap tides. In the PRE, the channels (Zone 2) were deepened by 49% (4.85m) from 1970s to 2010s, and the salt fluxes are increased by 78%, resulting in an increase of stratification by max. 400% in the channel area. Meanwhile, the west shoal was deepened by 28% along with a significant reduction in its water area, leading to an increase of stratification by max. 700%. These results suggest a highly amplified and irreversible impact of human-induced morphological change on estuarine environments in terms of stratification. It is worth noting that although direct human interventions including sand mining and land reclamation have been banned, other human activities which may also affect morphological change of the estuary, such as channel dredging and river damming, will still continue in future (Liu et al., 2018). An exclusion of potential morphological change caused by reduced sediment input from rivers due to damming or by extreme events (e.g. floods, typhoons) in the future scenario Run_2050s would lead to uncertainties of our estimation. To what extent these natural and anthropogenic drivers would lead to morphological change and consequence on estuarine circulation and stratification in future remains to be explored.

Our simulations show a minor impact of sea level rise (by 20 cm from 2010s to 2050s) on the stratification and circulation in the PRE. However, climate change impacts not only the sea level but also other environmental variables such as temperature and precipitation which have not been taken into account in this study so far. Climate change also seems to cause more frequent occurrence of extreme events such as cyclones (storms) and marine heat waves. The former may strongly affect the stratification at a short-term (as shown in our results), while the latter could cause higher temperature in the surface water, thus enhancing a thermal induced stratification [e.g., the southern North Sea, Chen et al. (2022)]. However, in typical estuarine environments

TABLE 2 Index of stability of stratification at the four sites in the wet season.

Station	Run_1970s	Run_2010s (ref. to 1970s)	Run_2050s (ref. to 2010s)
S1	17	1475(+8576.47%)	1683(+14.10%)
S2	1611	2238(+38.92%)	2384(+6.52%)
S3	208	285(+37.02%)	330(+15.79%)
S4	1045	1517(+45.17%)	1560(+2.83%)

The value represents the number of the time steps in the simulation when the maxium gradient Richardson number log10(Ri)>=1.

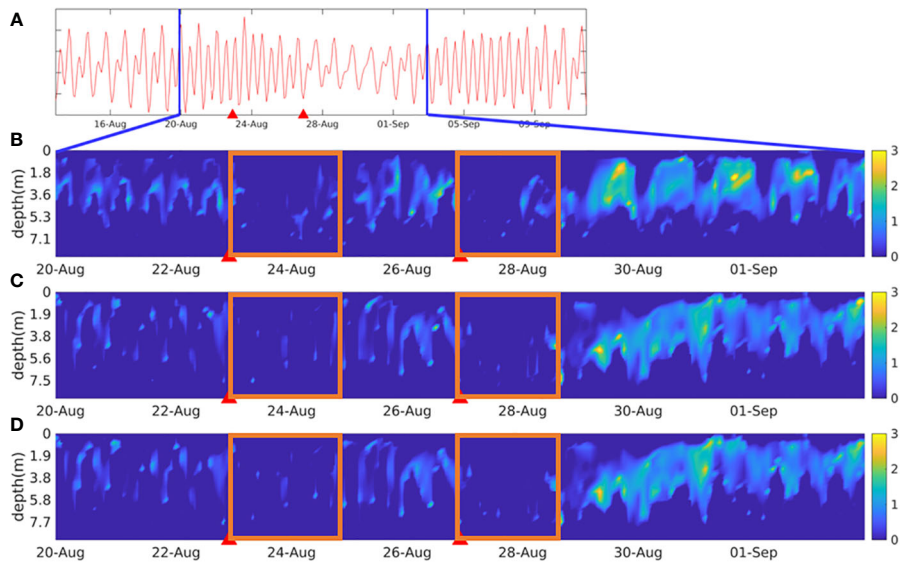

FIGURE 10
Time series of the **(A)** water elevation, and the gradient Richardson number R_i in the **(B)** Run_1970s, **(B)** Run_2010s, and **(D)** Run_2050s at site 2 (Zone 2). The arrival and duration of two typhoons (Hato and Pakhar) are marked by red triangles and orange rectangles, respectively.

such as the PRE where stratification is caused mainly by salinity gradient, we hypothesized that a change in temperature gradient by marine heat waves and enhanced solar radiation would not significantly affect the stratification. To test the impact of sea surface temperature increase on the stratification of PRE, a scenario with an increase of surface water temperature (above the pycnocline) at the open boundary by 2°C and enhanced atmospheric radiation over the entire model domain in summer (July and August). These results confirms our hypothesis and shows that the change in surface water temperature has only minor impact on stratification of the PRE, characterized by a change of the PEA within 5% from the reference level (Supplementary Table 1; Supplementary Figure 2).

Future climate change might affect stratification in the PRE mainly through modified river runoff. Hong et al. (2020) found that the rate of increase in stratification in response to the sea-level rise is higher during the high-flow conditions than that during the low-flow conditions. This might be related to the stability of the stratification, which shows a weaker vertical stratification with lower stability during dry season, and opposite in the wet season. Since river runoff is the main driving factor for monthly-to-seasonal variation

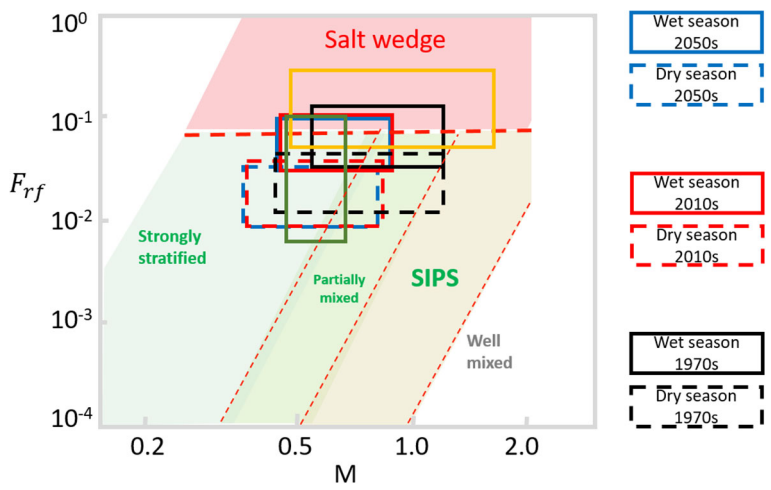

FIGURE 11
Estuarine parameter space with the freshwater Froude number (F_{rf}) and mixing number (M). The red solid line calculated from $\alpha^{-1/2}F_{rf}^{-1/3}M^2 \approx 1$, in which α=3.4, which divides the estuarine parameter space into estuaries that always remain stratified and those that experience boundary-generated mixing during a tidal cycle. The location of PRE in different ages and different seasons are indicated in the figure. The yellow rectangle is the location of North passage Yangtze River according to Chen (2018); the green rectangle represent the Hudson River according to Geyer and Maccready (2014). SIPS is Strain-Induced Periodic Stratification. Modified from Geyer and Maccready (2014).

of stratification in the PRE, how future climate change would affect monsoon intensity and associated river runoff and consequent impact on estuarine stratification remains to be further explored.

5 Conclusion

A high-resolution 3-D hydrodynamic model was used to investigate the impact of mainly human-induced morphological change (from 1970s till 2010s) and climate-induced sea level rise (from 1970s till 2050s) on the stratification in the PRE. The following conclusions are drawn from the simulation results.

1. Morphological change in the Lingding Bay (the main estuary of the PRE) from 1970s to 2010s results in a bay-scale enhancement of stratification by up to four times, with maximum enhancement (up to seven times) at the western shoal of the bay;
2. Stratification in the PRE becomes more sensitive to tidal and river runoff impact after the morphological change. The variation is greatly amplified by the spring-neap tidal cycle. The maximum enhancement in stratification occurs in the transition period from neap to spring tides due to the increase of advection of salinity variance;
3. The relationship between depth change and salt fluxes is nonlinear and varies among different morphological units. In the PRE, the eastern channel and the western shoal experience the greatest enhancement in both strength and stability of stratification caused by the morphological change;
4. Compared to an overwhelming impact of human-induced morphological change in the past few decades, future change of stratification driven by sea level rise would be further strengthened but to a much less extent. The maximum enhancement associated with sea level rise occurs in spring tides due to the increased negative straining;

Our results suggest a highly amplified and irreversible impact of human-induced morphological change on estuarine environments in terms of stratification, which should be taken into account in future planning of estuaries. The results of our researches might have potential implications for the estuarine management, in particular, human intervention such as the planning of land reclamation or sand mining in Lingding Bay, etc. As the human intervention is the main driving factor of variations of the hydrodynamic environment in PRE. With the deepening of channels as well as the average depth of Lingding Bay, the stratification becomes more stable and extends in space. Cui et al. (2019) found that the spatial distribution of coastal hypoxia can be well predicted by the overlapping zone between river plume and salt wedge. Therefore, the distribution of stratification is highly relevant to the occurrence of hypoxia in the PRE. Our model is suitable for further scenario studies to assess the impact of climate change and human intervention on estuaries.

Data availability statement

The original contributions presented in the study are included in the article/Supplementary Material. Further inquiries can be directed to the corresponding authors.

Author contributions

MM, WZ and CS contributed to conception and design of the study. JD provided the morphological data. MM collected the database, developed the model set-up and model validation and performed all analysis. WZ supervised the analysis of simulation results. MM and WZ wrote the first draft of the manuscript. All authors contributed to manuscript revision. All authors contributed to the article and approved the submitted version.

Funding

This study is a contribution to the Helmholtz PoF programme "The Changing Earth – Sustaining our Future" on its Topic 4: Coastal zones at a time of global change. It also contributes to the theme "C3: Sustainable Adaption Scenarios for Coastal Systems" of the Cluster of Excellence EXC 2037 'CLICCS - Climate, Climatic Change, and Society' – Project Number: 390683824 funded by the Deutsche Forschungsgemeinschaft (DFG, German Research Foundation) under Germany's Excellence Strategy. JD was supported by the National Natural Science Foundation of China, China (NSFC, Grant No. 41806100; NSFC-FDCT, Grant No., 42161160305).

Acknowledgments

Many thanks to Peter Arlinghaus and Lucas Porz for their help in the early stage of model build-up.

Conflict of interest

The authors declare that the research was conducted in the absence of any commercial or financial relationships that could be construed as a potential conflict of interest.

Publisher's note

Supplementary material

The Supplementary Material for this article can be found online at: https://www.frontiersin.org/articles/10.3389/fmars.2023.1072080/full#supplementary-material

References

Cameron, W. M., and Pitchard, D. W. (1963). "Estuaries." In The Sea. Ed. M. N. Hill. 2 306–324.

Chant, R. J., Sommerfield, C. K., and Talke, S. A. (2018). Impact of channel deepening on tidal and gravitational circulation in a highly engineered estuarine basin. *Estuaries Coasts* 41 (6), 1587–1600. doi: 10.1007/s12237-018-0379-6

Chegini, F., Holtermann, P., Kerimoglu, O., Becker, M., Kreus, M., Klingbeil, K., et al. (2020). Processes of stratification and destratification during an extreme river discharge event in the German bight ROFI. *J. Geophys. Res.: Oceans* 125 (8). doi: 10.1029/2019jc015987

Chen, W. (2018). *Dynamics of currents and sediment in estuaries with different density stratifications* (Doctoral dissertation, Utrecht University). Available at: https://dspace.library.uu.nl/handle/1874/362308.

Cheng, P., Valle-Levinson, A., and de Swart, H. E. (2011). A numerical study of residual circulation induced by asymmetric tidal mixing in tidally dominated estuaries. *J. Geophys. Res.: Oceans* 116 (C1). doi: 10.1029/2010JC006137

Chen, W., Staneva, J., Grayek, S., Schulz-Stellenfleth, J., and Greinert, J. (2022). The role of heat wave events in the occurrence and persistence of thermal stratification in the southern north Sea. *Natural Hazards Earth System Sci.* 22 (5), 1683–1698. doi: 10.5194/nhess-22-1683-2022

Chua, V. P., and Xu, M. (2014). Impacts of sea-level rise on estuarine circulation: An idealized estuary and San Francisco bay. *J. Mar. Syst.* 139, 58–67. doi: 10.1016/j.jmarsys.2014.05.012

Couldrey, M. P., Gregory, J. M., Dong, X., Garuba, O., Haak, H., Hu, A., et al (2022). Greenhouse-gas forced changes in the Atlantic meridional overturning circulation and related worldwide sea-level change. *Climate Dyn.* doi: 10.1007/s00382-022-06386-y

Cui, Y., Wu, J., Ren, J., and Xu, J. (2019). Physical dynamics structures and oxygen budget of summer hypoxia in the pearl river estuary. *Limnol. Oceanogr.* 64 (1), 131–148. doi: 10.1002/lno.11025

Dai, S., Yang, S., and Cai, A. (2007). Variation of sediment discharge of the pearl river basin from 1955 to 2005. *Acta GEOGRAPHICA SINICA-CHINESE EDITION-* 62 (5), 554.

Deng, J., Yao, Q., and Wu, J. (2020). Estuarine morphology and depositional processes in front of lateral river-dominated outlets in a tide-dominated estuary: A case study of the lingding bay, south China Sea. *J. Asian Earth Sci.* 196. doi: 10.1016/j.jseaes.2020.104382

Geyer, W. R., and MacCready, P. (2014). The estuarine circulation. *Annu. Rev. fluid mechanics* 46, 175–197. doi: 10.1146/annurev-fluid-010313-141302

Gong, W., and Shen, J. (2011). The response of salt intrusion to changes in river discharge and tidal mixing during the dry season in the modaomen estuary, China. *Continental Shelf Res.* 31 (7-8), 769–788. doi: 10.1016/j.csr.2011.01.011

Han, Z., Xie, H., Li, H., Li, W., Wen, X., and Xie, M. (2021). Morphological evolution of the lingding channel in the pearl river estuary over the last decades. *J. Coast. Res.* 37 (1), 104–112. doi: 10.2112/JCOASTRES-D-19-00187.1

Hong, B., Liu, Z., Shen, J., Wu, H., Gong, W., Xu, H., et al. (2020). Potential physical impacts of sea-level rise on the pearl river estuary, China. *J. Mar. Syst.* 201, 103245. doi: 10.1016/j.jmarsys.2019.103245

Hong, B., and Shen, J. (2012). Responses of estuarine salinity and transport processes to potential future sea-level rise in the Chesapeake bay. *Estuarine Coast. Shelf Sci.* 104-105, 33–45. doi: 10.1016/j.ecss.2012.03.014

Kennish, M. J. (2003). *Estuarine research, monitoring, and resource protection*. (Boca Raton, FI, USA: CRC Press). Available at: https://books.google.de/books?id=UdICWCidu9oC&redir_esc=y.

Li, X., Geyer, W. R., Zhu, J., and Wu, H. (2018b). The transformation of salinity variance: A new approach to quantifying the influence of straining and mixing on estuarine stratification. *J. Phys. Oceanogr.* 48 (3), 607–623. doi: 10.1175/JPO-D-17-0189.1

Li, L., He, Z., Xia, Y., and Dou, X. (2018a). Dynamics of sediment transport and stratification in changjiang river estuary, China. *Estuarine Coast. Shelf Sci.* 213, 1–17. doi: 10.1016/j.ecss.2018.08.002

Liu, Z., and Gan, J. (2020). A modeling study of estuarine–shelf circulation using a composite tidal and subtidal open boundary condition. *Ocean Model.* 147. doi: 10.1016/j.ocemod.2019.101563

Liu, F., Hu, S., Guo, X., Luo, X., Cai, H., and Yang, Q. (2018). Recent changes in the sediment regime of the pearl river (South china): Causes and implications for the pearl river delta. *Hydrol Processes* 32 (12), pp.1771–1785. doi: 10.1002/hyp.11513

Li, R., Xu, J., Li, X., Shi, Z., and Harrison, P. J. (2017). Spatiotemporal variability in phosphorus species in the pearl river estuary: influence of the river discharge. *Sci. Rep.* 7 (1), 1–13. doi: 10.1038/s41598-017-13924-w

Luo, L., Li, S., and Wang, D. (2009). Hypoxia in the pearl river estuary, the south China Sea, in July 1999. *Aquat. Ecosystem Health Manage.* 12 (4), 418–428. doi: 10.1080/14634980903352407

MacCready, P., Geyer, W. R., and Burchard, H. (2018). Estuarine exchange flow is related to mixing through the salinity variance budget. *J. Phys. Oceanogr.* 48 (6), 1375–1384. doi: 10.1175/JPO-D-17-0266.1

Mao, Q., Shi, P., Yin, K., Gan, J., and Qi, Y. (2004). Tides and tidal currents in the pearl river estuary. *Continental Shelf Res.* 24 (16), 1797–1808. doi: 10.1016/j.csr.2004.06.008

Masson-Delmotte, V., Zhai, P., Pirani, A., Connors, S. L., Péan, C., Berger, S., et al. (2021). Climate change 2021: the physical science basis. contribution of working group I to the sixth assessment report of the intergovernmental panel on climate change 2. (Cambridge, United Kingdom and New York, NY, USA: Cambridge University Press), 2391. doi: 10.1017/9781009157896

Pritchard, H. B. (1995). Estuarine circulation patterns: American Society of Civil Engineers Proceedings.

Ralston, D. K., and Geyer, W. R. (2019). Response to channel deepening of the salinity intrusion, estuarine circulation, and stratification in an urbanized estuary. *J. Geophys. Res.: Oceans* 124 (7), 4784–4802. doi: 10.1029/2019jc015006

Shen, Y., Jia, H., Li, C., and Tang, J. (2018). Numerical simulation of saltwater intrusion and storm surge effects of reclamation in pearl river estuary, China. *Appl. Ocean Res.* 79, 101–112. doi: 10.1016/j.apor.2018.07.013

Simpson, J. H., and Bowers, D. (1981). Models of stratification and frontal movement in shelf seas. *Deep Sea Res. Part A. Oceanogr. Res. Papers* 28 (7), 727–738. doi: 10.1016/0198-0149(81)90132-1

Tang, Y., Xi, S., Chen, X., and Lian, Y. (2016). Quantification of multiple climate change and human activity impact factors on flood regimes in the pearl river delta of China. *Adv. Meteorol.* 2016. doi: 10.1155/2016/3928920

Valentim, J. M., Vaz, L., Vaz, N., Silva, H., Duarte, B., Caçador, I., et al. (2013). Sea Level rise impact in residual circulation in tagus estuary and ria de aveiro lagoon. *J. Coast. Res.* 65 (10065), 1981–1986. doi: 10.2112/SI65-335.1

Wang, T., Geyer, W. R., and MacCready, P. (2017). Total exchange flow, entrainment, and diffusive salt flux in estuaries. *J. Phys. Oceanogr.* 47 (5), 1205–1220. doi: 10.1175/JPO-D-16-0258.1 https://www.hko.gov.hk/hko/publica/reprint/r556.pdf

Wong, L., Chen, J., and Dong, L. (2004). A model of the plume front of the pearl river estuary, China and adjacent coastal waters in the winter dry season. *Continental Shelf Res.* 24 (16), 1779–1795. doi: 10.1016/j.csr.2004.06.007

Wong, W., Li, K., and Yeung, K. (2003). Long term sea level change in Hong Kong. *Hong Kong Meteorol. Soc. Bull.* 13 (1-2), 24–40. Available at: https://www.hko.gov.hk/hko/publica/reprint/r556.pdf

Wu, Z. Y., Saito, Y., Zhao, D. N., Zhou, J. Q., Cao, Z. Y., Li, S. J., et al. (2016). Impact of human activities on subaqueous topographic change in lingding bay of the pearl river estuary, China, during 1955-2013. *Sci. Rep.* 6, 37742. doi: 10.1038/srep37742

Xu, H., Lin, J., and Wang, D. (2008). Numerical study on salinity stratification in the pamlico river estuary. *Estuarine Coast. Shelf Sci.* 80 (1), 74–84. doi: 10.1016/j.ecss.2008.07.014

Yuan, R., Zhu, J., and Wang, B. (2015). Impact of sea-level rise on saltwater intrusion in the pearl river estuary. *J. Coast. Res.* 31 (2), 477–487. doi: 10.2112/JCOASTRES-D-13-00063.1

Yu, L., Gan, J., Dai, M., Hui, C. R., Lu, Z., and Li, D. (2021). Modeling the role of riverine organic matter in hypoxia formation within the coastal transition zone off the pearl river estuary. *Limnol. Oceanogr.* 66 (2), 452–468. doi: 10.1002/lno.11616

Zhang, Y., Ren, J., and Zhang, W. (2020). Flocculation under the control of shear, concentration and stratification during tidal cycles. *J. Hydrol.* 586, 124908. doi: 10.1016/j.jhydrol.2020.124908

Zhang, Y., Ren, J., Zhang, W., and Wu, J. (2021b). Importance of salinity-induced stratification on flocculation in tidal estuaries. *J. Hydrol.* 596, 126063. doi: 10.1016/j.jhydrol.2021.126063

Zhang, Q., Sun, X., Zhang, K., Liao, Z., and Xu, S. (2021a). Trade-offs and synergies of ecosystem services in the pearl river delta urban agglomeration. *Sustainability* 13 (16), 9155. doi: 10.3390/su13169155

Zhang, Z., Wu, H., Yin, X., and Qiao, F. (2018). Dynamical response of changjiang river plume to a severe typhoon with the surface wave-induced mixing. *J. Geophys. Res.: Oceans* 123 (12), 9369–9388. doi: 10.1029/2018JC014266

Zhang, W., Yan, Y., Zheng, J., Li, L., Dong, X., and Cai, H. (2009). Temporal and spatial variability of annual extreme water level in the pearl river delta region, China. *Global Planetary Change* 69 (1-2), 35–47. doi: 10.1016/j.gloplacha.2009.07.003

Zhang, Y. J., Ye, F., Stanev, E. V., and Grashorn, S. (2016). Seamless cross-scale modeling with SCHISM. *Ocean Model.* 102, 64–81. doi: 10.1016/j.ocemod.2016.05.002

Zhao, M., Yang, D., Wang, P., and Shi, P. (2015). A market-based approach to marine sand resource management in the pearl river estuary, China. *Ocean Coast. Manage.* 105, 56–64. doi: 10.1016/j.ocecoaman.2014.12.012

Appendix B

Physical mechanisms, dynamics and interconnections of multiple estuarine turbidity maximum in the Pearl River estuary

frontiers | Frontiers in Marine Science

TYPE Methods
PUBLISHED 24 May 2024
DOI 10.3389/fmars.2024.1385382

OPEN ACCESS

EDITED BY
Wb Cheng,
Center, Taiwan

REVIEWED BY
Maarten Van Der Vegt,
Utrecht University, Netherlands
Yu-Pei Chang,
National Central University, Taiwan

*CORRESPONDENCE
Mengyao Ma
mengyao.ma@hereon.de
Wenyan Zhang
wenyan.zhang@hereon.de

RECEIVED 13 February 2024
ACCEPTED 09 May 2024
PUBLISHED 24 May 2024

CITATION
Ma M, Porz L, Schrum C and Zhang W (2024) Physical mechanisms, dynamics and interconnections of multiple estuarine turbidity maximum in the Pearl River estuary. *Front. Mar. Sci.* 11:1385382. doi: 10.3389/fmars.2024.1385382

Physical mechanisms, dynamics and interconnections of multiple estuarine turbidity maximum in the Pearl River estuary

Mengyao Ma[1,2]*, Lucas Porz[1], Corinna Schrum[1,2] and Wenyan Zhang[1]*

[1]Institute of Coastal Systems – Analysis and Modeling, Helmholtz-Zentrum Hereon, Geesthacht, Germany, [2]Institute of Oceanography, Center for Earth System Research and Sustainability, University of Hamburg, Hamburg, Germany

The formation and dynamics of individual estuarine turbidity maximum (ETM) in the Pearl River estuary (PRE) have been investigated but the temporal variability of the ETMs and interconnections among them remain poorly understood. To address these open questions, the distribution and transport of suspended particulate matter (SPM) in the PRE for the period of 2017–2020 are investigated by numerical modeling. The simulated sediment transport flux is decomposed into several major components associated with specific physical processes. Then, the relative contribution of each component to the formation of the ETMs is evaluated. Results suggest the coexistence of three prominent ETMs in the Lingding Bay of the PRE. They are formed by different physical mechanisms and characterized by remarkable seasonality in the spatial extension. In the two ETMs located at the west shoal and middle shoal, advection dominates the sediment transport flux, whilst tidal pumping plays a crucial role in maintaining the ETMs. A sharp bathymetric gradient leads to an entrapment of sediment flux within the bottom layer in the west channel ETM, a phenomenon referred to as topographical trapping. The interconnection analysis shows that the sediment transport between the ETMs varies with seasons, which is attributed to the variation of stratification driven by the monsoon-mediated river runoff. Our results provide new insights into the physical dynamics and interconnections of the ETMs in the PRE, which can serve as scientific base for estuarine sediment management and engineering.

KEYWORDS

estuarine turbidity maximum, advection, tidal pumping, interconnection, model sensitivity

1 Introduction

Estuaries, as part of the transition zone between land and ocean, are highly dynamic in terms of physical transport and biogeochemical cycling. They serve as transient or long-term sinks of sediments delivered by river runoff and tidal currents. Estuarine turbidity maxima (ETMs) are zones of elevated concentration of suspended sediments that often occur in estuaries, and exert a significant influence on the morphological development, biogeochemical cycling, and contaminant redistribution of estuaries (Wai et al., 2004; Etcheber et al., 2007; Cheng et al., 2013; Zhang et al., 2020; Moriarty et al., 2021).

ETMs are often located near the head of the salt intrusion where the suspended sediment concentration (SSC) is higher than that in the upstream and downstream sides of the estuary (Dyer, 1988). However, the SPM dynamics in the ETMs exhibit significant differences among estuaries, depending on local topography, fluvial, and tidal forcing. The formation of ETMs can be attributed to estuarine gravitational circulation, tidal pumping and straining, sediment resuspension and settling, river discharge, and topographical trapping (Burchard et al., 2018). Among all driving factors, tidal pumping is often reported as the dominant factor for ETM formation, which has been reported in well-mixed macrotidal estuaries (Yu et al., 2014), partially stratified estuaries (Scully and Friedrichs, 2007) and highly stratified estuaries (Garel et al., 2009). Tidal pumping denotes the barotropic, tide-induced transport of suspended sediment. It is considered to be mainly caused by tidal current asymmetry between the ebb and flood phase, and sediment lag effects (Uncles and Stephens, 1989; Brenon and Le Hir, 1999; Scully and Friedrichs, 2007). The latter refers to the phase lag between the velocity and the variation of SSC during the flood and ebb phase (Sommerfield and Wong, 2011). Tidal trapping occurs when the cross-sectionally averaged velocity and SPM signals are out of quadrature (MacVean and Stacey, 2011).

In estuaries with distinct seasonal variations in river runoff, variation of the ETM is also characterized by seasonality. For instance, in the Changjiang River, the ETM is located further upstream and with higher concentration in the dry season than in the wet season since the relative impact of tide currents is more significant in the dry season due to reduced river runoff (Hua et al., 2020). Seasonal enhancement of stratification due to increased river runoff can influence the concentration of the ETM by suppressing turbulence, which leads to a rapid accumulation of sediment near the bottom, as reported by Geyer (1993). In addition, seasonal change of wind-induced currents can also cause a landward or seaward shift of the ETM (Rao et al., 2011). In an idealized convergent partially mixed estuary investigated by Gong et al. (2023), it was demonstrated that the down-estuary wind enhances estuarine circulation and salt intrusion, thereby shifting the ETM landward and increasing SSC through an increase in bottom stress. Existing observations in numerous estuaries demonstrate that ETMs are not necessarily correlated with the limits of stratification or tidal propagation. Some ETMs appear to be spatially locked and are associated with bathymetric transitions (Burchard et al., 2018). Examples are seen in the Chesapeake Bay (North and Houde, 2001) and the Danshui River (Chen et al., 2015). Formation of ETMs due to topography-induced sediment convergence and enhanced deposition are also noted in the San Francisco Bay (Schoellhamer, 2000) and the Hudson River Estuary (Ralston et al., 2012).

In estuaries characterized by multiple ETMs, the response to a change in river runoff, tidal forcing, temperature, and salinity change may vary among the ETMs. For instance, a double ETM structure in the Nam Trieu estuary was found by Vinh and Ouillon (2021), with the downstream part of the double ETM resulting from gravitational circulation and the upstream part driven by tidal pumping.

The Pearl River Estuary (PRE) is the second largest river in terms of water discharge and the third largest river in terms of sediment loading in China (Liu et al., 2018). A rapid development of the economy and associated human activities, such as channel dredging, sand mining, and land reclamation, have caused an irreversible change in the estuarine circulation, stratification, and morphological change of the PRE during the past few decades (Ma et al., 2023). In the PRE, it has been reported that the formation of ETM is influenced by a combined effect of tides, river discharge, and topography, wherein sediment resuspension dominates the variation of ETM (Liu et al., 2016; Cui et al., 2022). According to existing observations, multiple ETMs are found in the upper and lower parts of the PRE (Wai et al., 2004; Yang and Liu, 2015b; Liu et al., 2016; Cui et al., 2022). ETMs in the upper estuary were observed between Qi'ao Island and Neilingding Island (Figure 1). The intensity and extent of the ETMs are weaker during the wet season than during the dry season as a result of variation of stratification, and the center of the ETMs moves upstream following the movement of salt wedge by a distance of ~10 km during wet seasons (Liu et al., 2016). Based on the analysis of observation data, Wai et al. (2004) proposed that gravitational circulation and tidal pumping are the principal formation mechanisms of the ETMs. However, a model study conducted by Liu et al. (2016) argued that sediment resuspension and vertical circulation are the major controlling factors of the ETMs in the upper estuary. In the lower estuary, an ETM was observed close to the west channel, in the west of Lantau island, in the wet season (Cui et al., 2022). In this ETM, particle resuspension induced by tidal pumping and straining significantly increases the concentration of SPM in the bottom layer.

In addition to the gravitational circulation and tides, complex geographical and topographical features of many estuaries exert a non-negligible influence on the dynamics of ETMs, including the sediment exchange between different geographical units (Leuven et al., 2019; Zhang et al., 2021a; Teng et al., 2022; Wang et al., 2022). The PRE is featured by a channel-shoal system superposed by various obstacles such as outcrops and islands (Figure 1). It has been reported that the lateral sediment flux from the channel to the west shoal leads to a large depositional rate (3.0–5.0 cm yr^{-1}) at the western part of the estuary, together with the formation of an ETM (Zhang et al., 2021a). However, according to our knowledge, there is no study investigating the dynamics of the ETMs across multiple time scales (from tides to multiple years) and potential interconnections between the ETMs in the PRE. Given the large natural topographic variation that is further complicated by

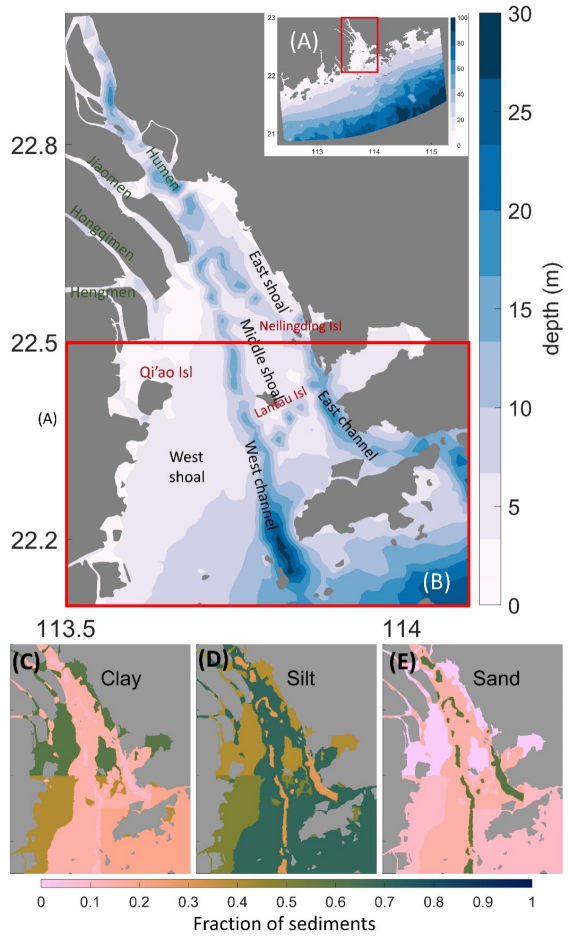

FIGURE 1
(A) The study area. The red box indicates the range of the Lingding Bay. The topographical features of the Lingding Bay are shown in **(B)**, the red box indicates the focus area in this study. The sediment map shows the spatial distribution of clay **(C)**, silt **(D)**, and sand **(E)**, respectively. Sediment data stem from Zhang et al. (2019) for the Lingding Bay and from Wang and Li (2014) for the outer estuary and shelf area.

intensive human activities and sea level rise (Yuan et al., 2015; Wu et al., 2016; Lin et al., 2021), a comprehensive understanding of the spatio-temporal dynamics of ETMs becomes increasingly vital.

In this study, we aim to fill the knowledge gap in understanding the spatio-temporal dynamics of ETMs across multiple time scales from tides, to multiple years and potential interconnections between the ETMs in the PRE. We applied a high-resolution 3-dimensional hydrodynamics-sediment transport model to investigate the sediment transport and dynamics of ETMs in the PRE from 2017 to 2020. Based on model validation by observation, we decomposed the simulated sediment transport into major components associated with specific physical mechanisms to identify the relative contribution and variability of the drivers. We then investigated the stability/variability of the ETMs and their future fates associated with climate change. The derived conclusions may help to inform coastal and estuarine spatial planning strategies in the context of climate change mitigation.

2 Study area

The PRE, with its major part located in the Lingding Bay, is situated in the south of China, connecting to the South China Sea (Figure 1). Morphology of the Lingding Bay is generally characterized by three distinct shoals separated by two navigation channels, namely the east channel and the west channel. The west shoal has the most extensive area and is proximate to the trio of Pearl River outlets, designated as Jiaomen, Hongqimen, and Hengmen, arrayed from north to south, respectively. The suspended sediment in the PRE has a mean concentration of ~200 mg L^{-1} and an annual flux of about 30 million tons, of which more than 90% is discharged during the wet season. About 80% of the discharged sediment is deposited within the estuary, and the rest is transported offshore to the continental shelf (Wai et al., 2004).

The characteristics of suspended sediment in terms of particle size and settling velocity spread over a wide spectrum in the PRE. The median grain size of suspended sediments is reported to vary between 10 and 100 $\mu m$and the settling velocity is between 0.001 and 0.02 cm s^{-1} (Xia et al., 2004). Sediment distribution map shows that the abundance of clay (diameter< 2 μm) is generally low in most areas except near the northeast and southwest coasts, while silt (diameter between 2 and 63 μm) is abundant in the whole PRE except for the waterways and channels, where the bottom is mostly (>70%) covered by sands (Figures 1D, E).

The tides in the PRE are of asymmetric, semi-diurnal and partially mixed type in which the tidal fluctuations between two consecutive tides may have different amplitudes. The tidal range is between 1.0 and 1.7 m in a major part of the estuary, with maximum value up to 3.7 m in some local parts (Mao et al., 2004). A gradual increase in the flood-to-ebb duration ratio is observed downstream and eastward, with a notable dependency of tidal duration asymmetry on river discharge rates. A substantially increased river discharge amplifies the ebb duration during the wet seasons (Mao et al., 2004).

3 Methods and data

3.1 Numerical model

3.1.1 Hydrodynamic setup

We applied the Semi-implicit Cross-scale Hydrodynamic Integrated System Model (SCHISIM) (Zhang et al., 2016). SCHISM solves the Reynolds averaged Navier-Stokes equations using unstructured grids, which allow us to adequately account for coastal dynamics over the complex topography with fine spatial resolution. Effect of wind-waves is included in SCHISM though a coupling to the third-generation, unstructured-grid Wind Wave Model III (WWM III).

The model domain covers the PRE and its eight river outlets spanning from 21 to 23°N in latitude and 112.4 to 115.25°E in longitude (Figure 1A). The grid resolution is ~50 m in the Lingding Bay and gradually coarsens to approximately 1000 at the open boundary on the South China Sea shelf. The vertical plane is divided

into 26 maximum layers. A terrain-following grid is employed near the bottom of the model domain. The number of vertical layers is different between shallow and deep water. In shallow water, the number of vertical layers is reduced, for instance, to a single layer in areas with depth less than 0.4 m. Whilst the number of layers becomes increasingly larger in deeper water, until reaching 26 layers in the deepest cell (~100 m) of the model domain. To ensure a high-resolution modeling for the bottom transport, the vertical grid has been designed with a resolution of approximately 0.5 m for the bottom-most layer throughout the entire model domain. The open boundary is forced by 8 major tidal constituents (M2, S2, N2, K2, K1, O1, P1, Q1) superposed by the regional circulation provided by the CMEMS product (doi.org/10.48670/moi-00021). Monthly discharge rates were specified at each of the river outlets. The ECMWF ERA5 reanalysis was used as atmospheric forcing. The model was used to reproduce hydrodynamics and sediment transport from July 2017 to September 2020. A detailed model configuration for hydrodynamics is provided in Ma et al. (2023), including the validation of water level variation and velocity field.

3.1.2 Sediment setup

The sediment model (SED3D) integrated into SCHISM, described in detail in Pinto et al. (2012), is adapted from the Community Sediment Transport Model (Warner et al., 2008). The sediment model calculates erosion, deposition, suspended load, and bed load transport of multiple sediment classes. Classes of suspended sediment are represented by tracer concentration values with sinking velocities dependent on grain size. The transport of these particles is managed by the implicit schemes of the hydrodynamic core. In this study, the critical shields parameter from Soulsby (1997) was used to specify the threshold for erosion of each sediment class. Bed load transport is neglected since it does not contribute to the dynamics of SPM and the formation of ETMs.

We implemented three sediment classes, namely clay, silt, and fine sands (Table 1), according to the sediment map from Zhang et al. (2019) for the Lingding Bay and that from Wang et al. (2014) for the outer estuary and shelf area. The initial fraction of each sediment class (Figures 1C–E) in the seabed was specified according to the compiled sediment map.

At the river boundary, the monthly sediment loading data obtained from the Sediment Report of China (http://www.mwr.gov.cn/sj/tjgb/zghlnsgb/) were implemented. In order to distinguish the source of SPM in the model domain, six sediment classes were defined in the simulation. These included three classes (clay, silt, and fine sand) explicitly delivered by river discharge during the simulation period, and three classes (clay, silt, and fine sand) initially from the local seabed in the study area.

with the intention of exploring the interconnections between the ETMs in the PRE, an additional dedicated model experiment was performed in which erodible silt (Table 1) is placed at the seabed of three sites where the nucleus of the three ETMs are located, as illustrated in Figure 2. Meanwhile, other parts of the seabed are specified as hard bottom and sediment input from the rivers, and the open boundary is set to zero, ensuring that there are no other sediment sources for the ETMs. The silt placed at each site is classified as an independent sediment class (e.g. silt from the TM_shoalw is labeled as Silt_TM_shoalw) despite that the same physical properties (Table 1) are used so that the transport of each class can be traced individually and their relative contribution to the ETMs can be quantified. The simulation period also covers the time from July 2017 to September 2020.

3.2 Data

Observation data provide important means for parameterization, initialization, calibration and validation of the model.

In General, fine-grained sediment can be classified into three-grain size classes, namely clay (0–0.004 mm), silt (0.004–0.063 mm), and sand (0.063–2 mm) according to Shepard (1954). In this study, the exact grain size of each class is configured (Table 1) based on observations from Xia et al. (2004) and Zhang et al. (2019). The settling velocity and erosion rate for each class are obtained from Xia et al. (2004) and Arlinghaus et al. (2022). For the erosion rate and critical shear stress of each class, the general formula by Winterwerp et al. (2012) are applied.

Data from Zhang et al. (2019) show that the area exhibits low clay abundance, with exceptions near the northeast and southeast coastlines. The sediment map exhibits a high abundance of silt, which is present throughout the PRE, with the exception of the channels, which are dominated by sand. The sand content exceeds 70% in channels.

The time series observation of SPM on 25–26 August 2018 at a site on the west shoal (Zhang et al., 2020) was used to calibrate the sediment model. The available data for the validation of the location of ETMs were obtained from a number of sources (Yang and Liu, 2015a; Liu et al., 2016; Cui et al., 2022). The distribution of SPM and salinity of a transect was utilized to validate the model result, which was derived from Cui et al. (2022). A full list of data sources is provided in Table 2.

TABLE 1 Configuration of sediment classes in the model.

Sediment class	D50 (mm)	Settling velocity (mm s^{-1})	Erosion rate (s m^{-1})	Critical shear stress for resuspension (Pa)
Clay	0.00184	0.0082	2.15×10^{-4}	0.4
Silt	0.0317	0.2	8.15×10^{-4}	0.11
Sand	0.303	25	3×10^{-5}	9.9

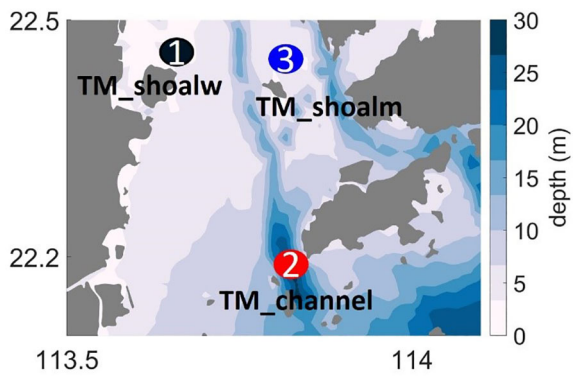

FIGURE 2
Location of the sites where erodible silt is placed in the experiment for analysis of interconnections between the ETMs.

3.3 Decomposition of sediment transport

Based on the analytical method of mass transport flux proposed by Dyer (1974), and using the relative depth as a vertical coordinate instead of absolute depth, Jilan and Kangshan (1986) decomposed cross-sectional currents for analysis of respective forcing. The same method was applied by (Wai et al., 2004) to investigate tidally averaged sediment transport, the sediment transport was decomposed into non-tidal drift, stokes drift, tidal pumping, vertical gravitational circulation, and a term resulting from scouring and settling activities.

Utilizing the aforementioned decomposition methodology, the terms derived from the model results were reassessed in terms of their actual contribution to sediment transport. This re-evaluation process ensures a more accurate understanding of each term's role within the sediment transport. We made the decomposition of sediment transportation as follows:

Sediment transport flux at each grid cell is calculated by:

$$f = \int_{-h}^{n} ucdz, \tag{1}$$

Where f is the sediment flux, h is the local water depth, η is the sea surface elevation, z is the vertical coordinate with zero at the mean sea level, $u(z)$ is the current velocity with a vertical structure and $c(z)$ is the SSC which also varies vertically.

h is composed of a tidally averaged value (h_0) and its deviation $h_t(t)$:

$$h(t) = h_0 + h_t(t)\,. \tag{2}$$

The current velocity u is composed of a vertical averaged value ($\bar{u}$) and its deviation ($u_v(z)$):

$$u(z) = \bar{u} + u_v(z), \tag{3}$$

where $\bar{u}$ varies with time (e.g., tides). Thus $\bar{u}$ is composed of a tidally averaged value u_0 and its deviation $u_t(t)$.

$$\bar{u}(t) = \overline{u_0} + \overline{u_t(t)} \tag{4}$$

Thus, the combination of Equations 3, 4 allows for the decomposition of current velocity to be expressed as follows:

$$u = \overline{u_0} + \overline{u_t(t)} + u_v(z,t) \tag{5}$$

Following the method for velocity decomposition, the concentration of sediment can also be decomposed into similar terms:

$$c = \overline{c_0} + \overline{c_t(t)} + c_v(z,t) \tag{6}$$

TABLE 2 Data sources used for model initialization (Init.), setup parameterization (Param.), forcing (Forc.), and model validation (Valid.).

Type	Use	Time	Description	Source/provider
Sediment fraction	Init.	1999–2007	Percentage of clay, silt, and sand at 240 sites sampled in July 1999 and 106 sites sampled in August 2007	(Zhang et al., 2019)
Sediment fraction	Init.	2007	Surface sediment map of the PRE	(Zhang et al., 2021a)
Sediment classes	Param.	January and July 1999	Particle size and settling velocity of SPM	(Xia et al., 2004)
Sediment classes	Param.	–	Setting velocity of clay	(Arlinghaus et al., 2022)
sediment model parameter	Param.	2002/2003 and 2014/2015	Model parameterization for erosion rates	(Porz et al., 2021)
Sediment loading	Forc.	2017–2020	Monthly sediment loading from the river outlets	Sediment report of China http://www.mwr.gov.cn/sj/tjgb/zghlnsgb/
Hydrodynamics	Forc.	2017–2020	Model setup for tides, river discharge, open boundary forcing, and atmospheric forcing	(Ma et al., 2023)
ETMs	Valid.	1978–2012	Spatial distribution of ETMs in the upper part of the PRE based on observation	(Yang and Liu, 2015b)
ETMs	Valid.	-	Distribution of ETMs in the upper part of the PRE based on model study	(Liu et al., 2016)
ETMs	Valid	August 2019	Observed vertical SPM distribution	(Zhang et al., 2021b)
ETMs	Valid.	July 2020	ETM in the lower part of the PRE based on observation	(Cui et al., 2022)

The instantaneous sediment transport flux is calculated based on the decomposition of depth (Equation 2), current velocity (Equation 5), and SPM concentration (Equation 6). The resulting equation is as follow:

$$f = (h_0 + h_t(t))\left(\overline{u_0} + \overline{u_t(t)} + u_v(z,t)\right)\left(\overline{c_0} + \overline{c_t(t)} + c_v(z,t)\right). \quad (7)$$

A complete decomposition of f (Equation 7) over a tidal cycle $\langle f \rangle$ is approximated by seven major flux terms:

$$\begin{aligned}\langle f \rangle &= h_0\overline{u_0 c_0} + \overline{c_0}\langle h_t\overline{u_t}\rangle + \overline{u_0}\langle h_t\overline{c_t}\rangle + h_0\langle \overline{u_t c_t}\rangle \\ &+ \langle h_t\overline{u_t c_t}\rangle + h_0\langle \overline{u_v c_v}\rangle + \langle \overline{h_t}\,\overline{u_v c_v}\rangle \\ &= T_1 + T_2 + T_3 + T_4 + T_5 + T_6 + T_7, \end{aligned} \quad (8)$$

In Equation 8, the brackets $\langle\ \rangle$ indicate the tidally averaged value, while the over bar symbol denotes the vertical average value. T_1 refers to the mean advective flux, T_2 accounts for the transport by stokes' drift related to tides wave, and T_3, T_4, T_5 are the tidal pumping terms that arise from the phase lag between variables related to the tidal cycle, with negative values corresponding to the phase lag between variables beyond $\pi/2$, T_6 *and* T_7 refer to the vertical gravitational circulation related to the estuarine exchange flow and the change of water depth partly caused by sediment scouring and settling, respectively.

The sediment transport in a single model layer (assuming $h = 1$) in which both current velocity and sediment concentration are vertically uniform, Equation 1 is simplified as:

$$f_b = uc \quad (9)$$

Following the aforementioned decomposition methodology, f_b (Equation 9) in a single layer can be decomposed into:

$$f_b = u_0c_0 + u_0c_t(t) + u_t(t)c_0 + u_t(t)c_t(t). \quad (10)$$

The terms $u_0c_t(t)$and $u_t(t)c_0$are much smaller than the other three terms after being averaged over the tidal cycles, and therefore Equation 10 can be further simplified as:

$$\langle f_b \rangle \approx u_0c_0 + \langle u_tc_t \rangle. \quad (11)$$

We computed the transport flux and its major terms in the bottom-most model layer. The Equation 11 can be rewritten as follows:

$$\langle f_b \rangle = T_{ba} + T_{bp}, \quad (12)$$

where subscript b denotes the bottom layer, T_{ba} represents the mean advective transport, T_{bp} is the tidal pumping term corresponding to the phase lag transport between velocity and sediment concentration associated with sediment resuspension and settling. These terms collectively govern the sediment transport dynamics in the bottom layer, in which the nucleus of the ETMs is located.

4 Results

4.1 Model validation

The hydrodynamic model has been validated in terms of water level, salinity, and temperature by Ma et al. (2023). In this study, the simulated suspended sediment distribution and associated hydrodynamic parameters are compared to observations.

4.1.1 Location of ETMs

In accordance with previous studies (Wai et al., 2004; Cui et al., 2022), the areas where the SSC surpasses 100 mg L^{-1} near the bottom are designated as ETMs. Our model result shows three ETMs in Lingding Bay in the wet season (Figure 3). One of them is located on the West shoal to the northeast of Qi'ao Isl (named TM_shoalw hereafter) and one on the Middle shoal to the east of Neilingding Isl (named TM_shoalm hereafter). These two ETMs have been observed and described by Yang and Liu (2015b); Liu et al. (2016), and Zhang et al. (2021b), and confirmed by our model results. The modeled concentration of SPM in the TM_shoalw is generally greater than in the TM_shoalm, which has also been reported by existing literature. In addition to the two ETMs on the shoals, a third ETM is located in the western channel (named TM_channel hereafter, Figure 3). This ETM had not been reported until the observation by (Cui et al., 2022).

Our simulation results are able to capture all three ETMs in the PRE that have been observed in the wet seasons in terms of spatial location and SSC level (Figure 3).

4.1.2 SPM dynamics

The assessment of simulated SPM dynamics is based on a comparison with observation data. Existing observations in the study area indicate that the distribution of SPM is constrained by salinity-induced stratification (Zhang et al., 2021b; Cui et al., 2022). The observation data shown in Figure 4A depicts the vertical profile of SPM along the transect, which exhibited a high concentration up to 300 mg L^{-1} in the bottom layer. The high concentration was observed at the salinity front. As illustrated in Figures 4B, C, the model output during the same period exhibited a similar distribution of salinity and SPM. The comparison between the modeled and observed distributions of salinity and SPM indicates

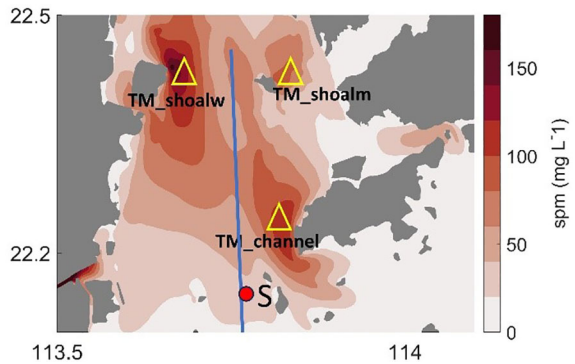

FIGURE 3
The spatial distribution of SSC in the bottom-most model layer in the wet season shows three ETMs in the study area in consistency with existing field observations. The blue line refers to the observation transect in Cui et al. (2022), and the red dot indicates the location of the site (S) where a lander was deployed in that study. Observation data from the transect and from site S were used to assess the model result.

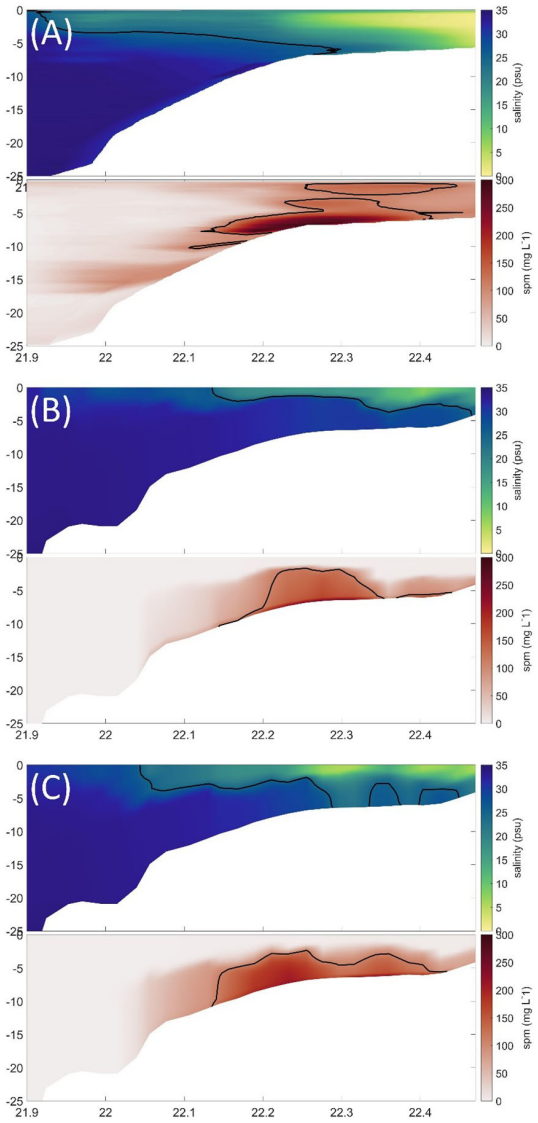

FIGURE 4
The distribution of sanility and SPM concentration along a transect in Lingding Bay. **(A)** Observed distribution of SPM concentration along the transect (during July 2020) by Cui et al., (2022). **(B)** and **(C)** snapshots of model results during a tidal cycle in the same day. The contour line of salinity of 25 psu and SPM concentration of 110 mg L^{-1} was marked by the black line in respective plots.

that the model reproduced the observations with a reasonable degree of accuracy.

The time series of current velocity demonstrates the dominance of tidal cycles at the observation site S. The variation of salinity and SSC exhibit a strong connection with tidal cycles and additionally controlled by the two-layer flow (low-salinity fresh water above saline water), as evidenced by both model results and observations (Figure 5). Besides a background concentration of 50–100 mg L^{-1}, enhanced near-bottom SPM concentration (150–200 mg L^{-1}) appearing in pulses are induced exclusively by strong tidal currents during the flooding phase at site S. This variation is also captured by our simulation results. Model results indicate an elevated bed shear stress during the flooding phase (Figure 5G), suggesting a tidal pumping effect at this site.

4.2 Formation mechanisms and dynamics of the ETMs

The physical mechanisms and dynamics of the ETMs are featured by distinct seasonality in the PRE. To provide a clearer depiction of the variation of the ETMs, the contour line of 100 mg L^{-1} is defined as the boundary of an ETM.

4.2.1 Spatial distribution

Our simulation results show that the physical mechanisms for the formation of the TM_shoalw and TM_shoalm show high similarity (Supplementary Figures S2, S3). These two ETMs are both formed by the convergence of SPM delivered by fresh riverine water and saline oceanic water. The formation of the TM_channel is driven by a different mechanism compared to the other two. The location of the nucleus of the ETMs remains relatively stable, despite that they exhibit different extension and SSC between wet and dry seasons. To avoid redundant process descriptions, we focus on the elucidation of the TM_shoalw (which shares similarity with the TM_shoalm) and the TM_channel.

In the TM_shoalw, the spatial average SSC exceeds 170 mg L^{-1} in the wet season, with a reduced level in the dry season. Notably, the spatial extent of the ETM is more pronounced during the wet season, whilst the location of its nucleus remains unchanged (Figures 6C, D). This stability in the nucleus location is attributed to the confluence of fresh riverine water and saline oceanic water, forming a distinct salinity front along the western shoal in both seasons, as illustrated in (Figures 6A, B). The estuarine front traps SPM, primarily due to the suppression of turbulence by stratification (Geyer, 1993; Largier, 1993). TM_shoalw is consistently located to the shoreward side of the front (Ma et al., 2023), effectively trapping SPM from both riverine and oceanic sources. The higher concentration of TM_shoalw in the wet season results from the larger river flow and sediment loading, given that the wet season accounts for approximately 70% of river flow and 85% of the sediment load annually.

In the TM_channel, the average SSC is 120 mg L^{-1} and 133 mg L^{-1} during the wet and dry seasons, respectively. The lower SSC in the TM_channel than in the TM_shoalw is due to the smaller fraction of silt in the channel which serves as the main source of SPM. An enhanced stratification occurs in the channel area in the wet season (Figure 6), which is induced by the extensive river plume that suppresses the saline water to the channel (Ma et al., 2023). The stratification reduces turbulence greatly, resulting in lower SSC in the TM_channel in the wet season compared to the dry season (Figure 6). The stratification also affects the spatial extent of the TM_channel. In the wet season, the TM_channel is mainly restricted to the deeper channel, whereas it extends upstream and to the shoals during the dry season. This pattern is clearly different from the TM_shoalw, which shrinks in the dry season.

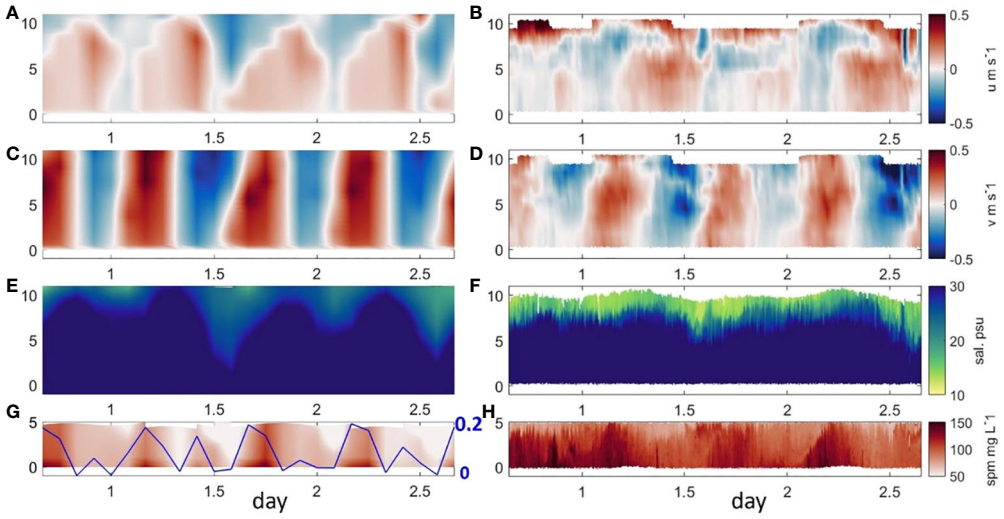

FIGURE 5
Vertical distribution of **(A, B)** eastward velocity u, **(C, D)** northward velocity v, **(E, F)** salinity, **(G, H)** SPM concentration at S site. The left panel is model result, and the right panel is observation data derived from (Cui et al., 2022). The solid line in **(G)** indicates simulated bed shear stress with axis on the right (unit: Pa).

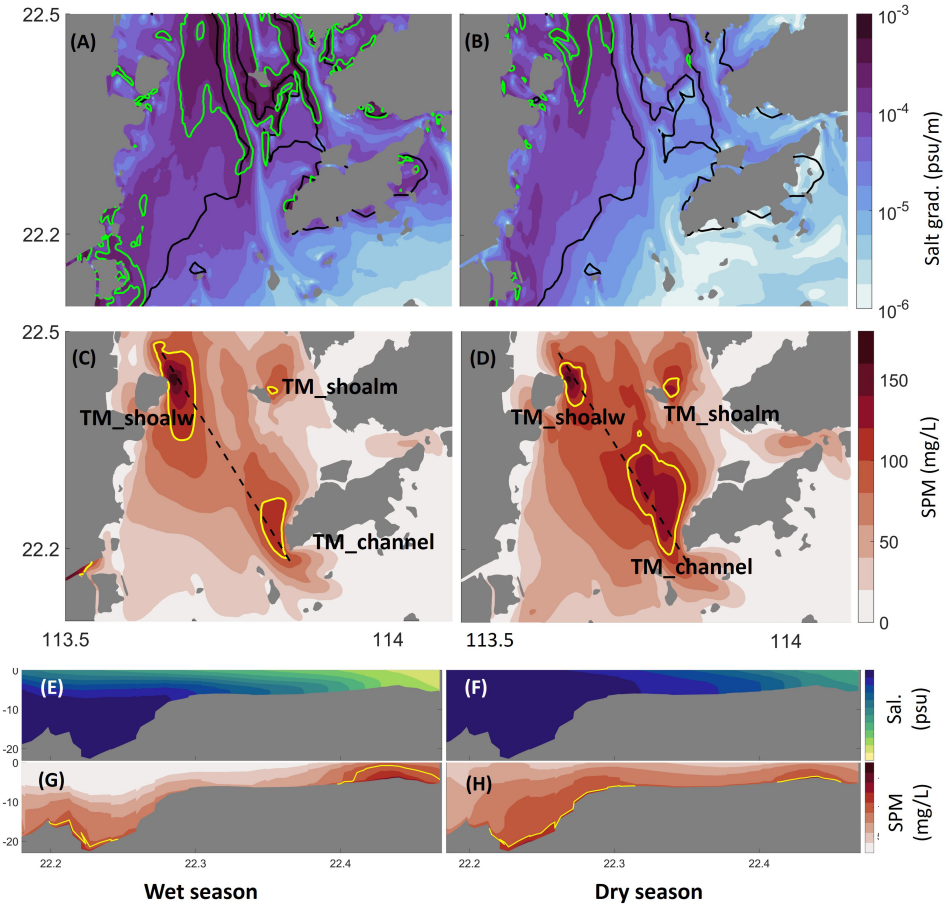

FIGURE 6
(A, B) Horizontal bottom water salinity gradient in the wet and dry seasons, respectively. The green line depicts the estuarine front according to Ma et al. (2023), and the green line marks the 7-m isobaths. **(C, D)** Seasonal average SSC in the bottom layer in the wet and dry seasons, respectively. The yellow lines mark the 100mg L^{-1} contours, and the dashed black line marks the transect which is plotted in **(E–H)**. **(E, G)** show the distribution of salinity and SSC along the transect in the wet season, respectively. **(F, H)** are for the same parameters but for the dry season.

4.2.2 Residual current and sediment flux

A comparison between the residual current and the residual sediment flux provides insight into the physical mechanisms for the formation of the ETMs. The simulated residual current and sediment flux in the bottom and surface layers in the wet and dry seasons are depicted in Figure 7. In the surface layer, the residual current predominantly exhibits a seaward direction in both the wet and dry seasons. In the lower reach of the estuary, the current is primarily influenced by the large-scale coastal current that is driven by the monsoon, that is, northeastward in the wet season and southwestward in the dry season (Zu and Gan, 2015). SPM in the surface water layer is mainly from the riverine sediment load and the residual transport direction generally follows the surface residual current, with elevated values in regions characterized by pronounced resuspension (Figures 7A, B).

The residual current and residual sediment flux in the bottom layer is significantly modulated by the estuarine morphology and tides (Figures 7C, D). The saline water intrudes into the estuary via the channel in the bottom layer, and the extension is much further upstream in the dry season than in the wet season. This significantly modifies the residual current and sediment transport flux at a seasonal scale. The bottom residual current on the west shoal is directed to the northwest, which results from a shear front between the west channel and the west shoal that is consistent with a previous study (Zhang et al., 2021a). The residual sediment flux follows the direction of the residual current within the channel. However, large discrepancies in their directions occur on the west shoal. This is due to the tidal asymmetry of SSC. In a major part of the west shoal, the bottom residual current points to the right relative to the residual sediment transport direction, indicating that the SSC is elevated during the ebbing phase compared to the flooding phase.

The formation of the TM_shoalw mainly results from a convergence of the residual transport. During the wet season, there is a notable convergence of residual current and sediment flux in both the surface and bottom layers. However, during the dry season, the convergence is weakened in the surface layer, leading to lower SSC than in the wet season.

In the TM_channel, the residual current and sediment transport are directed seaward in the surface layer, whereas landward transport occurs at the bottom. At the boundary between the west shoal and the west channel, an entrainment of SPM is induced by the counteracting surface and bottom residual transport, marking the boundary of the TM_channel. Along the west channel, a relatively sharp gradient in the bathymetry of Lantau Island on both landward and seaward sides creates a hole-like topography in the channel (Figure 1). Baroclinic circulation and stratification are locally intensified in this area (Figure 6), and hinder the landward SPM transport. This specific sediment trapping mechanism leading to the formation of ETM that is locked at topographic transitions independent of salinity is termed topographic trapping (Burchard et al., 2018).

4.2.3 Sediment sources

According to previous studies, a major portion of the riverine sediment is initially deposited in the estuary (Wai et al., 2004) and therefore contributes to the formation of the seabed in modern times. In this study, we distinguish the source of SPM in the ETMs

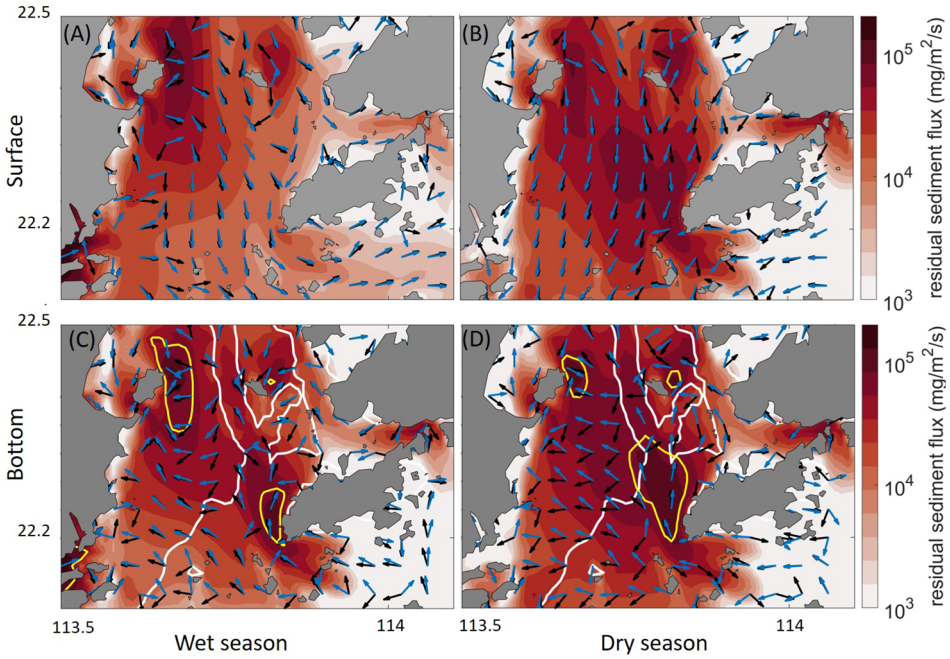

FIGURE 7
Residual current direction (blue arrows) and sediment transport flux (direction indicated by black arrows and magnitude indicated by the color) in the surface **(A, B)** and bottom layers **(C, D)**. **(A, C)** are for the wet season, whilst **(B, D)** are for the dry season. ETMs are indicated by the yellow lines in the bottom layer. The white line refers to the 7 m-isobaths.

between the sediment directly delivered by the river plume and local resuspension, despite that locally resuspended sediment may also have a terrestrial origin. The modeled fractions of SPM in the ETMs from these two sources are shown in Figure 6.

Our results show that local resuspension contributes to a major part of the SPM in all ETMs. In the wet season, SPM delivered directly by the river plume is also important for maintaining the two ETMs in the upper part of the estuary (Figure 8), whereas the ETM in the lower part of the estuary (TM_channel) is almost exclusively maintained by resuspended sediment. In the dry season, there is an enhanced contribution of local resuspension across all three ETMs, with the most pronounced observed in the TM_shoalm. In the TM_channel, local resuspended sediment almost entirely dominates.

4.3 Processes of SPM transport in the ETMs

The relative contribution of various sediment transport processes to the ETMs was quantified through a decomposition of the sediment transport flux (section 3.2).

4.3.1 Temporal variation

The time series of sediment transport terms averaged over the area of the TM_shoalw and TM_channel respectively, are shown in Figure 9. Results show that the sediment flux is largely modulated by river discharge and sediment loading. High water discharge and high river sediment loads occur in the wet season, whilst lower water discharge and river sediment loads occur in the dry season. During the simulation period, the wet season of 2018 experienced the lowest water discharge and sediment loading compared to the wet seasons of other years. This seasonal signal is clearly reflected in the advection and resuspension terms.

In the TM_shoalw, which is located close to the river outlets, sediment transport is featured by a generally southward-directed (i.e., seaward) net transport in the wet season and northward-directed (landward) net transport in the dry season jointly caused by the mean advection and tidal oscillations. At an hourly scale, the tidal oscillation-induced sediment flux can reach several times larger than the advective transport in magnitude. However, the tidal transport is largely balanced between landward and seaward transport when averaged weekly (7-day moving average) (Supplementary Figure S2). The mean advective transport is largely modulated by the river runoff and exhibits a distinct seasonality, featured by prominent seaward transport in wet seasons and landward transport in dry seasons (Figure 9E). The tidal pumping T_{bp} contributes to a significant fraction of sediment transport flux in the TM_shoalw, which is attributed to the large fraction of suspended fine-grained particles (e.g. clay) (Supplementary Figure S1). T_{bp} is generally positive (northward-directed) in the dry seasons and negative in the wet seasons, suggesting a different seasonal response of SSC to current velocity. Particularly, negative values of T_{bp} (Figure 9G) indicate a long phase lag between flow velocity and SSC which are in opposite phases, resulting mainly from a small settling velocity of clay. Two factors contribute to the significant presence of clay around Qi'so Island during the wet season. Firstly, Qi'ao Island's proximity to the outlet allowing it to receive substantial quantities of clay directly delivered by the river runoff. Secondly, SPM from the riverine runoff is trapped in this place due to a flow convergence (Figure 7).

In the TM_channel, the magnitude of sediment flux is larger than the TM_shoalw. In contrast to the TM_shoalw, the mean advective transport in the bottom layer of TM_channel is mostly northward (i.e., landward) driven by the gravitational circulation in the wet season. In the dry season, despite a higher SSC level (Figure 4) caused by enhanced mixing, the gravitational circulation is suppressed, leading to reduced mean advective sediment transport compared to the wet season Figure 9F. During the period of low river discharge, the advective sediment transport may even turn to a seaward direction. On a weekly scale (7-day moving average), the tidal pumping transport T_{bp} is generally positive and shows elevated values when river discharge is high, indicating a synchronized response of SSC and the current velocity that are with a small phase difference.

In each ETM zone, hourly-to-daily fluctuations of sediment flux are predominantly driven by tidal oscillations. However, at a longer time scale (weekly to yearly), variations in the net sediment flux patterns are primarily influenced by advection and tidal pumping.

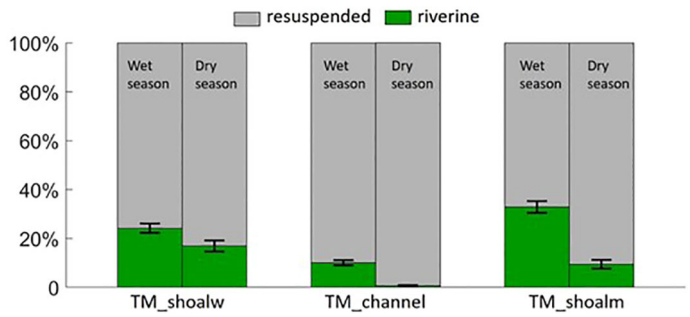

FIGURE 8
Fractions of SPM in the ETMs from the two sources (local resuspension and river plume) distinguished between wet and dry seasons according to the simulation results.

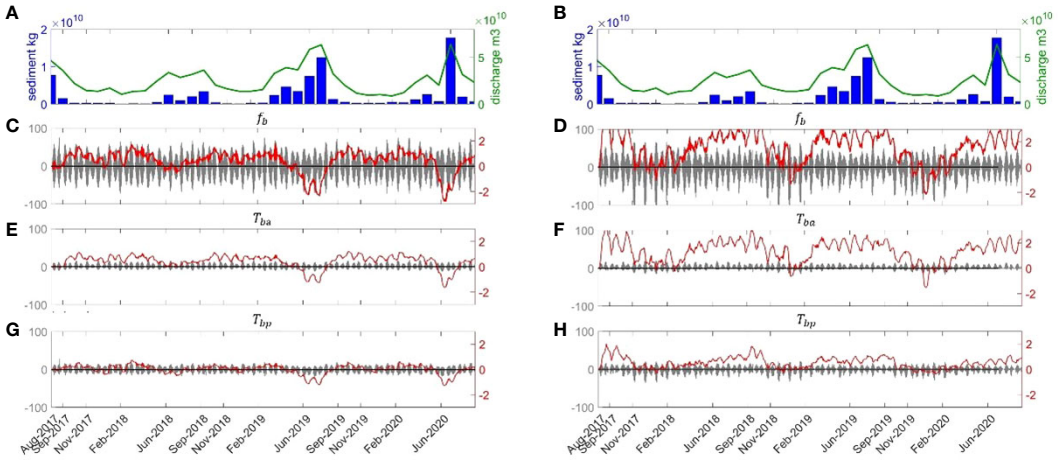

FIGURE 9
(A, B) Monthly averaged river discharge and sediment loading of the PRE. **(C, D)** Time series of modeled sediment flux f_b in the bottom layer of the TM_shoalw (left column) and TM_channel (right column) from August 2017 to September 2020. **(E, F)** Time series of the advective transport flux (T_{ba}) in the two ETMs. **(G, H)** Time series of transport flux due to tidal pumping (T_{bp}). Hourly data are indicated by the grey lines with the y-axis on the left and the 7-day moving average data are indicated by the red lines with y-axis on the right in **(C–H)**. Positive values indicate northward transport direction in **(C–H)**.

4.3.2 Spatial variation

The spatial distribution of seasonal averaged bottom sediment flux, integrated over three months of the wet and dry seasons, respectively, is calculated to examine their roles in the ETMs across distinct geographical units. The seasonal averaged terms were derived using the following equation:

$$T_{bin} = \frac{1}{t}\int_0^t T_b(t)dt \tag{13}$$

In the Equation 13, T_b represents f_b, T_{ba} and T_{bp} from Equation 12. These terms are averaged over the wet and dry seasons, respectively, yielding f_{bin}, T_{bain} and T_{bpin} for each grid cell over the PRE.

Results shown in Figures 10, 11 indicate that bottom sediment flux (f_{bin}) and all three terms (T_{bain}, T_{bpin}) are most pronounced in the west channel and influenced by bathymetrical gradients. The bottom sediment flux shows f_{bin} convergence in TM_ shoalw and strong advective transport in the west channel. The sharp depth gradient between 22.2N° and 22.3°N (Figures 6E–H) results in a decrease of northward transport, leading to topographic trapping of sediment in the channel. This effect is responsible for the formation of TM_channel (Figure 6). Despite a difference in the strength of the terms, their transport direction remains stable between the wet and dry seasons.

Compared to a consistent transport direction of each term in the western channel, the shoal area is featured by convergence and divergence in these terms, along with reduced strength (Figures 10, 11). The advective transport term T_{bain} shows convergence in the TM_shoalw both axially and laterally in in both wet and dry seasons. The divergence within the TM_shoalw is attributed to T_{bpin}, which shows tidally forced oscillation of the spatial extension of TM_shoalw.

Results in Figures 10, 11 indicate that the upstream of TM_shoalw is characterized by a landward sediment flux whereas the downstream of TM_shoalw is associated with a seaward sediment flux due to tidal pumping. Tidal pumping contributes to a net divergence of sediment flux. The same pattern was found in Yu et al. (2014). Upon the establishment of the ETM, tidal pumping predominantly dictates its mobility, aligning the ETM's movement with the flood and ebb tides. The pronounced value of T_{bpin} in the west shoal is located between 22.35N° and 22.45N° as shown in Figure 10, which is consistent with the swing of the ETM over a tidal cycle reported by Dong et al. (2020). The minimum value of T_{bpin} is located in the center of TM_shoalw. As proposed by Dyer (1995), the tidal pumping terms are likely to be a minimum at the locations near the peak of turbidity maximum, which is mainly associated with the asymmetry in the tidal flow (for details of the relationship between tidal asymmetry and tidal pumping, please refer to Supplementary Material).

4.4 Interconnections between ETMs

ETMs are spatially distributed across various morphological units within the PRE, yet exhibit interconnections, which are revealed by the experiments described in 3.1.

Results (Figure 12) show that on TM_shoalw, the sediment input from TM_channel and from TM_shoalm are comparable. This remote transport is markedly more pronounced in the wet seasons, approximately fivefold compared to the dry seasons. Two transport pathways exist from the west channel (TM_channel) to the west shoal (TM_shoalw): one follows the 'TM_channel-TM_shoalm-TM_shoalw' route across the middle shoal, and the other is the direct 'TM_channel-TM_shoalw' route. The former is influenced by the anti-clockwise circulation within the PRE (Figure 7). The latter can be attributed to lateral circulation, moving sediment from the west channel to the southern part of the west shoal, eventually reaching TM_shoalw (Figure 7).

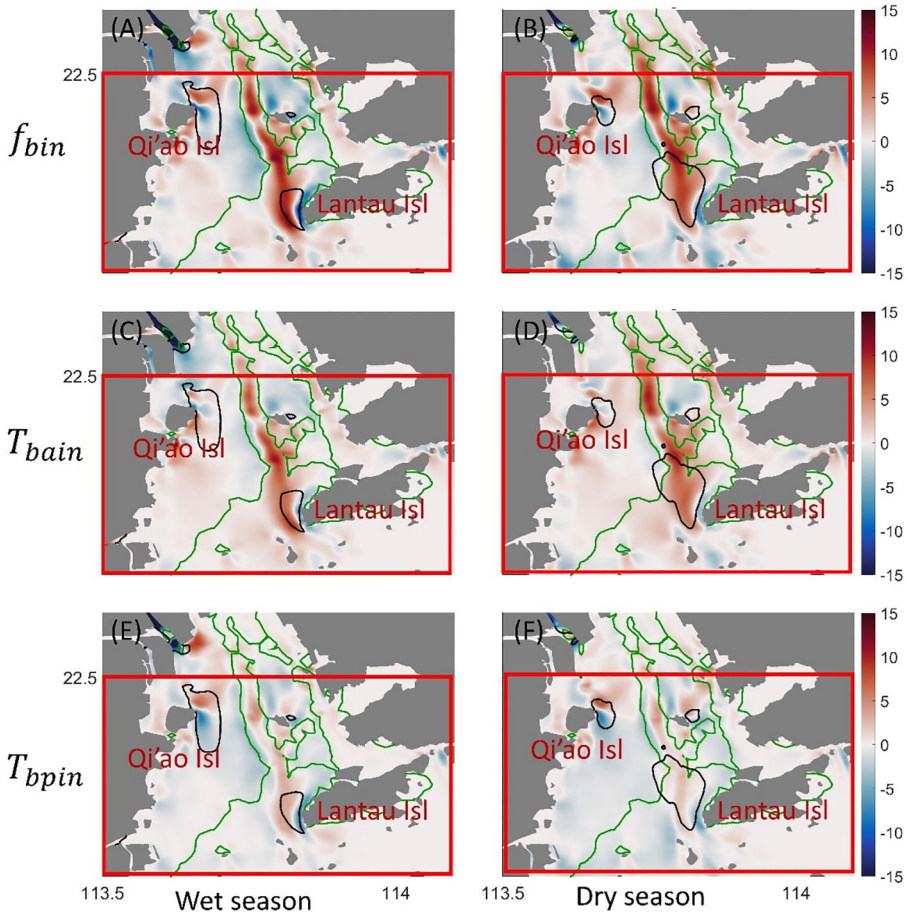

FIGURE 10
Spatial distribution of f_{bin}, T_{bain} and T_{bpin} in the bottom water layer in the wet (left column) and dry seasons (unit: m · mg · $s^{-1}L^{-1}$.). Positive (red color) and negative (blue color) values indicate northward and southward transport, respectively. The green lines indicate the 7-m isobaths, and the black polygons indicate the boundary of ETMs where SSC exceeds 100 mg L^{-1}. The red boxes indicate the focus area of this study.

Regarding TM_channel, sediment input from TM_shoalw is quite limited. This can be attributed to two primary factors. Firstly, the convergence effect results in sediment being predominantly trapped in TM_shoalw. Secondly, sediment transported out of the west shoal tends to settle in its southern part, as explained in section 4.2.2. Sediment transport from TM_shoalm to TM_channel is more pronounced during the dry seasons. This transport pattern is influenced by the seasonal stratification dynamics (Figure 12E). Intense stratification during the wet season impedes sediment movement from TM_shoalm to TM_channel. However, with the weakening of stratification in the wet season, this transport pathway becomes more active.

For TM_shoalm located in the middle shoal, sediment input from TM_shoalw is minor, primarily because the transport direction between the middle shoal and the west shoal is westward (as shown in Figure 7). The sediment movement from TM_channel to TM_shoalm is influenced by multiple factors. Firstly, salt intrusion at the bottom during the wet season amplifies this transport. Secondly, the enhanced river discharge from May to July causes the saltwater front to recede seaward, preventing sediment from reaching TM_shoalm. This suggests that sediment transport from TM_channel to TM_shoalm is contingent upon the establishment of stratification during the wet season and the location of the estuarine front.

Peaks in sediment transport arise from extreme short-term weather events. For instance, our results suggest that a tropical storm leads to significant sediment transport from TM_channel to TM_ shoalm (Figures 12D, F).

In summary, during the wet season, the presence of stratification and the anti-clockwise circulation of the PRE promotes a 'TM_channel-TM_shoalm-TM_shoalw' sediment transport pathway across the three ETMs and a 'TM_channel-TM_shoalw' pathway between two ETMs. In the dry season, as stratification diminishes, these transport pathways become less stringent, and sediment exchange between TM_channel and TM_shoalm becomes more active (Figure 13).

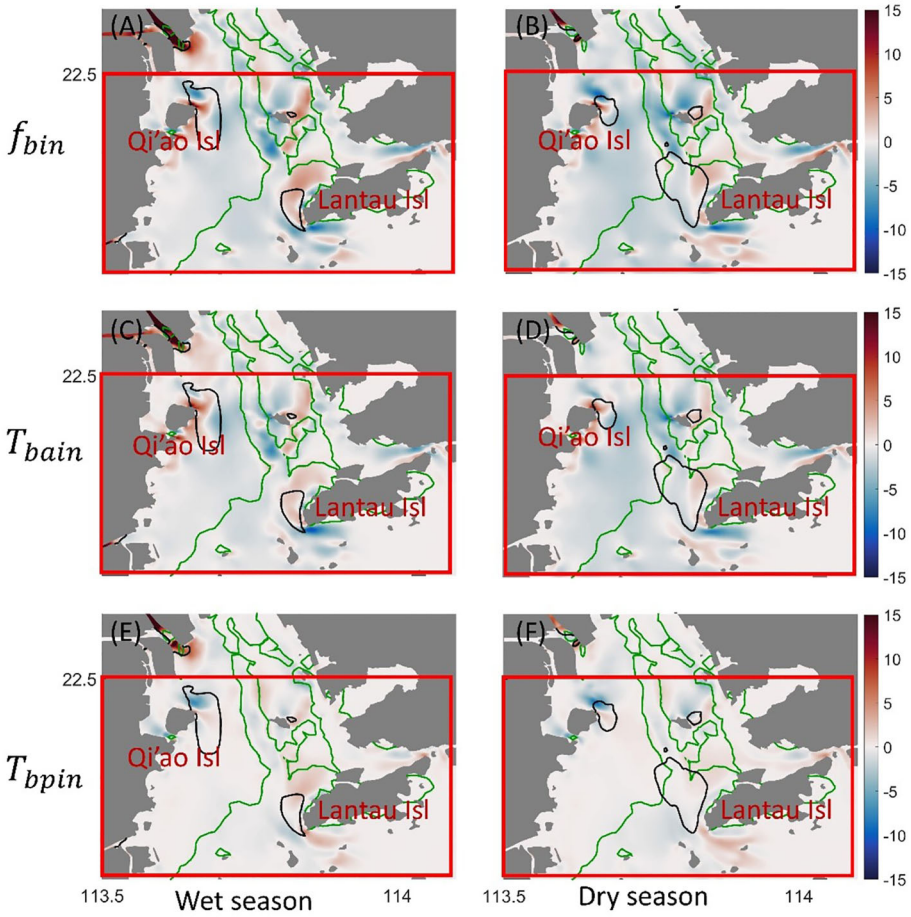

FIGURE 11
Spatial distribution of f_{bin}, T_{bain} and T_{bpin} in the bottom water layer in the wet (left column) and dry seasons (unit: $m \cdot mg \cdot s^{-1}L^{-1}$.). Positive (red color) and negative (blue color) values indicate eastward and westward transport, respectively. The green lines indicate the 7-m isobaths, and the black polygons indicate the boundary of ETMs where SSC exceeds 100 mg L^{-1}. The red boxes indicate the focus area of this study.

5 Discussion

5.1 Impact of morphology on ETM

Our modeling outcomes underscore the pivotal influence of morphological characteristics on the spatial distribution of ETMs within the PRE. Specifically, the two upstream ETMs (TM_shoalw and TM_shoalm) are situated in the west shoal and middle shoal, respectively, while the downstream ETM (TM_channel) is centered in the west channel, with an extension towards the west shoal. While prior research has identified ETM zones, the majority have been singularly focused on individual zones (Geyer et al., 2001; Sommerfield and Wong, 2011; Hua et al., 2020). Our model captures all three ETMs in the PRE, offering an opportunity for deepening the understanding of SPM distribution shaped by the interplay between morphological features and the estuarine circulation as well as interconnections among ETMs.

Tidal pumping-induced residual flow and sediment transport are pivotal in maintaining the ETM at the head of saltwater intrusion (Sommerfield and Wong, 2011; Li et al., 2014; Yu et al., 2014; Wan and Zhao, 2017). Moreover, ETMs are also observed at bathymetric transition zones (Schoellhamer, 2000; Geyer et al., 2001; Chen et al., 2015). The genesis of such ETMs can be attributed to topographical trapping (Burchard et al., 2018). Both formation mechanisms mentioned are manifested in this study. The two ETMs developed on the shoals, namely TM_shoalw and TM_shoalm, are sustained at the salinity fronts where residual transport from offshore and onshore directions converge (Figure 5). Despite that the formation of these two ETMs is caused by transport convergence, local resuspension contributes to a major portion of SPM in the ETMs (Figure 6). Interestingly, both ETMs are located on the eastern side of the islands, and the enhanced tidal currents in the island proximity are responsible for maintaining a high level of SSC in the two ETMS. Because these two ETMs are formed by the transport convergence at the front, their size variation is largely controlled by the movement of the salinity front between dry and wet seasons. By contrast, the ETM in the channel (TM_channel) is formed by topographic trapping and exhibits an extension towards the west shoal (Figure 4) during dry seasons whereas a shrinks in wet seasons. The extension of TM_channel results from lateral circulation driven by the baroclinic pressure gradient (Zhang et al., 2021a; Gong et al., 2022). The inversely co-varying dynamics

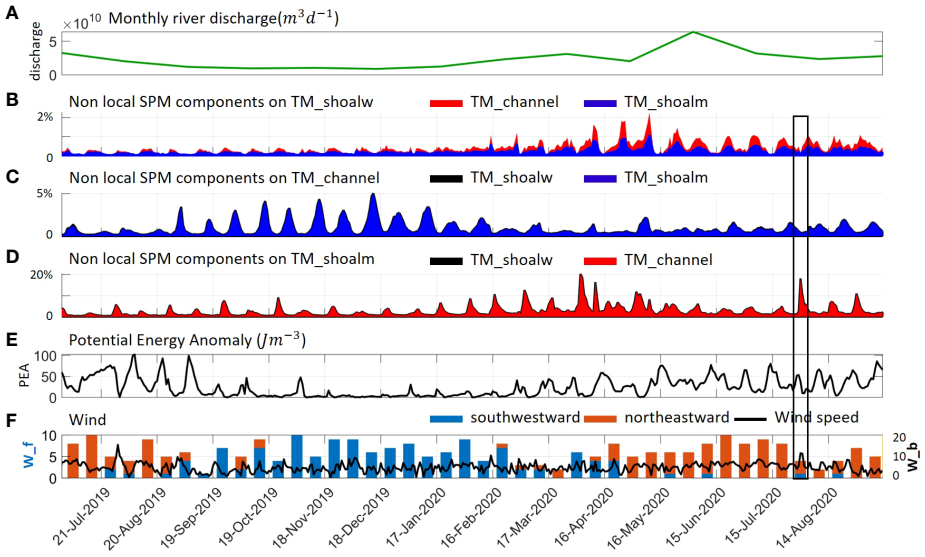

FIGURE 12
Interconnections between the ETMs as revealed from the simulation result of July 2019 - September 2020. **(A)** Monthly river discharge for the period of July 2019 – September 2020. **(B–D)** Temporal variation of local and non-local SPM components in each ETM zone; black, red, and blue denote the components of SPM originating from TM_shoalw, TM_channel, and TM_shoalm, respectively; The calculated potential energy anomaly (PEA) of site 3 is depicted in **(E)**. In the subplot **(F)**, the left y-axis represents the frequency of wind direction in 10 days, with blue indicating southwestward wind and red indicating northeastward wind. The right y-axis denotes the wind speed in meters per second(m/s). The black box indicates the passage of tropical storm Sinlaku from 31 July to 2 August 2020 (https://www.hko.gov.hk/en/publica/tc/tc2020/section3_2rpt.html).

between the ETMs in the upstream (TM_shoalw and TM_shoalm) and the ETM in the downstream promote an active exchange of sediment among the ETMs as shown in our simulation results.

5.2 Effect of stratification on ETMs and their interconnections

As described in section 4, the spatial variation of the ETMs and their interconnections are largely affected by stratification. While SPM transport from TM_shoalm to TM_shoalw and from TM_channel to TM_shoalw both intensify during the wet season, their transport pathways differ. The SPM transport from TM_shoalm to TM_shoalw is facilitated by the bay-wide anti-clockwise circulation (Xu et al., 2021). In contrast, the TM_channel to TM_shoalw transport route is not straightforward but via lateral circulation which is dependent on the salinity gradient. Despite the distinct transport pathways, the anti-clockwise circulation and the lateral circulation between the channel and the shoal are both amplified by enhanced stratification (Mao et al., 2004).

Remarkably, SPM transport from TM_shoalm to TM_channel intensifies during the dry season, which is associated with reduced river runoff. This enhanced transport is attributed to the diminished

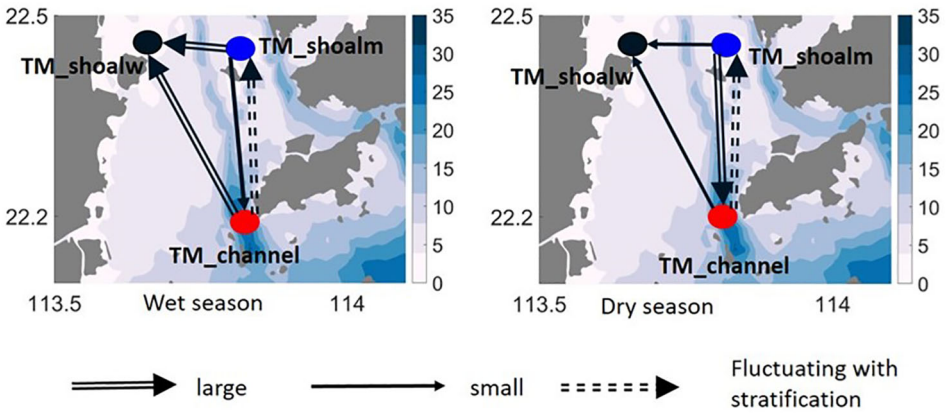

FIGURE 13
The interconnections between the ETMs in PRE. The seasonal average volume of sediment transport is categorized into two tiers, 'large' and 'small', using a threshold of 10^5 kg/d.

stratification during the dry season, leading to a dissolution of the front (Ma et al., 2023) which acts as a barrier between TM_shoalm and TM_channel, thereby augmenting SPM transport.

The SPM transport from TM_channel to TM_shoalm is not merely governed by the intensity of stratification. It is also associated with the latitudinal oscillation of the stratification. As shown in Figure 10, elevated river runoff in May and June (right after the dry season) results in pronounced stratification and diminishes the SPM transport from TM_channel to TM_shoalm. This phenomenon is attributed to the significant river runoff advancing the salinity front between TM_channel and TM_shoalm toward offshore, impeding the SPM transport from TM_channel to TM_shoalm.

In summary, the interconnections among the ETMs hinge not just on the intensity of stratification but also on the latitudinal oscillation of the estuarine front. Amid alterations in stratification, attributed to driving factors such as sea level rise, dredging, land reclamation (Schoellhamer, 2000; Wang et al., 2021; Cox et al., 2022; Ma et al., 2023), and/or deltaic land subsidence (Wang et al., 2017; Cao et al., 2021), it is also important to conder not only the effects of stratification intensity on ETMs (Geyer, 1993) but also the ramifications of shifts in stratification position and oscillation patterns.

The investigation of the interconnection of ETMs reveals that when multiple ETMs exist in an estuary, sediment management in the estuary must consider not only the formation mechanism and sediment source of a single ETM but also the dynamic mechanism that links various ETMs to each other.

5.3 Effect of flocculation on ETMs

Cohesive sediment, which typically ranges in size from 0.98 to 63 μm (Hjulström, 1935), is composed of particulate matter that is susceptible to aggregation, breakup, deposition, and erosion processes (Maggi, 2005; Manning et al., 2010). Turbulent mixing of the fluid causes the suspended aggregates to come in contact, inducing further aggregation and causing the growth of large aggregates. The frequency with which particles collide, grow, and break up is largely dependent on the intensity of turbulence (Malcherek, 1995; Maggi, 2005). To assess the effect of flocculation on the ETMs, we adopted the formulation (Equation 14) by Arlinghaus et al. (2022), which links the settling velocity of cohesive sediment to turbulence:

$$\omega = \omega_0 \frac{1 + mG}{1 + nG^2}, \tag{14}$$

where ω_0 is a reference settling velocity in still water (Table 1) depending on the particle grain size, $m$and $n$are empirical constants, and G is the turbulence shear.

Results are compared with the reference simulation (Figure 6) presented in previous parts of our study. The comparison indicates that in the dry season, with inclusion of the flocculation effect in the simulation, the spatial distribution of all three ETMs is quite similar to the reference simulation, only with a slight decrease of SSC in the channel (Figure 14). In the wet season, SSC in two ETMs (TM_shoalw and TM_shoalm) exhibits similar pattern with the reference result, whilst SSC in the TM_channel is lower than the threshold level (100 mg L^{-1}) for an ETM, albeit with locally elevated SSC in the same location. The similar distribution pattern of ETMs between simulations with and without flocculation in the PRE demonstrates that flocculation affects SSC in the ETMs, but it is not the driving mechanism for formation of ETMs. This result is consistent with studies in other estuaries (Manning et al., 2010; Xu et al., 2010).

5.4 Effect of wind-waves on ETMs

Surface wind-waves may alter the residual flow, water mixing and bottom stress, which in turn affects the transport and distribution of sediment in estuaries (Uncles and Stephens, 1997; Gong et al., 2022, 2023). A comparison between model results with and without wind-wave effect revealed that the overall SSC on the west shoal and in the west channel is enhanced by wave effect in both wet and dry seasons (Figure 14). This increase is believed to be attributed to the elevated bed shear stress, as shown in Supplementary Figure S11. In the simulation with wave effect, the bed shear stress exhibited a notable increase on the west shoal, resulting in an elevated SSC. A notable increase in SSC is also seen in the area between the west channel and west shoal, which is consistent with the findings of Zhang et al. (2021a) that waves enhance the sediment exchange between the shoal and the channel by eroding sediment on the side bank of west channel. The eroded sediment is subsequently transported toward the west shoal by tidal pumping. It is worthy of note that despite the notable increase in SSC within the estuary, the nucleus of the three ETMs remained the same in the simulations with and without wave effect.

5.5 Future scenarios of the ETMs in the PRE

According to a previous study by the authors (Ma et al., 2023), a dramatic historical change in the morphology of the PRE caused by human activities (land reclamation, channel dredging, and dumping, sand excavation) from the 1970s to 2010s has resulted in a bay-wide enhancement of stratification by up to four times, with maximum enhancement (up to seven times) on the western shoal of the Lingding Bay where TM_shoalw is located. In recent years, extensive human interventions including sand excavation and land reclamation have been banned. However, other local-scale human activities such as channel maintenance by dredging and indirect interventions such as reduced sediment discharge by river damming are likely to continue in the future (Liu et al., 2018). In this context, future change of stratification is likely to be driven mainly by sea level rise, land subsidence of the Pearl River delta as well as river runoff associated with monsoon intensity. The stratification is projected to be further strengthened albeit to a less extent than in past decades (Ma et aL., 2023). The projected future enhancement of stratification would possibly lead to an enhancement of the bay-wide anti-clockwise circulation and the

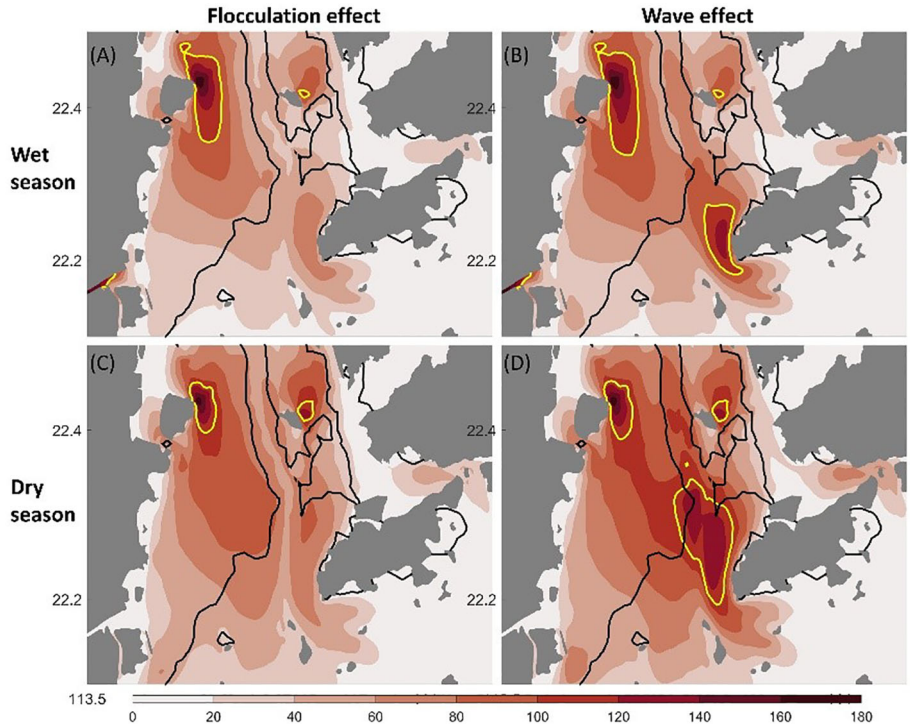

FIGURE 14
SSC in the bottom layer during the wet (top panel) and dry seasons in the sensitivity simulations. **(A, C)** SSC in the simulation with flocculation included; **(B, D)** SSC in the simulation with wind-waves included. The yellow line indicates the 100 mg L^{-1} contour line of SSC. The black line indicates the 7-m isobaths.

lateral circulation, promoting SPM transport between the ETMs and their interconnections.

Besides the impact of stratification, the largely reduced sediment input from rivers may also impact the ETMs to a considerable extent. Despite that sediment directly delivered by the river plumes contributes to only a small portion of the SPM in the ETMs (Figure 6), locally resuspended sediment in the ETMs may also have a terrestrial origin due to the fact that more than 80% of riverine sediment is initially deposited within the estuary. The reduction of riverine sediment supply would possibly lead to a deterioration of the deltaic deposit (Wu et al., 2016) and consequently impact the sediment source for the ETMs.

The elevated wave energy near the coast due to sea level rise and the narrowing of the estuary (Wei et al., 2021) indicate the potential for an increased influence of wave effect on sediment transport and distribution. Despite the numerous studies that have demonstrated the significant impact of wave effect on sediment transport (Madsen and Grant, 1976a; 1976b; Green and Coco, 2014; Chen et al., 2019) and the influence of flocculation on sediment distribution (Xu, 2009; Manning et al., 2010; Xu et al., 2010), impact of interactions between various factors, such as tides, wind-waves and flocculation, on the fate of ETMs has yet to be understood. Because of a nonlinear response of ETMs to changes in hydrodynamics and sediment supply, to what extent these climatic and anthropogenic drivers would lead to spatial and temporal variation of ETMs in the future remains to be explored.

6 Summary and conclusion

A high-resolution 3-dimensional hydrodynamics-sediment transport model was applied to investigate the sediment transport and dynamics of ETMs in the PRE from 2017 to 2020. Based on the simulation results that are confirmed by observation, the relative contribution of specific physical mechanisms for the formation of the ETMs, the temporal and spatial dynamics of the ETMs as well as their interconnections were investigated. The following main conclusions are drawn from the study:

1. Three ETMs exist in the Lingding Bay of the PRE, and they are formed by different physical mechanisms. The two upstream ETMs (TM_shoalw and TM_shoalm) situated on the shoals are a result of convergence of residual flow and sediment transport associated with tidal pumping. The downstream ETM located in the west channel (TM_channel) is formed mainly by topographical trapping.
2. All three ETMs exhibit distinct seasonal and spatial variations. Advection and tidal pumping are the main processes mediating the sediment flux of the ETMs. These factors are largely influenced by river runoff and stratification dynamics. The TM_shoalw exhibits spatial extension in wet seasons and shrinks in dry seasons, whereas TM_channel and TM_shoalm show an opposite pattern.

3. The ETMs are interconnected through sediment exchange. In the wet season, a 'TM_channel-TM_shoalm-TM_shoalw' sediment transport pathway across the three ETMs and a 'TM_channel-TM_shoalw' pathway between two ETMs are prominent. In the dry season, these transport pathways become less stringent, and sediment exchange between TM_channel and TM_shoalm becomes more active.

In the context of evolving estuarine dynamics, it is imperative to underscore the profound influence of both climate change and human activities on estuarine geomorphology and ecological systems. The ETM emerges as a salient component within this framework. Our findings elucidate that alterations in estuarine stratification, driven by climate changes and human activities, directly impact the formation of ETM, encompassing its spatial distribution, SPM concentration, and compositional attributes. It is paramount for future research endeavors to evaluate the multifaceted response of ETM to both climatic and anthropogenic challenges.

Data availability statement

The original contributions presented in the study are included in the article/Supplementary Material. Further inquiries can be directed to the corresponding authors.

Author contributions

MM: Conceptualization, Data curation, Methodology, Software, Validation, Writing – original draft, Writing – review & editing. LP: Data curation, Methodology, Writing – review & editing. CS: Supervision, Writing – review & editing. WZ: Methodology, Supervision, Writing – review & editing.

Funding

The author(s) declare financial support was received for the research, authorship, and/or publication of this article. This study is a contribution to the Helmholtz PoF program "The Changing Earth -Sustaining our Future" on its Topic 4: Coastal zones at a time of global change. It also contributes to the theme "C3: Sustainable Adaption Scenarios for Coastal Systems" of the Cluster of Excellence EXC 2037 'CLICCS -Climate, Climatic Change, and Society' -Project Number: 390683824 funded by the Deutsche Forschungsgemeinschaft (DFG, German Research Foundation) under Germany's Excellence Strategy. WZ acknowledges the support of the project "Morphological evolution of coastal seas -past and future" funded by the Deep-time Digital Earth program (https://www.ddeworld.org/) and the Sino-German Mobility Program: CHESS-Chinese and European Coastal Shelf Seas Ecosystem Dynamics-A Comparative Assessment (M-0053).

Acknowledgments

Many thanks to Peter Arlinghaus for his help in the early stage of model build-up and comments on scientific questions.

Conflict of interest

The authors declare that the research was conducted in the absence of any commercial or financial relationships that could be construed as a potential conflict of interest.

Publisher's note

Supplementary material

The Supplementary Material for this article can be found online at: https://www.frontiersin.org/articles/10.3389/fmars.2024.1385382/full#supplementary-material

References

Arlinghaus, P., Zhang, W., and Schrum, C. (2022). Small-scale benthic faunal activities may lead to large-scale morphological change-A model based assessment. *Front. Mar. Sci.* 9, 1011760. doi: 10.3389/fmars.2022.1011760

Brenon, I., and Le Hir, P. (1999). Modelling the turbidity maximum in the seine estuary (France): identification of formation processes. *Estuarine Coast. Shelf Sci.* 49 (4), 525–544. doi: 10.1006/ecss.1999.0514

Burchard, H., Schuttelaars, H. M., and Ralston, D. K. (2018). Sediment trapping in estuaries. *Annu. Rev. Mar. Sci.* 10, 371–395. doi: 10.1146/annurev-marine-010816-060535

Cao, A., Esteban, M., Valenzuela, V. P. B., Onuki, M., Takagi, H., Thao, N. D., et al. (2021). Future of Asian Deltaic Megacities under sea level rise and land subsidence: current adaptation pathways for Tokyo, Jakarta, Manila, and Ho Chi Minh City. *Curr. Opin. Environ. Sustainab* 50, 87–97. doi: 10.1016/j.cosust.2021.02.010

Chen, W.-B., Liu, W.-C., Hsu, M.-H., and Hwang, C.-C. (2015). Modeling investigation of suspended sediment transport in a tidal estuary using a three-dimensional model. *Appl. Math. Model.* 39, 2570–2586. doi: 10.1016/j.apm.2014.11.006

Chen, Y., Chen, L., Zhang, H., and Gong, W. (2019). Effects of wave-current interaction on the Pearl River Estuary during Typhoon Hato. *Estuarine Coast. Shelf Sci.* 228, 106364. doi: 10.1016/j.ecss.2019.106364

Cheng, L. I. U., Jueyi, S. U. I., Yun, H. E., and Hirshfield, F. (2013). Changes in runoff and sediment load from major chinese rivers to the pacific ocean over the period 1955–2010. *Int. J. Sediment Res.* 28 (4), 486–495. doi: 10.1016/S1001-6279(14)60007-X

Cox, J., Lingbeek, J., Weisscher, S., and Kleinhans, M. (2022). Effects of sea-level rise on dredging and dredged estuary morphology. *J. Geophys. Research: Earth Surface* 127, 1–20. doi: 10.1029/2022JF006790

Cui, Y., Wu, J., Tan, E., and Kao, S. J. (2022). Role of particle resuspension in maintaining hypoxic level in the Pearl River Estuary. *J. Geophys. Research: Oceans* 127, e2021JC018166. doi: 10.1029/2021JC018166

Dong, Y., Dehai, S., and Xianwen, B. (2020). Spring-neap tidal variation and mechanism analysis of the maximum turbidity in the Pearl River Estuary during flood season. *J. Trop. Oceanograph.* 39, 20–35. doi: 10.11978/2019035

Dyer, K. R. (1974). The salt balance in stratified estuaries. *Estuar. Coast. Mar. Sci.* 2, 273–281. doi: 10.1016/0302-3524(74)90017-6

Dyer, K. R. (1988). "Fine sediment particle transport in estuaries," in *Physical processes in estuaries* (Berlin, Heidelberg: Springer Berlin Heidelberg), 295–310.

Dyer, K. R. (1995). "Sediment transport processes in estuaries," in *Developments in sedimentology* (Elsevier), 423–449. doi: 10.1016/S0070-4571(05)80034-2

Etcheber, H., Taillez, A., Abril, G., et al. (2007). Particulate organic carbon in the estuarine turbidity maxima of the gironde, loire and seine estuaries: origin and lability. *Hydrobiologia* 588, 245–259. doi: 10.1007/s10750-007-0667-9

Garel, E., Pinto, L., Santos, A., and Ferreira, Ó. (2009). Tidal and river discharge forcing upon water and sediment circulation at a rock-bound estuary (Guadiana estuary, Portugal). *Estuarine Coast. Shelf Sci.* 84, 269–281. doi: 10.1016/j.ecss.2009.07.002

Geyer, W. R. (1993). The importance of suppression of turbulence by stratification on the estuarine turbidity maximum. *Estuaries* 16, 113–125. doi: 10.2307/1352769

Geyer, W. R., Woodruff, J. D., and Traykovski, P. (2001). Sediment transport and trapping in the Hudson River estuary. *Estuaries* 24, 670–679. doi: 10.2307/1352875

Gong, W., Wang, J., Zhang, G., and Zhu, L. (2023). Effect of axial winds and waves on sediment dynamics in an idealized convergent partially mixed estuary. *Mar. Geology* 107015. doi: 10.1016/j.margeo.2023.107015

Gong, W., Zhang, G., Zhu, L., and Zhang, H. (2022). Effects of swell waves on the dynamics of the estuarine turbidity maximum in an idealized convergent partially mixed estuary. *J. Mar. Syst.* 235, 103784. doi: 10.1016/j.jmarsys.2022.103784

Green, M. O., and Coco, G. (2014). Review of wave-driven sediment resuspension and transport in estuaries. *Rev. Geophysics* 52, 77–117. doi: 10.1002/rog.v52.1

Hjulström, F. (1935). *Studies of the morphological activity of rivers as illustrated by the River Fyris* (Doctoral dissertation). The Geological institution of the University of Upsala, Sweden.

Hua, X., Huang, H., Wang, Y., Yu, X., Zhao, K., and Chen, D. (2020). Seasonal estuarine turbidity maximum under strong tidal dynamics: three-year observations in the changjiang river estuary. *Water* 12, 1854. doi: 10.3390/w12071854

Jilan, S., and Kangshan, W. (1986). The suspended sediment balance in Changjiang Estuary. *Estuarine Coast. Shelf Sci.* 23, 81–98. doi: 10.1016/0272-7714(86)90086-7

Largier, J. L. (1993). Estuarine fronts: how important are they? *Estuaries* 16, 1–11. doi: 10.2307/1352760

Leuven, J. R. F. W., Pierik, H. J., Vegt, M., Bouma, T. J., and Kleinhans, M. G. (2019). Sea-level-rise-induced threats depend on the size of tide-influenced estuaries worldwide. *Nat. Climate Change* 9, 986–992. doi: 10.1038/s41558-019-0608-4

Li, M., Ge, J., Kappenberg, J., Much, D., Nino, O., and Chen, Z. (2014). Morphodynamic processes of the Elbe River estuary, Germany: the Coriolis effect, tidal asymmetry and human dredging. *Front. Earth Sci.* 8, 181–189. doi: 10.1007/s11707-013-0418-3

Lin, S., Liu, G., Niu, J., Wei, X., and Cai, S. (2021). Responses of hydrodynamics to changes in shoreline and bathymetry in the Pearl River Estuary, China. *Continental Shelf Res.* 229, 104556. doi: 10.1016/j.csr.2021.104556

Liu, F., Hu, S., Guo, X., Luo, X., Cai, H., and Yang, Q. (2018). Recent changes in the sediment regime of the Pearl River (South China): Causes and implications for the Pearl River Delta. *Hydrological Processes* 32, 1771–1785. doi: 10.1002/hyp.11513

Liu, R., Wang, Y., Gao, J., Wu, Z., and Guan, W. (2016). Turbidity maximum formation and its seasonal variations in the Zhujiang (Pearl River) Estuary, southern China. *Acta Oceanologica Sin.* 35, 22–31. doi: 10.1007/s13131-016-0897-7

Ma, M., Zhang, W., Chen, W., Deng, J., and Schrum, C. (2023). Impacts of morphological change and sea-level rise on stratification in the Pearl River Estuary. *Front. Mar. Sci.* 10. doi: 10.3389/fmars.2023.1072080

MacVean, L. J., and Stacey, M. T. (2011). Estuarine dispersion from tidal trapping: A new analytical framework. *Estuaries Coasts* 34, 45–59. doi: 10.1007/s12237-010-9298-x

Madsen, O. S., and Grant, W. D. (1976a). "Quantitative description of sediment transport by waves," in *Coastal engineering*, vol. 1976, 1092–1112. doi: 10.1061/9780872620834.065

Madsen, O. S., and Grant, W. D. (1976b). *Sediment transport in the coastal environment*. Cambridge, Mass.: Ralph M. Parsons Laboratory for Water Resources and Hydrodynamics, Dept. of Civil Engineering, Massachusetts Institute of Technology.

Maggi, F. (2005). *Flocculation dynamics of cohesive sediment* (Delft University of Technology: Faculty of Civil Engineering and Geosciences).

Malcherek, A. (1995). Mathematische Modellierung von Strömungen und Stofftransportprozessen in Ästuaren. Dissertation, Institut für Strömungsmeehanik und Elektronisch Rechnen im Bauwesen der Universiüit Hannover, Bericht Nr. 44/1995.

Manning, A., Langston, W., and Jonas, P. (2010). A review of sediment dynamics in the Severn Estuary: influence of flocculation. *Mar. pollut. Bull.* 61, 37–51. doi: 10.1016/j.marpolbul.2009.12.012

Mao, Q., Shi, P., Yin, K., Gan, J., and Qi, Y. (2004). Tides and tidal currents in the Pearl River Estuary. *Continental Shelf Res.* 24, 1797–1808. doi: 10.1016/j.csr.2004.06.008

Moriarty, J. M., Friedrichs, M. A. M., and Harris, C. K. (2021). Seabed resuspension in the chesapeake bay: Implications for biogeochemical cycling and hypoxia. *Estuaries Coasts* 44, 103–122. doi: 10.1007/s12237-020-00763-8

North, E. W., and Houde, E. D. (2001). Retention of white perch and striped bass larvae: biological-physical interactions in Chesapeake Bay estuarine turbidity maximum. *Estuaries* 24, 756–769. doi: 10.2307/1352883

Pinto, L., Fortunato, A., Zhang, Y., Oliveira, A., and Sancho, F. (2012). Development and validation of a three-dimensional morphodynamic modelling system for non-cohesive sediments. *Ocean Model.* 57, 1–14. doi: 10.1016/j.ocemod.2012.08.005

Porz, L., Zhang, W., and Schrum, C. (2021). Density-driven bottom currents control development of muddy basins in the southwestern Baltic Sea. *Mar. Geology* 438, 106523. doi: 10.1016/j.margeo.2021.106523

Ralston, D. K., Geyer, W. R., and Warner, J. C. (2012). Bathymetric controls on sediment transport in the Hudson River estuary: Lateral asymmetry and frontal trapping. *J. Geophys. Research: Oceans* 117 (C10). doi: 10.1029/2012JC008124

Rao, V. P., Shynu, R., Kessarkar, P. M., Sundar, D., Michael, G., Narvekar, T., et al. (2011). Suspended sediment dynamics on a seasonal scale in the Mandovi and Zuari estuaries, central west coast of India. *Estuarine Coast. Shelf Sci.* 91, 78–86. doi: 10.1016/j.ecss.2010.10.007

Schoellhamer, D. H. (2000). "Influence of salinity, bottom topography, and tides on locations of estuarine turbidity maxima in northern San Francisco Bay," in *Proceedings in marine science* (Amsterdam: Elsevier). 3, 343–357. doi: 10.1016/S1568-2692(00)80130-8

Scully, M. E., and Friedrichs, C. T. (2007). Sediment pumping by tidal asymmetry in a partially mixed estuary. *J. Geophys. Research: Oceans* 112 (C7). doi: 10.1029/2006JC003784

Shepard, F. P. (1954). Nomenclature based on sand-silt-clay ratios. *J. sedimentary Res.* 24, 151–158. doi: 10.1306/D4269774-2B26-11D7-8648000102C1865D

Sommerfield, C. K., and Wong, K. C. (2011). Mechanisms of sediment flux and turbidity maintenance in the Delaware Estuary. *J. Geophys. Research: Oceans* 116 (C1). doi: 10.1029/2010JC006462

Soulsby, R. (1997). *Dynamics of marine sands*. Thomas Telford Publishing. doi: 10.1680/doms.25844.fm

Teng, L., Cheng, H., Zhang, E., and Wang, Y. (2022). Lateral variation of tidal mixing asymmetry and its impact on the longitudinal sediment transport in turbidity maximum zone of salt wedge estuary. *J. Mar. Sci. Eng.* 10, 907. doi: 10.3390/jmse10070907

Uncles, R., and Stephens, J. (1997). Dynamics of turbidity in the Tweed estuary. *Estuarine Coast. Shelf Sci.* 45, 745–758. doi: 10.1006/ecss.1997.0232

Uncles, R. J., and Stephens, J. A. (1989). Distributions of suspended sediment at high water in a macrotidal estuary. *J. Geophys. Res.: Oceans* 94 (C10), 14395–14405. doi: 10.1029/JC094iC10p14395

Vinh, V. D., and Ouillon, S. (2021). The double structure of the Estuarine Turbidity Maximum in the Cam-Nam Trieu mesotidal tropical estuary, Vietnam. *Mar. Geology* 442, 106670. doi: 10.1016/j.margeo.2021.106670

Wai, O., Wang, C., Li, Y. S., and Li, X. (2004). The formation mechanisms of turbidity maximum in the Pearl River estuary, China. *Mar. pollut. Bull.* 48, 441–448. doi: 10.1016/j.marpolbul.2003.08.019

Wan, Y., and Zhao, D. (2017). Observation of saltwater intrusion and ETM dynamics in a stably stratified estuary: the Yangtze Estuary, China. *Environ. Monit. Assess.* 189, 1–14. doi: 10.1007/s10661-017-5797-6

Wang, H., Chen, Q., Hu, K., and La Peyre, M. K. (2017). A modeling study of the impacts of Mississippi River diversion and sea-level rise on water quality of a deltaic estuary. *Estuar. coasts* 40, 1028–1054. doi: 10.1007/s12237-016-0197-7

Wang, J., Dijkstra, Y. M., and de Swart, H. E. (2022). Turbidity maxima in estuarine networks: Dependence on fluvial sediment input and local deepening/narrowing with an exploratory model. *Front. Mar. Sci.* 9, 940081. doi: 10.3389/fmars.2022.940081

Wang, J., Tong, Y., Feng, L., Zhao, D., Zheng, C., and Tang, J. (2021). Satellite-observed decreases in water turbidity in the Pearl River Estuary: Potential linkage with sea-level rise. *J. Geophys. Research: Oceans* 126, e2020JC016842. doi: 10.1029/2020JC016842

Wang, P., Li, Q., and Li, C.-F. (2014). *Sedimentology* (Amsterdam: Elsevier). doi: 10.1016/B978-0-444-59388-7.00004-4

Warner, J. C., Sherwood, C. R., Signell, R. P., Harris, C. K., and Arango, H. G. (2008). Development of a three-dimensional, regional, coupled wave, current, and sediment-transport model. *Comput. geosciences* 34, 1284–1306. doi: 10.1016/j.cageo.2008.02.012

Wei, X., Cai, S., and Zhan, W. (2021). Impact of anthropogenic activities on morphological and deposition flux changes in the Pearl River Estuary, China. *Sci. Rep.* 11, 16643. doi: 10.1038/s41598-021-96183-0

Winterwerp, J., Van Kesteren, W., Van Prooijen, B., and Jacobs, W. (2012). A conceptual framework for shear flow–induced erosion of soft cohesive sediment beds. *J. Geophys. Research: Oceans* 117 (C10). doi: 10.1029/2012JC008072

Wu, Z. Y., Saito, Y., Zhao, D. N., Zhou, J. Q., Cao, Z. Y., Li, S. J., et al. (2016). Impact of human activities on subaqueous topographic change in Lingding Bay of the Pearl River estuary, China, during 1955-2013. *Sci. Rep.* 6, 37742. doi: 10.1038/srep37742

Xia, X., Li, Y., Yang, H., Wu, C., Sing, T., and Pong, H. (2004). Observations on the size and settling velocity distributions of suspended sediment in the Pearl River Estuary, China. *Continental Shelf Res.* 24, 1809–1826. doi: 10.1016/j.csr.2004.06.009

Xu, F. (2009). *Modeling study of flocculation effects on sediment transport in estuaries (State University of New York at Stony Brook)*. PhD Thesis, Stony Brook University, Stony Brook, United States.

Xu, F., Wang, D.-P., and Riemer, N. (2010). An idealized model study of flocculation on sediment trapping in an estuarine turbidity maximum. *Continental Shelf Res.* 30, 1314–1323. doi: 10.1016/j.csr.2010.04.014

Xu, H., Shen, J., Wang, D., Luo, L., and Hong, B. (2021). Nonlinearity of subtidal estuarine circulation in the Pearl River Estuary, China. *Front. Mar. Sci.* 8, 629403. doi: 10.3389/fmars.2021.629403

Yang, J., and Liu, W. (2015a). Evolution of the Maximum Turbidity Zone in the Lingding Bay of Pearl River Estuary over past 30 years. *Pearl River Water Transport* (16), 58–62.

Yang, J., and Liu, W. (2015b). Variation of the maximum turbidity zone during the flood season in the Pearl River Estuary over the past 30 years. *China Acad. J.* doi: 10.14125/j.cnki.zjsy.2015.16.034

Yu, Q., Wang, Y., Gao, J., Gao, S., and Flemming, B. (2014). Turbidity maximum formation in a well-mixed macrotidal estuary: The role of tidal pumping. *J. Geophys. Research: Oceans* 119, 7705–7724. doi: 10.1002/2014JC010228

Yuan, R., Zhu, J., and Wang, B. (2015). Impact of sea-level rise on saltwater intrusion in the Pearl River Estuary. *J. Coast. Res.* 31, 477–487. doi: 10.2112/JCOASTRES-D-13-00063.1

Zhang, G., Chen, Y., Cheng, W., Zhang, H., and Gong, W. (2021a). Wave effects on sediment transport and entrapment in a channel-shoal estuary: the pearl river estuary in the dry winter season. *J. Geophys. Research: Oceans* 126, e2020JC016905. doi: 10.1029/2020JC016905

Zhang, G., Cheng, W., Chen, L., Zhang, H., and Gong, W. (2019). Transport of riverine sediment from different outlets in the Pearl River Estuary during the wet season. *Mar. Geology* 415, 105957. doi: 10.1016/j.margeo.2019.06.002

Zhang, Y., Ren, J., and Zhang, W. (2020). Flocculation under the control of shear, concentration and stratification during tidal cycles. *J. hydrol.* 586, 124908. doi: 10.1016/j.jhydrol.2020.124908

Zhang, Y., Ren, J., Zhang, W., and Wu, J. (2021b). Importance of salinity-induced stratification on flocculation in tidal estuaries. *J. Hydrol.* 596, 126063. doi: 10.1016/j.jhydrol.2021.126063

Zhang, Y. J., Ye, F., Stanev, E. V., and Grashorn, S. (2016). Seamless cross-scale modeling with SCHISM. *Ocean Model.* 102, 64–81. doi: 10.1016/j.ocemod.2016.05.002

Zu, T., and Gan, J. (2015). A numerical study of coupled estuary–shelf circulation around the Pearl River Estuary during summer: Responses to variable winds, tides and river discharge. *Deep Sea Res. Part II: Top. Stud. Oceanograph.* 117, 53–64. doi: 10.1016/j.dsr2.2013.12.010

Appendix C

Evolution of Estuarine Turbidity Maximum in the Pearl River Estuary: historical development and future scenarios

Evolution of Estuarine Turbidity Maximum in the Pearl River Estuary: historical development and future scenarios

Mengyao. Ma[1, 2†], Wenyan. Zhang[1†], Lucas. Porz[1], Corinna. Schrum[1, 2]

[1]Institute of Coastal System, Helmholtz-Zentrum Hereon, Gessthacht, Germany

[2]Institute of Oceanography, University Hamburg, Hamburg, Germany

Corresponding authors: Mengyao Ma (mengyao.ma@hereon.de); Wenyan Zhang (wenyan.zhang@hereon.de)

Key Points:

- Long-term development of Estuarine Turbidity Maximum is dependent on human-induced modifications of the coast and sea level change
- Human-induced morphological change is the main driving factor for evolution of ETMs in the past
- ETMs in the Pearl River Estuary will likely become patchier and increasingly driven by baroclinicity

Abstract

Estuarine hydrodynamics and morphodynamics are highly sensitive to both anthropogenic and climatic impacts. The Pearl River Delta (PRD), which encompasses several megacities, has experienced pronounced land-use change over the past century. In the Pearl River Estuary (PRE), the predominant human-induced morphological development, coupled with climate drivers such as sea level and temperature rise, have collectively caused a notable change in the hydrodynamics and sediment dynamics. This resulted in notable modifications to the Estuarine Turbidity Maximum (ETM) which remain underexplored. Our study investigates how ETMs in the PRE evolved in response to various anthropogenic and climatic drivers during the past decades and their likely fates in the forthcoming decades by three-dimensional hydro-morphodynamic modeling. Our results demonstrate that the ETMs have evolved remarkably from a single and massive ETM in 1970s to several locally confined but interconnected ETMs in 2010s. Such change was mainly driven by human-induced morphological change associated with land-reclamation, river damming, sand mining, channel dredging and dumping. In the forthcoming decades, climate change will likely play a more important role in driving the change of ETMs due to an official cessation of land-reclamation and sand mining. The relative sea level rise resulting from global warming and land subsidence will likely decrease the concentration of suspended particulate matter (SPM) in the ETMs through enhanced stratification and reduced wind-wave resuspension of sediments, leading to a patchier distribution of ETMs with dynamics increasingly driven by baroclinicity.

Plain Language Summary

The Pearl River Estuary (PRE) has become narrower and deeper compared to its state 50 years ago. Human activities contributed to the morphological changes mostly. The coastline developed seaward due to land reclamation. The channel is dragged deeper to meet navigation needs. In future scenarios, the impact of sea level rise, land subsidence, potential changes in riverine sediment load and shifting wind conditions will also affect the sediment dynamics, thereby altering the situation of estuarine turbidity zones that are of critical importance for ecological functioning of estuaries.

Our study investigates decadal changes in the sediment dynamics and evolution of estuarine turbidity maxima (ETMs) in the PRE, employing a 3D hydrodynamic and sediment dynamic model to explore the driving mechanisms of the development of ETMs. Our results suggest that the estuarine morphology, sediment composition in the estuarine bed, relative sea level rise, and

riverine sediment load are the primary factors influencing the evolution of ETMs in the PRE. Our findings might provide guidance for sediment management in strongly engineered estuaries such as the PRE.

1 Introduction

An Estuarine Turbidity Maximum (ETM) refers to a zone in an estuary where highest concentration of suspended particulate matter (SPM) occurs. The formation of ETMs is a result of hydrodynamic and sediment dynamic processes, influenced by topography, fluvial and tidal forces, as well as SPM composition (Burchard et al, 2018; Geyer et al, 2001; Jay & Musiak, 1994; Yu et al, 2014). ETMs constitute an important ecological function of the estuary since high suspended sediment concentration (SSC) is often associated with oxygen deficiency and heavy metal accumulation (Cui et al, 2019; Gavhane et al, 2021; Niu et al, 2021; Song et al, 2021; Zhuang & Zhou, 2021).

Estuaries have undergone remarkable physical modifications in recent decades by human interventions, among which construction of dams upstream for hydroelectric power generation, dredging of channels for navigation, sand mining and large-scale land reclamation exert most prominent impacts on ETMs (Day et al, 2013). Impacts of several of the above-mentioned interventions have been extensively studied. For instance, the construction of dams modifies ETMs by reducing the amount of suspended sediment load (Walling, 2008) and altering the composition of suspended sediment (Luo et al, 2012). It is reported that in the Yangtze Estuary, the spatial extent of the ETM has decreased by 22% and the ETM center have migrated landward by 7 km during the flood season after the construction of the Three Gorges Dam (Zhao et al, 2023). Sediment dredging may not only alter the location of ETMs but also provide additional source for SPM. It is found that extensive dredging in the lower part of Ems Estuary has induced a removal of a consolidated sediment layer in the surface riverbed and consequently created a new sediment source to sustain high SSC in the ETM (Jonge, 1983). A numerical modeling study of the Ems estuary showed that the deepening of tidal channels during the period of 1965 - 2005 have also induced a reduction in hydraulic drag which is most likely responsible for a landward shift of the ETM (de Jonge et al, 2014). In contrast to the impact of dredging, land reclamation reduces sediment supply from land and may lead to a significant decline in the SSC and seaward migration of ETM, as is the case in the north channel of the Yangtze Estuary (Teng et al, 2021).

Apart from human interventions, relative sea level rise (rSLR) also significantly influences the development of ETMs through modification of tides-river runoff interactions and bed shear stress (Burchard et al, 2018; Geyer et al, 2001; Yu et al, 2014). In the Rhine-Meuse-Scheldt delta, the rSLR-induced shift in tidal asymmetry, from a mixed regime of ebb and flood dominance to ebb dominance, alters the direction of the residual sediment transport, thereby favoring sediment export (Jiang et al, 2020). Under high greenhouse gas emission scenarios, the climate change-induced (eustatic) sea level is predicted to reach between 0.6 and 1.0 m by 2100 above present day's level (Oppenheimer et al, 2019). The impact of rSLR is even more critical in regions characterized by land subsidence. For example, a land subsidence reaching up to 22 cm yr^{-1} between 2007 and 2009 has been reported for the western Indonesia (Chaussard et al, 2013), which is much larger than the eustatic SLR rate. Large river deltas are especially vulnerable to the joint impact of climate change-induced and land subsidence-induced SLR. It has been evidenced that land subsidence and eustatic sea-level rise have exerted an influence on the reduction of delta growth over the past decades based on an analysis of 86% of the world's deltaic regions (Nienhuis & van de Wal, 2021). However, how estuaries and ETMs would respond to an accelerated rSLR in the forthcoming decades remain largely elusive (Weisscher et al, 2023).

Another impact of climate change on estuarine sediment dynamics is through modification in atmospheric forcing. Global warming may alter wind speed and direction at both global and reginal levels. At the regional scale, different trends in wind speed and direction may emerge in the future (Kulkarni et al, 2013). For example, a pronounced increase in the mean wind speed by 0.5 m/s in the northern part of the Baltic Sea and a notable decline in the Mediterranean by 2.0 m/s have been projected (Walter et al, 2006). A study by De Winter et al (2013) suggested a shift in wind direction, with more extreme wind from the west, in the North Sea during 2050-2100. Even a small change in winds may exert a remarkable influence on sediment transport in coastal environments by altering the residual circulation and waves (Bauer et al, 2012; Weisse et al., 2021).

Estuaries with large, densely populated river deltas are particularly vulnerable to the impact of both climatic and anthropogenic stressors. To mitigate negative impacts for a sustainable management of estuaries, it is thus important to understand how estuaries respond to drivers of contemporary and future changes. This study aims to explore plausible future scenarios of estuarine hydro-morphodynamics, sediment transport and ETMs associated with a densely populated large river delta, namely the Pear River Delta (PRD), that has been increasingly stressed

by climate change and anthropogenic activities. To this end, we firstly investigated the historical development of ETMs in the Pear River Estuary (PRE) from 1970s till 2010s and quantified the impact of individual driving factors as well as their combined effect based on 3-dimensional numerical modeling. We then projected future development of the ETMs till 2050s in a set of scenarios representing plausible change in the rSLR and other important climate driving factors (intensity and direction of the East Asian monsoon) for the region. The derived outcomes may help to inform coastal and estuarine spatial planning strategies in the context of climate change mitigation.

2 Study area and previous research

The Pearl River Estuary (PRE) is situated in southern China (Figure 1a), encompassing several megacities, including Guangzhou, Shenzhen, Zhuhai, and Hong Kong. The PRE is a semi-enclosed, bell-shaped estuary that connects the Pearl River with the South China Sea. Two deep channels (the west and the east channels) divide the estuary into three shallow shoals (the west shoal, the middle shoal, and the east shoal). Freshwater is discharged into the estuary via eight river outlets, namely Humen, Jiaomen, Hongqimen, Hengmen, Modaomen, Jitimen, Hutiaomen, and Yamen. The total river discharge of all outlets reaches 40,000 $m^3 s^{-1}$ during the summer months (June – August, so-called the wet season), with a notable decline to 4,000 $m^3 s^{-1}$ during the winter months (December – February, so-called the dry season) (Li et al, 2024; Tang et al, 2009). Approximately 40% of the Pearl River's total discharge and suspended sediment load is transported through the Hengmen, Hongqimen, and Jiaomen outlets into the west shoal (Ou et al, 2019). Hydrodynamics and sediment dynamic in the PRE are influenced by two alternating monsoons: the southwesterly monsoon during the summer and the northeasterly monsoon during the winter. The estuarine circulation in the PRE is primarily influenced by tidal movements. M2 and K1 are two dominant tidal constituents, followed by O1 and S2. This results in a semi-diurnal mixed tidal regime in the PRE (Mao et al, 2004). During both the wet and dry seasons, waves propagating from the open sea are significantly attenuated upon entering the PRE, with their energy dissipated by a large number of islands in the outer estuary and the shallow water depth along the propagation (Liu & Cai, 2019).

Dramatic changes that occurred throughout the estuary and its delta due to residential and industrial complexes being built at a breakneck speed have greatly altered the morphological, hydrological, hydrodynamical and biogeochemical environments in the past decades (Wei et al, 2023). The time series of annual riverine freshwater discharge from 1954 to 2020 show minor fluctuations around a stable level without a visible trend (Liu et al, 2018; Wu et al, 2016). By contrast, the riverine sediment load in the PRE experienced a notable decreasing trend from 1980s to 2020s. In the 1970s, the annual mean riverine sediment load was ~94 Mt yr^{-1} (Niu et al, 2020).The annual mean riverine sediment loading dropped to ~34 Mt yr^{-1} in 2010s. This dramatic reduction of sediment loading results from dam construction in the upper river from 1970s to 2010s (Lin et al, 2022; Wu et al, 2016). As consequence, reservoirs in the Pearl River basin are heavily silted by sediments, with approximately 70% of the total sediment load from upstream trapped by reservoirs in the West River basin (Wang & Hong, 2021). A combined effect of reduction in sediment load, sand mining, channel dredging, and land reclamation has led to a remarkable morphological change of PRE in the past few decades (Ma et al, 2023; Wu et al, 2016).

Along with a morphological change, the types of sediment in the estuarine bed have also undergone remarkable change, with clay dominance in 1970s altered to silt dominance in 2010s (Figure 1).

The historical change in morphology and sedimentary types in the PRE is mainly driven by human activities, and to a certain extent by climate change. Tide gauge records show that the annual mean rSLR was at a rate of 3.1 mm yr^{-1} for the period of 1954-2023 (www.hko.gov.hk). This rate has been corrected for land settlement (Wong et al, 2003). The average land subsidence rate in the Pearl River Delta is ~2.5 $mm\ yr^{-1}$ with maximum up to 6 $mm\ yr^{-1}$ based on the InSAR data from 2007 to 2010 (Wang et al, 2012).

SPM distribution in the PRE is constrained by topographic features (channels, islands, shoals), as well as by tides, river runoff and monsoon. Existing studies have identified two prominent ETMs (defined as zones with SSC $\geq$ 100 mg L^{-1}) in the upper part of the estuary, one located adjacent to the northern Qi'ao Island and one adjacent to the northeastern Neilingding Island, which are generated by flow convergence (Liu et al, 2016; Yang & Liu, 2015). In recent years, another ETM in the lower part of the estuary, located in the channel adjacent to the Lantau Island, has been identified (Cui et al, 2022; Ma et al, 2024). Existing literature indicate that gravitational circulation and tidal pumping are the principal mechanisms of the formation of the upstream ETMs (Wai et al, 2004), whilst topographical trapping is mainly responsible for the formation of the ETM in the

downstream (Ma et al, 2024). A combined effect of climate change and human activities has also greatly altered the ETMs in the past decades. Long-term observations show that a northeast-southwest large turbidity zone has evolved into multiple independent ETMs due to the morphological changes since 1970s (Yang & Liu, 2015). Wang et al (2021) examined the correlation between water turbidity and various factors including sediment load, wind speed, tidal range, and sea level. Their analysis highlighted that SLR could lead to both longitudinal and lateral landward retreat of ETMs, directly contributing to the decline of water turbidity. An interplay of multiple processes influences the spatial and temporal variations of ETMs in the PRE. However, disentangling the impact of individual process on the historical and plausible future development of ETMs remains a challenge.

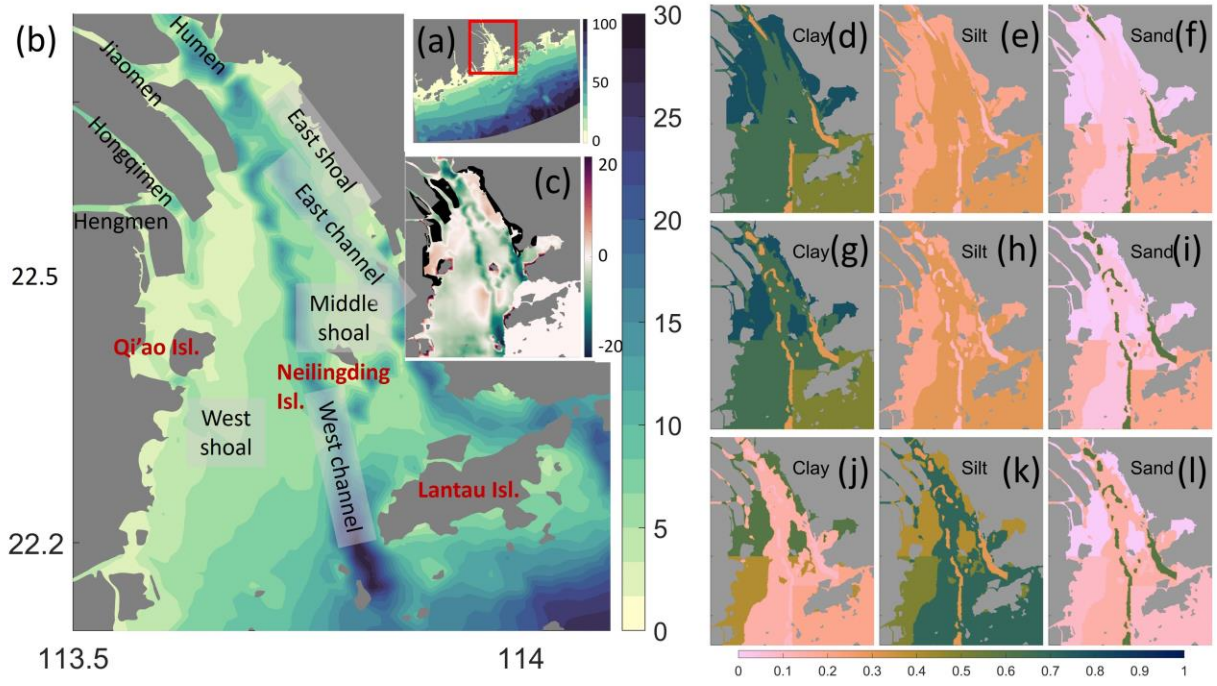

Figure 1 Maps of the study area. (a) Location of the PRE in south China. The red box indicates the range of the Lingiding Bay as the focus of this study. (b)Topographic features of the Lingding Bay. (c) Morphological change in the Lingding Bay from 1970s to 2010s. Black polygons refer to the land reclaimed during this period. Negative values (in green color) indicates a deepening of the bathymetry in 2010s compared to 1970s, vice versa. The seabed sediment maps in (d)-(f) indicate the fractions of clay, silt, and sand in 1970s, respectively. Slightly modified sediment maps based on those for 1970s used for the simulation scenario 2010s_bed are shown in (g)-(i), respectively. Sediment maps based on field measurements in 2010s are shown in (j)-(l), respectively.

3 Numerical model and analysis methods

3.1 Numerical model and setup

The numerical model used in this study is the Semi-implicit Cross-scale hydroscience Integrated system model SCHISM (Zhang et al, 2016). SCHISM addresses the Reynolds-averaged Navier-Stokes equation using a semi-implicit Galerkin finite element method on an unstructured horizontal grid. Vertical velocities and transport are computed with a finite volume method approach for a flexible number of vertical layers. This feature is particularly advantageous for modeling transitions between areas of varying depth and resolution. Effect of wind-waves is included in SCHISM though a coupling to the third-generation, unstructured-grid Wind Wave Model III (WWM III, Roland (2008)). The SCHISM framework also includes a sediment module SED3D (Pinto et al, 2012). Sediment is divided into multiple classes, each defined by specific parameters including grain size, density, settling velocity, erosion rate and critical shear stress for erosion. The model differentiates between cohesive and non-cohesive sediment. Non-cohesive sediments (sands) can be transported in both suspension and bedload depending on the shear stress and settling velocity, while cohesive sediment (clay and silt) is transported in suspension. The transport of each predefined sediment class is computed independently.

3.1.1 Data for numerical modeling

Several observational datasets obtained *via* field surveys and gauge stations in the study area as well as regional and global hydrographic and atmospheric datasets and projections were used for model setup, calibration and assessment of performance. A summary of these datasets is given in Table 1.

Table 1. Data sources used for model initialization (Init.), parameterization (Param.), forcing (Forc.), and model validation (Valid).

type	use	time	description	Source
Morphology of 1970s	Init.	1970s	Nautical charts of 1970s	(Deng et al, 2020)
Discharge & Riverine	Forc.	1954–2018	Annual runoff and sediments load of Boluo gauging station in the Pearl River basin	(Luo et al, 2020)

sediments loading				
Sediment loading	Forc.	2017-2020	Monthly sediment loading from the river outlets	Sediment report of China
Hydrodynamics	Forc.	2017-2020	Model setup for tides, river discharge, open boundary forcing and atmospheric forcing	(Ma et al, 2023)
Hydrodynamics	Forc	2017-2020	Model set up for boundary current forcing	CMEMS
Atmospheric forcing	Forc	2017-2020	Model set up for atmospheric forcing	ERA-interim
Tides	Forc	2017-2020	Model set up for boundary tidal forcing	TPXO
Sediments fraction	Init.	1999-2007	Percentage of clay, silt, and sand at 240 sites sampled in July 1999 and 106 sites sampled in August 2007	(Zhang et al, 2019)
Sediment classes	param	January and July 1999	Particle size and settling velocity of SPM	(Xia et al, 2004)
Sediment classes	param		Setting velocity of clay	(Arlinghaus et al, 2022)
seiment model parameter	Param.	2002/2003 and 2014/2015	Model parameterization for erosion rates	(Porz et al, 2021)
ETMs of 1970s	Vaild.	Wet season of 1978	Spatial distribution of ETMs in the PRE based on observation	(Yang & Liu, 2015)

Sea level rise rate in the past	Forc.	1954-2023	Annual variations in sea level rise	Hong Kong Observatory
Sea level rise rate in future	Forc.	-	In the IPCC Sixth Assessment Report, the latest monitoring and simulation results indicate that the current rate of sea level rise is accelerating (3.7 mm/a) and will continue to rise in the future	(Tong et al, 2022)
Land subsidence rate	Forc.	2015-2018	The subsidence rate obtained through InSAR, with an average of approximately 2.5 mm per year and a maximum of up to 6 mm per year.	(Wang et al, 2012)

3.1.2 Model configuration - hydrodynamics

The model domain spans roughly from 21 to 23°N in latitude and 112.4 to 115.25°E in longitude (Figure 1 a), with a high grid resolution (~50 m) in the Lingding Bay and coarsening resolution (till ~1000 m) toward the open boundary on the outer shelf of the South China Sea. A terrain-following grid is utilized and the vertical plane is subdivided into a maximum of 26 layers. The number of vertical layers decreases from deep water (~100 m water depth) toward shallow water, until to a single layer in areas with a depth of less than 0.4 m. To guarantee a high-resolution modelling of the bottom transport, a thickness of 0.5 m for the bottom-most layer is configured for the entire model domain. Eight primary tidal constituents (M2, S2, N2, K2, K1, O1, P1, Q1) were specified at the open boundary, with tidal data extracted from the TPXO-atlas (Egbert & Erofeeva, 2002). Additionally, daily-averaged data of water level, current (u, v), salinity, and temperature obtained from the Copernicus Marine Environment Monitoring Service (CMEMS, doi.org/10.48670/moi-00021) were specified at the open boundary.

The river boundary was forced by monthly freshwater discharge and sediment load at the eight major outlets obtained from the China Sediment Report (http://www.mwr.gov.cn, see also Supporting Information Figure S1). This dataset has been widely used in studies of the PRE (Liu et al, 2018; Liu et al, 2022; Wu et al, 2016).

Atmospheric forcing for our model includes hourly wind, air pressure, precipitation, and net solar radiation obtained from the European Centre for Medium Range Weather (ECMWF) ERA-interim (Hersbach et al, 2018). This dataset is proven to be consistent with the wind speeds and wind directions measured in Macau Airport (Hong et al, 2022).

3.1.3 Model configuration - sediment

We implemented three sediment classes, namely clay, silt, and fine sands, according to field measurements (Li & Li, 2018; Ma et al, 2024; Xia et al, 2004; Zhang et al, 2019). The sediment fraction of each class for 1970s and 2010s are depicted in Figure 1 with data sources listed in Table 1. The observed time series of SSC from Zhang et al (2020) were utilized to calibrate the sediment model, as detailed in our previous study (Ma et al., 2024).

3.1.4 Scenarios design

To disentangle the impact of individual driving factors and their joint effect for historical as well as plausible future development of the ETMs in the PRE, a set of scenarios for simulation (Table 2) was designed and explained below:

1) Two scenarios, namely 1970s_REF and 1970s_SED, were designed for 1970s. The scenario 1970s_REF is based on historical data of seabed sediment composition, coastline, bathymetry, and riverine sediment load from the 1970s. Its simulation result, namely the location and spatial extent of ETMs, was assessed against historical data. Therefore, this scenario serves as a reference for the 1970s. The scenario 1970s_SED is used to quantify the impact of a reduction in riverine sediment loading on ETMs. The sediment loading measured in 2010s (reduced by 2/3 compared to that in 1970s) was used in this scenario. All other model settings remained the same as the 1970s_REF.
2) Two scenarios, namely 2010s_REF and 2010s_BED, were designed for 2010s. Similar to 1970s_REF, the scenario 2010s_REF is based on measurement data from 2010s and serves as a reference for 2010s. The scenario 2010s_BED is used to quantify the impact of a change in the seabed sediment composition on the ETMs. The bed sediment maps in 1970s, which shows a much larger fraction of clay content and smaller fraction of silt content than those in 2010s (Figure 1), were used in this scenario. All other settings remained the same as the 2010s_REF.

3) Four scenarios, namely 2100s_SLR30, 2100s_SLR100, 2100s_SLR100_SED0.5, 2100_SLR100_SED1.5, were designed for future projections. We consider two trajectories of rSLR, namely 2100s_SLR30 and 2100s_SLR100, corresponding to the SSP1-2.6 (2.0°C warming) and SSP5-8.5 (5.0°C warming) sea level rise scenarios presented in the IPCC Sixth Assessment Report (Ruane, 2024). The rSLR of +100 cm incorporates land subsidence which has been estimated as 2-3 mm yr^{-1} in the PRD (Wang et al, 2012). The pure impact of rSLR was investigated in 2100s_SLR30 and 2100s_SLR100. In these two scenarios, the mean sea level was increased by 30 cm (2100s_SLR30) and 100 cm (2100s_SLR100), respectively, whilst other settings remained the same as the 2010s_REF. In addition to a rSLR by 100 cm, two scenarios, namely 2100s_SLR100_SED0.5 and 2100s_SLR100_SED1.5, were designed to test the sensitivity of ETMs to a change in the riverine sediment load. The scenario 2100s_SLR100_SED0.5 assumed a further reduction of the sediment load by 50% compared to the present-day level, whereas an increase by 50% (compared to the present-day level) was adopted in the scenario 2100s_ SLR100_SED1.5.
4) Two additional scenarios, 2100s_SLR100_WD and 2100s_SLR100_WDWS, are employed to examine the influence of fluctuating wind conditions on ETMs. A study by Hong et al. (2022) shows that the mean wind direction in the PRE in summer (June, July and August) over the period of 1979 - 2020 experienced an anticlockwise rotation by 0.36° per year, along with a decrease in the mean wind speed by 0.03 m yr^{-1}. To test the sensitivity of ETMs to a potential future change in the wind direction and speed, two scenarios (2100s_SLR100_WD and 2100s_SLR100_WDWS) were designed. 2100s_SLR100_WD assumed an anticlockwise rotation by 40° in the mean wind direction in summer months (June, July and August) compared to present-day conditions, whilst 2100s_SLR100_WDWS additionally included a decrease in the mean wind speed by 70% in summer months. All other settings in these two scenarios remained the same as the 2100s_SLR100. Wind rose plot for the wind shifting are available in Figure S2.
5) In the last three scenarios, the impact of wave effects on ETMs in the 1970s, 2010s, and 2100s is assessed. In accordance with the scenarios designated as 1970s_REF, 2010s_REF, and 2100s_SLR100, the wave model was activated within the aforementioned scenarios.

These scenarios were designated as 1970s_REF_wave, 2010s_REF_wave, and 2100s_SLR100_wave, respectively.

Table 2. Model scenarios with configuration in the initial morphology (Mor.), riverine sediment load (Sed. load), seabed sediment composition (Sed. Comp.), mean sea level (SL), wind condition (wind cond.) which involve wind direction (WD) and wind speed (WS), wave model (activate: No/Yes) designed for this study.

Scenarios	*Mor.*	*Sed. load*	*Sed. Comp.*	*SL*	*Wind cond.*	*Wave model*
1970s_REF	1970s	1970s	1970s	1970s	2010s	No
1970s_SED	1970s	2010s	1970s	1970s	2010s	No
2010s_BED	2010s	2010s	1970s	2010s	2010s	No
2010s_REF	2010s	2010s	2010s	2010s	2010s	No
2100s_SLR30	2010s	2010s	2010s	2010s+30cm	2010s	No
2100s_SLR100	2010s	2010s	2010s	2010s+100cm	2010s	No
2100s_SLR100_SED0.5	2010s	2010s*0.5	2010s	2010s+100cm	2010s	No
2100s_SLR100_SED1.5	2010s	2010s*1.5	2010s	2010s+100cm	2010s	No
2100s_SLR100_WD	2010s	2010s	2010s	2010s+100cm	2010s $-40°$ WD	No
2100s_SLR100_WDWS	2010s	2010s	2010s	2010s+100cm	2010s $-40°WD$ 40% WS	No
1970s_REF_wave	1970s	1970s	1970s	1970s	2010s	Yes
2010s_REF_wave	2010s	2010s	2010s	2010s	2010s	Yes
2100s_SLR100_wave	2010s	2010s	2010s	2010s+100cm	2010s	Yes

292

293 ## 3.2 Analysis method

294 ### 3.2.1 Potential energy anomaly

295 In this study, the potential anergy anomaly (PEA) φ (Simpson & Bowers, 1981) is employed as a
296 metric of stratification. The value of φ is calculated by:

297 $$\varphi = \frac{1}{H}\int_{-h}^{\eta}(\bar{\rho} - \rho)gzdz. \quad (1)$$

298 The vertical density profile over the water column of depth $H = \eta + h$, where η is the free surface,
299 h is the bed level, $\bar{\rho}$ is the depth-average density, z is the vertical coordinate, and g is the
300 gravitational acceleration. The value of φ indicates the work required per unit of volume to achieve
301 complete vertical mixing of the water column.

302 ### 3.2.2 Sediment flux decomposition

303 Based on the analytical method of mass transport flux proposed by Dyer (1974), and using the
304 relative depth as a vertical coordinate instead of absolute depth, Jilan & Kangshan (1986)
305 decomposed cross-sectional currents for analysis of respective forcing. The same method was
306 applied by (Wai et al, 2004) to investigate tidally averaged sediment transport. The sediment
307 transport was decomposed into terms related to non-tidal drift, stokes drift, tidal pumping, vertical
308 gravitational circulation, and a term resulting from scouring and settling.
309 By interpolating the model result into fixed depths in the vertical plane, the sediment transport flux
310 in each vertical layer was decomposed into (Gong et al, 2014):

311 $$\overline{uc} \approx (\bar{u})(\bar{c}) + \overline{u_t c_t}, \quad (2)$$

312 where u is the current velocity along the major axis in that layer, c is the sediment concentration
313 in the same layer, and the over bar represents the time average over a 25-hour period in this study.
314 The subscript t denotes tidal variations, u_t and c_t refer to tidal variations of current velocity and
315 sediment concentration, respectively. $\overline{uc}$ signifies the total net sediment transport flux. $(\bar{u})(\bar{c})$
316 represents the mean advective sediment flux, and $\overline{u_t c_t}$ represents the flux associated with tidal
317 pumping. The application of this equation to the bottom layer can be used to identify the major
318 driving mechanism for formation of ETM as elucidated by (Ma et al, 2024).
319 In this study, we applied Eq. (2) to calculate the sediment flux in the bottom layer of the PRE. This
320 is expressed by:

321 $$f_b \approx T_{ba} + T_{bp}, \quad (3)$$

where f_b is the sediment flux ($\overline{uc}$) in the bottom layer, T_{ba} represents the mean advective sediment flux component ($(\bar{u})(\bar{c})$) in the bottom layer, and T_{bp} represents the sediment flux associated with tidal pumping ($\overline{u_t c_t}$) in the bottom layer.

4 Results

4.1 Model validation

The hydrodynamic model has been validated in terms of water level, salinity, and temperature for the reference simulation for 2010s (2010s_ref) by Ma et al (2023). Simulated SPM dynamics, location of ETMs and their spatial extent in 2010s in the PRE have also been validated against measurement data by Ma et al. (2024). The results of the reference simulation for 2010s (2010s_ref) indicate the presence of three ETMs during the wet season. Two of them are situated in the upper part of the PRE, with the ETM on the west shoal designated as TM_shoalw and the ETM on the middle shoal designated as TM_shoalm (Figure 2c). The ETM located in the west channel is designated as TM_channel. The presence of TM_shoalw and TM_shoalm ETMs has been confirmed by several field studies (Liu et al, 2016; Yang & Liu, 2015; Zhang et al, 2021b). The TM_channel was firstly identified by Wai et al (2004) and further confirmed by Cui et al (2022). In this study, model assessment is focused on the spatial extent of ETMs and SSC in 1970s.

A sketch map made by Yang & Liu (2015) based on field measurements in 1978 summer shows a turbidity zone located between the river mouth of Humen and the Qi'ao island (Figure 2b) with SSC between 80 and 300 mg L^{-1}. The location of the nucleus (>160 mg L^{-1}) of the ETM is located adjacent to the northern tip of the Qi'ao island. The area of the turbidity zone (>80 mg L^{-1}) and the nucleus of the ETM are generally reproduced by our reference simulation result (1970s_ref) for 1970s (Figure 2), albeit the turbidity zone in the model result exhibits a larger extent than in the observation.

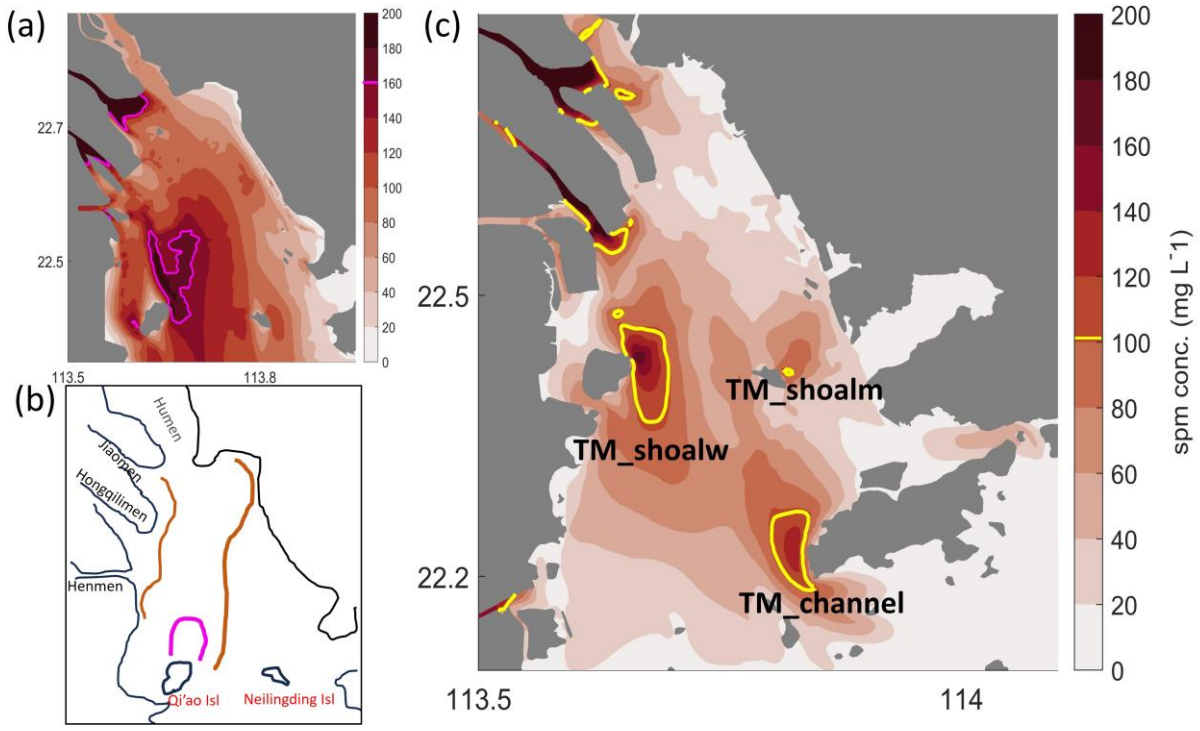

Figure 2 (a) Distribution of bottom SSC in the wet season of the scenario 1970s_REF. The magenta polygons represent the nucleus of ETMs (SSC ≥160 mg L^{-1}). (b)Map of the observed turbidity zone in the wet season in 1978 derived from Yang & Liu (2015). The magenta line delineates the ETM nucleus (>160 mg L^{-1}), and the brown lines indicate the turbidity zone where observed SSC is between 80 and 300 mg L^{-1} (c) Distribution of bottom SSC in the wet season of the scenario 2010s_ref. The yellow polygons represent the boundary of ETMs (bottom SSC =100 mg L^{-1}).

4.2 Historical development of the ETMs: 1970s - 2010s

The scenarios 1970s_REF, 1970s_SED, 2010s_BED, 2010s_REF, and 2100s_SLR30 were designed to understand the historical evolution of ETMs in the PRE. The influencing factors include changes in the coastline and riverine sediment load, transformation in the bed sediment from clay-dominance to silt-dominance, and relative sea level rise. Simulated SSC in the bottom layer of each of these scenarios is illustrated in Figure 3. A comparison between the results indicates remarkable changes of bottom SSC and ETMs from 1970s to 2010s.

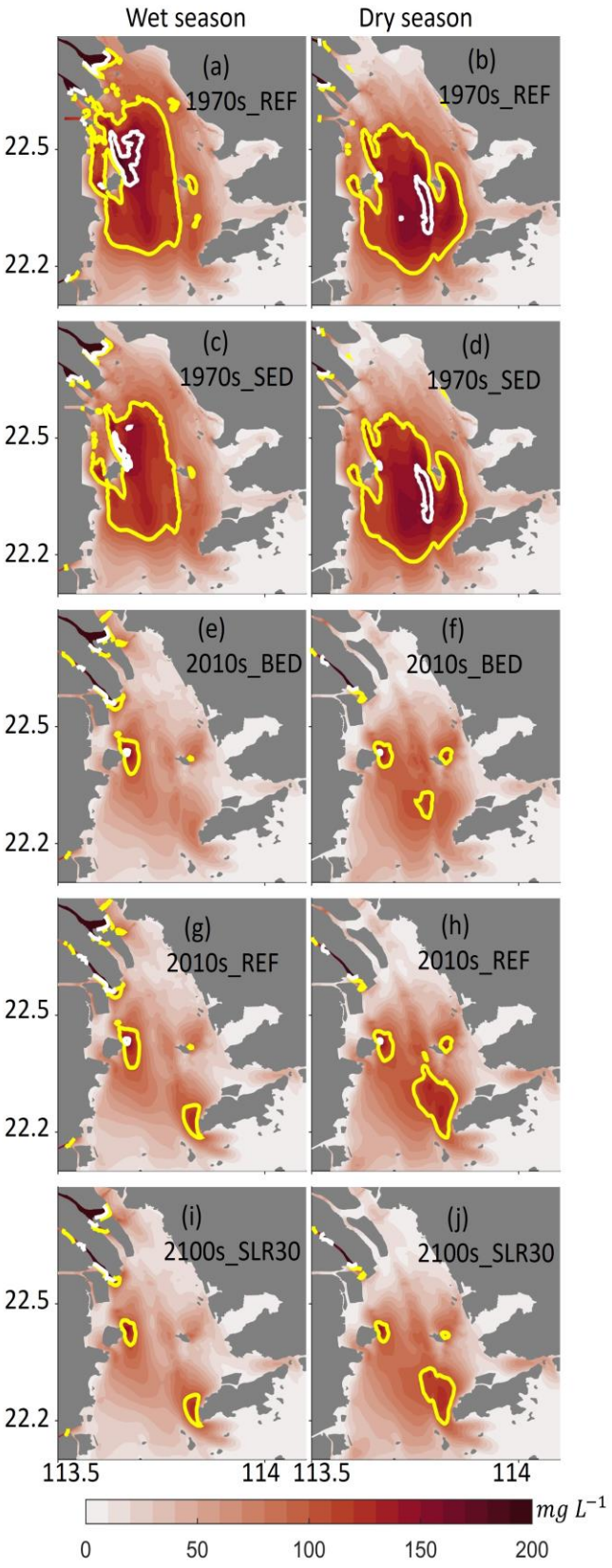
Wet season
Dry season
(a) 1970s_REF
(b) 1970s_REF
(c) 1970s_SED
(d) 1970s_SED
(e) 2010s_BED
(f) 2010s_BED
(g) 2010s_REF
(h) 2010s_REF
(i) 2100s_SLR30
(j) 2100s_SLR30
22.5
22.2
113.5
114
$mg\ L^{-1}$
0
50
100
150
200

359

Figure 3. Simulated bottom SSC distribution in the wet season (left column) and dry season in the 1970s_REF, 1970s_SED, 2010s_BED, 2010s_REF, and 2100s_SLR30 scenario. The contour lines of 100 mg L^{-1} and 160 mg L^{-1} are marked by yellow and white color, respectively. The distribution of sediments across different classes is illustrated in Figure S3.

4.2.1 Impact of sediment load reduction

From 1970s to 2010s, there was a notable decline in the quantity of sediment discharged into the Pearl River. A comparison between the scenario 1970s_REF (Figure 3a, b) and 1970s_SED (Figure 3c, d) reveals the impact of the sediment load reduction on ETMs. In the wet season, the reduction in sediment load results in a notable decrease in the spatial extent of ETM. For instance, the nucleus of the ETM where bottom SSC ≥160 mg L^{-1} declines by approximately 50% in the reduced sediment load scenario (1970s_SED) compared to the reference scenario (1970s_REF).

A natural seasonal reduction in sediment load from the wet season to the dry season results in a notable change of the ETM, which is characterized by a shrink along the N-S axis and expansion toward the east. Such change is seen in both scenarios, indicating that the long-term reduction of annual riverine sediment load has minor effect on the seasonal variation of ETM. The nucleus of the ETM (SSC ≥ 160 mg L^{-1}) also exhibits a spatial migration from the wet season to the dry season, which is not affected by the long-term reduction of riverine sediment load.

4.2.2 Impact of morphological change

From the 1970s to the 2010s, the PRE experienced a continuous shrink in its water area due to land reclamation and a deepening of the channels due to dredging (Figure 1). Adopting the same configuration in seabed sediment distribution, riverine loading and external forcing but with different morphology, the difference between the scenario 1970s_SED and 2010s_BED reveals the impact of morphological change on the ETMs (Figure 3 c-f).

The comparison between the two scenarios indicates that the morphological change has the largest impact on the bottom SSC and ETMs among all driving factors. Bottom SSC is significantly reduced, and the massive spatial extent of the ETM in 1970s has diminished and evolved into several much smaller ETMs in 2010s. The comparison of sediment residual flux between 1970s_SED and 2010s_BED in the wet season (Figure 4 a, c) reveals a shrinking trend of the ETM on the west shoal. The ETM in the 1970s (Figure 4 a) covered the northern part of the west shoal and extended east of the Neilingding Island. However, following the morphological change, the ETM has experienced a significant reduction, resulting in a smaller ETM on the west shoal (i.e. TM_shoalw) in 2010s (Figure 4 c). The deepening of bathymetry has resulted in a significant

391 increase in saltwater intrusion, which has led to an intensification of convergence on the west shoal,
392 as well as an enhanced stratification which suppress the resuspension of sediment. This is the
393 primary reason for the shrinking of the ETM on the west shoal. Additionally, changes in the
394 coastline have influenced the distribution of SSC. The seaward extension of land and the narrowing
395 of tributary outlets have facilitated the transportation of riverine sediment away from the tributary
396 outlets. Similarly, during the dry season, the same shrinking pattern is confirmed on the west shoal
397 (Figure 4 b, d). It is noteworthy that an ETM occurs at the junction between the west shoal and
398 west channel during the dry season in the scenario 2010s_BED (Figure 4 d). The underlying reason
399 for this occurrence is the existence of a shear gradient between the channel and the shoal, which
400 gives rise to a residual sediment transport from the channel to the shoal. This residual sediment
401 transport converges with the southward directed residual sediment transport on the shoal, forming
402 the ETM between the west shoal and west channel. Overall, the morphological change resulted in
403 a more concentrated distribution of ETM on the west shoal, accompanied by a notable reduction
404 in SSC in the PRE. Nevertheless, this is not responsible for the formation of ETM in the west
405 channel.
406

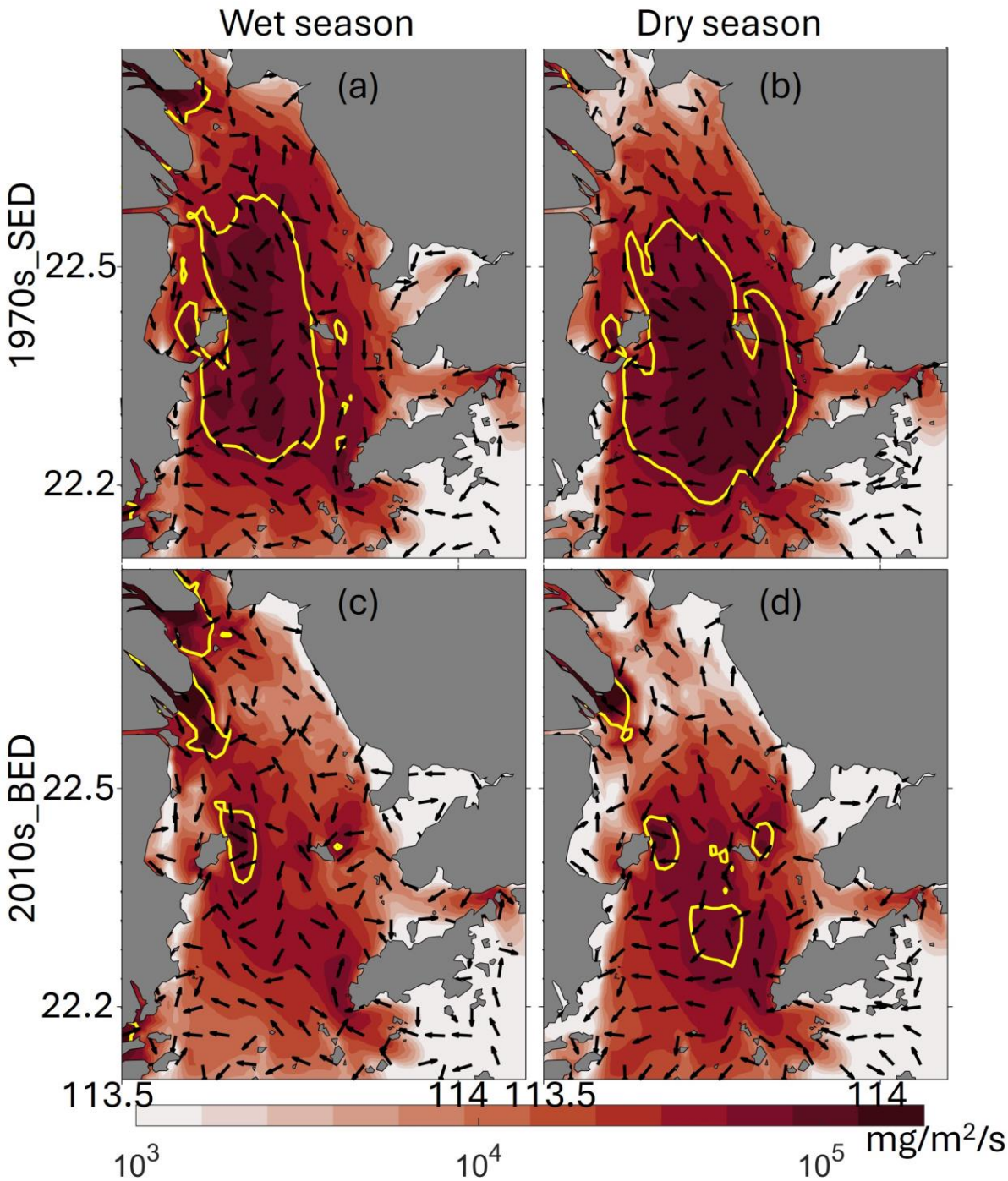

Figure 4 Residual sediment flux of 1970s_SED and 2010s_BED. The first row (a, b) show the residual sediment flux rate and direction of 1970s_SED; the second row (c, d) show the residual sediment flux rate and direction of 2010s_BED. The black arrow shows the direction of residual sediment flux. The yellow line indicates the SSC contour 100 mg L^{-1}.

4.2.3 Impact of change in sediment type

In addition to a reduction in riverine sediment load, human activities (sand mining, channel dredging and dumping) have also affected the composition of sediments on the estuarine bed. Clay content has largely been depleted since 1970s and the present-day estuarine bed is dominated by silts (Figure 1). Adopting the same configuration in the model setting except for the sediment composition in the estuarine bed, the difference between the scenario 2010s_BED and 2010s_REF reveals the impact of a change in sediment composition on the ETMs. A comparison between the results of these two scenarios indicates that SSC in the PRE is enhanced by a change from clay-dominance to silt-dominance in the estuarine bed, leading to a larger spatial extent of ETMs (Figure 3e-h). The most significant change occurs in the channel, where the ETM becomes not only larger but also persistent throughout the year. In the clay-dominance scenario (2010s_BED), this ETM appears only in the dry season. Therefore, the confluence of morphological change and change in sediment type on riverine bed yielded a verifiable ETM distribution pattern for the 2010s.

4.2.4 Impact of relative Sea level rise

The relative sea level rise (rSLR) in the PRE is affected by both eustatic SLR and regional land subsidence. The impact of rSLR on the historical development of ETMs from 1970s to 2010s is assessed by comparing the scenarios 2010s_REF and 2100s_SLR30, in which all model settings are the same except for a rSLR of 30 cm in the latter. A comparison between the results in these two scenarios indicate that the bottom SSC is decreased due to the rSLR, leading to reduced spatial extent of the ETMs (Figure 3 g-j). The ETM on the middle shoal (TM_Shoalm) is no longer persistent throughout the year but appears only in the dry season. The reason for the change is that the rSLR enhances the stratification, which in turn reduces the SSC on the shoal (Figure 5). During the wet season, stratification is significantly enhanced in the upper part of the PRE, particularly in the vicinity of the Humen outlet. Consequently, the reduction in bottom SSC is more pronounced in the two ETMs located in this region (TM_shoalw and TM_shoalm). In the dry season, the change in stratification caused by the rSLR is relatively mild due to greatly reduced freshwater discharge from the rivers leading to enhanced vertical mixing by tides. In the lower part of the PRE, a slight reduction in stratification by the rSLR occurs in the channel area during the wet season. Such reduction in stratification does not impact the ETM (TM_channel) in the channel. In the dry season, the reduction in stratification is further enhanced in the channel and extended further upstream. This leads to a notable decrease of the extent of the TM_channel. The reason for

this is that the rSLR causes a weakening of stratification in the channel and in the meanwhile also reduces bottom shear stress there. The impact of reduced resuspension due to lower bottom shear stress prevails the impact of enhanced mixing related to weaker stratification, leading to a decline of SSC in the TM_channel, particularly in its northwest part (Supporting Information Figure S4).

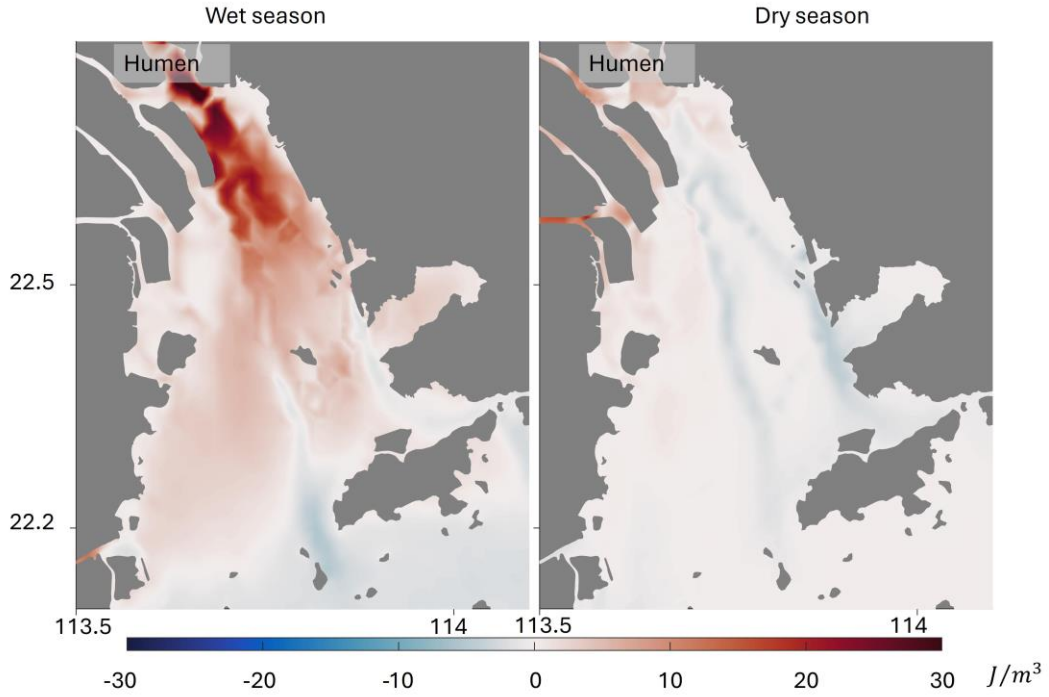

Figure 5 The depth average PEA difference between 2010s_REF and 2100S_SLR30 in the wet (left panel) and dry seasons. Positive and negative values indicate enhancement and weakening of stratification by the rSLR, respectively.

4.3 Future scenarios

In the future projections, impact of accelerated rSLR, change in riverine sediment loading and monsoon are assessed.

4.3.1 Impact of accelerated relative sea level rise

The rSLR is expected to continue and accelerated in the forthcoming decades due to global warming. A comparison between the scenarios 2100s_SLR30, 2100s_SLR100 with reference to 2010s_REF (Figure 6) helps to unravel the impact of the accelerated rSLR. Results suggest that the accelerated rSLR (2100s_SLR100) results in a substantial reduction of SSC, particularly on the shoals (TM_shoalm and TM_shaolw), with a maximum reduction up to ~60 mgL^{-1} in the bottom SSC compared to the reference scenario 2010s_REF. This reduction is ~ 3 times higher compared to the impact of a rSLR following the same rate in the past decades (2100s_SLR30,

Figure 6 a). The increasing of SSC in Hongqilimen in the wet season (Figure 6 c) may be attributed to the landward movement of stratification, which resulted in a convergence of sediment flux in Hongqilimen. As the rSLR the ETMs exhibit a shrinking trend in extent and a decreasing trend in SSC in both the wet sea and the dry season(Figure 6). The area of TM_shoalm exhibited a notable decline of approximately 50% under the rSLR of 30 cm during the wet season, and a more modest reduction of approximately 25% during the dry season. Conversely, the area of TM_channel demonstrated a relatively minor change in both seasons (Figure 6 a, b). Under a rSLR of 100 cm, more than 90% area of TM_shoalw disappears in the wet season (Figure 6 c), while the reduction percentage is 80% in the dry season (Figure 6 d). The reduction of area of TM_channel becomes more prominent than that with a rSLR of 30cm (Figure 6 c, d). Especially in the dry season, the area of TM_channel decreases by ~80% with a rSLR of 100cm (Figure 6 d). Similarly, the TM_shaolm almost disappears with a rSLR of 100 cm.

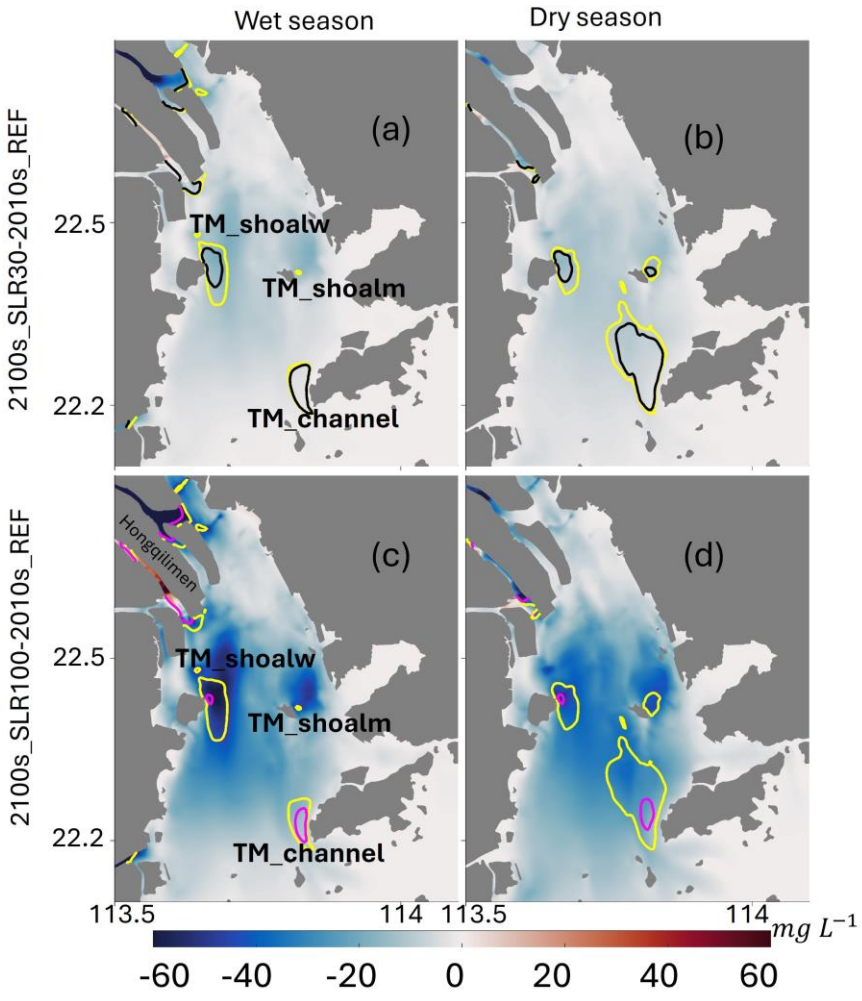

Figure 6 The SSC difference and change of ETMs between scenario 2100s_SLR30 and 2010s_REF, 2100s_SLR100 and 2010s_REF. (a, b) 2100s_SLR30-2010s_REF in wet season and dry season; (c, d) 2100s_SLR100-2010s_REF in wet season and dry season. The yellow line indicates 100 mg L^{-1} in 2010s_REF, the black line indicates 100 mg L^{-1} in 2100s_SLR30, and the magenta line indicates 100 mg L^{-1} in 2100s_SLR100. The blue color indicates a reeducation on SSC, while the red indicates an increase in the colorbar.

4.3.2 Impact of varying sediment loading under rSLR

As explained in section 4.2.1, a reduction in sediment loading results in a general decline in SSC over the entire PRE for the period of 1970s-2010s. The impact of riverine sediment loading on future development of the ETMs is assessed here in the context of accelerated rSLR. Results of the two scenarios, namely 2100s_SLR100_0.5SED which assumes a further reduction in sediment load by 50% and 2100s_SLR100_1.5SED which assumes an increase in sediment load by 50% compared to the 2100s_SLR100, the differences between 2100s_SLR100 and 2100s_SLR100_0.5SED, as well as 2100s_SLR100 and 2100s_SLR100_1.5SED are presented in Figure 7. The compare between 2100s_SLR100 and 2100s_SLR100_0.5SED show that the decrease of sediment load lead to reduction on bottom SSC, and this reduction effect gradually decreases away from the tributary outlets, moreover the reduction effect is more obviously in the wet season than it in the dry season (Figure 7 a,b). In the wet season, the reduction of bottom SSC in the TM_shoalw zone is about 7%, 6.57% in the TM_shoalm zone, and 0.73% in the TM_channel zone.The increase of sediment load by 50% result in an increase on bottom SSC, and show the same pattern as the reduction in Figure 6 a,b. In the wet season, the increasing of bottom SSC in the TM_shoalw zone is about 7%, 6% in the TM_shoalm zone, and 0.73% in the TM_channel zone. The comparison between the 2100s_SLR100_0.5SED and the 2100s_SLR100_1.5SED scenarios reveals an elevation on bottom SSC resulting from the increase of sediment load (Figure 7 e, f). An increase in sediment load to three times of the present-day value has a notable impact on bottom SSC, with SSC values increased by approximately 15% in the TM_shoalw zone, 14% in the TM_shoalm zone, and 1.47% in the TM_channel zone. However, this is only slightly higher than the impact of a ~67% decrease in sediment load on bottom SSC during the 1970s, with the decreasing value of bottom SSC being 11% in the TM_shoalw zone, 9.8% in the TM_shoalm, and 2.65% in the TM_channel zone (Figure 3, a-c). When this comparison is extended to the entire Lingding Bay, the large increase in sediment load leads to a 39.56% increase of bottom SSC in the 2100s, while the increase in the 1970s is 14.7%. This indicates that the PRE may become increasingly starved in the SPM following the morphological change and rSLR.

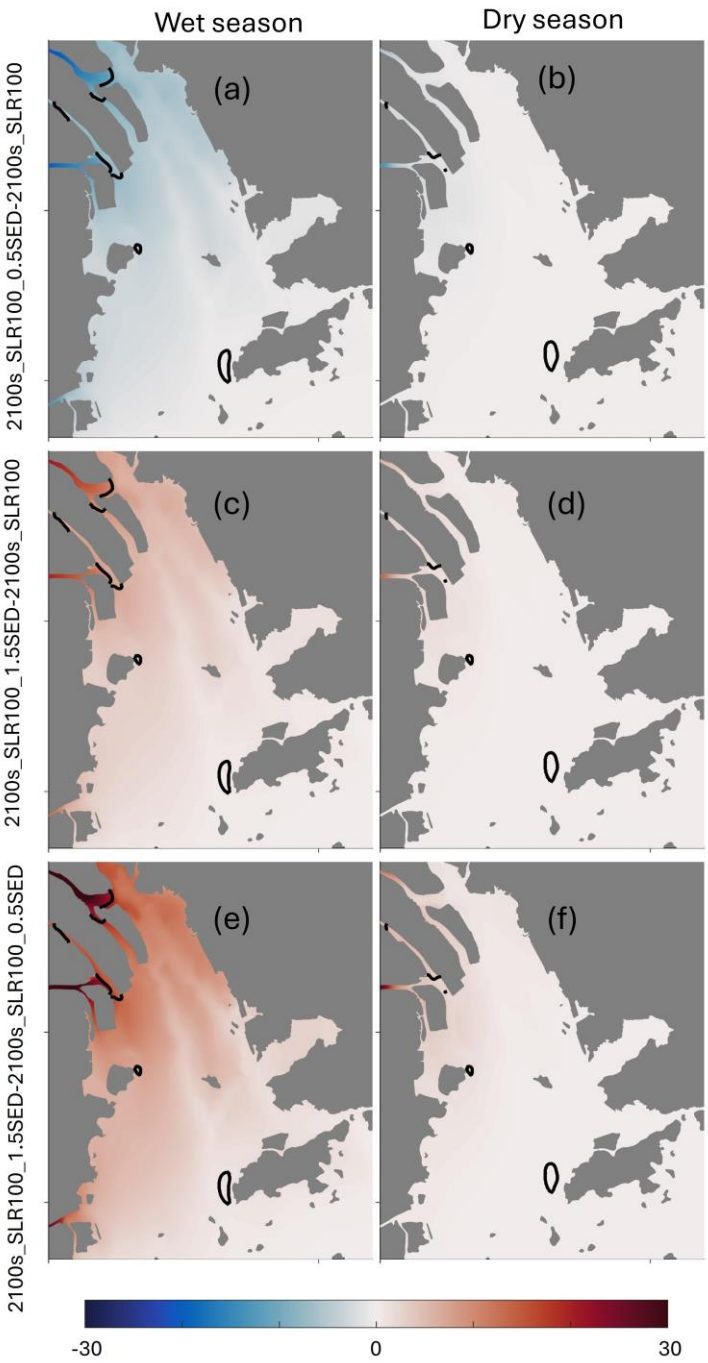

Figure 7 The differences between bottom SSC distribution in the wet season and dry season of the 2100s_SLR100, 2100s_SLR100_0.5SED and 2100s_SLR100_1.5SED scenarios. (a, b) is the difference of bottom SSC between 2100s_SLR100_0.5SED and 2100s_SLR100. (c, d) is the difference of bottom SSC between 2100s_SLR100_1.5SED and 2100s_SLR100. (e, f) is the difference of bottom SSC between 2100s_SLR100_1.5SED and 2100s_SLR100_0.5SED. The left column presents the results of the wet season; the right column presents the results of the dry season. The black line represent the location of ETMs in 2100s_SLR100..

4.3.3 Impact of change in the monsoon

Impact of potential change in the summer monsoon can be identified by comparing the results from the scenarios 2100s_SLR100_WD and 2100s_SLR100_WDWS with reference to 2100s_SLR100. The impact of an anticlockwise rotation by 40° in the mean wind direction in summer months (June, July and August) is seen by the difference between 2100s_SLR100_WD and 2100s_SLR100 (Figure 8 d). A shift in the mean wind direction from southwest to southeast in summer period results in a general increase in bottom SSC in the PRE, except for the western region of the Lantau Island where the TM_channel is situated. The reason is that the southeasterly wind counteracts the riverine outflow and associated sediment export from the outlets, resulting in a longer residual time in the PRE. This promotes settling of fine-grained sediments including clay and silt inside the Lingding Bay. Meanwhile, long distance transport of sediment to the TM_channel area is weakened due to changed circulation pattern, resulting in a reduction of SSC in the TM_channel (Figure 8 g). As a result, the spatial extent of TM_shoalw has increased, while the TM_channel has diminished (Figure 8 a, b ,c) under the impact of a change in the mean wind direction in summer months (June, July and August).

The impact of reduced wind speed in summer on the distribution of bottom SSC is seen by comparing the results from 2100s_SLR100_WD and 2100s_SLR100_WDWS (Figure 8 e). A reduction in wind speed by 60% results in a decline of bottom SSC by up to 15 mg L^{-1} in the northern part of the western shoal and an increase of bottom SSC by up to 10 mg L^{-1} in the southern part of the shoalIn the middle shoal, bottom SSC is generally decreased. By contrast, bottom SSC in the channels is increased. The most remarkable increase of bottom SSC occurs in the TM_channel adjacent to the Lantao Island by up to 15 mg L^{-1}. The spatial extent of TM_shoalw has diminished, which is likely due to the reduction in wind speed resulting in diminished resuspension on west shoal. The elevated SSC in the southern part of west shoal suggests that the diminished SPM in the northern part has been transported to the southern of the shoal. The spatial extent of the TM_channel increased as a consequence of the reduction in wind speed. This can be attributed to the fact that the formation mechanism of the TM_channel is driven by topographic trapping(Ma et al, 2023). The reduced wind speed resulted in an enhanced residual sediment flux in the west channel (Figure 8 h), which resulting from the decreased shear stress between west channel and west shoal.

The combined effect of wind direction rotation and wind speed reduction is seen by comparing the result of 2100s_ SLR100_WDWS and 2100s_SLR100 (Figure 8 f, i). The change of wind direction and speed jointly lead to a lower bottom SSC in the northern part of the western shoal and higher bottom SSC in the southern part of the shoal. Bottom SSC is generally increased on the middle shoal and in the channels. The increase of bottom SSC in the TM_channel by a reduction of wind speed prevails the decrease by changed wind direction there. The reduction in wind speed results in a decrease in shear stress on the bank at the edge of the channel, which reduces lateral transport of SPM between the channel and the west shoal and thereby allowing a greater proportion of SPM to remain within the channel.

The impact of changes in the summer monsoon can be further explained by the residual sediment transport flux (Figure 8). The direction of the residual sediment transport flux on the west shoal exhibits an eastward shift following a change in the wind direction (Figure 8 f). This indicates that the landward sediment transport was enhanced on the west shoal, resulting in elevated SSCs in this area due to convergence with the seaward sediment transport from the river mouths. A reduction in wind speed leads to a decrease of the residual sediment transport flux in the vicinity of the outlets. By contrast, residual sediment transport flux in the southern part of the west shoal as well as in the channel adjacent to the Lantao Island where TM_channel is located experiences a remarkable increase (Figure 8 g). The joint effect of changes in wind direction and speed leads to similar changes of the residual sediment transport flux to the impact of wind speed reduction (Figure 8 h), with further enhanced landward transport on the southern part of the west shoal, inside the channels and on a vast part of the middle shoal.

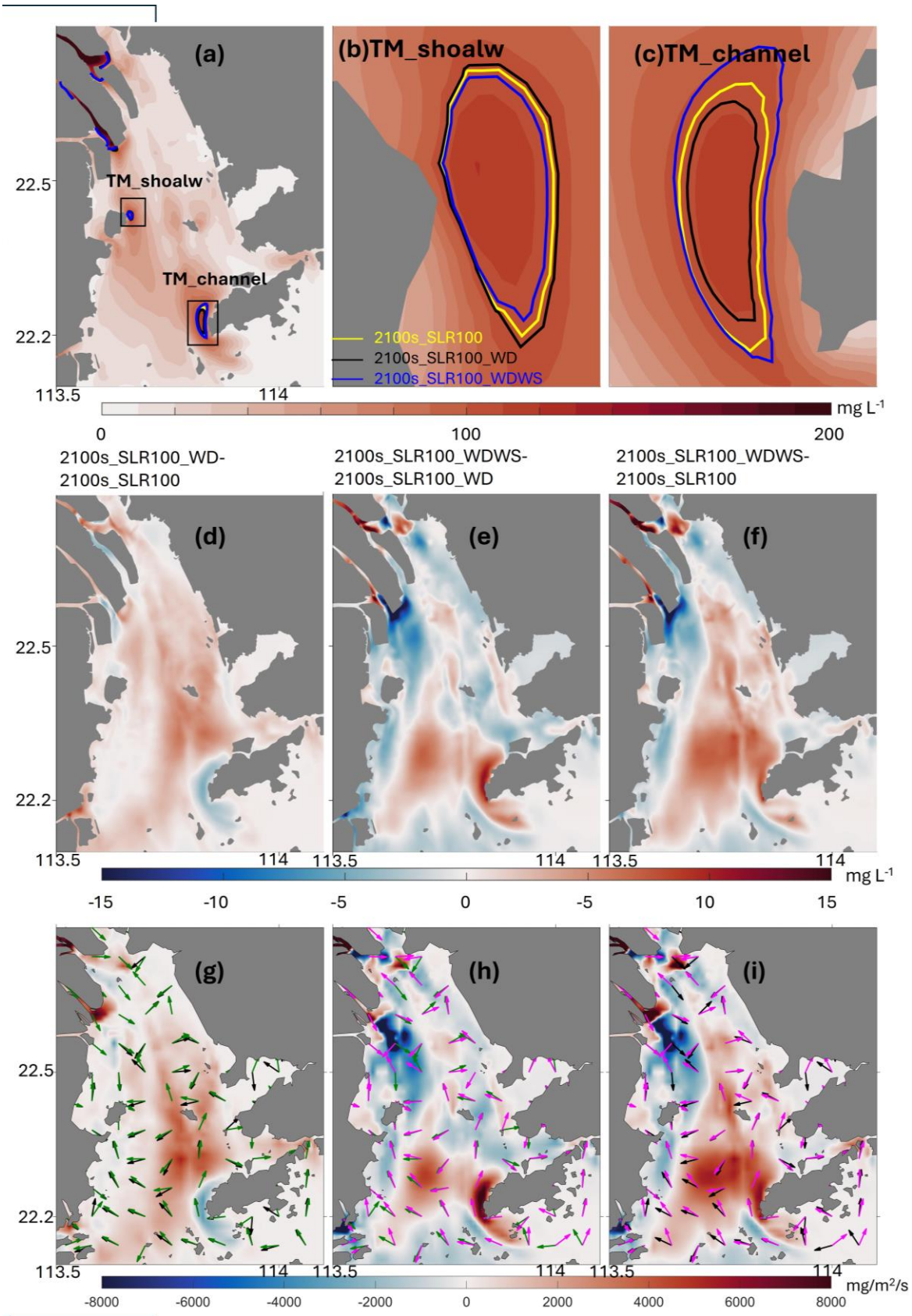
(a)
(b)TM_shoalw
(c)TM_channel
TM_shoalw
TM_channel
2100s_SLR100
2100s_SLR100_WD
2100s_SLR100_WDWS
22.5
22.2
113.5
114
mg L-1
0
100
200
2100s_SLR100_WD-
2100s_SLR100
2100s_SLR100_WDWS-
2100s_SLR100_WD
2100s_SLR100_WDWS-
2100s_SLR100
(d)
(e)
(f)
-15
-10
-5
0
-5
10
15
(g)
(h)
(i)
mg/m2/s
-8000
-6000
-4000
-2000
0
2000
4000
6000
8000

564

Figure 8 Change of ETMs, difference of bottom SSC, and difference of residual current between scenarios of wind condition shifting in the wet season. The bottom SSC of 2100s_SLR100 is shown in (a), with the zoom-in of TM_shaolw in (b), and (c) shows the zoom in of TM_channel. (d) Bottom SSC difference between 2100s_SLR100 and 2100s_SLR100_WD; (e) bottom SSC difference between 2100s_SLR100_WDWS and 2100s_SLR100_WD. (f) bottom SSC difference between 2100s_SLR100_WDWS and 2100s_SLR100. (g) the sediment residual flux difference between 2100S_SLR100 and 2100s_SLR100_WD, the green arrow is the direction of sediment residual flux in 2100s_SLR100_WD. (h) the sediment residual flux difference between 2100s_SLR100_WDWS and 2100s_SLR100_WD, the magenta arrow is the direction of sediment residual flux in 2100s_SLR100_WDWS. (i) the sediment residual flux difference between 2100s_SLR100_WDWS and 2100s_SLR100.

5 Discussion

5.1 Impact of the changing tides

The variation of tides can exert a considerable influence on estuarine hydrodynamics and the importance of tidal asymmetry in sediment transport has been quantified in various studies (Burchard et al, 2018; Scully & Friedrichs, 2007; Zhang et al, 2019). As reported by Dijkstra et al (2019) the channel deepening in the Ems River estuary between the 1960s and early 2000s occurred concurrently with an increase in the SSC, which rose from moderate levels (~1 kg/m^3) to high levels (>10 kg/m^3). Model analysis demonstrates that the deepening of the channel and the sediment-induced damping of turbulence near the bottom increase the M2 and M4 tidal asymmetry, which consequently results in an increase in the magnitude of sediment import with enhanced flood levels (Winterwerp & Wang, 2013). In the Tagus estuary in Portugal, the strong ebb-dominance of this estuary will decrease significantly due to the decrease of intertidal area resulting from the SLR (Bertin et al, 2015). In estuaries, the flood-dominated area normally promotes net landward sediment transport, whereas the ebb-dominated area promotes net seaward sediment transport (Guo et al, 2019). The alteration in tidal asymmetry will consequently affect the sedimentation, which in turn will alter the geomorphology of the estuary over a long-time scale. This may result in further changes in tidal dynamics through a feedback loop.

In our previous study (Ma et al (2024), tidal pumping due to tidal asymmetry is found to play a pivotal role in the formation of ETMs in the PRE. This study illustrates the tidal pumping effect of the bottom sediment flux in two scenarios, namely the 1970s_SED and 2010s_REF, under the impact of morphological change. The impact of rSLR on tidal pumping is analyzed by comparing another two scenarios, namely 2100S_SLR30 and 2100S_SLR100. In scenario 1970s_SED (Figure 8 a e i), the sediment flux was predominantly advective. The sediment flux on the West Shoal exhibits a southward direction, while the sediment flux in the West Channel demonstrates a

northward movement, driven by both advection and tidal pumping. Following morphological changes in 21010s_REF, the convergence due to tidal pumping on the West Shoal (eastern north of Qi'ao Island) becomes evident where the TM_shoalw is situated (Figure 9 j). The effect of tidal pumping is diminished with rSLR in scenarios 2100s_SLR30 and 2100s_SLR100 (Figure 9 k l), corresponding with the observed reduction in TM_shoalw. The tidal dynamic changes can be seen by the tidal ellipse in Figure 10. Morphological changes cause an increase in tidal ellipticity, a reduction of peak velocity (Figure 10 b) during the tidal cycle, as well as spatial differences in the orientation of tidal ellipse (Figure 10 d) in the upper part of the PRE. As the primary tidal ellipse typically aligns with the coastline, the clockwise orientation of the ellipse is consistent with the clockwise rotation of the west coastline (Figure 1 c, Supporting Information Figure_S9).

The modified tidal dynamics resulting from morphological changes and rSLR can influence the transport of sediments, leading to variations in the concentration and/or location of ETMs, as well as alterations in SPM distribution. The altered tidal asymmetry may also affect the long-term sedimentary patterns of the estuary. These sediment transport patterns will, over time, affect the estuary shape (Khojasteh et al, 2022; Masselink et al, 2007; Zarzuelo et al, 2019).

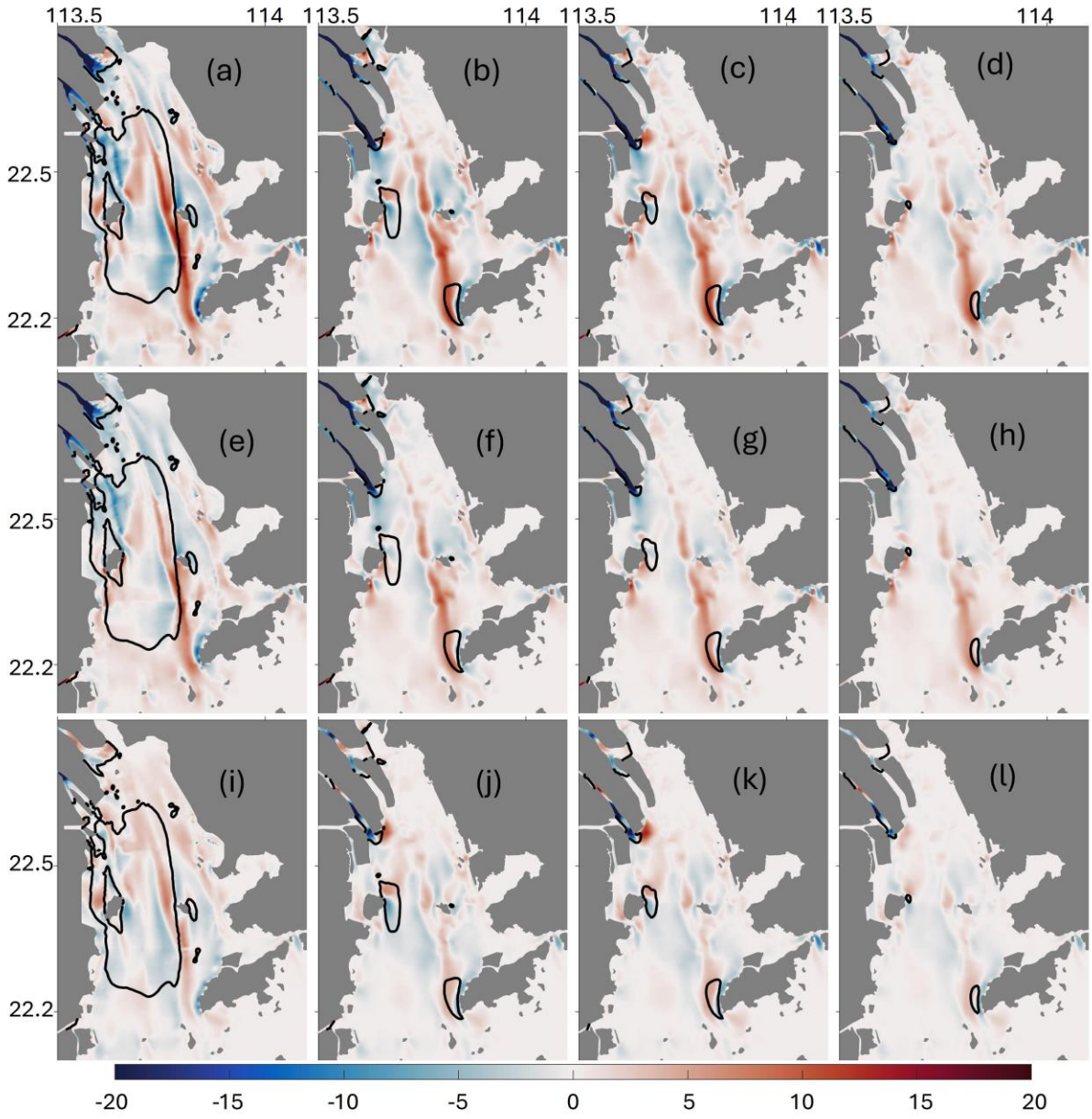

Figure 9 Spatial distribution of tidal pumping (Tbpin) in the bottom water layer of scenarios: 1970s_SED, 2010s_REF, 2100s_SLR30, 2100s_SLR100 in the wet (unit: $m \cdot mg \cdot s^{-1}L^{-1}$.). Positive (red color) and negative (blue color) values indicate northward and southward transport, respectively. The black line indicates the location of ETMs in different scenarios.

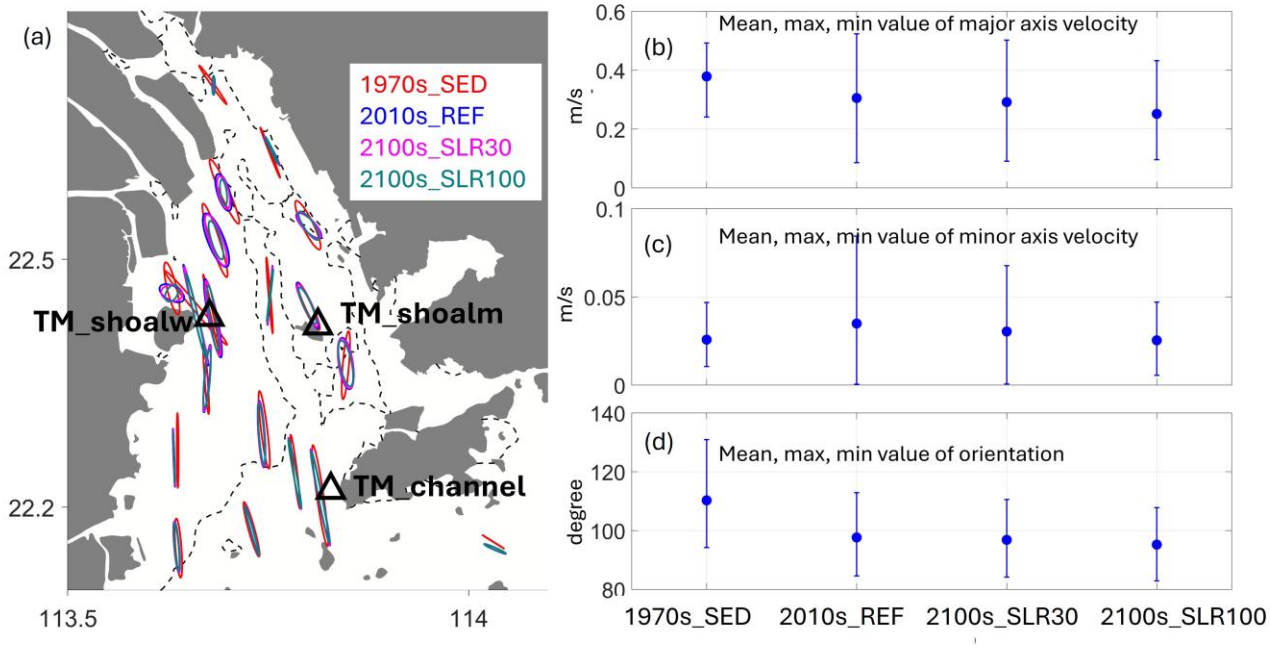

Figure 10 Tidal ellipse of scenarios 1970s_SED, 2010s_REF, 2100s_SLR30 and 2100s_SLR100 in wet season.

5.2 Impact of waves

Wind waves can significantly impact ETMS through sediment resuspension. In the Seine Estuary, it is found that the suspended mass in the ETM caused by energetic wave conditions is three times higher that is caused by mean tides (Grasso et al., 2018). Christie et al (1999) reported that wave activity maintains elevated SSC over high water level. This suspended sediment was transported offshore during ebb tides in stormy conditions in the Humber Estuary. Wave effects in sediment transport can be significantly influenced by typhoon(Chen et al, 2019), and morphological change (Tönis et al, 2002). In the PRE, modeled SSC is elevated by 1.3~1.5 times with inclusion of wave-enhanced bottom shear stress compared to that without wave effect during a typhoon landfall (Yang et al, 2022). As reported by Lin et al (2022), the narrowing of the PRE estuary due to land reclamation has resulted in a general increase in wave-induced bottom stress in the estuary leading an increase in the area of SSC greater than 100 mgL^{-1} by 183.4%.

To assess the impact of wave effect in different time periods, the results of scenarios with and without wave effect are compared (Figure 11). The discrepancy in the bottom SSC between 1970s_SED and 2010s_REF reveals the impact of morphological change (from 1970s to 2010s) on the wave effect and the discrepancy in the bottom layer SSC between 2100s_SLR30 and 2100s_SLR100 reveals the impact of rSLR on wave effect.

635 The comparisons indicate that the location of the ETMs is not affected by waves. A minor
636 expansion of ETM during the wet season of 1970s is seen with wave effect included. The most
637 significant wave effect is a modification of the SPM distribution in the bottom water. In the
638 scenario 1970s_SED, wave-induced enhancement of bottom shear stress elevates the bottom SSC
639 over the entire PRE in the wet season (Figure 11 a). During the dry season, wind waves result in a
640 notable increase of bottom SSC on the west shoal by ~7 mg/L but a slight reduction of bottom
641 SSC on the middle and east shoals (Figure 11 b). In comparison to 1970s_sed, the increase of SSC
642 by waves in 2010s_ref is relatively modest. The wave-induced increase of SSC is less than 5 mg/L
643 on the west shoal. In the scenario with a rising sea level, the impact of waves on SSC is further
644 reduced. In the scenario 2100s_SLR100, the wave-induced SSC increase is 3.5 mg/L. During the
645 dry season when winds are blowing from the land to the sea, wave effects are weakened compared
646 to the wet season (Figure 11 b, d, f).
647 The wave-induced increase of bottom SSC on the west shoal is consistent with the findings of the
648 study by Zhang et al (2021a). Their study suggests that waves exert a considerably stronger
649 influence on bottom shear stress on the shoal than in the channels. Concurrently, waves enhance
650 the westward lateral flow, thereby driving sediment from the channel to the west shoal. This is
651 also demonstrated in our model results shown in Figure 11.

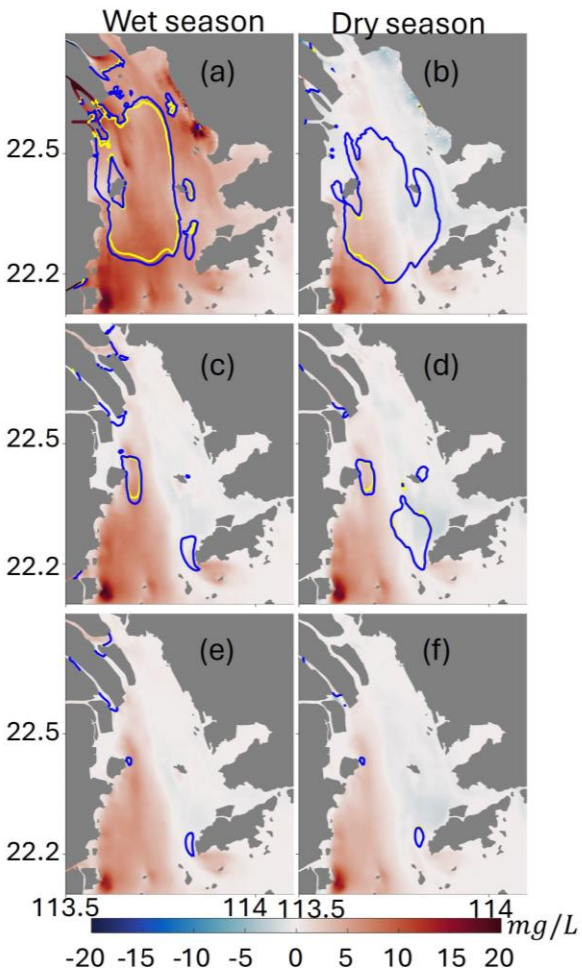

Figure 11 illustrates the difference between scenarios with and without a wave effect. The left column depicts the wet season, while the right column depicts the dry season. The first panel (a, b) depicts scenario 1970s_SED, the second panel (c, d) depicts scenario 2010s_REF, and the third panel (e, f) depicts scenario 2100s_SLR100. Each panel compares the scenario with and without wave effect. The yellow line indicates the location of ETMs without wave effect. The blue line indicates the locations of ETMs with wave effect.

5.3 Implications of results

A diachronic analysis of an estuary is a crucial undertaking to predict its future fates. In the industrial age, when human activities flourish, the effects of climate change and human impact on estuaries are becoming increasingly pronounced. This is leading to significant alterations in the factors that maintain estuary hydrodynamic and sediment dynamic(Grasso & Le Hir, 2019; Hutton et al, 2017; Sottolichio et al, 2013). Each estuary exhibits unique natural geographical conditions. However, the modifications implemented by humans are broadly similar, including activities such as dredging, damming and land reclamation. On the other hand, climate change occurs globally.

The joint effect of climate change and human activities has led to similar response of estuaries during the past decades (Cloern et al, 2016; Talke & de Swart, 2006; Wang et al, 2017) and likely similar fates in future. Successful examples in mitigation of climate change and anthropogenic impact in some estuaries thus have global implications. Our work presents an effort towards a comprehensive understanding of the evolution of ETMs and may contribute to development of guidelines for mitigation in one of the largest estuaries worldwide.

The study by Cui et al. (2022) shows that resuspension is a main process for controlling the SSC in the bottom water. In present-day conditions, medium silts are found to dominate the suspended sediments in the PRE (Wei et al, 2021; Xia et al, 2004).Our results show that a change from clay-dominance to silt-dominance in the estuarine bed from 1970s to 2010s results in enhanced SSC which sustain the ETMs. Therefore, we propose that the main sediment source of the ETMs in the PRE has shifted from a direct riverine sediment discharge in 1970s to erosion of local estuarine bed in 2010s and future. Such shift of sediment source has also been reported in various estuaries, such as the Ems River estuary (Talke & de Swart, 2006) and the Changjiang River estuary (Sun et al, 2019), as a consequence of river damming and other human activities. This shift is likely to alter both sedimentation and biogeochemical environments of estuaries in a profound manner in near future(Cloern et al, 2016).

6 Conclusions

This study examines the impact of anthropogenic and climatic drivers on historical development as well as possible future fates of ETMs in the PRE. Since 1970s, the Pearl River Delta and its estuary (PRE) have experienced significant changes in its morphology in conjunction with a rapid economic growth and land use change. The most considerable changes during the past decades include a continuous narrowing of the estuary by massive land reclamation, increase in the depth of the navigation channels by dredging, reduction of riverine sediment load by damming, sand mining on the shoals, and enhanced land subsidence due to extraction of ground water. In 2010s, an official cessation of land-reclamation and sand mining has been implemented. It is expected that climate change will likely play a more important role in driving the change of hydro-morphodynamics and evolution of ETMs in the forthcoming decades.

In this study, based on validated hydro-morphodynamic model results for 1970s and 2010s, we have designed in total 13 scenarios to investigate the response of ETMs to the aforementioned influencing factors in the PRE. Main outcomes are listed below:

1. An ETM with a relatively large spatial extent between the river mouth of Humen and the Qi'ao island (>30 km in length) existed in 1970s according to both observation and our model results. This ETM evolved into several locally confined but interconnected ETMs in 2010s. Human-induced morphological change mainly associated with land reclamation and deepening of bathymetry by channel dredging and sand mining is the main driver behind such change.
2. Sediment composition in the estuarine bed has also been altered significantly during the past decades. Clay content has largely been depleted since 1970s and the present-day estuarine bed is dominated by silts. The SSC in the PRE is enhanced by a change from clay-dominance to silt-dominance in the estuarine bed, sustaining the multiple ETMs. The most significant change occurs in the channel, where the ETM becomes not only larger but also persistent throughout the year.
3. A remarkable reduction in riverine sediment load from 1970s to 2010s leads to a notable decrease in the spatial extent of ETMs in the wet season. However, it has minor effect on the dynamics of ETMs in the dry season. Our results also show that the PRE has become increasingly starved in SPM along with the morphological change and this trend will likely remain with an accelerated rSLR.
4. The rSLR during the past decades leads to a mild reduction of the spatial extent of the ETMs from 1970s to 2010s. In the forthcoming decades, an accelerated rSLR will likely result in a substantial reduction of SSC in the PRE, particularly on the shoals, with a maximum reduction by up to ~ 3 times larger than the impact of a rSLR following the same rate in the past decades and thereby greatly reduce the spatial extent of ETMs in the PRE.
5. A gradual shift in the mean wind direction and reduction in wind speed in summer during the past decades have a minor influence on ETMs when compared to the effect of morphological change. However, in future scenarios, a continuous change of wind direction and speed would jointly lead to a lower bottom SSC in the northern part of the western shoal and higher bottom SSC in the southern part of the shoal and the channels, which consequently affect the spatial extent of the ETMs.

6. Wind waves exert a considerable impact on SSC in the 1970s and sustain the ETM on the shoal. An increase of the mean water depth of the PRE from 1970s to 2010s by human activities leads to a weakening of the wave effect in a vast part of the estuary except for the western shoal. The same pattern is projected in future scenarios.

Acknowledgements

The author(s) declare financial support was received for the research, authorship, and/or publication of this article. This study is a contribution to the Helmholtz PoF program "The Changing Earth -Sustaining our Future" on its Topic 4: Coastal zones at a time of global change. It also contributes to the theme "C3: Sustainable Adaption Scenarios for Coastal Systems" of the Cluster of Excellence EXC 2037 'CLICCS -Climate, Climatic Change, and Society' -Project Number: 390683824 funded by the Deutsche Forschungsgemeinschaft (DFG, German Research Foundation) under Germany's Excellence Strategy. WZ acknowledges the support of the project "Morphological evolution of coastal seas -past and future" funded by the Deep-time Digital Earth program (https://www.ddeworld.org/) and the Sino-German Mobility Program: CHESS-Chinese and European Coastal Shelf Seas Ecosystem Dynamics-A Comparative Assessment (M-0053).

MM: Conceptualization, Data curation, Methodology, Software, Validation, Writing – original draft, Writing – review & editing. WZ: Methodology, Supervision, Writing – review & editing. LP: Data curation, Methodology, Writing – review & editing. CS: Supervision, Writing – review & editing.

Open Research

References

Arlinghaus, P., Zhang, W. & Schrum, C. (2022) Small-scale benthic faunal activities may lead to large-scale morphological change-A model based assessment. *Frontiers in Marine Science*, 9, 1011760.

Bauer, B. O., Davidson-Arnott, R. G., Walker, I. J., Hesp, P. A. & Ollerhead, J. (2012) Wind direction and complex sediment transport response across a beach–dune system. *Earth Surface Processes and Landforms*, 37(15), 1661-1677.

Bertin, X., Azevedo, A., Guerreiro, M., Fortunato, A. B., Freire, P., Rilo, A., Taborda, R., Freitas, M. C., Andrade, C. & Silva, T. (2015) Evolution of the hydrodynamics of the Tagus estuary (Portugal) in the 21st century. *Revista de Gestão Costeira Integrada-Journal of Integrated Coastal Zone Management*, 15(1), 65-80.

Burchard, H., Schuttelaars, H. M. & Ralston, D. K. (2018) Sediment trapping in estuaries. *Annual review of marine science*, 10, 371-395.

Chaussard, E., Amelung, F., Abidin, H. & Hong, S.-H. (2013) Sinking cities in Indonesia: ALOS PALSAR detects rapid subsidence due to groundwater and gas extraction. *Remote sensing of environment*, 128, 150-161.

Chen, Y., Chen, L., Zhang, H. & Gong, W. (2019) Effects of wave-current interaction on the Pearl River Estuary during Typhoon Hato. *Estuarine, Coastal and Shelf Science*, 228, 106364.

Christie, M., Dyer, K. & Turner, P. (1999) Sediment flux and bed level measurements from a macro tidal mudflat. *Estuarine, Coastal and Shelf Science*, 49(5), 667-688.

Cloern, J. E., Abreu, P. C., Carstensen, J., Chauvaud, L., Elmgren, R., Grall, J., Greening, H., Johansson, J. O. R., Kahru, M. & Sherwood, E. T. (2016) Human activities and climate variability drive fast-paced change across the world's estuarine–coastal ecosystems. *Global change biology*, 22(2), 513-529.

Cui, Y., Wu, J., Ren, J. & Xu, J. (2019) Physical dynamics structures and oxygen budget of summer hypoxia in the Pearl River Estuary. *Limnology and Oceanography*, 64(1), 131-148.

Cui, Y., Wu, J., Tan, E. & Kao, S. J. (2022) Role of particle resuspension in maintaining hypoxic level in the Pearl River Estuary. *Journal of Geophysical Research: Oceans*, 127(8), e2021JC018166.

Day, J. W., Yanez-Arancibia, A. & Kemp, W. M. (2013) Human impact and management of coastal and estuarine ecosystems. *Estuarine Ecology*, 483-495.

de Jonge, V. N., Schuttelaars, H. M., van Beusekom, J. E., Talke, S. A. & de Swart, H. E. (2014) The influence of channel deepening on estuarine turbidity levels and dynamics, as exemplified by the Ems estuary. *Estuarine, Coastal and Shelf Science*, 139, 46-59.

De Winter, R., Sterl, A. & Ruessink, B. (2013) Wind extremes in the North Sea Basin under climate change: An ensemble study of 12 CMIP5 GCMs. *Journal of Geophysical Research: Atmospheres*, 118(4), 1601-1612.

Deng, J., Yao, Q. & Wu, J. (2020) Estuarine morphology and depositional processes in front of lateral river-dominated outlets in a tide-dominated estuary: A case study of the Lingding Bay, South China Sea. *Journal of Asian Earth Sciences*, 196, 104382.

Dijkstra, Y. M., Schuttelaars, H. M., Schramkowski, G. P. & Brouwer, R. L. (2019) Modeling the transition to high sediment concentrations as a response to channel deepening in the Ems River Estuary. *Journal of Geophysical Research: Oceans*, 124(3), 1578-1594.

Dyer, K. R. (1974) The salt balance in stratified estuaries. *Estuarine and coastal marine science*, 2(3), 273-281.

Egbert, G. D. & Erofeeva, S. Y. (2002) Efficient inverse modeling of barotropic ocean tides. *Journal of Atmospheric and Oceanic technology*, 19(2), 183-204.

Gavhane, S., Sapkale, J., Susware, N. & Sapkale, S. (2021) Impact of heavy metals in riverine and estuarine environment: A review. *Res. J. Chem. Environ*, 25(5), 226-233.

Geyer, W. R., Woodruff, J. D. & Traykovski, P. (2001) Sediment transport and trapping in the Hudson River estuary. *Estuaries*, 24, 670-679.

Gong, W., Jia, L., Shen, J. & Liu, J. T. (2014) Sediment transport in response to changes in river discharge and tidal mixing in a funnel-shaped micro-tidal estuary. *Continental Shelf Research*, 76, 89-107.

Grasso, F. & Le Hir, P. (2019) Influence of morphological changes on suspended sediment dynamics in a macrotidal estuary: diachronic analysis in the Seine Estuary (France) from 1960 to 2010. *Ocean Dynamics*, 69(1), 83-100.

Grasso, F., Verney, R., Le Hir, P., Thouvenin, B., Schulz, E., Kervella, Y., Khojasteh Pour Fard, I., Lemoine, J. P., Dumas, F. & Garnier, V. (2018) Suspended sediment dynamics in the macrotidal Seine Estuary (France): 1. Numerical modeling of turbidity maximum dynamics. *Journal of Geophysical Research: Oceans*, 123(1), 558-577.

Guo, L., Wang, Z. B., Townend, I. & He, Q. (2019) Quantification of tidal asymmetry and its nonstationary variations. *Journal of Geophysical Research: Oceans*, 124(1), 773-787.

Hersbach, H., Bell, B., Berrisford, P., Biavati, G., Horányi, A., Muñoz Sabater, J., Nicolas, J., Peubey, C., Radu, R. & Rozum, I. (2018) ERA5 hourly data on single levels from 1979 to present. *Copernicus climate change service (c3s) climate data store (cds)*, 10(10.24381).

Hong, B., Xue, H., Zhu, L. & Xu, H. (2022) Climatic change of summer wind direction and its impact on hydrodynamic circulation in the pearl river estuary. *Journal of Marine Science and Engineering*, 10(7), 842.

Hutton, P. H., Rath, J. S. & Roy, S. B. (2017) Freshwater flow to the San Francisco Bay-Delta estuary over nine decades (Part 1): Trend evaluation. *Hydrological Processes*, 31(14), 2500-2515.

Jay, D. A. & Musiak, J. D. (1994) Particle trapping in estuarine tidal flows. *Journal of Geophysical Research: Oceans*, 99(C10), 20445-20461.

Jiang, L., Gerkema, T., Idier, D., Slangen, A. & Soetaert, K. (2020) Effects of sea-level rise on tides and sediment dynamics in a Dutch tidal bay. *Ocean Science*, 16(2), 307-321.

Jilan, S. & Kangshan, W. (1986) The suspended sediment balance in Changjiang Estuary. *Estuarine, Coastal and Shelf Science*, 23(1), 81-98.

Jonge, V. d. (1983) Relations between annual dredging activities, suspended matter concentrations, and the development of the tidal regime in the Ems estuary. *Canadian Journal of Fisheries and Aquatic Sciences*, 40(S1), s289-s300.

Khojasteh, D., Lewis, M., Tavakoli, S., Farzadkhoo, M., Felder, S., Iglesias, G. & Glamore, W. (2022) Sea level rise will change estuarine tidal energy: A review. *Renewable and Sustainable Energy Reviews*, 156, 111855.

Kulkarni, S., Deo, M. & Ghosh, S. (2013) Impact of climate change on local wind conditions, *International Conference on Hydraulics and Water Resources (HYDRO), Chennai, India, Dec*.

Li, T. & Li, T.-J. (2018) Sediment transport processes in the Pearl River Estuary as revealed by grain-size end-member modeling and sediment trend analysis. *Geo-Marine Letters*, 38, 167-178.

Li, X., Chrysagi, E., Klingbeil, K. & Burchard, H. (2024) Impact of islands on tidally dominated river plumes: A high-resolution modeling study. *Journal of Geophysical Research: Oceans*, 129(7), e2023JC020272.

Lin, S., Niu, J., Liu, G., Wei, X. & Cai, S. (2022) Variations of suspended sediment transport caused by changes in shoreline and bathymetry in the Zhujiang (Pearl) River Estuary in the wet season. *Acta Oceanologica Sinica*, 41(10), 54-73.

Liu, F., Hu, S., Guo, X., Luo, X., Cai, H. & Yang, Q. (2018) Recent changes in the sediment regime of the Pearl River (South China): Causes and implications for the Pearl River Delta. *Hydrological Processes*, 32(12), 1771-1785.

Liu, G. & Cai, S. (2019) Modeling of suspended sediment by coupled wave-current model in the Zhujiang (Pearl) River Estuary. *Acta Oceanologica Sinica*, 38, 22-35.

Liu, R., Wang, Y., Gao, J., Wu, Z. & Guan, W. (2016) Turbidity maximum formation and its seasonal variations in the Zhujiang (Pearl River) Estuary, southern China. *Acta Oceanologica Sinica*, 35, 22-31.

Liu, Z., Fagherazzi, S., Liu, X., Shao, D., Miao, C., Cai, Y., Hou, C., Liu, Y., Li, X. & Cui, B. (2022) Long-term variations in water discharge and sediment load of the Pearl River Estuary: Implications for sustainable development of the Greater Bay Area. *Frontiers in Marine Science*, 9, 983517.

Luo, X., Gao, H., Wu, Z., Li, S., Shang, J. & Zhao, D. (2020) Large-scale Long Time-series InSAR Land Subsidence Research in the Pearl River Estuary.

Luo, X., Yang, S. & Zhang, J. (2012) The impact of the Three Gorges Dam on the downstream distribution and texture of sediments along the middle and lower Yangtze River (Changjiang) and its estuary, and subsequent sediment dispersal in the East China Sea. *Geomorphology*, 179, 126-140.

Ma, M., Porz, L., Schrum, C. & Zhang, W. (2024) Physical mechanisms, dynamics and interconnections of multiple estuarine turbidity maximum in the Pearl River estuary. *Frontiers in Marine Science*, 11, 1385382.

Ma, M., Zhang, W., Chen, W., Deng, J. & Schrum, C. (2023) Impacts of morphological change and sea-level rise on stratification in the Pearl River Estuary. *Frontiers in Marine Science*, 10, 1072080.

Mao, Q., Shi, P., Yin, K., Gan, J. & Qi, Y. (2004) Tides and tidal currents in the Pearl River Estuary. *Continental Shelf Research*, 24(16), 1797-1808.

Masselink, G., Auger, N., Russell, P. & O'HARE, T. (2007) Short-term morphological change and sediment dynamics in the intertidal zone of a macrotidal beach. *Sedimentology*, 54(1), 39-53.

Nienhuis, J. H. & van de Wal, R. S. (2021) Projections of global delta land loss from sea-level rise in the 21st century. *Geophysical Research Letters*, 48(14), e2021GL093368.

Niu, L., Li, J., Luo, X., Fu, T., Chen, O. & Yang, Q. (2021) Identification of heavy metal pollution in estuarine sediments under long-term reclamation: ecological toxicity, sources and implications for estuary management. *Environmental Pollution*, 290, 118126.

Niu, L., Luo, X., Hu, S., Liu, F., Cai, H., Ren, L., Ou, S., Zeng, D. & Yang, Q. (2020) Impact of anthropogenic forcing on the environmental controls of phytoplankton dynamics between 1974 and 2017 in the Pearl River estuary, China. *Ecological Indicators*, 116, 106484.

Oppenheimer, M., Glavovic, B., Hinkel, J., Van de Wal, R., Magnan, A. K., Abd-Elgawad, A., Cai, R., Cifuentes-Jara, M., Deconto, R. M. & Ghosh, T. (2019) Sea level rise and implications for low lying islands, coasts and communities.

Ou, S., Yang, Q., Luo, X., Zhu, F., Luo, K. & Yang, H. (2019) The influence of runoff and wind on the dispersion patterns of suspended sediment in the Zhujiang (Pearl) River Estuary based on MODIS data. *Acta Oceanologica Sinica*, 38, 26-35.

Pinto, L., Fortunato, A., Zhang, Y., Oliveira, A. & Sancho, F. (2012) Development and validation of a three-dimensional morphodynamic modelling system for non-cohesive sediments. *Ocean Modelling*, 57, 1-14.

Porz, L., Zhang, W. & Schrum, C. (2021) Density-driven bottom currents control development of muddy basins in the southwestern Baltic Sea. *Marine Geology*, 438, 106523.

Roland, A. (2008) *Development of WWM II (Wind Wave Model II) -Spectral Wave Modeling on Unstructured Meshes*. Translated from English by, *PhD*. Darmstadt: Technische Universität Darmstadt.

Ruane, A. C. (2024) Synthesis Report of the IPCC Sixth Assessment Report (AR6).

Scully, M. E. & Friedrichs, C. T. (2007) Sediment pumping by tidal asymmetry in a partially mixed estuary. *Journal of Geophysical Research: Oceans*, 112(C7).

Simpson, J. H. & Bowers, D. (1981) Models of stratification and frontal movement in shelf seas. *Deep Sea Research Part A. Oceanographic Research Papers*, 28(7), 727-738.

Song, G., Liu, S., Zhang, J., Zhu, Z., Zhang, G., Marchant, H. K., Kuypers, M. M. & Lavik, G. (2021) Response of benthic nitrogen cycling to estuarine hypoxia. *Limnology and Oceanography*, 66(3), 652-666.

Sottolichio, A., Hanquiez, V., Périnotto, H., Sabouraud, L. & Weber, O. (2013) Evaluation of the recent morphological evolution of the Gironde estuary through the use of some preliminary synthetic indicators. *Journal of Coastal Research*(65), 1224-1229.

Suh, S.-W. (2016) Tidal asymmetry and energy variation due to sea-level rise in a macro tidal bay. *Journal of Coastal Research*(75), 765-769.
Sun, X., Fan, D., Liu, M., Liao, H. & Tian, Y. (2019) Persistent impact of human activities on trace metals in the Yangtze River Estuary and the East China Sea: evidence from sedimentary records of the last 60 years. *Science of the Total Environment*, 654, 878-889.
Talke, S. A. & de Swart, H. E. (2006) Hydrodynamics and morphology in the Ems/Dollard estuary: Review of models, measurements, scientific literature, and the effects of changing conditions.
Tang, L., Sheng, J., Ji, X., Cao, W. & Liu, D. (2009) Investigation of three-dimensional circulation and hydrography over the Pearl River Estuary of China using a nested-grid coastal circulation model. *Ocean Dynamics*, 59, 899-919.
Teng, L., Cheng, H., de Swart, H. E., Dong, P., Li, Z., Li, J. & Wang, Y. (2021) On the mechanism behind the shift of the turbidity maximum zone in response to reclamations in the Yangtze (Changjiang) Estuary, China. *Marine Geology*, 440, 106569.
Tong, Z., Yong-Qiang, Y., Cun-De, X., Li-Juan, H. & Zhan, Y. (2022) Interpretation of IPCC AR6 report: monitoring and projections of global and regional sea level change. *Advances in Climate Change Research*, 18(1), 12.
Tönis, I., Stam, J. & Van de Graaf, J. (2002) Morphological changes of the Haringvliet estuary after closure in 1970. *Coastal Engineering*, 44(3), 191-203.
Wai, O., Wang, C., Li, Y. S. & Li, X. (2004) The formation mechanisms of turbidity maximum in the Pearl River estuary, China. *Marine Pollution Bulletin*, 48(5-6), 441-448.
Walling, D. (2008) The changing sediment loads of the world's rivers. *Annals of Warsaw University of Life Sciences-SGGW. Land Reclamation*(39).
Walter, A., Keuler, K., Jacob, D., Knoche, R., Block, A., Kotlarski, S., Müller-Westermeier, G., Rechid, D. & Ahrens, W. (2006) A high resolution reference data set of German wind velocity 1951-2001 and comparison with regional climate model results. *Meteorologische Zeitschrift*, 15(6), 585-596.
Wang, C., Zhao, Y., Zou, X., Xu, X. & Ge, C. (2017) Recent changing patterns of the Changjiang (Yangtze River) Estuary caused by human activities. *Acta Oceanologica Sinica*, 36, 87-96.
Wang, H., Wright, T. J., Yu, Y., Lin, H., Jiang, L., Li, C. & Qiu, G. (2012) InSAR reveals coastal subsidence in the Pearl River Delta, China. *Geophysical Journal International*, 191(3), 1119-1128.
Wang, J. & Hong, B. (2021) Threat posed by future sea-level rise to freshwater resources in the Upper Pearl River Estuary. *Journal of Marine Science and Engineering*, 9(3), 291.
Wang, J., Tong, Y., Feng, L., Zhao, D., Zheng, C. & Tang, J. (2021) Satellite-observed decreases in water turbidity in the Pearl River Estuary: Potential linkage with sea-level rise. *Journal of Geophysical Research: Oceans*, 126(4), e2020JC016842.
Wei, D., Meyer, H. & Bacchin, T. K. (2023) Spatial Dynamics in the Pearl River Delta and Development Strategies, *Adaptive Urban Transformation: Urban Landscape Dynamics, Regional Design and Territorial Governance in the Pearl River Delta, China*Springer International Publishing Cham, 37-59.
Weisse, R., Dailidienė, I., Hünicke, B., Kahma, K., Madsen, K., Omstedt, A., Parnell, K., Schöne, T., Soomere, T., Zhang, W., & Zorita, E. (2021) Sea level dynamics and coastal erosion in the Baltic Sea region. *Earth Syst. Dynam*., 12, 871–898.
Wei, X., Cai, S., Zhan, W. & Li, Y. (2021) Changes in the distribution of surface sediment in Pearl River Estuary, 1975–2017, largely due to human activity. *Continental Shelf Research*, 228, 104538.
Weisscher, S. A., Adema, P. H., Rossius, J. E. & Kleinhans, M. G. (2023) The effect of sea-level rise on estuary filling in scaled landscape experiments. *The Depositional Record*, 9(2), 363-379.
Winterwerp, J. C. & Wang, Z. B. (2013) Man-induced regime shifts in small estuaries—I: theory. *Ocean Dynamics*, 63, 1279-1292.
Wong, W., Li, K. & Yeung, K. (2003) Long term sea level change in Hong Kong. *Hong Kong Meteorological Society Bulletin*, 13(1-2), 24-40.
Wu, Z., Saito, Y., Zhao, D., Zhou, J., Cao, Z., Li, S., Shang, J. & Liang, Y. (2016) Impact of human activities on subaqueous topographic change in Lingding Bay of the Pearl River estuary, China, during 1955–2013. *Scientific reports*, 6(1), 37742.
Xia, X., Li, Y., Yang, H., Wu, C., Sing, T. & Pong, H. (2004) Observations on the size and settling velocity distributions of suspended sediment in the Pearl River Estuary, China. *Continental Shelf Research*, 24(16), 1809-1826.
Yang, J. & Liu, W. (2015) Evolution of the Maximum Turbidity Zone in the Lingding Bay of Pearl River Estuary over past 30 years. *珠江水运*(16), 58-62.
Yang, Y., Guan, W., Deleersnijder, E. & He, Z. (2022) Hydrodynamic and sediment transport modelling in the Pearl River Estuary and adjacent Chinese coastal zone during Typhoon Mangkhut. *Continental Shelf Research*, 233, 104645.

Yu, Q., Wang, Y., Gao, J., Gao, S. & Flemming, B. (2014) Turbidity maximum formation in a well-mixed macrotidal estuary: The role of tidal pumping. *Journal of Geophysical Research: Oceans*, 119(11), 7705-7724.

Zarzuelo, C., D'Alpaos, A., Carniello, L., López-Ruiz, A., Díez-Minguito, M. & Ortega-Sánchez, M. (2019) Natural and human-induced flow and sediment transport within tidal creek networks influenced by ocean-bay tides. *Water*, 11(7), 1493.

Zhang, G., Chen, Y., Cheng, W., Zhang, H. & Gong, W. (2021a) Wave effects on sediment transport and entrapment in a channel-shoal estuary: the pearl river estuary in the dry winter season. *Journal of Geophysical Research: Oceans*, 126(4), e2020JC016905.

Zhang, G., Cheng, W., Chen, L., Zhang, H. & Gong, W. (2019) Transport of riverine sediment from different outlets in the Pearl River Estuary during the wet season. *Marine Geology*, 415, 105957.

Zhang, Y., Ren, J. & Zhang, W. (2020) Flocculation under the control of shear, concentration and stratification during tidal cycles. *Journal of hydrology*, 586, 124908.

Zhang, Y., Ren, J., Zhang, W. & Wu, J. (2021b) Importance of salinity-induced stratification on flocculation in tidal estuaries. *Journal of Hydrology*, 596, 126063.

Zhang, Y. J., Ye, F., Stanev, E. V. & Grashorn, S. (2016) Seamless cross-scale modeling with SCHISM. *Ocean Modelling*, 102, 64-81.

Zhao, L., Xin, P., Cheng, H. & Chu, A. (2023) Change of turbidity maximum in Yangtze Estuary after construction of the Three Gorges Dam. *Continental Shelf Research*, 258, 104983.

Zhuang, W. & Zhou, F. (2021) Distribution, source and pollution assessment of heavy metals in the surface sediments of the Yangtze River Estuary and its adjacent East China Sea. *Marine Pollution Bulletin*, 164, 112002.

Advancing earth and space sciences

Supporting Information for

[JGR Oceans]

Additional Supporting Information (Files uploaded separately)

Figure S1 monthly freshwater discharge and sediment load at the eight major outlets obtained from the China Sediment Report (http://www.mwr.gov.cn)
Figure S2 the wind rose of data from ECWMF and the wind data after -40 rotation and wind speed decreased by 70%.
Figure S3 the clay, silt, and sand distribution of scenarios (1970s_REF, 1970s_SED, 2010s_BED, 2010s_REF, and 2100s_SLR30) in the wet season and dry season.
Figure S4 the difference of stratification and bottom shear stress between 2010s_REF and 2100S_SLR30 in the wet season and the dry season.

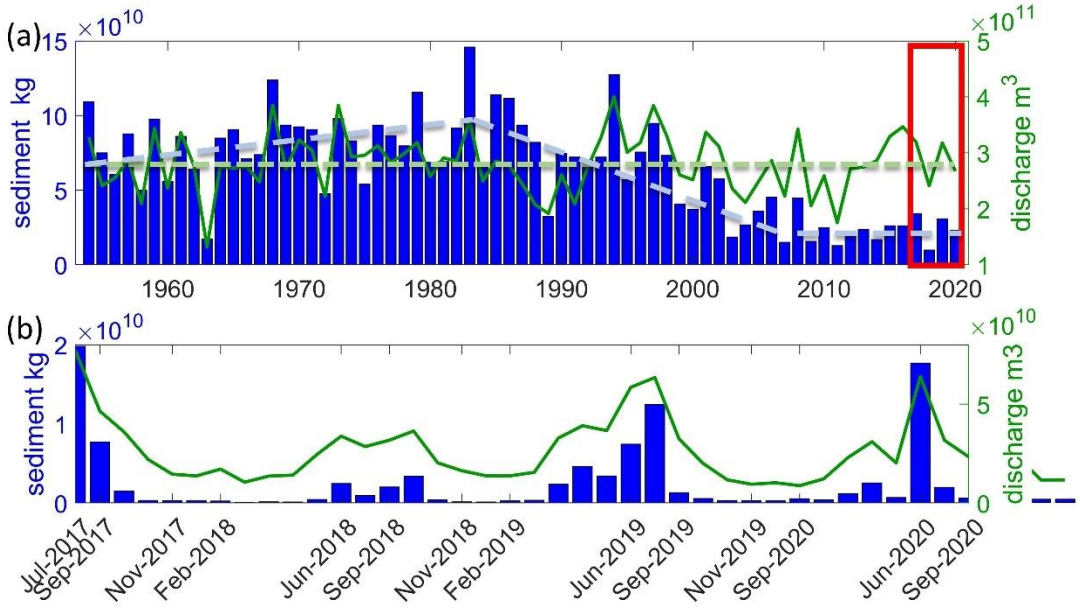

Figure S5 monthly freshwater discharge and sediment load at the eight major outlets obtained from the China Sediment Report (http://www.mwr.gov.cn)

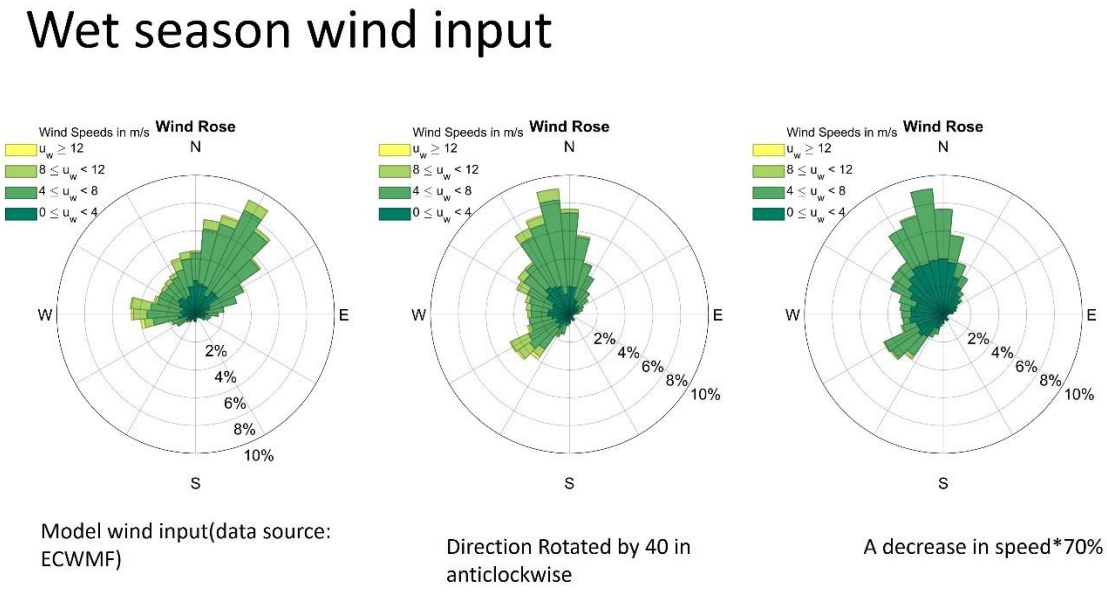

Figure S6 the wind rose of data from ECWMF and the wind data after -40 rotation and wind speed decreased by 70%.

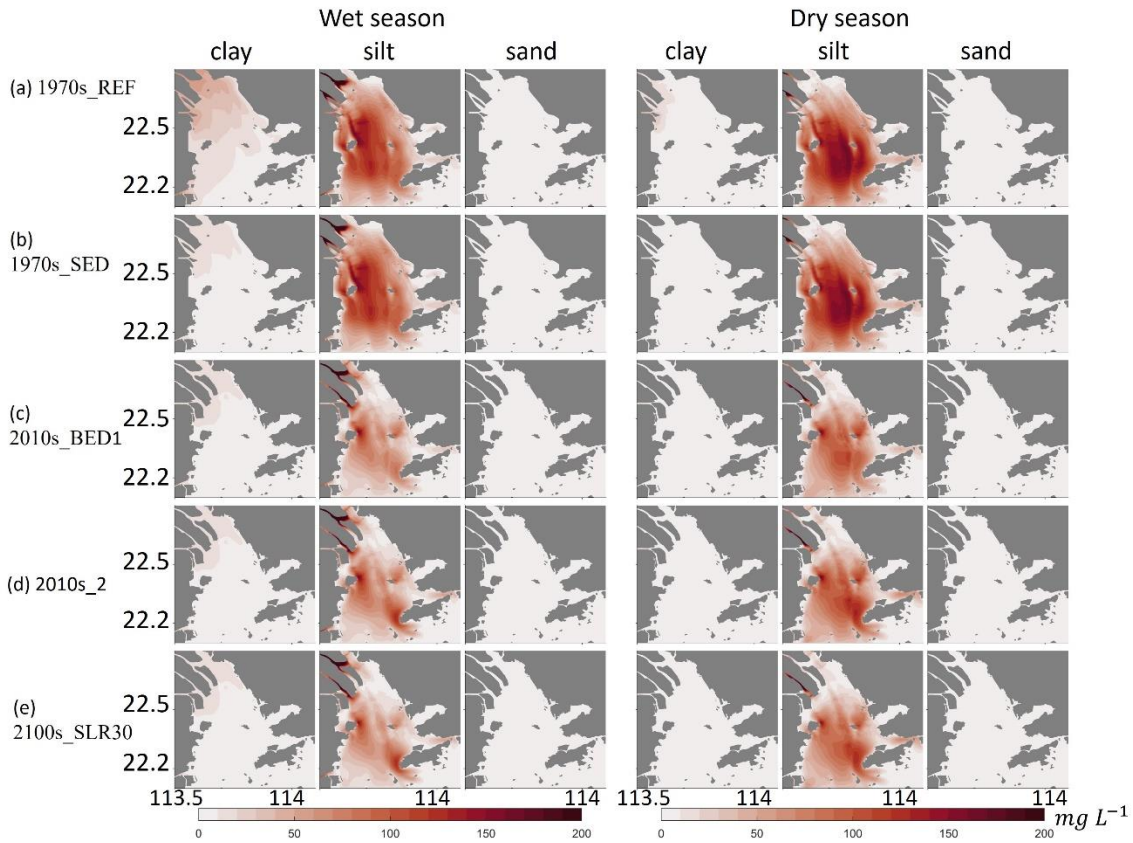

Figure S7 the clay, silt, and sand distribution of scenarios (1970s_REF, 1970s_SED, 2010s_BED, 2010s_REF, and 2100s_SLR30) in the wet season and dry season.

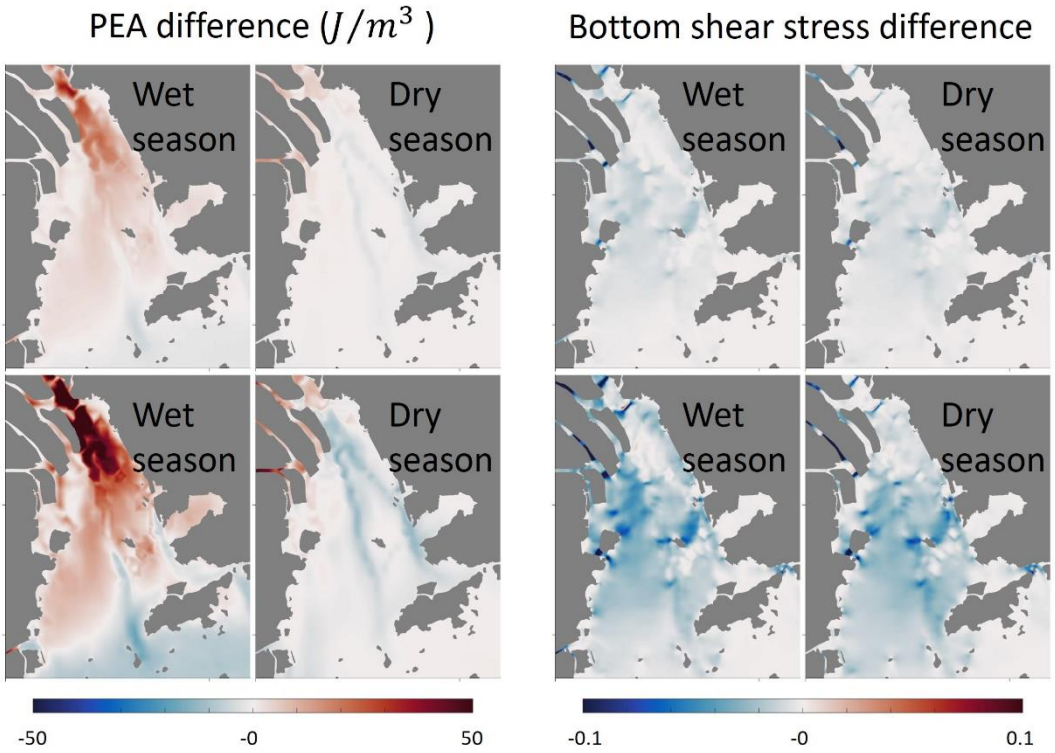

Figure S8 the difference of stratification and bottom shear stress between 2010s_REF and 2100S_SLR30 in the wet season and the dry season.

References

Abidin, H., H. Andreas, I. Gumilar, T. P. Sidiq, and Y. Fukuda (2013), Land subsidence in coastal city of Semarang (Indonesia): characteristics, impacts and causes, *Geomatics, Natural Hazards and Risk*, *4*(3), 226-240.

Arlinghaus, P., W. Zhang, and C. Schrum (2022), Small-scale benthic faunal activities may lead to large-scale morphological change-A model based assessment, *Frontiers in Marine Science*, *9*, 1011760.

Arlinghaus, P. P., C. Schrum, I. Kröncke, and W. Zhang (2023), Benthos as a key driver of morphological change in coastal regions, *EGUsphere*, *2023*, 1-28.

Barnard, P. L., D. H. Schoellhamer, B. E. Jaffe, and L. J. McKee (2013), Sediment transport in the San Francisco Bay coastal system: an overview, *Marine Geology*, *345*, 3-17.

Baross[1], J. A. (1994), Elevated'microbial loop'activities in the Columbia River estuarine turbidity maximum John A. Baross[1], Byron Crump[1] & Charles A. Simenstad[2] 1. School of Oceanography, WB-10, University of Washington, Seattle, WA 98195, USA 2. Fisheries Research Institute, WH-10, School of Fisheries, University of Washington, *Changes in fluxes in estuaries: Implications from science to management*, 459.

Bartholomä, A., A. Kubicki, T. H. Badewien, and B. W. Flemming (2009), Suspended sediment transport in the German Wadden Sea—seasonal variations and extreme events, *Ocean Dynamics*, *59*(2), 213-225.

Bi, S., H. Lai, D. Guo, X. Liu, G. Wang, X. Chen, S. Liu, H. Yi, Y. Su, and G. Li (2022), Spatio-temporal variation of bacterioplankton community structure in the Pearl River: impacts of artificial fishery habitat and physicochemical factors, *BMC Ecology and Evolution*, *22*(1), 10.

Biggs, R. B., J. H. Sharp, T. M. Church, and J. M. Tramontano (1983), Optical properties, suspended sediments, and chemistry associated with the turbidity maxima of the Delaware Estuary, *Canadian Journal of Fisheries and Aquatic Sciences*, *40*(S1), s172-s179.

Bindoff, N. L., and T. J. McDougall (2000), Decadal changes along an Indian Ocean section at 32 S and their interpretation, *Journal of Physical Oceanography*, *30*(6), 1207-1222.

Borsje, B. W., B. K. van Wesenbeeck, F. Dekker, P. Paalvast, T. J. Bouma, M. M. van Katwijk, and M. B. de Vries (2011), How ecological engineering can serve in coastal protection, *Ecological Engineering*, *37*(2), 113-122.
Burchard, H., and H. Baumert (1998), The formation of estuarine turbidity maxima due to density effects in the salt wedge. A hydrodynamic process study, *Journal of Physical Oceanography*, *28*(2), 309-321.
Burchard, H., H. M. Schuttelaars, and D. K. Ralston (2018a), Sediment trapping in estuaries, *Annual review of marine science*, *10*, 371-395.
Burchard, H., H. M. Schuttelaars, and D. K. Ralston (2018b), Sediment trapping in estuaries, *Annual review of marine science*, *10*(1), 371-395.
Campbell, D. E., and R. W. Spinrad (1987), The relationship between light attenuation and particle characteristics in a turbid estuary, *Estuarine, Coastal and Shelf Science*, *25*(1), 53-65.
Chakraborty, S. K. (2021), River pollution and perturbation: Perspectives and processes, *Riverine Ecology Volume 2: Biodiversity Conservation, Conflicts and Resolution*, 443-530.
Chakrapani, G. J. (2005), Factors controlling variations in river sediment loads, *Current science*, 569-575.
Chan, F. K. S., L. E. Yang, J. Scheffran, G. Mitchell, O. Adekola, J. Griffiths, Y. Chen, G. Li, X. Lu, and Y. Qi (2021), Urban flood risks and emerging challenges in a Chinese delta: The case of the Pearl River Delta, *Environmental Science & Policy*, *122*, 101-115.
Chen, N., M. D. Krom, Y. Wu, D. Yu, and H. Hong (2018), Storm induced estuarine turbidity maxima and controls on nutrient fluxes across river-estuary-coast continuum, *Science of the Total Environment*, *628*, 1108-1120.
Chen, Y., L. Chen, H. Zhang, and W. Gong (2019), Effects of wave-current interaction on the Pearl River Estuary during Typhoon Hato, *Estuarine, Coastal and Shelf Science*, *228*, 106364.
Cheng, Z., I. Jalon-Rójas, X. H. Wang, and Y. Liu (2020), Impacts of land reclamation on sediment transport and sedimentary environment in a macro-tidal estuary, *Estuarine, Coastal and Shelf Science*, *242*, 106861.
Chowdhury, M. S. N., M. La Peyre, L. D. Coen, R. L. Morris, M. W. Luckenbach, T. Ysebaert, B. Walles, and A. C. Smaal (2021),

Ecological engineering with oysters enhances coastal resilience efforts, *Ecological Engineering*, *169*, 106320.
Christie, M., K. Dyer, and P. Turner (1999), Sediment flux and bed level measurements from a macro tidal mudflat, *Estuarine, Coastal and Shelf Science*, *49*(5), 667-688.
Cloern, J. E. (1987), Turbidity as a control on phytoplankton biomass and productivity in estuaries, *Continental shelf research*, *7*(11-12), 1367-1381.
Cloern, J. E., P. C. Abreu, J. Carstensen, L. Chauvaud, R. Elmgren, J. Grall, H. Greening, J. O. R. Johansson, M. Kahru, and E. T. Sherwood (2016), Human activities and climate variability drive fast - paced change across the world's estuarine–coastal ecosystems, *Global change biology*, *22*(2), 513-529.
Colby, L. H., S. D. Maycock, F. A. Nelligan, H. J. Pocock, and D. J. Walker (2010), An investigation into the effect of dredging on tidal asymmetry at the river murray mouth, *Journal of Coastal Research*, *26*(5), 843-850.
Cox, J., J. Lingbeek, S. Weisscher, and M. Kleinhans (2022), Effects of Sea - Level Rise on Dredging and Dredged Estuary Morphology, *Journal of Geophysical Research: Earth Surface*, *127*(10), e2022JF006790.
Cui, Y., J. Wu, E. Tan, and S. J. Kao (2022), Role of particle resuspension in maintaining hypoxic level in the Pearl River Estuary, *Journal of Geophysical Research: Oceans*, *127*(8), e2021JC018166.
Dai, M., Y. Zhao, F. Chai, M. Chen, N. Chen, Y. Chen, D. Cheng, J. Gan, D. Guan, and Y. Hong (2023), Persistent eutrophication and hypoxia in the coastal ocean, *Cambridge Prisms: Coastal Futures*, *1*, e19.
Dankers, P., and J. Winterwerp (2007), Hindered settling of mud flocs: Theory and validation, *Continental shelf research*, *27*(14), 1893-1907.
de Jonge, V. N., H. M. Schuttelaars, J. E. van Beusekom, S. A. Talke, and H. E. de Swart (2014), The influence of channel deepening on estuarine turbidity levels and dynamics, as exemplified by the Ems estuary, *Estuarine, Coastal and Shelf Science*, *139*, 46-59.
De Winter, R., A. Sterl, and B. Ruessink (2013), Wind extremes in the North Sea Basin under climate change: An ensemble study of 12

CMIP5 GCMs, *Journal of Geophysical Research: Atmospheres*, *118*(4), 1601-1612.
Du, Y., G. Feng, L. Liu, H. Fu, X. Peng, and D. Wen (2020), Understanding land subsidence along the coastal areas of Guangdong, China, by analyzing multi-track MTInSAR data, *Remote Sensing*, *12*(2), 299.
Duy Vinh, V., S. Ouillon, and D. Van Uu (2018), Estuarine Turbidity Maxima and variations of aggregate parameters in the Cam-Nam Trieu estuary, North Vietnam, in early wet season, *Water*, *10*(1), 68.
Eisma, D. (1986), Flocculation and de-flocculation of suspended matter in estuaries, *Netherlands Journal of Sea Research*, *20*(2-3), 183-199.
Elmilady, H., M. Van der Wegen, D. Roelvink, and A. Van der Spek (2022), Modeling the morphodynamic response of estuarine intertidal shoals to sea - level rise, *Journal of Geophysical Research: Earth Surface*, *127*(1), e2021JF006152.
Fettweis, M., and M. Baeye (2015), Seasonal variation in concentration, size, and settling velocity of muddy marine flocs in the benthic boundary layer, *Journal of Geophysical Research: Oceans*, *120*(8), 5648-5667.
Forrester, J., N. Leonardi, J. R. Cooper, and P. Kumar (2024), Seagrass as a nature-based solution for coastal protection, *Ecological Engineering*, *206*, 107316.
Gameiro, C., J. Zwolinski, and V. Brotas (2011), Light control on phytoplankton production in a shallow and turbid estuarine system, *Hydrobiologia*, *669*, 249-263.
Gao, G. D., X. H. Wang, X. W. Bao, D. Song, X. P. Lin, and L. L. Qiao (2018), The impacts of land reclamation on suspended-sediment dynamics in Jiaozhou Bay, Qingdao, China, *Estuarine, Coastal and Shelf Science*, *206*, 61-75.
Geyer, W. R. (1993), The importance of suppression of turbulence by stratification on the estuarine turbidity maximum, *Estuaries*, *16*, 113-125.
Geyer, W. R., and P. MacCready (2014), The estuarine circulation, *Annual review of fluid mechanics*, *46*(1), 175-197.
Geyer, W. R., J. D. Woodruff, and P. Traykovski (2001), Sediment transport and trapping in the Hudson River estuary, *Estuaries*, *24*, 670-679.

Giosan, L., J. Syvitski, S. Constantinescu, and J. Day (2014), Climate change: Protect the world's deltas, *Nature*, *516*(7529), 31-33.
Glangeaud, L. (1938), Transport et sédimentation dans l'estuaire et a l'embouchure de la Gironde. Caracteres Petrographiques des Formations Fluviatiles, Saumatres, Littordes, et Néritiques, *Bulletin of Geological Society of France*, *8*, 599-630.
Grasso, F., and P. Le Hir (2019), Influence of morphological changes on suspended sediment dynamics in a macrotidal estuary: diachronic analysis in the Seine Estuary (France) from 1960 to 2010, *Ocean Dynamics*, *69*(1), 83-100.
Grasso, F., R. Verney, P. Le Hir, B. Thouvenin, E. Schulz, Y. Kervella, I. Khojasteh Pour Fard, J. P. Lemoine, F. Dumas, and V. Garnier (2018), Suspended sediment dynamics in the macrotidal Seine Estuary (France): 1. Numerical modeling of turbidity maximum dynamics, *Journal of Geophysical Research: Oceans*, *123*(1), 558-577.
Green, M. O., and G. Coco (2014), Review of wave-driven sediment resuspension and transport in estuaries, *Reviews of Geophysics*, *52*(1), 77-117.
Gutiérrez, J., C. Jones, J. Byers, K. Arkema, K. Berkenbusch, J. Commito, C. Duarte, S. Hacker, J. Lambrinos, and I. Hendriks (2011), 7.04—Physical ecosystem engineers and the functioning of estuaries and coasts, *Treatise on estuarine and coastal science*, 53-81.
Haigh, I. D., M. D. Pickering, J. M. Green, B. K. Arbic, A. Arns, S. Dangendorf, D. F. Hill, K. Horsburgh, T. Howard, and D. Idier (2020), The tides they are a-Changin': A comprehensive review of past and future nonastronomical changes in tides, their driving mechanisms, and future implications, *Reviews of Geophysics*, *58*(1), e2018RG000636.
Heininger, P., I. Keller, I. Quick, R. Schwartz, and S. Vollmer (2015), Sediment management on river-basinscale: The river Elbe, *Sediment Matters*, 201-247.
Hesse, R. F., A. Zorndt, and P. Fröhle (2019), Modelling dynamics of the estuarine turbidity maximum and local net deposition, *Ocean Dynamics*, *69*, 489-507.
Holland, E. A., M. Garschagen, C. Adler, S. Crate, H. Jacot des Combes, B. Glavovic, S. Harper, G. Kofinas, S. O'Donoghue, and B. Orlove (2022), Special Report on Oceans and Cryosphere in a Changing Climate.

Hong, B., Z. Liu, J. Shen, H. Wu, W. Gong, H. Xu, and D. Wang (2020), Potential physical impacts of sea-level rise on the Pearl River Estuary, China, *Journal of marine systems*, *201*, 103245.
Hong, B., H. Xue, L. Zhu, and H. Xu (2022), Climatic change of summer wind direction and its impact on hydrodynamic circulation in the pearl river estuary, *Journal of Marine Science and Engineering*, *10*(7), 842.
Hua, X., H. Huang, Y. Wang, X. Yu, K. Zhao, and D. Chen (2020), Seasonal estuarine turbidity maximum under strong tidal dynamics: three-year observations in the Changjiang River Estuary, *Water*, *12*(7), 1854.
Hutton, P. H., J. S. Rath, and S. B. Roy (2017), Freshwater flow to the San Francisco Bay - Delta estuary over nine decades (Part 1): Trend evaluation, *Hydrological Processes*, *31*(14), 2500-2515.
Iglesias, I., F. Buschman, G. Simone, F. Amorim, A. Bio, L. Vieira, H. Boisgontier, L. Zaggia, V. Moschino, and F. Madricardo (2024), Hydrodynamics of a highly stratified small estuary and the influence of nearby river plumes, *Estuarine, Coastal and Shelf Science*, *304*, 108843.
Jay, D. A., and J. D. Musiak (1994), Particle trapping in estuarine tidal flows, *Journal of Geophysical Research: Oceans*, *99*(C10), 20445-20461.
Jay, D. A., S. A. Talke, A. Hudson, and M. Twardowski (2015), Estuarine turbidity maxima revisited: Instrumental approaches, remote sensing, modeling studies, and new directions, *Developments in sedimentology*, *68*, 49-109.
Jordan, P., and P. Fröhle (2022), Bridging the gap between coastal engineering and nature conservation? A review of coastal ecosystems as nature-based solutions for coastal protection, *Journal of coastal conservation*, *26*(2), 4.
Kappenberg, J., G. Schymura, and H.-U. Fanger (1995), Sediment dynamics and estuarine circulation in the turbidity maximum of the Elbe River, *Netherland Journal of Aquatic Ecology*, *29*, 229-237.
Kessarkar, P. M., V. Purnachandra Rao, R. Shynu, I. M. Ahmad, P. Mehra, G. Michael, and D. Sundar (2009), Wind-driven estuarine turbidity maxima in Mandovi Estuary, central west coast of India, *Journal of Earth System Science*, *118*, 369-377.

Khojasteh, D., W. Glamore, V. Heimhuber, and S. Felder (2021), Sea level rise impacts on estuarine dynamics: A review, *Science of The Total Environment*, *780*, 146470.
Kikstra, J. S., Z. R. Nicholls, C. J. Smith, J. Lewis, R. D. Lamboll, E. Byers, M. Sandstad, M. Meinshausen, M. J. Gidden, and J. Rogelj (2022), The IPCC Sixth Assessment Report WGIII climate assessment of mitigation pathways: from emissions to global temperatures, *Geoscientific Model Development*, *15*(24), 9075-9109.
King, E., D. Conley, G. Masselink, N. Leonardi, R. McCarroll, and T. Scott (2019), The impact of waves and tides on residual sand transport on a sediment‐poor, energetic, and macrotidal continental shelf, *Journal of Geophysical Research: Oceans*, *124*(7), 4974-5002.
Kösters, F., I. Grabemann, and R. Schubert (2014), On SPM dynamics in the turbidity maximum zone of the Weser Estuary, *Die Küste*, *81*, 393-408.
Kulkarni, S., M. Deo, and S. Ghosh (2013), Impact of climate change on local wind conditions, paper presented at International Conference on Hydraulics and Water Resources (HYDRO), Chennai, India, Dec.
Lee, D. Y., D. P. Keller, B. C. Crump, and R. R. Hood (2012), Community metabolism and energy transfer in the Chesapeake Bay estuarine turbidity maximum, *Marine Ecology Progress Series*, *449*, 65-82.
Lee, J.-Y., J. Marotzke, G. Bala, L. Cao, S. Corti, J. P. Dunne, F. Engelbrecht, E. Fischer, J. C. Fyfe, and C. Jones (2021), Future global climate: scenario-based projections and near-term information, in *Climate change 2021: The physical science basis. Contribution of working group I to the sixth assessment report of the intergovernmental panel on climate change*, edited, pp. 553-672, Cambridge University Press.
Li, H., Q. Yang, S. Mo, J. Huang, S. Wang, R. Xie, X. Luo, and F. Liu (2022), Formation of turbidity maximum in the modaomen estuary of the Pearl River, China: the roles of mouth bar, *Journal of Geophysical Research: Oceans*, *127*(12), e2022JC018766.
Li, J.-L., N. Salam, P.-D. Wang, L.-X. Chen, J.-Y. Jiao, X. Li, W.-D. Xian, M.-X. Han, B.-Z. Fang, and X.-Z. Mou (2018a), Discordance between resident and active bacterioplankton in free-living and particle-associated communities in estuary ecosystem, *Microbial ecology*, *76*, 637-647.

Li, M., J. Ge, J. Kappenberg, D. Much, O. Nino, and Z. Chen (2014), Morphodynamic processes of the Elbe River estuary, Germany: the Coriolis effect, tidal asymmetry and human dredging, *Frontiers of earth science*, *8*(2), 181.
Li, R., N. Jiao, A. Warren, and D. Xu (2018b), Changes in community structure of active protistan assemblages from the lower Pearl River to coastal Waters of the South China Sea, *European Journal of Protistology*, *63*, 72-82.
Li, X., C. Lu, Y. Zhang, H. Zhao, J. Wang, H. Liu, and K. Yin (2020), Low dissolved oxygen in the Pearl River estuary in summer: Long-term spatio-temporal patterns, trends, and regulating factors, *Marine pollution bulletin*, *151*, 110814.
Lin, J., and A. Y. Kuo (2001), Secondary turbidity maximum in a partially mixed microtidal estuary, *Estuaries*, *24*, 707-720.
Lin, S., G. Liu, J. Niu, X. Wei, and S. Cai (2021), Responses of hydrodynamics to changes in shoreline and bathymetry in the Pearl River Estuary, China, *Continental Shelf Research*, *229*, 104556.
Lin, S., J. Niu, G. Liu, X. Wei, and S. Cai (2022), Variations of suspended sediment transport caused by changes in shoreline and bathymetry in the Zhujiang (Pearl) River Estuary in the wet season, *Acta Oceanologica Sinica*, *41*(10), 54-73.
Liu, B., S. Peng, Y. Liao, and H. Wang (2019), The characteristics and causes of increasingly severe saltwater intrusion in Pearl River Estuary, *Estuarine, coastal and shelf science*, *220*, 54-63.
Liu, F., S. Hu, X. Guo, X. Luo, H. Cai, and Q. Yang (2018), Recent changes in the sediment regime of the Pearl River (South China): Causes and implications for the Pearl River Delta, *Hydrological Processes*, *32*(12), 1771-1785.
Liu, R., Y. Wang, J. Gao, Z. Wu, and W. Guan (2016), Turbidity maximum formation and its seasonal variations in the Zhujiang (Pearl River) Estuary, southern China, *Acta Oceanologica Sinica*, *35*, 22-31.
Liu, Y., Q. Lin, J. Feng, F. Yang, H. Du, Z. Hu, and H. Wang (2020), Differences in metabolic potential between particle-associated and free-living bacteria along Pearl River Estuary, *Science of The Total Environment*, *728*, 138856.
Lu, Z., and J. Gan (2015), Controls of seasonal variability of phytoplankton blooms in the Pearl River Estuary, *Deep Sea Research Part II: Topical Studies in Oceanography*, *117*, 86-96.

Ma, M., L. Porz, C. Schrum, and W. Zhang (2024), Physical mechanisms, dynamics and interconnections of multiple estuarine turbidity maximum in the Pearl River estuary, *Frontiers in Marine Science*, *11*, 1385382.
Ma, M., W. Zhang, W. Chen, J. Deng, and C. Schrum (2023), Impacts of morphological change and sea-level rise on stratification in the Pearl River Estuary, *Frontiers in Marine Science*, *10*, 1072080.
MacCready, P. (1999), Estuarine adjustment to changes in river flow and tidal mixing, *Journal of Physical Oceanography*, *29*(4), 708-726.
Mai, Y.-z., Z.-n. Lai, X.-h. Li, S.-y. Peng, and C. Wang (2018), Structural and functional shifts of bacterioplanktonic communities associated with spatiotemporal gradients in river outlets of the subtropical Pearl River Estuary, South China, *Marine pollution bulletin*, *136*, 309-321.
Mao, Q., P. Shi, K. Yin, J. Gan, and Y. Qi (2004), Tides and tidal currents in the Pearl River Estuary, *Continental Shelf Research*, *24*(16), 1797-1808.
Megina, C., Í. Donázar-Aramedía, J. M. Miró, J. García-Lafuente, and J. C. García-Gómez (2023), The hyperturbid mesotidal Guadalquivir estuary during an extreme turbidity event: Identifying potential management strategies, *Ocean & Coastal Management*, *246*, 106903.
Miu, C. (2005), A Stronger Pearl River Delta Government Initiatives.
Nilsson, C., C. A. Reidy, M. Dynesius, and C. Revenga (2005), Fragmentation and flow regulation of the world's large river systems, *science*, *308*(5720), 405-408.
Niu, L., H. Cai, L. Jia, X. Luo, W. Tao, Y. Dong, and Q. Yang (2021), Metal pollution in the Pearl River Estuary and implications for estuary management: The influence of hydrological connectivity associated with estuarine mixing, *Ecotoxicology and Environmental Safety*, *225*, 112747.
Niu, L., X. Luo, S. Hu, F. Liu, H. Cai, L. Ren, S. Ou, D. Zeng, and Q. Yang (2020), Impact of anthropogenic forcing on the environmental controls of phytoplankton dynamics between 1974 and 2017 in the Pearl River estuary, China, *Ecological Indicators*, *116*, 106484.
North, E., S. Chao, L. Sanford, and R. Hood (2004), The influence of wind and river pulses on an estuarine turbidity maximum: Numerical studies and field observations in Chesapeake Bay, *Estuaries*, *27*, 132-146.

Ou, S., H. Zhang, and D.-x. Wang (2009), Dynamics of the buoyant plume off the Pearl River Estuary in summer, *Environmental Fluid Mechanics*, *9*, 471-492.
Palmer, K., C. Watson, and A. Fischer (2019), Non-linear interactions between sea-level rise, tides, and geomorphic change in the Tamar Estuary, Australia, *Estuarine, Coastal and Shelf Science*, *225*, 106247.
Panin, N., and D. Jipa (2002), Danube River sediment input and its interaction with the north-western Black Sea, *Estuarine, Coastal and Shelf Science*, *54*(3), 551-562.
Papenmeier, S., K. Schrottke, and A. Bartholomä (2014), Over time and space changing characteristics of estuarine suspended particles in the German Weser and Elbe estuaries, *Journal of Sea Research*, *85*, 104-115.
Passeri, D. L., S. C. Hagen, S. C. Medeiros, M. V. Bilskie, K. Alizad, and D. Wang (2015), The dynamic effects of sea level rise on low-gradient coastal landscapes: A review, *Earth's Future*, *3*(6), 159-181.
Pein, J. U., E. V. Stanev, and Y. J. Zhang (2014), The tidal asymmetries and residual flows in Ems Estuary, *Ocean Dynamics*, *64*, 1719-1741.
Postma, H. (1967), Sediment transport and sedimentation in the estuarine environment, *American Association of Advanced Sciences*, *83*, 158-179.
Qian, W., S. Zhang, C. Tong, J. Sardans, J. Peñuelas, and X. Li (2022), Long-Term Patterns of Dissolved Oxygen Dynamics in the Pearl River Estuary, *Journal of Geophysical Research: Biogeosciences*, *127*(7), e2022JG006967.
Ralston, D. K., and W. R. Geyer (2019), Response to channel deepening of the salinity intrusion, estuarine circulation, and stratification in an urbanized estuary, *Journal of Geophysical Research: Oceans*, *124*(7), 4784-4802.
Ralston, D. K., W. R. Geyer, and J. C. Warner (2012), Bathymetric controls on sediment transport in the Hudson River estuary: Lateral asymmetry and frontal trapping, *Journal of Geophysical Research: Oceans*, *117*(C10).
Ren, T., W. Gong, L. Gao, and F. Zhao (2024), Understanding land subsidence in the Pearl River Delta region of China based on InSAR observations, *Engineering Geology*, *339*, 107646.

Sanford, L. P., W. Panageotou, and J. P. Halka (1991), Tidal resuspension of sediments in northern Chesapeake Bay, *Marine Geology*, *97*(1-2), 87-103.
Sanford, L. P., S. E. Suttles, and J. P. Halka (2001), Reconsidering the physics of the Chesapeake Bay estuarine turbidity maximum, *Estuaries*, *24*, 655-669.
Schoellhamer, D. H. (2000), Influence of salinity, bottom topography, and tides on locations of estuarine turbidity maxima in northern San Francisco Bay, in *Proceedings in marine science*, edited, pp. 343-357, Elsevier.
Schulz, E., F. Grasso, P. Le Hir, R. Verney, and B. Thouvenin (2018), Suspended sediment dynamics in the macrotidal Seine Estuary (France): 2. Numerical modeling of sediment fluxes and budgets under typical hydrological and meteorological conditions, *Journal of Geophysical Research: Oceans*, *123*(1), 578-600.
Scown, M. W., F. E. Dunn, S. C. Dekker, D. P. van Vuuren, S. Karabil, E. H. Sutanudjaja, M. J. Santos, P. S. Minderhoud, A. S. Garmestani, and H. Middelkoop (2023), Global change scenarios in coastal river deltas and their sustainable development implications, *Global Environmental Change*, *82*, 102736.
Scully, M. E., and C. T. Friedrichs (2007), Sediment pumping by tidal asymmetry in a partially mixed estuary, *Journal of Geophysical Research: Oceans*, *112*(C7).
Shenliang, C., Z. Guoan, and Y. Shilun (2003), Temporal and spatial changes of suspended sediment concentration and resuspension in the Yangtze River estuary, *Journal of Geographical Sciences*, *13*, 498-506.
Sottolichio, A., V. Hanquiez, H. Périnotto, L. Sabouraud, and O. Weber (2013), Evaluation of the recent morphological evolution of the Gironde estuary through the use of some preliminary synthetic indicators, *Journal of Coastal Research*(65), 1224-1229.
Sottolichio, A., P. Le Hir, and P. Castaing (2000), Modeling mechanisms for the stability of the turbidity maximum in the Gironde estuary, France, in *Proceedings in Marine Science*, edited, pp. 373-386, Elsevier.
Sun, F.-L., Y.-S. Wang, M.-L. Wu, Y.-T. Wang, and Q. Li (2011), Spatial heterogeneity of bacterial community structure in the sediments of the Pearl River estuary, *Biologia*, *66*(4), 574-584.

Swapna, P., J. Jyoti, R. Krishnan, N. Sandeep, and S. Griffies (2017), Multidecadal weakening of Indian summer monsoon circulation induces an increasing northern Indian Ocean sea level, *Geophysical Research Letters*, *44*(20), 10,560-510,572.
Talke, S. A., and H. E. de Swart (2006), Hydrodynamics and morphology in the Ems/Dollard estuary: Review of models, measurements, scientific literature, and the effects of changing conditions.
Talke, S. A., H. E. de Swart, and V. De Jonge (2009), An idealized model and systematic process study of oxygen depletion in highly turbid estuaries, *Estuaries and coasts*, *32*, 602-620.
Tang, J., Y. P. Wang, Q. Zhu, J. Jia, J. Xiong, P. Cheng, H. Wu, D. Chen, and H. Wu (2019), Winter storms induced high suspended sediment concentration along the north offshore seabed of the Changjiang estuary, *Estuarine, Coastal and Shelf Science*, *228*, 106351.
Te Slaa, S., Q. He, D. S. van Maren, and J. C. Winterwerp (2013), Sedimentation processes in silt-rich sediment systems, *Ocean Dynamics*, *63*, 399-421.
Tönis, I., J. Stam, and J. Van de Graaf (2002), Morphological changes of the Haringvliet estuary after closure in 1970, *Coastal Engineering*, *44*(3), 191-203.
Torres, R. J., D. M. Abessa, F. C. Santos, L. A. Maranho, M. B. Davanso, M. R. do Nascimento, and A. A. Mozeto (2009), Effects of dredging operations on sediment quality: contaminant mobilization in dredged sediments from the Port of Santos, SP, Brazil, *Journal of soils and sediments*, *9*, 420-432.
Uncles, R., M. Barton, and J. Stephens (1994), Seasonal variability of fine-sediment concentrations in the turbidity maximum region of the Tamar Estuary, *Estuarine, Coastal and Shelf Science*, *38*(1), 19-39.
Uncles, R., and J. Stephens (2010), Turbidity and sediment transport in a muddy sub-estuary, *Estuarine, Coastal and Shelf Science*, *87*(2), 213-224.
Uncles, R., J. Stephens, and C. Harris (2006), Runoff and tidal influences on the estuarine turbidity maximum of a highly turbid system: the upper Humber and Ouse Estuary, UK, *Marine Geology*, *235*(1-4), 213-228.
Valentim, J. M., L. Vaz, N. Vaz, H. Silva, B. Duarte, I. Caçador, and J. M. Dias (2013), Sea level rise impact in residual circulation in Tagus

estuary and Ria de Aveiro lagoon, *Journal of Coastal Research*(65), 1981-1986.
van Maanen, B., and A. Sottolichio (2018), Hydro-and sediment dynamics in the Gironde estuary (France): Sensitivity to seasonal variations in river inflow and sea level rise, *Continental Shelf Research*, *165*, 37-50.
van Rijn, L., and B. Grasmeijer (2018), Effect of channel deepening on tidal flow and sediment transport—part II: muddy channels, *Ocean Dynamics*, *68*(11), 1481-1501.
Wai, O., C. Wang, Y. S. Li, and X. Li (2004), The formation mechanisms of turbidity maximum in the Pearl River estuary, China, *Marine Pollution Bulletin*, *48*(5-6), 441-448.
Walling, D. (2008), The changing sediment loads of the world's rivers, *Annals of Warsaw University of Life Sciences-SGGW. Land Reclamation*(39).
Walter, A., K. Keuler, D. Jacob, R. Knoche, A. Block, S. Kotlarski, G. Müller-Westermeier, D. Rechid, and W. Ahrens (2006), A high resolution reference data set of German wind velocity 1951-2001 and comparison with regional climate model results, *Meteorologische Zeitschrift*, *15*(6), 585-596.
Wang, B., M. Xin, X. Sun, Q. Wei, and X. Zhang (2016), Does reduced sediment load contribute to increased outbreaks of harmful algal blooms off the Changjiang Estuary?, *Acta Oceanologica Sinica*, *35*, 16-21.
Wang, C., W. Li, S. Chen, D. Li, D. Wang, and J. Liu (2018), The spatial and temporal variation of total suspended solid concentration in Pearl River Estuary during 1987–2015 based on remote sensing, *Science of the Total Environment*, *618*, 1125-1138.
Wang, C., Y. Zhao, X. Zou, X. Xu, and C. Ge (2017), Recent changing patterns of the Changjiang (Yangtze River) Estuary caused by human activities, *Acta Oceanologica Sinica*, *36*, 87-96.
Wang, F. C. (1988), Dynamics of saltwater intrusion in coastal channels, *Journal of Geophysical Research: Oceans*, *93*(C6), 6937-6946.
Wang, G., W. Cao, Y. Yang, W. Zhou, S. Liu, and D. Yang (2010), Variations in light absorption properties during a phytoplankton bloom in the Pearl River estuary, *Continental Shelf Research*, *30*(9), 1085-1094.

Wang, H., T. J. Wright, Y. Yu, H. Lin, L. Jiang, C. Li, and G. Qiu (2012), InSAR reveals coastal subsidence in the Pearl River Delta, China, *Geophysical Journal International*, *191*(3), 1119-1128.
Wang, J., and B. Hong (2021), Threat posed by future sea-level rise to freshwater resources in the Upper Pearl River Estuary, *Journal of Marine Science and Engineering*, *9*(3), 291.
Wang, J., Y. Tong, L. Feng, D. Zhao, C. Zheng, and J. Tang (2021a), Satellite - observed decreases in water turbidity in the Pearl River Estuary: potential linkage with sea - level rise, *Journal of Geophysical Research: Oceans*, *126*(4), e2020JC016842.
Wang, Y.-H., S.-L. Cai, Y.-D. Yang, Z.-Y. Zhong, and F. Liu (2021b), Morphological consequences of upstream water and sediment changes and estuarine engineering activities in Pearl River Estuary channels over the last 50 years, *Science of The Total Environment*, *765*, 144172.
Wang, Y., J. Pan, J. Yang, Z. Zhou, Y. Pan, and M. Li (2020), Patterns and processes of free - living and particle - associated bacterioplankton and archaeaplankton communities in a subtropical river - bay system in South China, *Limnology and Oceanography*, *65*, S161-S179.
Wang, Z. B., C. Jeuken, and H. De Vriend (1999), Tidal asymmetry and residual sediment transport in estuaries*Rep.*, Deltares (WL).
Wei, X., S. Cai, P. Ni, and W. Zhan (2020), Impacts of climate change and human activities on the water discharge and sediment load of the Pearl River, southern China, *Scientific Reports*, *10*(1), 16743.
Wei, X., S. Cai, and W. Zhan (2021), Impact of anthropogenic activities on morphological and deposition flux changes in the Pearl River Estuary, China, *Scientific Reports*, *11*(1), 16643.
Weng, Q. (2007), A historical perspective of river basin management in the Pearl River Delta of China, *Journal of Environmental Management*, *85*(4), 1048-1062.
Wigley, T. M. (2009), The effect of changing climate on the frequency of absolute extreme events, *Climatic Change*, *97*(1), 67-76.
Winterwerp, J. C. (2011), Fine sediment transport by tidal asymmetry in the high-concentrated Ems River: indications for a regime shift in response to channel deepening, *Ocean Dynamics*, *61*(2), 203-215.
Wong, L.-A., J. Chen, H. Xue, L. Dong, J. Su, and G. Heinke (2003), A model study of the circulation in the Pearl River Estuary (PRE) and

its adjacent coastal waters: 1. Simulations and comparison with observations, *Journal of Geophysical Research: Oceans*, *108*(C5).
Woodruff, J. D., W. R. Geyer, C. K. Sommerfield, and N. W. Driscoll (2001), Seasonal variation of sediment deposition in the Hudson River estuary, *Marine Geology*, *179*(1-2), 105-119.
Wright, L., and B. Thom (1977), Coastal depositional landforms: a morphodynamic approach, *Progress in Physical geography*, *1*(3), 412-459.
Wu, C., C. Ji, B. Shi, Y. Wang, J. Gao, Y. Yang, and J. Mu (2019), The impact of climate change and human activities on streamflow and sediment load in the Pearl River basin, *International Journal of Sediment Research*, *34*(4), 307-321.
Wu, S., H. Cheng, Y. J. Xu, J. Li, and S. Zheng (2016a), Decadal changes in bathymetry of the Yangtze River Estuary: Human impacts and potential saltwater intrusion, *Estuarine, Coastal and Shelf Science*, *182*, 158-169.
Wu, Z., J. D. Milliman, D. Zhao, Z. Cao, J. Zhou, and C. Zhou (2018), Geomorphologic changes in the lower Pearl River Delta, 1850–2015, largely due to human activity, *Geomorphology*, *314*, 42-54.
Wu, Z., Y. Saito, D. Zhao, J. Zhou, Z. Cao, S. Li, J. Shang, and Y. Liang (2016b), Impact of human activities on subaqueous topographic change in Lingding Bay of the Pearl River estuary, China, during 1955–2013, *Scientific reports*, *6*(1), 37742.
Xiong, H., J. Ren, H. Liu, J. Deng, L. Ye, B. Shi, and J. Wu (2024), Pearl River Delta, in *Delta Sustainability: A Report to the Mega-Delta Programme of the UN Ocean Decade*, edited by W. Zhang and H. d. Vriend, pp. 237-261, Springer Nature Singapore, Singapore, doi:10.1007/978-981-97-7259-9_13.
Xiong, H., Y. Zong, G. Huang, and S. Fu (2020), Human drivers accelerated the advance of Pearl River deltaic shoreline in the past 7500 years, *Quaternary Science Reviews*, *246*, 106545.
Xu, F., D.-P. Wang, and N. Riemer (2010), An idealized model study of flocculation on sediment trapping in an estuarine turbidity maximum, *Continental Shelf Research*, *30*(12), 1314-1323.
Yang, F., X. Ji, W. Zhang, H. Zou, W. Jiang, and Y. Xu (2022a), Characteristics and Driving Mechanisms of Salinity Stratification during the Wet Season in the Pearl River Estuary, China, *Journal of Marine Science and Engineering*, *10*(12), 1927.

Yang, J., and C. Chen (2007), An optimal algorithm for retrieval of chlorophyll, suspended sediments and gelbstoff of case II waters in Zhujiang River estuary, *Journal of tropical oceanography*, *26*(5).
Yang, J., and W. Liu (2015), Evolution of the Maximum Turbidity Zone in the Lingding Bay of Pearl River Estuary over past 30 years, *珠江水运*(16), 58-62.
Yang, Y., W. Guan, E. Deleersnijder, and Z. He (2022b), Hydrodynamic and sediment transport modelling in the Pearl River Estuary and adjacent Chinese coastal zone during Typhoon Mangkhut, *Continental Shelf Research*, *233*, 104645.
Yang, Y., Y. Li, Z. Sun, and Y. Fan (2014), Suspended sediment load in the turbidity maximum zone at the Yangtze River Estuary: The trends and causes, *Journal of Geographical Sciences*, *24*, 129-142.
Yu, Q., Y. Wang, J. Gao, S. Gao, and B. Flemming (2014), Turbidity maximum formation in a well‐mixed macrotidal estuary: The role of tidal pumping, *Journal of Geophysical Research: Oceans*, *119*(11), 7705-7724.
Yu, Y., H. Zhang, and C. Lemckert (2013), Seasonal variations of the salinity and turbidity in the Brisbane River estuary, Queensland, Australia, *Journal of Coastal Research*(65), 1253-1258.
Zeng, Z., W. W. Cheung, S. Li, J. Hu, and Y. Wang (2019), Effects of climate change and fishing on the Pearl River Estuary ecosystem and fisheries, *Reviews in Fish Biology and Fisheries*, *29*, 861-875.
Zhang, G., Y. Chen, W. Cheng, H. Zhang, and W. Gong (2021a), Wave effects on sediment transport and entrapment in a channel‐shoal estuary: the pearl river estuary in the dry winter season, *Journal of Geophysical Research: Oceans*, *126*(4), e2020JC016905.
Zhang, G., W. Cheng, L. Chen, H. Zhang, and W. Gong (2019), Transport of riverine sediment from different outlets in the Pearl River Estuary during the wet season, *Marine Geology*, *415*, 105957.
Zhang, M., Q. Dong, T. Cui, C. Xue, and S. Zhang (2014), Suspended sediment monitoring and assessment for Yellow River estuary from Landsat TM and ETM+ imagery, *Remote Sensing of Environment*, *146*, 136-147.
Zhang, Q., X. Sun, K. Zhang, Z. Liao, and S. Xu (2021b), Trade-offs and synergies of ecosystem services in the Pearl River Delta urban agglomeration, *Sustainability*, *13*(16), 9155.

Zhang, S., X. X. Lu, D. L. Higgitt, C.-T. A. Chen, J. Han, and H. Sun (2008), Recent changes of water discharge and sediment load in the Zhujiang (Pearl River) Basin, China, *Global and Planetary Change*, *60*(3-4), 365-380.
Zhang, W., Y. Xu, A. Hoitink, M. Sassi, J. Zheng, X. Chen, and C. Zhang (2015a), Morphological change in the Pearl River delta, China, *Marine Geology*, *363*, 202-219.
Zhang, Y., J. Ren, W. Zhang, and J. Wu (2021c), Importance of salinity-induced stratification on flocculation in tidal estuaries, *Journal of Hydrology*, *596*, 126063.
Zhang, Y., Z. Wang, Y. Xue, and J. Wu (2015b), Visco-elasto-plastic compaction of aquitards due to groundwater withdrawal in Shanghai, China, *Environmental Earth Sciences*, *74*, 1611-1624.
Zhu, C., D. S. van Maren, L. Guo, J. Lin, Q. He, and Z. B. Wang (2021), Effects of sediment‐induced density gradients on the estuarine turbidity maximum in the Yangtze Estuary, *Journal of Geophysical Research: Oceans*, *126*(5), e2020JC016927.
Zu, T., and J. Gan (2015), A numerical study of coupled estuary–shelf circulation around the Pearl River Estuary during summer: Responses to variable winds, tides and river discharge, *Deep Sea Research Part II: Topical Studies in Oceanography*, *117*, 53-64.

Acknowledgements

I have been extremely fortunate to have learned from and benefited from the project, and work with many wonderful and brilliant people.

I would like to express my sincerest gratitude to my principal supervisor, Prof. Corinna Schrum. Her guidance and support have been most instrumental in my scientific career, providing me with invaluable knowledge and insights. She is always able to provide clear direction with an optimistic and confident approach. And in the personal conversations, she's always so warm and patient.

I would also like to express my gratitude to my co-supervisor, Dr. Wenyan Zhang. I would like to thank him for his dedicated effort and meticulous guidance. In particular, he conducted multiple reviews of my articles, offering valuable insights and suggestions on pivotal aspects. He exemplifies a capacity for flexible thinking and possesses a profound depth of knowledge.

My hearty thanks to my colleagues at the Department of Sediment Transport and Morphodynamics. Lucas always comes with calm and patient whether at work or in private. He is always available for any discussion and provide the most practical suggestions based on his in-depth knowledge of sediment. Peter is the most energetic one who can always bring happiness. He's a nice colleague at work, always giving it his all. And in life, he's a sweat friend, always there to support and bring a smile. Thanks to my officemate Jialing and Yuxin. The conversation with Jialing and is always relax and interesting. Special thanks to Yuxin for the comments on my dissertation. Thanks for David, Jiayue, Veronika, Ruemeysa, Bo, Zhentao, Chao. I would like to thank all colleagues who have worked at KSS, either currently or previously. I have enjoyed working with you all and have many memories that I will always treasure. Thanks to other PhD students, both current and former: Seyed, Philipp, Jan, Nils, Benjamin. Special thanks go to Jan, Nils, Johannes Pein for their invaluable help when I started with SCHISM. I would like to express my many thanks to Enpei for the enjoyable holiday period we have experienced. I'd like to thank Sabine Billerbeck for always being so helpful and answering any administrative questions I have.

My January, thank you for being found me, hearing me, bringing me spring. I am looking forward to stars in front of us.

Thanks to Lizhang for your ongoing assistance and support. I couldn't have done my PhD without you. Thanks for my family, they give me courage to move forward.

Eidesstattliche Versicherung | Declaration on Oath

Hiermit erkläre ich an Eides statt, dass ich die vorliegende Dissertationsschrift selbst verfasst und keine anderen als die angegebenen Quellen und Hilfsmittel benutzt habe. Sofern im Zuge der Erstellung der vorliegenden Dissertationsschrift generative Künstliche Intelligenz (gKI) basierte elektronische Hilfsmittel verwendet wurden, versichere ich, dass meine eigene Leistung im Vordergrund stand und dass eine vollständige Dokumentation aller verwendeten Hilfsmittel gemäß der Guten wissenschaftlichen Praxis vorliegt. Ich trage die Verantwortung für eventuell durch die gKI generierte fehlerhafte oder verzerrte Inhalte, fehlerhafte Referenzen, Verstöße gegen das Datenschutz- und Urheberrecht oder Plagiate.

Ort, Datum
Unterschrift

I hereby declare and affirm that this doctoral dissertation is my own work and that I have not used any aids and sources other than those indicated.

If electronic resources based on generative artificial intelligence (gAI) were used in the course of writing this dissertation, I confirm that my own work was the main and value-adding contribution and that complete documentation of all resources used is available in accordance with good scientific practice. I am responsible for any erroneous or distorted content, incorrect references, violations of data protection and copyright law or plagiarism that may have been generated by the gAI.

City, date
Signature